UNIVERSITY OF LJUBLJANA
FACULTY OF MATHEMATICS AND PHYSICS
DEPARTMENT OF PHYSICS
Chair of Meteorology

Rahela Žabkar

High-resolution spatial and temporal dynamics of tropospheric ozone in complex terrain

Doctoral thesis

ADVISOR: prof. dr. Jože Rakovec
CO-ADVISOR: prof. dr. Darko Koračin

Ljubljana, 2009

UNIVERZA V LJUBLJANI
FAKULTETA ZA MATEMATIKO IN FIZIKO
ODDELEK ZA FIZIKO
Katedra za meteorologijo

Rahela Žabkar

Prostorsko in časovno podrobna dinamika troposferskega ozona v razgibanem reliefu

Doktorska disertacija

MENTOR: prof. dr. Jože Rakovec
SOMENTOR: prof. dr. Darko Koračin

Ljubljana, 2009

Zahvala

Zahvalila bi se rada vsem, ki so mi tako ali drugacče pomagali pri nastanku tega dela. V prvi vrsti gre zahvala mentorju prof. dr. Jožetu Rakovcu in somentorju prof. dr. Darku Koračinu za njune nasvete in usmerjanje, pa tudi za podporo pri nastanku tega dela. Hvala doc. dr. Marku Žagarju, ker je s svojimi predlogi pripomogel k izboljšanju disertacije.

Hvala dr. Martinu Horvatu ter kolegom z Agencije RS za okolje, ki so mi pomagali pri izvedbi računskih simulacij. Hvala mag. Tanji Bolte, ker mi je neštetokrat priskočila na pomoč s podatki in različnimi informacijami. Hvala doc. dr. Nedjeljki Žagar, njeni nasveti so mi pogosto predstavljali vodilo pri delu, mag. Mateji Iršič Žibert pa hvala za rešilno bilko.

Hvala staršem. Omogočili so mi, da stopim na pot znanja in mi bili ves čas v oporo. Hvala moževi mami Nuši, ker je popazila na fante v moji odsotnosti.

Hvala sinovom Luki, Janu in Binetu. V moj vsakdan vnašajo smeh, mojemu življenju dajejo smisel, ob njih se učim pomembno ločevati od manj pomembnega.

Hvala možu Janezu, ker je vedno ob meni in z mano. Tudi v trenutkih, ko to ni najbolj enostavno.

Abstract

The highest frequency of exceedances of ozone threshold values during the warm months in Slovenia is usually limited to the Mediterranean part of the country, separated from central Slovenia with the Alpine-Dinaric mountain ridge. The rest of Slovenia generally experiences lower ozone daily maxima with occasionally exceeded thresholds.

The thesis focuses on the characteristics of temporal and spatial dynamics of the high ozone episodes in Slovenia. One of the interesting issues is also the question of the impact of Po River Basin emissions on Slovenian ozone levels. With the trajectory analysis, performed for the warm parts of two years, the influence of air masses origin on the near ground ozone levels is studied. Nevertheless, the main purpose of this research remains to be the exploration of the dynamics of selected high ozone episodes with a coupled meteorological-photochemistry WRF-Chem model.

As part of the research the ability of WRF-Chem model to follow the measured meteorological parameters and the near ground ozone levels at measuring sites spread over the complex terrain of Slovenia is evaluated. In addition, different experiments are performed with the aim to estimate the sensitivity of simulated near ground ozone to different sources of uncertainties, such as quantity and speciation of anthropogenic emissions, initial and boundary chemical conditions, model horizontal resolution and the meteorological representation of the planetary boundary layer.

According to the results of these experiments, simulated ozone levels are most sensitive to the initial chemistry conditions during the first 2 or 3 days of an episode (simulation). Although in the next days the influence of chemical initial conditions significantly decreases, under certain conditions they can become important again even after 6 or 7 days of simulation. Nevertheless, for the complex terrain of Slovenia the model representation of meteorological conditions in the planetary boundary layer appears to be problematic during the discussed stagnant anticyclonic situations.

Results of simulations show that all three analyzed episodes generally express a similar temporal evolution, consisting of three phases, closely related to the synoptic situation. On the basis of the characteristics distinctive of each of these phases, the phenomenon of the northern Adriatic sea the origin of polluted trajectories (revealed by trajectory analysis), as well as the higher frequency of extreme ozone values in the Mediterranean Slovenia, can be explained.

Keywords

Tropospheric ozone; planetary boundary layer; model sensitivity; WRF-Chem model; complex terrain

PACS

92.60.Wc, 92.60.Fm, 92.60.Hf

Povzetek

V Sloveniji je pogostnost preseganj dovoljenih vrednosti ozona v topli polovici let največja na Primorskem. Vzhodno od Mediteranskega dela, ki ga od preostale Slovenije ločuje Alpsko-Dinarska gorska pregrada, so koncentracije (oz. gostote v zraku) ozona običajno nižje, vendar pa so tudi v tem delu države občasno izmerjene ekstremno visoke vrednosti ozona.

V disertaciji raziskujem značilnosti časovne in prostorske dinamike epizod z visokimi izmerjenimi gostotami ozona v Sloveniji. Eno od vprašanj, ki ga obravnavam, je med drugim tudi vpliv Padske nižine na onesnaženost zraka z ozonom pri nas. S statistično analizo trajektorij, narejeno za toplo polovico dveh let, preiskujem vpliv izvora zračnih mas na prizemne vrednosti ozona na nekaj izbranih merilnih mestih. Osrednja tema mojega dela pa je vsekakor študija dinamike izbranih epizod s sklopljenim meteorološko-fotokemijskim modelom WRF-Chem.

V sklopu disertacije sem med drugim analizirala sposobnost modela, da sledi dejanskim vrednostim izmerjenih meteoroloških spremenljivk in ozona v razgibanem reliefu Slovenije. Poleg tega so bili z namenom analizirati občutljivost simuliranih vrednosti ozona na različne vire negotovosti, narejeni nekateri ekperimenti, v katerih ocenjujem in primerjam vpliv negotovosti v antropogenih emisijah, začetnih in robnih kemijskih pogojih, horizontalni ločljivosti modela in meteorološkem opisu planetarne mejne plasti zraka na simulirane vrednosti ozona.

Rezultati teh eksperimentov so pokazali, da so simulirane vrednosti ozona prve 2 do 3 dni epizod oziroma simulacij najbolj občutljive na začetne kemijske pogoje. Kljub temu, da v nadaljnih dneh vpliv začetnih kemijskih pogojev pade, pa v določenih okoliščinah, lahko celo po 6 ali 7 dneh simulacije, postanejo ponovno bolj pomembni. Poleg tega se je izkazalo, da je za podrobnejše modeliranje ozona nad razgibanim območjem Slovenije v primeru stagnantnih anticiklonalnih situacij najbolj problematičen meteorološki opis planetarne mejne plasti zraka v modelu.

Na osnovi rezultatov simulacij lahko zaključimo, da je za časovni razvoj obravnavanih epizod značilen potek v treh fazah, vezanih na sinoptično situacijo. S pomočjo značilnosti vsake od teh faz lahko razložimo tako izvor onesnaženih trajektorij iznad severnega Jadrana (rezultat analize trajektorij), kot tudi večjo pogostost pojavljanja najvišjih koncentracij ozona na območju Mediteranske Slovenije.

Ključne besede

Troposferski ozon; planetarna mejna plast; občutljivost modela; model WRF-Chem; razgiban relief

PACS

92.60.Wc, 92.60.Fm, 92.60.Hf

Contents

1 Introduction **1**
1.1 Meteorology and air pollution . . . 5
1.1.1 Planetary boundary layer . . . 8
1.1.1.1 Turbulence . . . 8
1.1.1.2 Turbulence closure . . . 9
1.2 Chemical Processes in PBL . . . 10
1.2.1 Basic photochemical transformations of oxidized nitrogen species . . . 10
1.2.1.1 The role of free radicals . . . 11
1.2.1.2 Tropospheric sinks of ozone . . . 12
1.2.2 The role of VOCs in photochemical ozone formation . . . 13
1.2.2.1 Sources, sinks and reservoirs of HO_x . . . 14
1.2.3 Sensitivity of O_3 to NO_x and VOC concentration . . . 15

2 Trajectory Analysis of Ozone Pollution in Slovenia **17**
2.1 Methodology . . . 18
2.1.1 Selected locations and their ozone characteristics . . . 18
2.1.2 Computation of trajectories . . . 21
2.1.3 The k-means clustering . . . 21
2.1.4 Analysis of cluster variables . . . 22
2.1.5 Concentration-weighted trajectory (CWT) . . . 22
2.2 Results of trajectory analysis . . . 23
2.2.1 The trajectory clusters and local ozone concentrations . . . 23
2.2.2 Concentration weighted trajectories and number density fields . . . 26
2.3 Discussion . . . 28

3 The WRF-Chem modeling System **31**
3.1 Model dynamics . . . 31
3.2 Discretization of governing equations . . . 33
3.3 Physical parameterizations . . . 33
3.3.1 Land surface model . . . 34
3.3.1.1 5-layer thermal diffusion scheme . . . 34
3.3.1.2 Noah LSM . . . 35
3.3.2 Planetary boundary layer schemes . . . 36
3.3.2.1 YSU PBL scheme . . . 36
3.3.2.2 MYJ PBL scheme . . . 37
3.3.3 Surface layer physics parameterizations . . . 38
3.4 WRF-Chem chemistry . . . 39
3.4.1 Chemical mechanism . . . 39
3.4.2 Biogenic emissions . . . 41
3.4.3 Anthropogenic emissions . . . 41
3.4.4 Dry deposition . . . 41
3.5 Model setup and initialization . . . 41

3.6 Monitoring sites used for model validation . . . 43

4 Preparation of Anthropogenic Emission Database 45
4.1 Spatial disaggregation of emissions . . . 47
4.2 Temporal disaggregation of emissions . . . 55
4.3 Speciation of organic gases . . . 58

5 Numerical Simulations of High Ozone Episodes 61
5.1 Episode I: 4 - 14 August 2003 . . . 63
5.1.1 Synoptic situation and ozone characteristics . . . 63
5.1.2 Reference simulation . . . 66
5.1.3 Impact of different model PBL schemes and LSMs . . . 72
5.1.4 Impact of horizontal resolution . . . 90
5.1.5 Impact of anthropogenic VOC speciation . . . 91
5.1.6 Impact of bulk ±30% changes in VOC and NO_x emissions . . . 93
5.1.7 Impact of chemical initial and lateral boundary conditions . . . 98
5.1.8 Impact of meteorology re-initialization . . . 101
5.2 Episode II: 10 - 11 June 2004 . . . 103
5.2.1 Synoptic situation and ozone characteristics . . . 103
5.2.2 Model results . . . 104
5.3 Episode III: 19 - 26 June 2005 . . . 110
5.3.1 Synoptic situation and ozone development . . . 110
5.3.2 Model results . . . 112

6 Discussion 119

7 Conclusions 127

Bibliography 129

Appendices 136

A Statistical scores used for model evaluation 139

B Weighting factor maps for spatial disaggregation of EMEP emissions 141

C Tables associated with preparation of anthropogenic emissions 145

D WRF-Chem model namelist options used for reference simulations 149

E High ozone days in years 2003 - 2005 153

F Time series of near ground variables for experiments of Episode I 155

G Results of sensitivity tests for Episode II 165

Daljši slovenski povzetek 168

Chapter 1

Introduction

Air quality is of great interest to society, because it affects human health (Bernard et al., 2001; Levy et al., 2001), crops (Heck et al., 1982), forests (Ollinger et al., 1996; Staff and Tyler, 1996), and other ecosystems. One of major air pollutants continues to be tropospheric ozone, which is together with other secondary photochemical pollutants formed through the complex interactions between nitrogen oxides (NO_x) and volatile organic compounds (VOCs) in the presence of sunlight.

This study focuses on the characteristics of high ozone episodes in Slovenia. Although some statistical approaches are used as well, the main purpose is to explore the dynamics of these episodes with a coupled meteorological-photochemistry model.

The history of tropospheric ozone goes back to the 1940s, when ozone was first identified as the most recognized gas-phase by-product of photochemical smog in Los Angeles. Since then research has focused on several aspects of photochemical air pollution, including: a detailed elucidation of photochemical mechanisms and rates (Hough, 1988; Stockwell et al., 1990; Carter, 2008), development of monitoring networks and measurements in urban centers and later also in suburban and rural environments, the creation and development of chemical transport models (e.g. Seinfeld and Pandis, 1998) and field measurement techniques for testing the model results. If at the beginning the tropospheric ozone was recognized as a local urban problem, about 20 years ago it was realized that it is of concern on a much larger scale (Volz and Kley, 1988; Staehelin and Smith, 1991). Moreover, according to measurements fairly high ozone levels can be achieved also at rural stations far away from emission sources (Sillman, 1999; Kalabokas et al., 2000; Wotawa et al., 2000).

In Slovenia the first attempt toward the recognition and understanding of the near ground ozone phenomena was made at the beginning of the 1990s, with the implementation of the first continuous ozone measurements in 1992. To date the total number of ozone ground level stations has increased to 18 sites, spread over the country (Fig. 1.1). Measurements show that the annual number of days with at least one hourly warning ozone threshold value (180 $\mu g/m^3$) exceedance ranges from a few days in the interior of the country to up to 25 days at stations close to the Adriatic Sea in the southwestern part of Slovenia. The highest number of ozone exceedances recorded in the southwestern part of Slovenia (Table 1.2 and 1.2) can be partly attributed to meteorological conditions typical of Mediterranean climate (high temperatures, a lot of sunshine, a low number of precipitation days). But since local emissions in this part of the country are not significant (originate mainly from traffic), they cannot explain the measured degree of pollution. Considerably lower ozone values measured at Maribor station (Table 1.2 and 1.2) are a consequence of ozone titration with NO_x from the nearby road emissions. Ozone values measured at this station are considered to be underestimated and

not representative for the city of Maribor.

In a scope of the Vertical Ozone Transports in the Alps (VOTALP, VOTALP II; Wotawa and Kromp-Kolb, 2000) and some other projects the heavily industrialized Po Basin was identified as important source region of Alpine ozone precursors (Seibert et al., 1997; Wotawa and Kromp-Kolb, 2000; Kaiser et al., 2007). The thesis that regional transport from Po Basin explains the high ozone measured in the southwestern part of the Slovenia was thus set up, but has not been verified yet. In addition, high ozone concentrations are occasionally measured not only at urban stations in the interior of Slovenia, but also at sparsely inhabited rural areas like Iskrba near Kočevska Reka. The motivation for this thesis were re-occurring questions regarding the origins of polluted air masses as well as spatial and temporal characteristics of the photochemical pollution during the episodes.

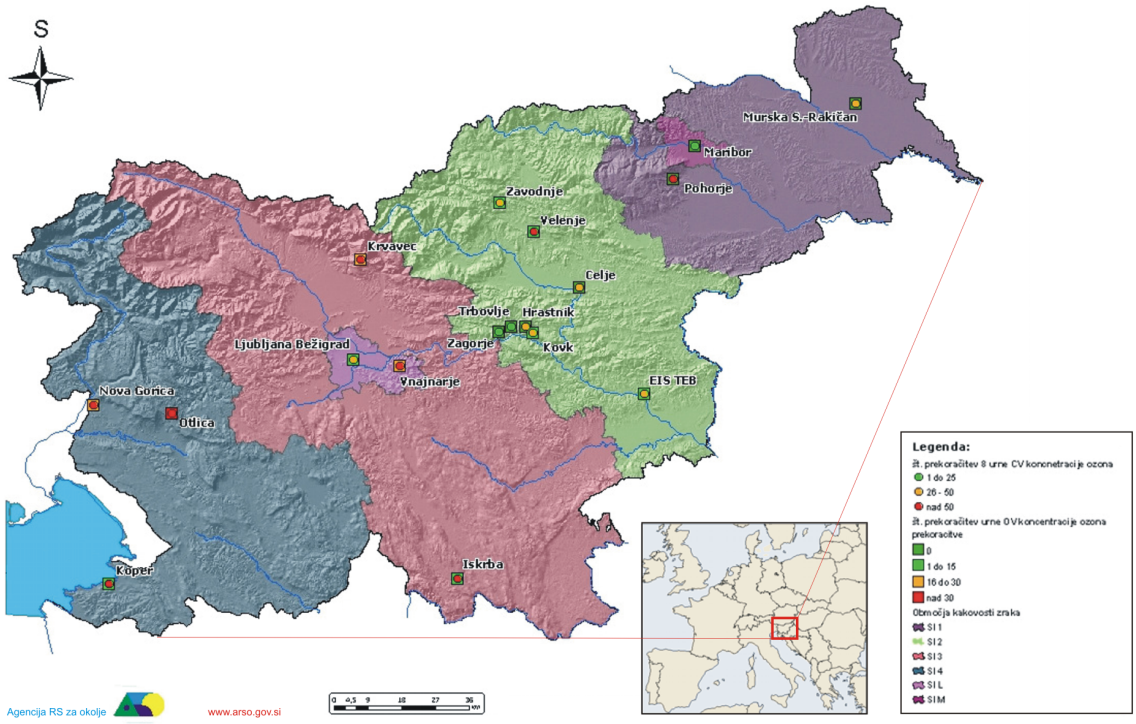

Figure 1.1: Ozone measuring sites in Slovenia colored according to the number of exceedances of 1 hour warning value (180 $\mu g/\mathrm{m}^3$) and 8 hour 2010 target value (120 $\mu g/\mathrm{m}^3$) in year 2007. Circles denote yearly number of 8 hour target value exceedances (green: 1 - 15, orange: 26 - 50, red: more than 50), squares denote yearly number of exceedances of ozone hourly warning value (green: zero, light green: 1 - 15, orange: 16 - 30, red: more than 30). The territory of Slovenia is divided and colored according to air quality zones. (source: ARSO, 2008)

Practical motivation was that Slovenian legislation (transposed from Directive 2002/3/EC of the European Parliament and of the Council of 12 February 2002) demands predictions of ozone threshold value exceedances. Moreover, if the exceedence is forecasted also its duration and spatial extension should be predicted. To meet these legislation demands not only the understanding of the meteorological and other circumstances leading to high ozone levels was necessary, but also the modeling system had to be established.

Table 1.1: Number of days with exceeded 8-hour target value for ozone at some Slovenian sites (the highest average 8-hour floating value above 120 $\mu g/m^3$). Red color indicates the exceedances of the maximum annual permitted limit of 25 days. nd - data not available. Source: MOP ARSO.

	2000	2001	2002	2003	2004	2005	2006	2007
Ljubljana	49	40	25	81	32	38	47	43
Maribor	6	3	4	19	1	0	7	4
Celje	28	34	33	78	18	43	39	35
Velenje	12	1	57	87	6	10	66	61
Nova Gorica	nd	nd	36	105	46	43	56	51
Murska Sobota	nd	nd	nd	101	15	31	28	34
Iskrba	nd	nd	nd	94	38	60	67	61
Otlica	nd	nd	nd	nd	nd	nd	90	98

Table 1.2: Number of hours with ozone value above 180 $\mu g/m^3$. nd - data not available. Source: MOP ARSO.

	2000	2001	2002	2003	2004	2005	2006	2007
Ljubljana	3	1	4	18	4	11	10	8
Maribor	0	0	0	0	0	0	0	0
Celje	0	3	0	2	0	0	3	0
Velenje	0	0	1	5	0	0	6	14
Nova Gorica	nd	nd	26	102	27	33	34	19
Murska Sobota	nd	nd	nd	6	0	1	0	0
Iskrba	nd	nd	nd	11	1	0	1	7
Otlica	nd	nd	nd	nd	nd	nd	69	44

In the thesis the temporal and spatial dynamics of the episodes with high near ground ozone levels in Slovenia are studied with a coupled meteorological-photochemistry model. A WRF-Chem model (Grell et al., 2005), which has been in the time of this research in its last stage before the official release, and has already been available in a beta version, was used. The advantage and the novelty of the WRF-Chem model is that meteorological and chemical processes are fully coupled, as are the meteorological and chemical processes in the real atmosphere. Otherwise, it has been a common practise today to use two different models for air quality simulations: the meteorological model for providing description of the atmospheric conditions, and the transport-chemical one for modeling transport, dispersion and chemical transformations of pollutants. However, the separation of meteorology and chemistry can present a significant source of uncertainties arising from incomplete or inconsistent meteorological coupling between the two models (Seaman, 2000) at the parametrization levels. In any case the usage of two separate models causes a significant loss of information about atmospheric processes that have a time scale shorter than is the frequency of the meteorological model outputs (usually 1 hour).

The task of ozone modeling was challenging, because many complex processes are involved in the ozone formation and most of them potentially present a significant source of model uncertainties. For example, the planetary boundary layer meteorology, specially the representation of mixing heights and local air circulations, which usually govern the high ozone episodes, still represent a challenge for today's models. Similar holds for the nighttime

boundary layer height, especially during low-wind and high stability conditions. Although the highest near ground ozone levels occur during the daytime, the nighttime processes affect the daytime ozone levels. The emissions, their spatial and temporal variability, as well as description of chemical processes in model (specially nighttime chemistry) are another source of model uncertainties. In addition, not only production from local sources, but also the regional transport of pollutants and their accumulation in air masses may have significant influence on final ozone concentrations and has to be represented well by the model. Consequently, beside characterizing the circumstances leading to the high ozone episodes in Slovenia, the aim of this research was also to estimate the ability of model to follow the evolution of measured ozone levels as well as to estimate the sensitivity of simulated ozone to different potential sources of uncertainties.

At the beginning the plan was to focus on ozone in Ljubljana and its surroundings, mainly because we were able to acquire the detailed emissions only for this region. Nevertheless, during the course of research it became clear, that Ljubljana although as a capital city characterized by significant emissions, cannot be studied apart from the rest of Slovenia. Often high measured ozone in Ljubljana coincides with high ozone levels measured also at other Slovenian sites with less (or sometimes no) significant local emissions. Whereas, in addition, the ozone exceedances most often occur in the Mediterranean part of the country, the area of interest was expanded to the whole Slovenia.

Conceptual sequence of the chapters in thesis to some extent reflects the time course of the research work. In the continuation of this introductory chapter the planetary boundary layer (PBL), where the tropospheric ozone phenomena occur, is briefly described. Some generally known effects of the meteorological conditions on the air pollution are summarized, and examples of relations between the ozone and meteorological parameters for Slovenian sites are shown as well. The presentation of main chemical processes governing the ozone formation and destruction in the PBL concludes this chapter.

Chapter 2 presents results of the trajectory statistical analysis, showing the influence of the air masses origin on the measured near ground ozone in Slovenia. Despite the complexity of the processes involved, some certain characteristics of the high ozone episodes in Slovenia are revealed through the trajectory analysis as well. In the chapter the characteristics of the near ground ozone phenomenon at four Slovenian stations are also explored, which gives this chapter some introductory properties. The value of the trajectory statistical analysis is also that this study (with different approach and other model used than WRF-Chem) is completely independent of photochemistry modeling, which gives the possibility to compare results of two different approaches. Trajectories calculated in Chapter 2 are also included in the presentation of the episodes in one of the following chapters.

Chapter 3 briefly introduces the WRF-Chem modeling system and the setup and initialization procedure used in simulations. In Chapter 4 the construction of the anthropogenic emissions is described. Anthropogenic emissions constitute an important part of modeling system, but were prior to my research available only in a lacking and/or inappropriate form. Another source of primarily air pollutants represent biogenic emissions. For the estimation of the biogenic emissions in the WRF-Chem model incorporated routines were used. In these routines the quantity of these emissions is calculated on the basis of the land-cover category, near ground air temperature and solar radiation.

Chapter 5 presents main results from the analysis of selected ozone episodes, including description of synoptic situations, characteristics of ozone measurements and results of simulations. Since only a limited number of studies have been performed with a WRF-Chem model so far the influence of some meteorological parametrization schemes on simulated ozone

is systematically tested. This sensitivity is further compared to other sensitivities: ozone sensitivity to chemical boundary and initial conditions, changed emissions and model horizontal resolution. Based on the experiences from these sensitivity tests the results of simulations are evaluated. Some characteristics of the temporal and spatial ozone variability in Slovenia during the course of these episodes are also shown.

Chapter 6 presents final discussion. The thesis is concluded with Chapter 7, which briefly summarizes the results and exposes main findings.

1.1 Meteorology and air pollution

Near-surface concentrations of pollutants are highly affected by meteorological conditions in a variety of ways: horizontal transport, turbulent diffusion, depositions, formation of secondary species, heterogeneous chemistry, are all influenced by meteorological parameters. The common meteorological conditions favorable for high ozone concentrations include high sunlight intensity, low winds and high air temperatures, making episodes of high ozone concentrations generally a summer phenomenon. Stagnant air masses allow pollutants to accumulate, while high air temperatures and sunlight intensity promote photochemical transformations (Sillman and Samson, 1995). Such atmospheric conditions are usually related to stagnant high pressure synoptic systems, under which meso-scale circulations, like up- and down-slope winds, thermal heat island circulations, sea breezes, and valley channeled winds, become a major mechanism for dispersing, mixing and transporting air pollutants. These local (thermal) winds, when they enable recirculation of polluted air from previous days, together with clear sky and high temperature provide conditions for high ozone episodes in areas with significant emission sources (Millan et al., 1996; Tov et al., 1997; Liu and Hsiao, 2002; Rosenthal et al., 2003). Characteristic for episodes driven by meso-scale circulations is the gradually increased ozone daily maxima with each consecutive day of the episode.

Some examples of how the the local and larger scale meteorological conditions influence the transport and dispersion of atmospheric pollutants (Jacobson, 2002):

Ground temperatures:
Warm ground surfaces produce thick mixing depths and consequently low pollution mixing ratios.
Warm surfaces enhance convection, causing surface air to mix with air aloft and resulting in faster near-surface winds and greater dispersion.
Temperatures affect rates of several processes including rates of biogenic gas emissions from trees, chemical reactions and gas-to-particle conversion.

Soil moisture:
Increases in soil liquid water can cool the ground, reduce convection and mixing depths, and slow near-surface winds. The net effect is to enhance pollutant buildup.

Urban heat island:
Urban construction material surfaces increase surface temperature, resulting in increased mixing depths, faster near-surface winds and lower near-surface concentrations of pollutants.

Sea/valley breezes:
Sea breeze transfers primary pollutants emitted near the coast into inland.
The breeze forms the elevated pollution layers by lifting and injecting polluted air into the inversion layer during its return flow to the ocean.

Atmospheric stability:
Affects plume dimension and dispersion and concentrations of pollutants downwind.

Winds:
Fast winds tend to clear out chemically produced pollution faster than do the slow winds.
Wind direction determines where air pollutants are transported to/from.
Long range transport enhances the local-regional-hemispheric pollution buildup via transferring the pollutants/precursors from the source regions downwind.

Clouds:
Reduce the penetration of UV radiation, therefore decreasing rates of photolysis below them.
Pollutants dissolve in cloud water and are either rained out or returned to the air upon cloud evaporation. Rain-forming clouds help to cleanse the atmosphere.
Clouds enhance the aerosol formation via in-cloud chemistry.

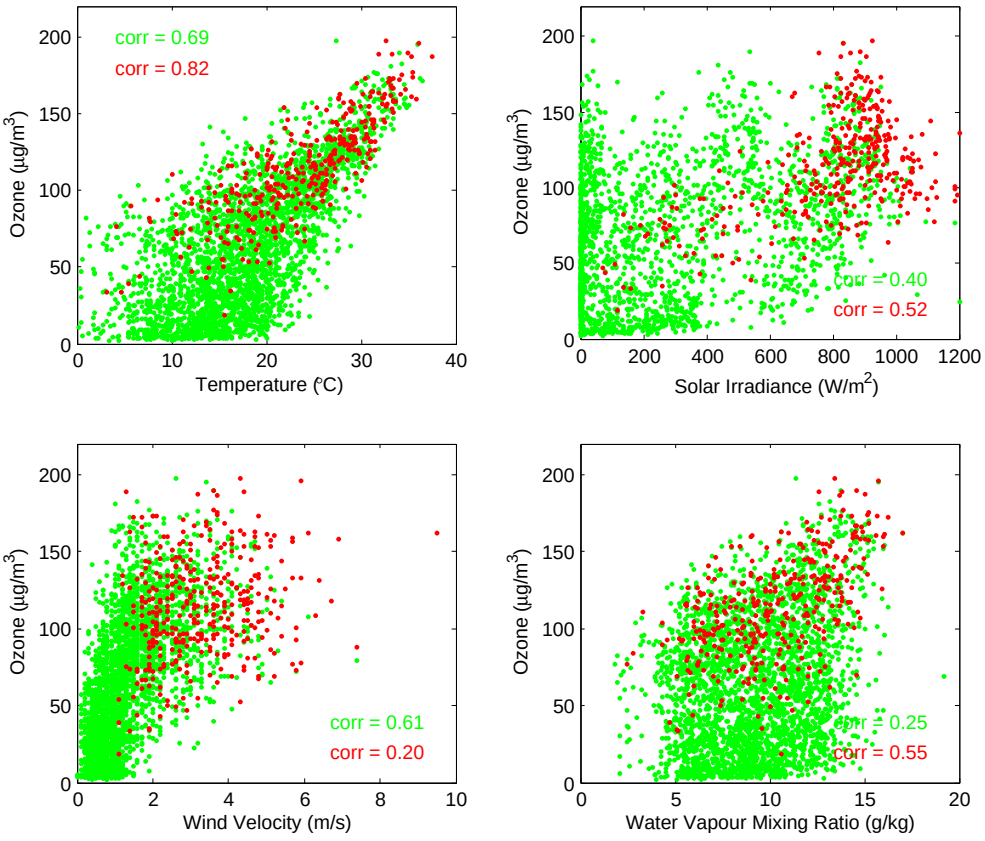

Figure 1.2: Scatter plots between the near ground ozone and temperature, solar irradiance, wind velocity or water vapor mixing ratio, measured at Ljubljana during the warm parts (April - September) of years 2003 and 2004. Green dots: point-by-point comparison of all hourly measured values. Red: the same but for daily maxima. The values of correlation coefficient are added to the plot.

In the case of ozone, in addition to these general effects, the influences of meteorological factors on photochemical reactions (presented in Section 1.2 below) must be taken into account. Figures 1.2 and 1.3 show scatter plots between measured ozone in Ljubljana and Nova

Gorica, and four basic meteorological variables. The significant correlation between ozone and temperature was expected, because hundreds of chemical reactions involved depend on the temperature. A large contributor to this behavior is the temperature dependant decomposition rate of peroxyacetylnitrate (PAN), which act as a reservoir species for NO_2 (Sillman and Samson, 1995). Scatter plots for solar irradiance show, that a certain degree of solar irradiance is required, while above this level ($\approx$ 700-800 W/m^2) other conditions determine the exact degree of ozone production. Positive correlation between all hourly values of wind velocity and ozone is because low nighttime ozone coincides with weak nighttime winds and vice versa for the daytime. In Nova Gorica days with the strongest daily winds experience lower daily ozone maxima, while for Ljubljana this is not necessary the case. The characteristics of the high ozone episodes, presented in the thesis, will explain the reasons why is it so. Water vapor mixing ratio in Ljubljana and Nova Gorica positively correlates with ozone, but the correlation coefficient is relatively weak. In general water vapor has competing effects on ozone levels (Sillman and Samson, 1995; Dawson et al., 2007). It participates in chemical transformations, and its final effect on ozone production depends on the NO_x/VOC mixture in a location.

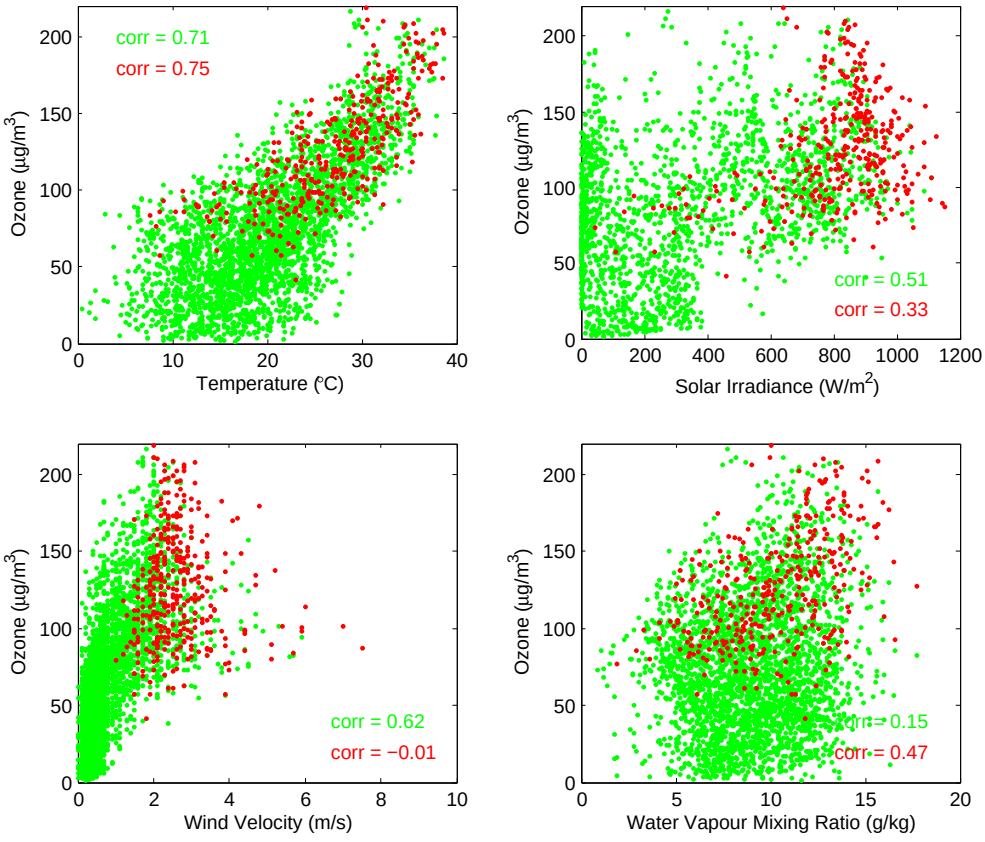

Figure 1.3: The same as Fig. 1.2 but for Nova Gorica.

1.1.1 Planetary boundary layer

Planetary boundary layer (PBL) is the lower layer of the atmosphere, which is directly influenced by the earth surface. In this layer as a consequence of anthropogenic and biogenic near-ground emissions, tropospheric ozone is formed. The efficiency of the ozone production depends directly on the meteorological conditions inside the PBL.

The influence of the earth surface on PBL include frictional drag, evapotranspiration, terrain induced flow modifications, heat and momentum transfer, and pollution emissions. It is the layer that dissipates the energy from the upper atmosphere. as a consequence of these earth surface influences PBL experiences a diurnal cycle of temperature, humidity, wind, and pollution variations. Its depth may range from 30 m in stable to 3 km and more in highly convective conditions.

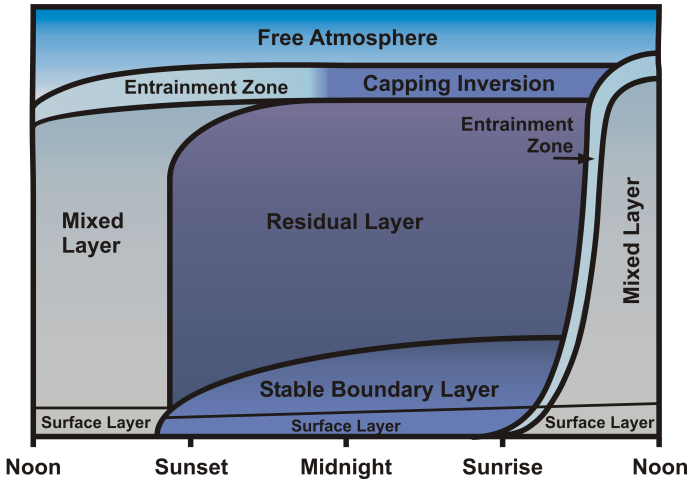

Figure 1.4: Evolution of planetary boundary layer during fair weather conditions. Adopted from Stull (2000).

In fair weather PBL develops in time as sketched in Figure 1.4. During daytime there is often a statically unstable **mixed layer**. At night, a statically **stable boundary layer** forms under a statically neutral **residual layer**. The residual layer contains pollutants and moisture from the previous mixed layer(s), but is not very turbulent.

The bottom 20 to 200 m of the PBL is **surface layer**, where frictional drag, heat conduction and evaporation from the surface cause substantial changes of wind speed, temperature and humidity with height.

Entrainment zone, with intermittent turbulence, separates the **free atmosphere** from the mixed layer. At night turbulence in the entrainment zone ceases, leaving a nonturbulent separation layer called the **capping inversion**, which is strongly statically stable.

Free atmosphere is that portion of the earth's atmosphere above the planetary boundary layer in which the effect of the earth's surface friction on the air motion is negligible and in which the air is usually treated (dynamically) as an ideal fluid.

1.1.1.1 Turbulence

Turbulence, the superposition of many small-scale swirls of motion (eddies), is one of the causes of the unique nature of the PBL. Near surface even a fairly weak wind causes a large

velocity shear, which leads to a development of turbulent eddies. Such shear- induced eddies, together with convective eddies caused by surface heating, are very effective in transferring momentum to the surface and transferring latent and sensible heat away from the surface.

In the turbulent field variables (wind components u, v and w, potential temperature θ, pressure p, humidity q etc.) can be written as a sum of the slow varying mean variables ($\overline{u}$, $\overline{v}$, $\overline{w}$, $\overline{\theta}$, $\overline{q}$...) and the rapidly varying turbulent components (u', v', w', T', q'). In the governing equations for the atmosphere (i.e., the first law of thermodynamics, ideal gas law, equations of motion, water conservation, and the continuity equation) after applying the separation of dependant variables into mean and fluctuating part, then averaging the equations and subtracting the equation for mean variables, additional terms appear. For example, in the equations of motion (Holton, 1992):

$$\frac{\overline{D}\overline{u}}{dt} = -\frac{1}{\rho_0}\frac{\partial \overline{p}}{\partial x} + f\overline{v} - \left[\frac{\partial \overline{u'u'}}{\partial x} + \frac{\partial \overline{u'v'}}{\partial y} + \frac{\partial \overline{u'w'}}{\partial z}\right] + \overline{F}_{rx}, \tag{1.1}$$

$$\frac{\overline{D}\overline{v}}{dt} = -\frac{1}{\rho_0}\frac{\partial \overline{p}}{\partial y} - f\overline{u} - \left[\frac{\partial \overline{u'v'}}{\partial x} + \frac{\partial \overline{v'v'}}{\partial y} + \frac{\partial \overline{v'w'}}{\partial z}\right] + \overline{F}_{ry}, \tag{1.2}$$

$$\frac{\overline{D}\overline{w}}{dt} = -\frac{1}{\rho_0}\frac{\partial \overline{p}}{\partial z} + g\frac{\overline{\theta}}{\theta_0} - \left[\frac{\partial \overline{u'w'}}{\partial x} + \frac{\partial \overline{v'w'}}{\partial y} + \frac{\partial \overline{w'w'}}{\partial z}\right] + \overline{F}_{rz}, \tag{1.3}$$

where g is acceleration of gravity, f Coriolis parameter, and F_{rx}, F_{ry} and F_{rz} the components of internal frictional (viscous) force $\mathbf{F_r}$. Terms in square brackets represent additional turbulent fluxes. For example, $\overline{w'u'}$ is a vertical turbulent flux of zonal momentum. Similarly, $\overline{w'\theta'}$ in thermodynamic equation would be a vertical turbulent heat flux.

Above the PBL the turbulent fluxes are weak and terms in square brackets can be neglected, while inside PBL the magnitudes of the turbulent flux terms are of the same order as are the other terms.

The sum of diagonal terms in square brackets in Equations (1.1)-(1.3) gives an overall measure of the intensity of turbulence, called the turbulence kinetic energy (TKE):

$$TKE = \frac{1}{2}\left[\overline{u'u'} + \overline{v'v'} + \overline{w'w'}\right]. \tag{1.4}$$

The prognostic equation for TKE/$m = e$, derived from equation of motion, is:

$$\frac{\partial \overline{e}}{\partial t} = -\overline{u_i}\frac{\partial \overline{e}}{\partial x_i} + \delta_{i3}\frac{\overline{u_i'\theta'}}{\theta_0}g - \overline{u_i'u_j'}\frac{\partial \overline{u_i}}{\partial x_i} - \frac{\partial \overline{u_i'e}}{\partial x_i} - \frac{1}{\rho_0}\frac{\partial \overline{u_i'p'}}{\partial x_i} - \epsilon, \tag{1.5}$$

where terms on the right represent, respectively: advection of TKE (1), buoyant production/consumption (2), mechanical or shear production/loss term (3), turbulent transport (4), pressure correlation term (5) and viscous dissipation of TKE (6).

1.1.1.2 Turbulence closure

Due to turbulence the set of atmospheric equations inside the PBL is mathematically not closed. It has more unknown variables than equations. To work around this problem in mesoscale meteorological models the net effect of all eddies is parameterized (approximated). Such an approximation is called turbulence closure, because it mathematically closes the governing equations.

There are many types of closures. Most common are local closures, which neglect the large eddies and assume that turbulent eddies act in a manner analogous to molecular diffusion.

Such turbulence closure is for for example a traditional K-theory (Pasquill and Smith, 1983), where turbulent terms are approximated like:

$$\overline{u'w'} = -K_m \left(\frac{\partial \overline{u}}{\partial z} \right), \quad \overline{v'w'} = -K_m \left(\frac{\partial \overline{v}}{\partial z} \right), \quad \overline{\theta'w'} = -K_h \left(\frac{\partial \overline{\theta}}{\partial z} \right). \tag{1.6}$$

K_m and K_h are the eddy viscosity and eddy diffusivity coefficients with units $\mathrm{m^2 s^{-1}}$, which are further estimated.

In Chapter 3 two WRF-Chem turbulence parameterizations are briefly presented. Analysis of simulations in Chapter 5 will show that the type of model PBL turbulence parametrization can have significant influence on model results.

1.2 Chemical Processes Governing the Ozone Formation in the PBL

The present section presents a basic description of the chemical mechanisms leading to the generation of a variety of secondary photochemical pollutants. The emphasis is on the gas-phase photochemical transformations of nitrogen oxides and volatile organic compounds, and their role in the formation of ozone (O_3) in the planetary boundary layer.

The gas-phase chemistry of the troposphere involves the oxidation of organic molecules in the presence of oxides of nitrogen under the action of sunlight. Atmospheric oxidation proceeds via chains of free radical reactions. For organic molecules these chains can be long and complex. To drive these reactions, external source of energy (solar radiation) is required.

A variety of oxidized products, commonly referred to as secondary photochemical pollutants, are formed in the planetary boundary layer (PBL), but ozone can be considered as the principal product of tropospheric chemistry. The only ozone-forming reaction that occurs in the atmosphere is that between atomic (O) and molecular oxygen (O_2). In the stratosphere the source od atomic oxygen is dissociation of O_2. Solar ultraviolet radiation of wavelengths (λ) less than 242 nm slowly dissociates molecular oxygen. Since only sunlight of wavelengths exceeding 290 nm reaches the troposphere, the source of atomic oxygen in troposphere cannot be O_2 dissociation, which requires radiation of wavelengths shorter than this. In the troposphere that source is provided by nitrogen dioxide (NO_2). Many other secondary pollutants (e.g. peroxy acetyl nitrate, PAN) that are formed on local or regional scales in the PBL may also have adverse impact on health and/or play wider roles in global atmospheric chemistry.

Further information on tropospheric chemistry can be found in sources like Finlayson-Pitts and Pitts (1999), Jenkin and Clemitshaw (2000), Seinfeld and Pandis (1998), Hobbs (1998) and many others. At writing this chapter, we rely mainly on Finlayson-Pitts and Pitts (1999) and Jenkin and Clemitshaw (2000). These two sources are the reference through the whole Chapter 1.2. If other sources are are used, they are referenced accordingly.

1.2.1 Basic photochemical transformations of oxidized nitrogen species

Nitrogen oxides are released into the troposphere from a variety of biogenic and anthropogenic sources. The largest single source is the combustion of fossil fuels, leading to nitrogen oxides emissions mainly in the form of NO. A small fraction (less then 10 %) may be released as NO_2 (PORG, 1997), or is produced close to the point of emission from reaction of NO with O_2:

$$2\mathrm{NO} + \mathrm{O_2} \rightarrow 2\mathrm{NO_2}. \tag{1.7}$$

The rate of this reaction is strongly dependent on the NO concentration. At high NO levels, close to the emission source, the rate of conversion is rapid (e.g. 0.5 % s^{-1} at 1 ppmv NO). The significance of reaction (1.7) decreases dramatically as NO is diluted. Under most tropospheric conditions reaction (1.7) is insignificant and the dominant pathway, by which NO is converted to NO_2, is via the reaction with O_3:

$$NO + O_3 \rightarrow NO_2 + O_2. \tag{1.8}$$

The timescale at typical boundary layer concentrations for this reaction is ca. 1 min. During daylight hours NO_2 is concerted back to NO as a result of photolysis, which also leads to the regeneration of O_3:

$$NO_2 + h\nu(\lambda < 420 \text{ nm}) \rightarrow NO + O(^3P), \tag{1.9}$$

$$O(^3P) + O_2 + M \rightarrow O_3 + M. \tag{1.10}$$

M represents a catalyst; N_2 or O_2 or another third molecule that absorbs the excess vibrational energy and thereby stabilizes the O_3 molecule formed. There are no significant sources of ozone in the atmosphere other than reaction (1.10). In the absence of competing interconversion reactions last three reactions (1.8) - (1.10) constitute a steady-state cycle in which the concentrations of NO and NO_2 are related to the O_3 concentration by the following expression (Leighton, 1961):

$$[O_3] = \frac{j_{1.9}[NO_2]}{k_{1.8}[NO]}. \tag{1.11}$$

$j_{1.9}$ (s^{-1}) is the rate of NO_2 photolysis (reaction 1.9) and $k_{1.8}$ (conc.$^{-1}s^{-1}$) is the rate coefficient for the reaction of NO with O_3 (reaction 1.8). The expression (1.11) has been named *photostationary state relation*. It suggests that the steady-state O_3 concentration is proportional to the $[NO_2]/[NO]$ ratio and the maximum steady-state O_3 concentration would be achieved with initial charge of pure NO_2. As a result of rapid interconversion, the behaviour of NO and NO_2 is highly coupled and they are usually collectively referred to as NO_x.

1.2.1.1 The role of free radicals

In real troposphere the O_3 mixing ratios are much greater than O_3 concentrations reached, if governed solely by reactions (1.8) - (1.10). In order to explain high observed atmospheric ozone levels it is necessary that reactions other than (1.8) - (1.10) must be invoked. These other reactions involve interconversions of NO_x species in the presence of free radicals. Free radicals in chemistry are atoms, molecules or ions with usually highly reactive unpaired electrons.

Free radicals are mainly produced in the troposphere as intermediates in the photochemical oxidation of carbon monoxide (CO) and volatile organic compounds (VOC), as described in the Section 1.2.2. For example, the hydroperoxy radical (HO_2) and organic peroxy radicals (RO_2) both perturb the photostationary state by providing additional NO to NO_2 routes to supplement reaction (1.8):

$$HO_2 + NO \rightarrow OH + NO_2, \tag{1.12}$$

$$RO_2 + NO \rightarrow RO + NO_2. \tag{1.13}$$

Since these conversions of NO to NO_2 do not consume O_3, the subsequent reactions (1.9) and (1.10) represent a net source of O_3. The net production rate of O_3 resulting from this fast photochemistry followed by reactions (1.9) and (1.10) is given by:

$$\frac{d[O_3]}{dt} = (k_{1.12}[HO_2] + \Sigma k_{1.13}[RO_2])[NO]. \tag{1.14}$$

Free radicals concentration is a strong function of location, time of day, cloud cover... The ozone production rate is thus very variable. Nevertheless, O_3 production rates for rural site in summertime may be of the order of 5 - 10 ppbv h^{-1} (Jenkin and Clemitshaw, 2000). Observed deviations of O_3 concentrations from equation (1.11) are usually interpreted in terms of the presence of significant amount of the peroxy radicals.

1.2.1.2 Tropospheric sinks of ozone

An important sink of tropospheric ozone is the reaction with HO_2:

$$HO_2 + O_3 \rightarrow OH + 2O_2. \tag{1.15}$$

Apparently, HO_2 can act as O_3 source (reaction 1.12) or sink (reaction 1.15), where the net role of HO_2 is dictated by the local concentration of NO_x. Since other reactions involving the same species occur at the same time and the competition among species for some reactions exists, the calculation of crossover concentration for NO_x between O_3 production and destruction is rather complicated. But its approximate value is usually considered to be about 30 ppt (Seinfeld and Pandis, 1998).

The principal photochemical sink of O_3 in troposphere is through $O(^1D)$:

$$\begin{aligned} O_3 + h\nu &\rightarrow O + O_2, & (1.16)\\ &\rightarrow O(^1D) + O_2. & (1.17) \end{aligned}$$

Ozone photolysis produces both ground-state O (reaction 1.16) and excited singlet $O(^1D)$ (reaction 1.17). The ground-state O atom combines rapidly with O_2 to reform O_3, so reaction (1.16) has no net chemical effect. When $O(^1D)$ is produced, it must catalytically react with another atmospheric species. Most often $O(^1D)$ collides with N_2 or O_2, removing the excess of energy:

$$O(^1D) + M \rightarrow O + M. \tag{1.18}$$

Since the oxygen then reacts with O_2 into O_3, this path is just another null cycle. Occasionally, however, $O(^1D)$ collides with H_2O and produces two hydroxy radicals:

$$O(^1D) + H_2O \rightarrow 2OH. \tag{1.19}$$

This net sink of O_3 depends on the concentration of water vapor. The removal path is most effective in low latitudes at low altitudes, with intense radiation and high humidity, where as much as 10 % of the $O(^1D)$ produced reacts with H_2O to to generate OH.
Total local loss rate of O_3 from reactions (1.15) and (1.19) is then:

$$\frac{d[O_3]}{dt} = k_{1.19}[O(^1D)][H_2O] + k_{1.15}[HO_2][O_3]. \tag{1.20}$$

The local lifetime of O_3 can be estimated on the basis of its local rate of either production or loss, as long as the local O_3 concentration is more or less in balance as a result of photochemical loss and production mechanisms. O_3 lifetimes in the troposphere vary significantly depending on altitude, latitude and season. They are shorter in the summer because of higher solar fluxes and near surface because of higher water vapor concentrations. Increasing NO_x weakens the net photochemical sink of O_3 in the background troposphere, leading to an overall increase of O_3.

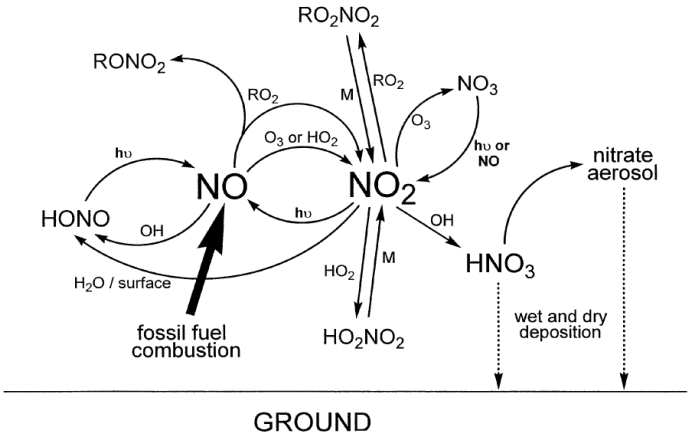

Figure 1.5: Daytime interconversions of oxidized nitrogen compounds in the troposphere. (Jenkin and Clemitshaw, 2000)

Other chemical transformations of NO_x lead to the generation of a variety of inorganic and organic oxidized nitrogen compounds, among others higher oxides (NO_3 and N_2O_5), oxyacids (HNO_3, HO_2NO_2 and HONO), organic peroxy nitrates (RO_2NO_2), organic nitrates ($RONO_2$) and aerosol nitrate. The majority of these species are generated during daylight, while formation of higher oxides (NO_3 and N_2O_5) is greatest for nighttime tropospheric chemistry.

1.2.2 The role of VOCs in photochemical ozone formation

An enormous variety of VOCs may be emitted from anthropogenic and biogenic sources and either or both categories can make a major contribution to photochemical O_3 formation. The process is initiated by sunlight dissociating certain stable molecules, leading to the formation of hydrogen-containing free radicals (HO_x). In the presence of NO_x these free radicals catalyse the oxidation of VOCs, ultimately to CO_2 and H_2O. Partially oxidized organic species such as aldehydes, ketones and CO are produced as intermediate oxidation products, with O_3 formed as a by-product.

An example of such chemistry is shown in Fig. 1.6, where VOCs are denoted as RH. The oxidation of organic compound (RH) is here initiated by reaction with the hydroxyl radical (OH), leading to the following rapid sequence of reactions:

$$\mathrm{OH + RH \rightarrow R + H_2O}, \tag{1.21}$$

$$\mathrm{R + O_2 + M \rightarrow RO_2 + M}, \tag{1.22}$$

$$\mathrm{RO_2 + NO \rightarrow RO + NO_2}, \tag{1.13}$$

$$\mathrm{RO + O_2 \rightarrow R_{-H}O + HO_2}, \tag{1.23}$$

$$\mathrm{HO_2 + NO \rightarrow OH + NO_2}. \tag{1.12}$$

$$\mathrm{2(NO_2 + h\nu \rightarrow NO + O)}, \tag{1.24}$$

$$\mathrm{2(O_2 + O + M \rightarrow O_3 + M)} \tag{1.25}$$

$$\text{Net: RH + 4 } O_2 \text{ + 2 h}\nu \rightarrow \mathrm{R_{-H}O} + 2\ O_3 + H_2O$$

In the cycle OH is regenerated. Reactions (1.12) and (1.13), involving the RO_2, play a key role in O_3 formation by oxidizing NO to NO_2. As explained in Section 1.2.1.1, NO_2 is efficiently photodissociated to generate O_3 by reactions (1.9) and (1.10). The oxidation of one molecule of RH to $R_{-H}O$ (catalysed by HO_x and NO_x) is accompanied by the generation of two molecules of O_3. As seen in reactions (1.17)- (1.19) and discussed in the following section, O_3 photolysis is a major source of HO_x radicals. Via the chemistry described above, O_3 stimulates its own production.

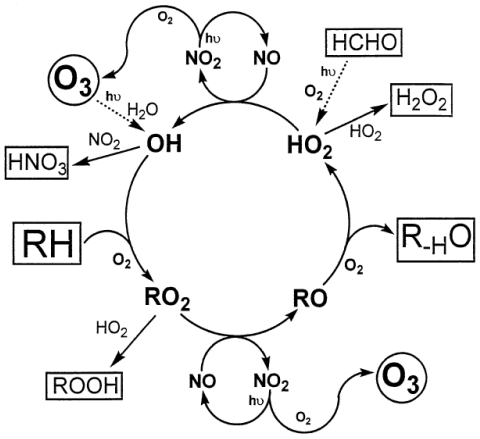

Figure 1.6: Schematic representation of the free radical-catalyzed oxidation of a hydrocarbon RH to its first generation oxidized product $R_{-H}O$. Illustrated is the key role of the NO_x species, which leads to the generation of O_3 as a by-product. The major sources and sinks of the free radicals are also shown. (Jenkin and Clemitshaw, 2000)

The further oxidation of the first generation product $R_{-H}O$ also follows the same general pattern (i.e. generating O_3), and subsequent organic products are oxidized until CO_2 is eventually produced. The rate of oxidation of VOCs and therefore production of O_3 is governed by the ambient concentration of the catalytic HO_x radicals.

1.2.2.1 Sources, sinks and reservoirs of HO_x

HO_x radicals are generated by photolysis of certain atmospheric trace species. A strict definition of HO_x radicals would include only OH and HO_2, but in the present discussion organic radicals (RO_2) are also classified as HO_x.

The potential radical precursors in the lower troposphere are species which absorb light at wavelengths longer than ca. 290 nm, which penetrates to the lower atmosphere. In global terms, the most important tropospheric source of free radicals results from the photolysis of O_3 (reactions 1.16 - 1.19). Another important contribution of free radical production is photolysis of aldehydes RCHO, specially the photolysis of HCHO:

$$\mathrm{HCHO} + h\nu \rightarrow \mathrm{H} + \mathrm{HCO}, \tag{1.26}$$

$$\mathrm{H} + \mathrm{O_2} + \mathrm{M} \rightarrow \mathrm{HO_2} + \mathrm{M}, \tag{1.27}$$

$$\mathrm{HCO} + \mathrm{O_2} \rightarrow \mathrm{HO_2} + \mathrm{CO}. \tag{1.28}$$

Photolysis of HCHO (reaction 1.26) dominates radical production under urban conditions, when the concentrations of O_3 are suppressed due to reaction with NO (reaction 1.8) and

the concentration of HCHO is elevated due to high local emissions or production rates from hydrocarbon oxidation. Clearly, the photolysis of HCHO and also other RCHO play an important role in the initialization of the summertime pollution at urban locations, when initial O_3 concentrations may be significantly suppressed.

Another source of free radicals is photolysis of HONO:

$$\mathrm{HONO} + h\nu \rightarrow \mathrm{OH} + \mathrm{NO}, \tag{1.29}$$

which potentially provides a pulse for free radical production in the early morning, when photolysis rate of O_3 and aldehydes is very slow due to the long atmospheric pathlength. Significant source of HO_x radicals throughout the day is also oxidation of alkenes by reaction with O_3, but more detailed discussion is beyond the scope of this basic introduction.

HO_x radicals are removed from the atmosphere by a variety of termination reactions. The products of these reactions are usually reservoirs, since the possibility of HO_x regeneration through thermal decomposition or photolysis exists. However, specially for reservoirs with longer lifetimes it is likely, that the removal processes (physical and chemical ones) become competitive or even dominant. The formation of reservoirs thus present a sink for HO_x radicals. The most significant tropospheric sinks for HO_x radicals involve either reactions between two HO_x species:

$$\mathrm{HO_2} + \mathrm{HO_2} \rightarrow \mathrm{H_2O_2} + \mathrm{O_2}, \tag{1.30}$$

$$\mathrm{RO_2} + \mathrm{HO_2} \rightarrow \mathrm{ROOH} + \mathrm{O_2}, \tag{1.31}$$

$$\mathrm{OH} + \mathrm{HO_2} \rightarrow \mathrm{H_2O} + \mathrm{O_2}, \tag{1.32}$$

or reactions of HO_x with NO_x species:

$$\mathrm{OH} + \mathrm{NO_2} + \mathrm{M} \rightarrow \mathrm{HNO_3} + \mathrm{M}, \tag{1.33}$$

$$\mathrm{RO_2} + \mathrm{NO} + \mathrm{M} \rightarrow \mathrm{RONO_2} + \mathrm{M}. \tag{1.34}$$

Reactions (1.33) and (1.13) involving NO_x are much more important over the polluted areas. Actually, the reaction(1.33) totally dominates radical removal at urban levels of NO_2 and presents the main contribution also under rural conditions.

1.2.3 Sensitivity of O_3 to NO_x and VOC concentration

The dependence of O_3 production on the initial amounts of VOC and NO_x is frequently represented as an O_3 diagram of the form shown in Figure 1.7. Such diagrams are a contour plots of maximum O_3 concentrations achieved as a function of initial VOC and NO_x concentrations. They are obtained from a large number of simulations with varying initial VOC and NO_x concentrations, while all other variables (solar radiation, temperature...) are constant.

It is evident from Figure 1.7 that for having high O_3 concentrations both VOC and NO_x must be sufficiently high. Very low NO_x in the presence of high VOC (or vice versa) do not lead to high O_3 concentrations.

Moreover, the influence of changing the concentration of NO_x or VOC on the O_3 production depends on the relative concentrations of NO_x and VOCs. When the relative concentration $[NO_x]/[VOC]$ is high, the condition is referred to as VOC sensitive (or VOC limited in Fig. 1.7). As indicated in the previous subsection, the dominant chain terminating reaction under these

circumstances is (1.33), while reaction (1.21) leads to O_3 formation. Thus under these conditions decrease of VOCs would decrease the final O_3 concentration. In contrast, a decrease of NO_x would increase the rate of O_3 formation.

At high [VOC]/[NO_x] ratios, or NO_x sensitive (NO_x limited in Fig. 1.7) conditions, the dominant chain terminating reactions are (1.30) and 1.31. This circumstance is more readily achieved at higher radical concentration, so that the [VOC]/[NO_x] ratio required for NO_x sensitive conditions to prevail is also influenced by intensity of solar radiation. Under NO_x sensitive conditions O_3 formation correlates positively with [NO_x] and is in almost insensitive to the changes in VOC concentrations. However, the variation of the concentration of some VOCs has an effect on O_3 formation under NO_x sensitive conditions, because the degradation of some VOCs can lead to the significant removal of NO_x as organic nitrates and peroxy nitrates.

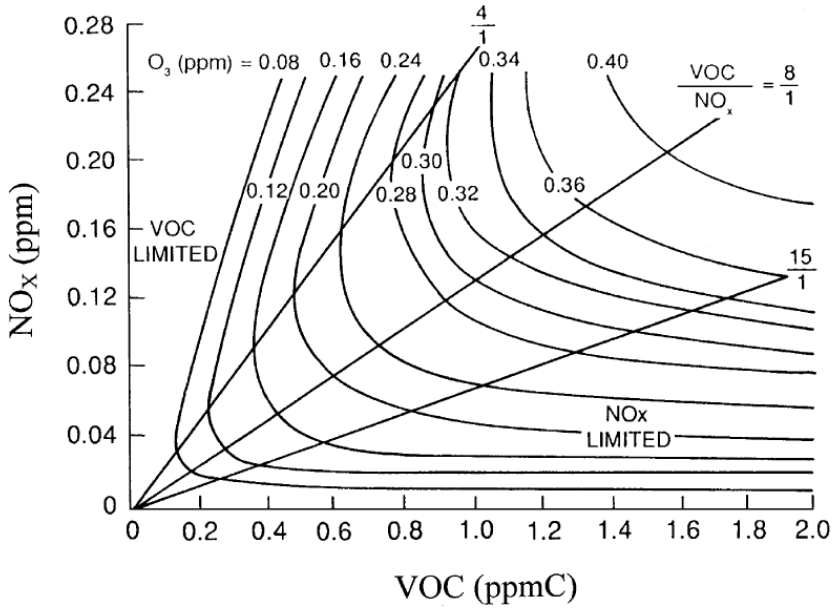

Figure 1.7: Isopleth diagram illustrating peak O_3 concentrations generated from various initial concentrations of NO_x and a specified VOC mixture using the US EPA empirical kinetic modeling approach. Reagent concentrations are significantly greater than typically observed in the PBL, but the characteristic shape of the O_3 isopleths as a function of VOC/NO_x ratio applies also to lower reagent concentrations. (Dodge, 1977)

Reduction of O_3 is best achieved by a reduction of NO_x concentration under NO_x sensitive conditions and by a decrease in the VOC concentration under VOC sensitive conditions. The conditions encountered in the boundary layer over Europe is usually varying between the two extremes for a given mass trajectory (Jenkin and Clemitshaw, 2000).

Chapter 2

Trajectory Analysis of Ozone Pollution in Slovenia

This chapter summarizes the main results of a trajectory-based analysis, in which the influence of the air masses origin on the summertime near-ground ozone in Slovenia is studied. The content of this chapter contributes to the understanding of the ozone pollution in Slovenia,presents the starting point for further research, and gives the coupled meteorological-photochemistry modeling a deeper meaning. In addition, the inclusion of trajectory study enables the comparison of the results of two different independent approaches (statistical approach and photochemical modeling for selected episodes) and different models used. A more detailed presentation of the trajectory analysis can be found in Žabkar et al. (2008).

As already explained in Introduction, the highest ozone levels usually occur in the southwestern part of Slovenia close to the Adriatic Sea, while occasionally very high ozone levels are measured also at other stations in the interior of the country. The number of days with exceeded ozone threshold values during the warm part of the year varies from a few days for the capital city of Ljubljana, to up to 25 days with daily maxima over 180 μg/m^3 (warning hourly threshold value) for the Mediterranean stations. Measurements show that ozone concentrations close to the ground are high and the threshold values (primarily the 8 hour target value) are exceeded also in the sparsely inhabited rural areas all over Slovenia. This implies that transport of polluted air masses has an important influence on the photochemical pollution.

In some previous studies (Seibert et al., 1997; Wotawa et al., 2000; Kaiser et al., 2007) Po Basin was identified as an important source region of the Alpine ozone precursors. The conclusions of these studies lead to the following question: Do the Po Basin emissions have significant impact on ozone concentrations across all Slovenia, or only in the southwestern part with the highest measured occurrence of the exceeding ozone concentrations? For urbanized areas, like the capital city of Ljubljana, the assumption is that high ozone concentrations occur mainly due to local emissions of primary pollutants. With no significant local emission sources close to a rural measuring station in Iskrba, the transport of polluted air masses might play a dominant role, but the contributions of relatively nearby urban plumes and the long-range transport of ozone rich air to this site remain to be investigated.

Four observation sites were selected in order to assess ozone pollution over Slovenia. Three-dimensional backward trajectories were calculated for the warm parts (April - September) of the years 2003 and 2004, based on meteorological fields with relatively high spatial and temporal resolution of 9.5 km and 1 hour, respectively. The resolution was considerably

higher than in previous related studies (Seibert et al., 1997; Kaiser et al., 2007; Cristofanelli et al., 2007; Ricco et al., 2007; Galvez, 2007). For example Seibert et al. (1997) used three different types of back trajectories, the highest resolution trajectories were calculated on the basis of ECMWF fields with a horizontal resolution 0.5° and temporal resolution 3 hours. The high resolution of the trajectories in our research is vital because of a very complex topography in this part of Europe and because we are investigating the origin of the polluted air masses for low altitude measuring sites. Both the regional transport from remote emission areas as well as relatively nearby urban plumes (up to 50 km distant) can influence the measured ozone concentrations at these stations.

Trajectory analysis consisted of two parts. In the first part we classified the trajectories into groups of similar trajectories, using the k-means trajectory clustering procedure. We analyzed inter-cluster variations of measured ozone concentrations and basic meteorological variables at the receptor sites. In the second part, concentration-weighted trajectories (CWT Seibert et al., 1994) in combination with number density (ND) of "polluted trajectories" (i.e. trajectories with high measured ozone at receptor points) were applied to identify the locations of potential pollution sources. The CWT method distributes the ozone concentration along the trajectories evenly and is able to distinguish major sources from moderate ones by calculating concentration gradients. ND results represent potential source directions rather than locations. In addition, the trailing effect, where areas upwind and/or downwind of receptor point are likely to be identified as sources as well, must be taken into account. Thus, combining the two methods yields better information about the source areas.

2.1 Methodology

2.1.1 Selected locations and their ozone characteristics

Measurement stations at Nova Gorica (suburban), Ljubljana (urban), Mt. Krvavec (elevated) and Iskrba (rural) were selected for a detailed analysis (Fig. 2.1). The stations are not under the influence of direct emission sources and are considered to be representative for ozone concentrations in their surroundings.

Nova Gorica (NG) at the border with Italy is the westernmost station with a Mediterranean climate. Hot summers with a low number of precipitation days promote photochemical ozone production. The exceeded ozone concentrations were in years 2003 - 2005 the most frequent of all the sites: altogether 162 hours with ozone concentration above 180 μg/m^3 were measured. There are some moderate local emission sources in the vicinity, mainly from traffic. Major potential sources are located within a radius of about 40 km (i.e. Udine, Monfalcone, Trieste).

Ljubljana (LJ), the capital of Slovenia, represents the urban ozone case. The population of Ljubljana is about 300.000 and the city is located in a basin (over 20 km W-E by some 40 km N-S). There were altogether 33 hours with ozone concentration exceeding 180 μg/m^3 in the years 2003 - 2005. The direct impact of nearby emissions on the measured ozone is relatively weak except during the rush hour. The measured ozone concentrations are supposed to be representative for the Ljubljana region.

Mt. Krvavec (KV) is located on the foothills of the eastern Alps within the Alpine climate zone. The site is situated about 30 km north of Ljubljana and lies on a ridge surrounded by peaks between 1500 and 2500 meters above sea level. Threshold values are occasionally exceeded: 23 hours with ozone above 180 μg/m^3 in the years 2003 - 2005. High average ozone concentrations are due to the absence of nighttime ozone removal, which is more important at the lower altitude stations (Fig. 2), and is typical for a site located above the stable nocturnal

boundary layer (Scheel et al., 1997). At least occasionally intrusions of upper-tropospheric and stratospheric ozone can affect ozone levels at this elevated site, as well. KV has already been studied by Kaiser et al. (2007), but we decided to include it in our study with higher spatial and temporal resolution of meteorological fields and different methods used for trajectory analysis.

Iskrba (IS) is located on a plateau, in a grassy glade, surrounded by forest with predominantly coniferous trees covering the hills and mountains at an altitude of approximately 800 - 1200 meters. The rest is grassland (not grazed by domestic animals) and partly also farmed (grass, pasture). Occasional high-level ozone concentrations measured at this rural background station (16 hours above 180 μg/m^3 in 2003 - 2005) suggest advection of polluted air. Major potential source emission areas are at least 40 km away, such as Rijeka (Croatia, 40 km to the southwest) or Ljubljana (50 km to the northwest), while the highly industrialized Italian cities in the west are rather distant.

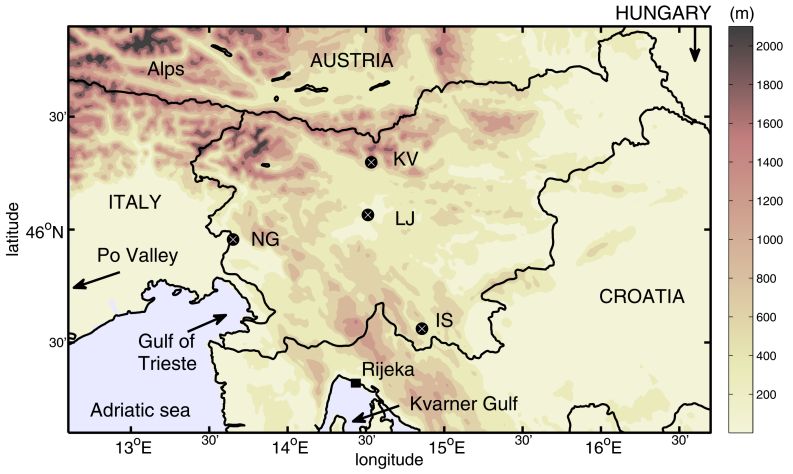

Figure 2.1: Orography of Slovenia at 1 km resolution and locations of selected ozone measuring sites.

The first insight into the ozone concentration statistics is provided by average daily and seasonal ozone concentrations for the four stations (Fig. 2.2). For stations at lower altitudes (LJ, NG, IS) the diurnal ozone cycles are very pronounced. Daily maxima in the warm part of the year (April - September) are on average the highest at NG, which is probably a consequence of both polluted air and very favorable weather conditions for ozone formation. Surprisingly, the average daily maxima during these months are slightly lower at LJ (urban) than at IS (rural). To some extent this could be explained by local emissions in Ljubljana resulting in somewhat lower measured ozone values. Nevertheless, the measured ozone concentrations in IS are unusually high and require further explanation. Nighttime ozone minima for the three stations can be explained by the nocturnal destruction by NO_x scavenging and dry deposition. A comparison of average nighttime ozone values shows the highest ozone reduction for IS and the lowest for NG, with the LJ curve being similar to NG. The effective nighttime ozone destruction at IS can be explained by the formation of stable nighttime boundary layer above the glade, where the measurement site is located. Dry deposition and local biogenic NO soil emissions, produced by microorganisms and bacteria in the nearby conifer forests (Pilegaard et al., 2006), in coincidence with the suppressed vertical mixing deplete the ozone in the near

the ground layer. The amount of local biogenic NO emissions are small but sufficient, because of inefficient ozone replenishment from the boundary layer due to the reduced vertical mixing. Effective dry deposition of ozone as well as other pollutants is a consequence of the higher surface roughness and the surface area of the forest. The nighttime air mixing over town (LJ and NG) is not entirely suppressed and the nocturnal emissions are due to rare traffic, resulting in higher nighttime ozone concentrations at these stations. In addition, typical local diurnal circulations develop during the calm weather conditions associated with highest daily ozone maxima. Consequently, ozone formed during the day, and transported outside the urban areas toward surrounding hills by daytime winds, slowly drains back during the night, resulting in slightly higher nocturnal ozone concentrations. Distinct minima in the morning are caused by the morning rush hour (note that 5:00 UTC = 7:00 CEST).

During the night and sometimes even during the day the KV site lies above the boundary layer formed in the Ljubljana basin. If this is the case the KV site is disconnected from the emission sources situated in the basin (beside Ljubljana city also smaller towns, villages and main traffic lines) and experiences ozone levels typical of the lower free troposphere. For this reason there is an absence of the nighttime ozone removal (Fig. 2.2) in the diurnal ozone cycle for KV site. A slight ozone minimum at about 10:00 UTC corresponds to the time when the fresh locally polluted air from Ljubljana basin due to daytime increase of the boundary layer above the basin reaches the station and causes the ozone decrease. The diurnal ozone cycle at KV is typical for a higher mountain stations and is similar to the lower free troposphere variations (e.g. Balzhanov, 1994; Scheel et al., 1997).

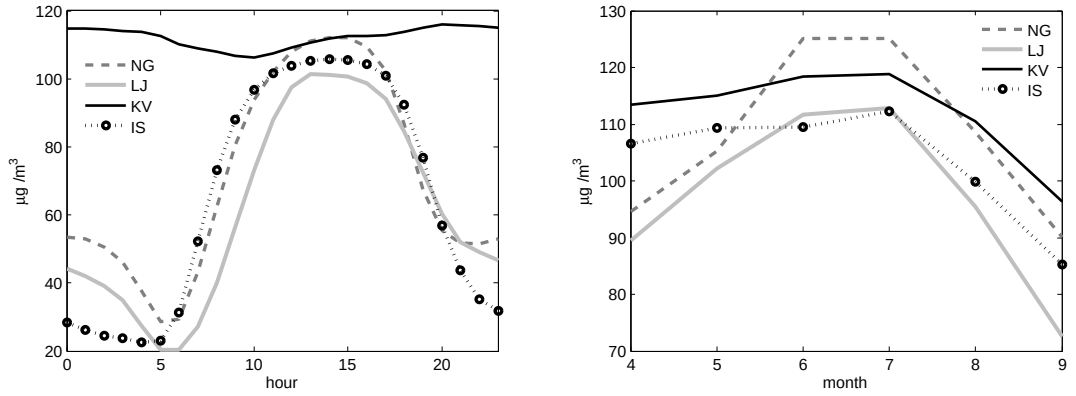

Figure 2.2: Left: Average daily variations of ozone concentration at Nova Gorica (NG), Ljubljana (LJ), Krvavec (KV) and Iskrba (IS) for the months June and July from 2003 to 2006. Hours represent UTC. Right: Average monthly values for the warm period of the years 2003 to 2006. For NG, LJ and IS average monthly values were calculated based on the daytime ozone (hourly values from 11 to 17 UTC were considered), while for KV hourly concentrations throughout the day were taken into account.

For the comparison of monthly variations (right panel in Fig. 2.2) only hourly values from 11:00 to 17:00 UTC were taken into account to eliminate an impact of the nighttime ozone removal for the three low level stations. For KV all hourly values were considered. Both regional stations (KV and IS) are characterized by relatively high ozone levels in the spring, almost comparable to the summertime maxima. High ozone concentrations in spring may be due to the winter accumulation of precursors in air masses, causing high ozone concentrations with the onset of favorable springtime weather conditions. Other possible explanations may

be the influence of stratosphere-troposphere exchange (i.e. stratospheric intrusions), specially in the case the elevated KV site, or another process synoptic-scale pollutant transport. Since many remote locations in the Northern Hemisphere experience a spring ozone peak, the possible causes of high spring ozone levels ate these sites have already been extensively studied. The conclusions of different studies were reviewed by Monks (2000), who concluded there was still no consensus on the formation mechanisms. The two stations (LJ, NG) exhibit distinct summer maxima, associated with the photochemical production of ozone from VOCs and NO_x under the influence of intensive solar irradiance at polluted sites (Lefohn et al., 1992; Derwent and Davies, 1994; Logan, 1985, 1989; Scheel et al., 1997).

2.1.2 Computation of trajectories

The meteorological fields used for trajectory calculations were computed with operational hydrostatic ALADIN/SI model (Team, 2003). ALADIN is a spectral limited area model with a terrain-following hybrid pressure coordinate, a semi-implicit semi-Lagrangian advection scheme and different parameterizations of physical processes such as boundary layer and turbulence formulation following Louis et al. (1982), shallow convection parametrization (Geleyn, 1987), gravity wave drag, the ISBA (Interaction Soil Biosphere Atmosphere) soil-vegetation scheme (Giard and Basil, 2000), a radiation scheme according to Ritter and Geleyn (1992) and implemented diagnostic cloudiness and large-scale precipitation scheme with Kessler-type cloud microphysics (Kessler, 1969).

The spatial domain of ALADIN model spanned from 2° W to 28° W and from 36° N to 54° N. The horizontal resolution was 9.5 km and 37 vertical levels extended from the ground to the 5 hPa level, where the lowest model levels were located approximately 17, 65, 141, 245, 373 meters etc. above above ground level. The temporal resolution of wind fields used for trajectory calculations was 1 hour.

Three-dimensional backward trajectories were calculated by using the FLEXTRA trajectory model (Stohl et al., 1995; Stohl and Seibert, 1998) for arrival levels 50 meters above the model topography. They were calculated for eight arrival times per day (00, 03, ..., 21 UTC) for the warm periods (months from April to September) of years 2003 and 2004. Each trajectory calculation started 96 hours prior to the arrival time. Their positions were stored at one-hour time intervals.

2.1.3 The k-means clustering

To aggregate trajectories into groups with similar characteristics the k-means clustering algorithm was applied (Moody and Galloway, n.d.). This algorithm iteratively allocates the set of N objects (trajectories in our case) among a predetermined number of clusters k, until the sum of distances from each object to its cluster centroid over all clusters cannot be decreased any further. Before the algorithm is initialized, the k initial cluster centroids (seeds) must be defined. Since the procedure is only guaranteed to converge to a local solution, which can significantly differ from the global one, the initial selection of seeds might significantly impact the classification. Our strategy concerning this issue was to use the "multiple random starts" procedure, where the initial seeds were randomly selected k trajectories from total. The clustering procedure was then repeated many (800) times and among the obtained results the one with the minimum sum of distances of all trajectories from its cluster centroids was selected and used in further analysis. Only the results of clustering with only the last 24 hours of each trajectory considered in clustering procedure are presented. The main reason

for that was that a significant number of longer trajectories (48 hours and longer) escaped out of the domain, while clustering algorithm requires the equal length of trajectories included in procedure. Actually, we performed the whole analysis also with 48 hours of trajectories (the clustering procedure and the subsequent analysis) and the results were in general very similar to the results from the 24 hour trajectories. Consequently, we decided to present the results of analysis of the complete set of 24 hour long trajectories rather than of the reduced set of longer trajectories.

The Euclidean distance between trajectories was calculated from 24 points, no data measured at the arrival point was considered in the clustering process. We decided not to explicitly include altitude of the trajectory points in the distance calculations. It is actually built-in implicitly because winds tend to be faster at higher altitudes, thus longer trajectories tend to be associated with higher altitudes. A similar approach was also used by some other authors (e.g. Hafner et al., 2007).

The procedure for selecting the final number of clusters is described in Žabkar et al. (2008). The aim of this procedure was to choose and analyze a stable and objective clustering solution, representing true main pathways, i.e. the solution which does not change considerably by adding or eliminating trajectories. For IS and KV the trajectory classification into 6 clusters, and for LJ and NG the classification into 7 clusters was selected and is presented below.

2.1.4 Analysis of cluster variables

Hourly values of measured meteorological variables (temperature, relative humidity and precipitation) and ozone concentrations (representing a mixture of transported and local pollution) at the time of arrival at the trajectory destination points were assigned to each computed trajectory. The measured data was provided by the Environmental Agency of the Republic of Slovenia. Values of these variables were analyzed for each trajectory cluster. Tukey's least significant difference (LSD) multiple comparison procedure (Hochberg and Tamhane, 1987) and Kruskal-Wallis test (Hollander and Wolfe, 1973) were then used for the pair wise comparisons of average cluster values to determine clusters that significantly differ in these variables, particularly in ozone. LSD procedure is a simple t-test, while Kruskal-Wallis test is a nonparametric version of the classical one-way ANOVA, which does not assume a-priori a normal distribution of data. Another characteristic of the Kruskal-Wallis test is smaller sensitivity to outliers. The ranks in the Kruskal-Wallis test are obtained by sorting all the cluster values (e.g. ozone concentrations) into ascending order and then calculating mean rank of concentrations for each cluster.

2.1.5 Concentration-weighted trajectory (CWT)

A method of weighting trajectories with associated concentrations was introduced by Seibert et al. (1994). In this procedure, each grid cell is assigned a concentration obtained by averaging trajectory-associated concentrations that had crossed the grid cell:

$$C_{ij} = \frac{1}{\sum_{k=1}^{N} n_{ijk}} \sum_{k=1}^{N} C_k n_{ijk} \tag{2.1}$$

C_{ij} is weighted concentration in the (i, j) grid cell, C_k is concentration of k-th trajectory at the receptor point, N is the total number of trajectory endpoints in (i, j) grid, and n_{ijk} is the number of k-th trajectory endpoints in the (i, j) grid cell. The denominator corresponds to (i, j) grid cell number density ND_{ij}.

2.2 Results of trajectory analysis

2.2.1 The trajectory clusters and local ozone concentrations

The average cluster trajectories for stations NG, LJ, KV and IS are presented in Fig. 2.3. The influence of the Alpine barrier dictates the main airflow characteristics. There are two dominant paths of air masses reaching Slovenia: from the SW and from the NE. The trajectories from these two main directions are initially disaggregated with respect to the trajectory lengths, resulting in one cluster of slow and short trajectories originating from the NE and one from the SW. The long and fast moving trajectories are further disaggregated into groups originating from more distant westerly and easterly areas. There are generally two long trajectory clusters with low altitudes, one from the SSE and the other from the SW. Longer trajectories from the N are further split into a cluster east of the Alps over Eastern Austria and a cluster (or two) descending over the Alps from the NW.

Basic characteristics of air masses approaching the measuring sites (in correspondence to the trajectory clusters) are summarized in Table 2.1, including ozone concentration, air temperature, relative humidity and precipitation. Clusters are uniformly labeled for all the stations and they generally follow the cluster average ozone maximum: clusters 1 of short trajectories from SW with the highest maximum, followed by cluster 2 of (again short) trajectories from NW, etc. Cluster 7 of long trajectories across the Alps is the one with the lowest maximum.

In addition to the air mass origin, the prevalent local meteorological conditions associated with a specific cluster also play an important role in the ozone pollution. Some basic characteristics of the average cluster meteorological variables can be deduced from Table 2.1. For clusters with average values that significantly differ in the value of the variable at significance level 0.05 (according to the LSD multiple comparisons), the numbers are emphasized in bold. Air masses, originating from the north and crossing the Alps, are usually associated with the significantly lower temperatures at the sites (e.g. clusters 7 and 5) - in spite of adiabatic heating of descending air in cluster 7. Adiabatic heating is expected to contribute to the temperatures in cluster 6, as well. The percentage of precipitation days is higher in clusters of trajectories originating from the south, associated with the Mediterranean cyclone. High temperatures are generally positively correlated with the ozone formation - the correlation coefficient between ozone and temperature daily maxima is 0.75, 0.82, 0.47, 0.74 for NG, LJ, KV and IS, respectively. The average relative humidity (RH) has in our case no evident impact on the ozone. This is partly due to different reasons for high and low humidity values. For example, the highest RH in cluster 7 for LJ is mainly associated with very low temperatures in this cluster, while for KV high RH in cluster 2 stems from air moistening above the Adriatic Sea. The correlation coefficients between daily ozone maxima and daily RH minima are now -0.5, -0.63, -0.45 and -0.70 for NG, LJ, KV and IS, respectively. Like RH, the precipitation enabling wet deposition of air pollutants is negatively correlated to measured ozone.

Figure 2.4 shows characteristics of the 3-hourly ozone maxima associated with the cluster trajectories arriving at 12:00 and 15:00 UTC to NG, LJ and IS. Including all trajectories and associated ozone values for the three stations would result in lower average ozone concentrations due to nighttime ozone reduction. For KV without a pronounced daily cycle all cluster trajectories with associated 3-hourly ozone maximum were taken into account. For example, the 3-hourly maximum ozone data for 12 UTC includes maximum hourly values from 11:00 to 13:00 UTC. Box-and-whisker plots are presented in the upper panel of Fig. 2.4, and the

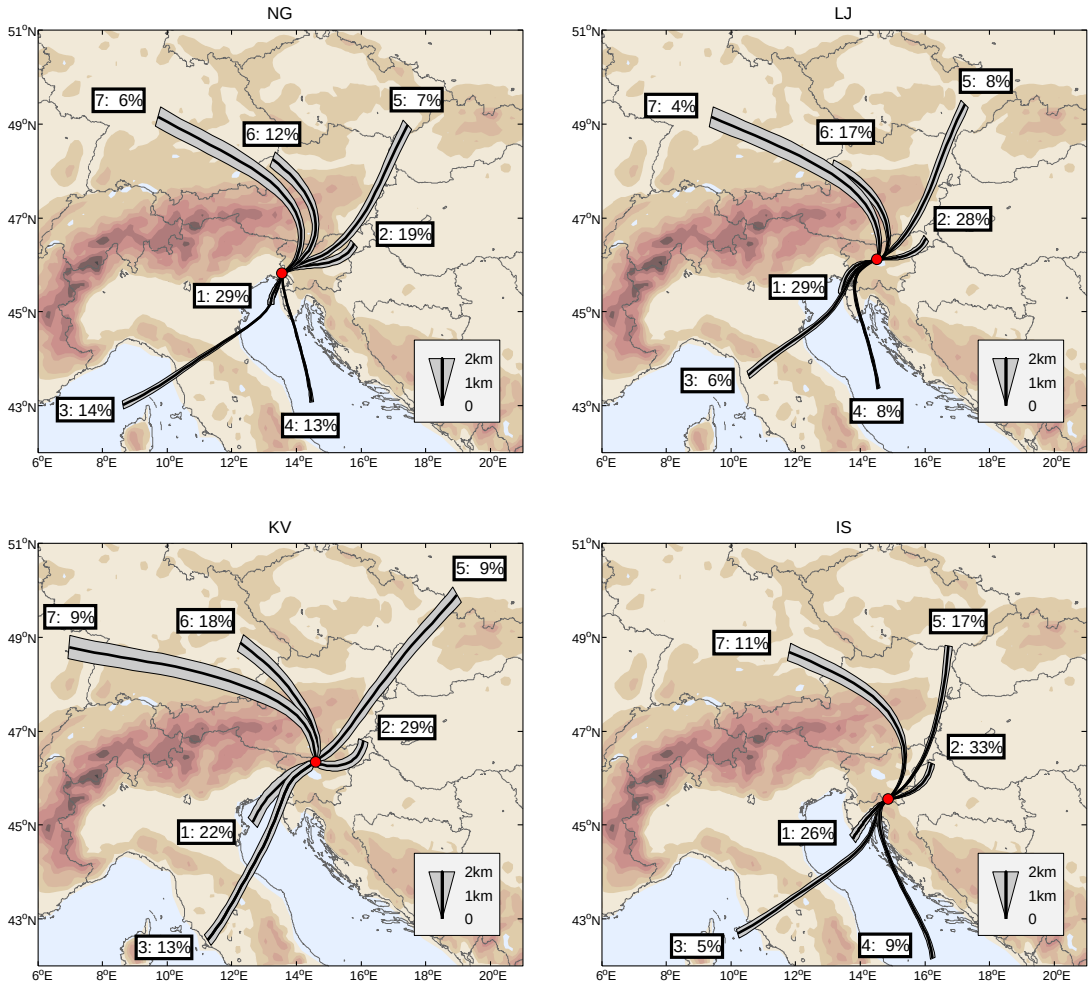

Figure 2.3: Average cluster trajectories for Nova Gorica (NG), Ljubljana (LJ), Krvavec (KV) and Iskrba (IS). Text boxes denote the cluster number and the percentage of trajectories involved in cluster. Path widths measure average above ground level (AGL) of cluster trajectories. ALADIN topography (resolution 9.5 km) above 500 m AMSL, with the contour intervals 500 m are shown in the background.

Kruskal-Wallis test results for the null hypothesis that ozone concentrations from any two clusters come from distributions with equal median (at 0.05 significance level) are shown in the lower panel of Fig. 2.4.

For the pairs of clusters with non-overlapping ranks, the difference in medians of ozone concentrations is significant at 0.05 level. The daily maxima in Table 2.1 are for all stations associated with cluster of short trajectories from the SW. These clusters include stagnant anticyclone situations with light winds, highest daily temperatures and high solar irradiance, which are the most favorable situations for ozone formation. Note that ozone concentrations in short clusters from the NE with similar local meteorological conditions, sometimes on average even more favorable for ozone formation (higher average temperatures and less precipitation days), have maximum ozone concentrations slightly lower than those from the SW. Moreover, the differences between these two clusters (1 and 2) are significant for all measuring sites according to t-test results for maximum ozone concentrations (numbers in bold style in Ta-

Table 2.1: Number of trajectories, meteorological variables and ozone concentrations for stations NG, LJ, KV and IS associated with clusters in Fig. 2.3. Ozone (O3 in μg/m^3), temperature (T in $^\circ C$) and relative humidity (RH in %) are averaged over all trajectories, regardless of the time of arrival. Daily maxima are assigned to the trajectories arriving at 12:00 and 15:00 UTC and then averaged over all cluster 12:00 and 15:00 UTC trajectories. Ozone daily minima are assigned to and averaged over the 6:00 UTC trajectories, while accumulated daily precipitation (RR in mm) was assigned to all cluster 12:00 UTC trajectories. Significantly different average values (t-test, 0.05 significance level) are written in bold style.

Cluster	N	O_3	O_3 max	O_3 min	T	Tmax	RH	RR*
NG: O_3(annual) = 51 μg/m^3								
1	923	75.0	**140.9**^{a}	18.8	20.2	27.6	64.5	7 (21/5)
2	570	74.6	128.9	22.0	22.1	**29.2**^{a}	59.6	5 (10/-)
3	277	**86.3**^{a}	130.1	23.5	21.4	26.5	66.2	17 (20/6)
4	373	72.9	125.2	16.9	19.6	25.4	69.5	12 (12/2)
5	236	75.9	109.2	31.5	19.9	25.7	**51.3**^{c}	5 (4/-)
6	308	67.7	107.8	26.7	19.6	25.9	56.9	11 (10/2)
7	218	**58.3**^{c}	**92.6**^{c}	21.1	**15.2**^{c}	**21.5**^{c}	59.7	9 (9/2)
LJ: O_3(annual) = 45 μg/m^3								
1	744	69.4	**127.3**^{a}	14.0	19.3	25.6	68.1	13.5 (35/9)
2	824	60.4	114.9	13.3	18.8	24.6	71.9	11.1 (22/3)
3	211	**77.0**^{a}	107.5	22.6	17.8	22.5	70.0	17.3 (8/3)
4	231	**78.9**^{a}	117.8	23.0	18.3	23.5	70.3	18.0 (14/5)
5	264	56.1	106.8	10.8	**15.4**^{d}	21.8	69.1	4.0 (5/-)
6	434	58.9	101.1	16.8	17.4	22.3	70.2	12.8 (16/4)
7	196	**39. 5**^{c}	**77.1**^{c}	10.4	**10.7**^{c}	**14.2**^{c}	**81.0**^{a}	9.8 (5/1)
KV: O_3(annual) = 99 μg/m^3								
1	638	**123.4**^{a}	**136.7**^{a}	**105.5**^{a}	11.2	15.0	75.5	17.0(39/11)
2	834	116.3	128.1	100.3	12.1	16.6	77.5	9.6 (33/4)
3	359	116.0	125.4	98.0	8.8	11.8	**87.8**^{a}	13.3 (17/4)
5	254	113.0	120.5	100.7	**6.5**^{d}	10.5	80.8	3.6 (6/-)
6	528	**105.3**^{d}	115.3	92.4	8.7	12.4	78.3	8.8 (21/3)
7	252	**96.3**^{c}	**103.7**^{c}	**83.8**^{c}	**5.4**^{c}	**8.1**^{c}	80.3	8.4 (9/1)
IS: O_3(annual) = 57 μg/m^3								
1	802	63.9	**128.7**^{a}	7.6	15.3	23.9	73.6	11.3 (28/6)
2	895	59.6	115.2	6.8	15.8	23.4	74.0	11.3 (24/2)
3	185	**83.7**^{b}	115.0	27.4	15.6	20.4	74.4	16.9 (13/4)
4	288	**84.7**^{b}	121.0	**41.0**^{a}	15.5	21.7	73.7	14.3 (13/5)
5	439	65.7	107.1	13.8	13.3	19.0	76.4	7.9 (19/1)
7	298	61.7	**96.4**^{c}	16.3	**10.8**^{c}	**16.4**^{c}	77.7	13.0 (13/3)

* (x/y) is precipitation frequency in days, a - above 1 mm, b - above 20 mm
[a] average cluster value significantly higher than any other average cluster value
[b] average cluster value significantly higher than any except one average cluster value
[c] average cluster value significantly lower than any other average cluster value
[d] average cluster value significantly lower than any except one average cluster value

ble 2.1) and for the three measuring sites (except LJ) according to Kruskal-Wallis test results for 3 hourly maximum (Fig. 2.4 lower panel). Since cluster 2 has the highest ozone from all northern clusters, the difference between the short SW cluster and all northern clusters is significant. The difference between the short SW cluster and long southern clusters are usually not significant according to the Kruskal-Wallis test (NG cluster 3, LJ and IS cluster 4). Ozone

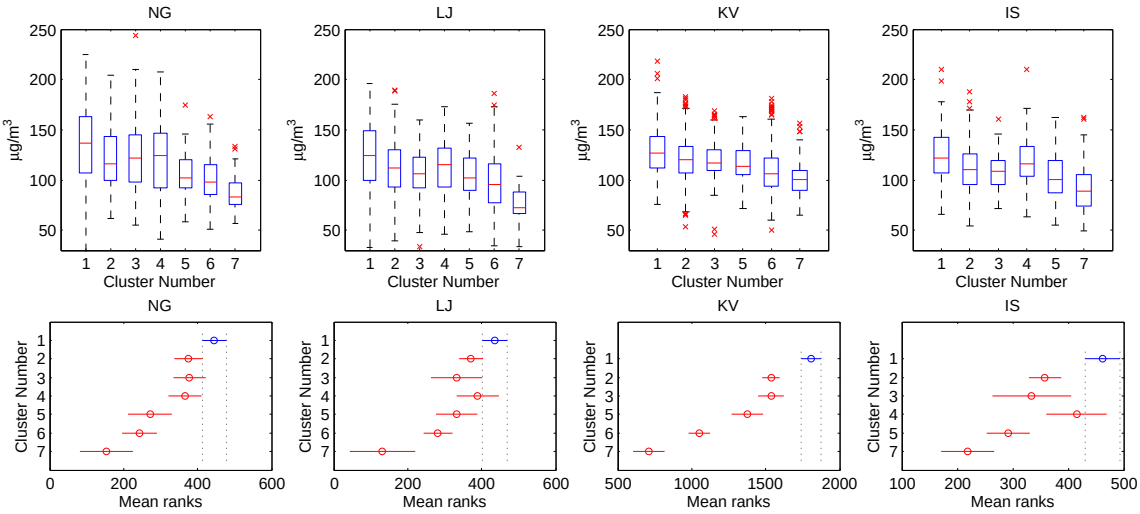

Figure 2.4: Analysis of average cluster ozone mixing ratios for NG, LJ, KV and IS, cluster centroids are shown in Fig. 2.3. Upper panel: box-and-whisker plots of the 3 hourly ozone maximum associated with trajectories arriving at 12:00 and 15:00 UTC for sites NG, LJ and IS; for KV all trajectories are taken into account. Boxes extend from the lower quartile, over median to the upper quartile values. The whiskers specify 1.5 times the interquartile range and crosses beyond the whiskers represent outliers. Lower panel: mean ranks of Kruskall-Wallis test for the same data sets.

concentrations associated with cluster 7 significantly differ from all the other clusters for all the stations regardless of the statistical test applied. Cluster 7 of long trajectories from NW across the Alps is thus the cluster with lowest ozone concentrations. The ozone in other long northern clusters is also low. This is due to the low temperatures (northern flow) and strong winds (long trajectories) that prevent efficient ozone formation. Since prevalent meteorological conditions in these clusters are unsuitable for effective ozone formation, meteorological conditions rather than air mass origins explain low ozone concentrations.

2.2.2 Concentration weighted trajectories and number density fields

A method of weighting trajectories with associated concentrations (CWT) in combination with trajectory number density (ND) fields offers additional information about pathways of polluted air mass and potential source locations. Almost all NG polluted trajectories (Fig. 2.5) travel over the north Adriatic Sea, over the Gulf of Trieste and reach NG from the south. There are some rare exceptions, namely trajectories originating either in northern Italy and reaching NG from the west, or originating in central Slovenia and reaching NG from the east. It must be also taken into account, that due to the local topography, southern flow toward Soča Valley north of NG usually develops in the fair weather conditions. The resulting trailing effect, where areas upwind and downwind of the sources are likely to be identified as sources as well, is eliminated in the CWT field, where the pattern at the Po River estuary indicates contribution of the Po Basin polluted air masses. The CWT field over the Adriatic Sea for NG is otherwise more or less homogeneous (except over the central Adriatic Sea, due to faster

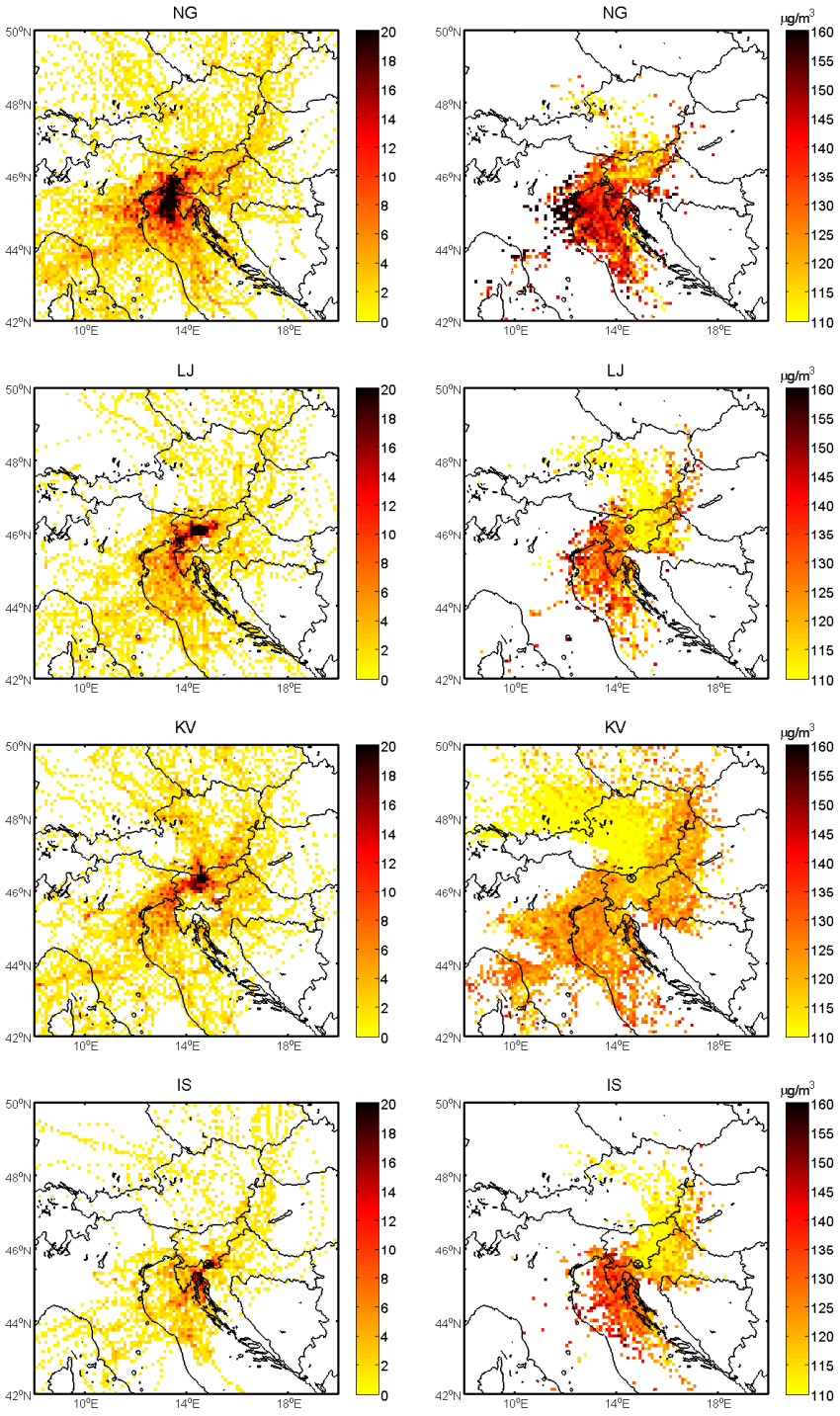

Figure 2.5: Analysis of 96-hour trajectories associated with 3h ozone maximum measured at receptor points NG, LJ, KV, and IS. Left panel: number density ND of trajectories with 3h ozone maximum above 160 μg/m^3. Right panel: CWT fields, where only grid values with at least 10 trajectory end points are presented (for NG, LJ, IS with at least 10 trajectory points in hours 12:00 - 15:00 UTC). Grid mesh has a resolution of 10 km.

trajectories), and has noticeably higher values than over Slovenia. Results are thus similar to conclusions of the cluster analysis. The highest ozone concentrations probably occur due to polluted air masses spread over the Mediterranean while a passage over emission areas in western Istria and the Gulf of Trieste enhances the total pollution.

Similar conclusions are valid for IS. ND for IS indicates that the most polluted air masses travel over the Gulf of Kvarner with industrial emission sources located on the coast and enhanced coastal traffic during the peak summer tourist season. Homogeneous CWT values over a broader coastal area and over the Adriatic Sea indicate that ozone polluted air masses are probably spread over a larger area south of Slovenia. The contribution of emissions located around Rijeka and surroundings most likely causes the final addition to the total ozone resulting in exceeding threshold values at the IS station.

The pollution accumulated in the Mediterranean air masses presents a contribution even for LJ, or rather a baseline, to which local emissions (which are probably dominant) are added. There are some "polluted" trajectories, approaching from the east, but the SW pattern of ND for LJ is prevalent. Similarly, the CWT field indicates cleaner NE trajectories towards LJ than SW trajectories.

The most distinct ND pattern for KV again occurs from the SW. In contrast to the other stations, there are three additional trails approaching from the N, NE and E, indicating that regional transport from Central and Eastern Europe is not always altogether negligible. The CWT values for KV are less variable. Regions over the north Adriatic Sea and northern Italy are associated with the highest CWT values, but the CWT values for eastern and northeastern flows are almost the same. Actually the only distinct pattern of CWT for KV is a significantly cleaner airflow of trajectories crossing the Alps and reaching the site from the north.

2.3 Discussion

In the present chapter, a trajectory-based analysis has been applied to reveal the origins of ozone-polluted air masses for four measuring sites in Slovenia. Results of cluster analysis show that for all the stations the highest average ozone concentrations are associated with southwesterly flow of air masses. The lowest measured ozone is for all the stations related to the cluster of long NW trajectories, crossing the Alps and approaching Slovenia from the north. This "clean" air pathway is probably in a great deal due to the meteorological conditions, unfavorable for ozone formation.

A significant influence of Central Europe pollution cannot be confirmed for NG, LJ and IS. There are only some rare northern trails in ND and CWT fields for these sites, suggesting that high ozone values are rarely associated with air masses originating from the north. The results as well did not confirm a direct pathway of polluted air from the Po River Basin to Slovenia, only the CWT field for NG shows a pattern toward the Po Basin. But still there may be a substantial indirect influence of this heavily industrialized area to the overall northern Mediterranean air pollution.

Stratospheric intrusions (SI) may beside regional transport and local emissions as well occasionally affect the near ground ozone levels. Especially the elevated sites (like KV in Slovenia) are more exposed to this natural phenomenon (Schuepbach et al., 1999). For the urban areas elevated ozone concentrations due to intrusions from stratosphere are rare, but as well documented (e.g. Lisac et al., 1993; Klaic et al., n.d.). There are two main mechanisms causing SI of ozone, namely the descending flow near the cold front and the large scale anticyclonic subsidence (e.g. Wakamatsu et al., 1989). For Slovenia the cases with SI of

ozone are thus most likely to occur for trajectories with the NW origin. Since clusters from NW have significantly lower ozone (see KV, Fig. 2.3 and 2.4), and also the CWT fields show the lowest ozone values for NW trajectories, SI are not expected to considerably influence average ozone levels at any of analyzed stations (including KV). Nevertheless, only case by case analysis would enable the isolation of days with predominant contribution of SI on ozone concentrations. Since the influence of the SI were not of the primarily interest in the present study, we did not further investigate the contribution of SI at KV and other stations. The question about the influence of stratospheric ozone intrusions, specially as potential origin of ozone polluted air masses at elevated stations in spring, thus remains unanswered and is left for the future research.

A common origin of ozone rich air masses for all stations and from all analysis seems to be the area over the northern Adriatic Sea, which is rather unexpected. Since there are no significant precursor emissions (except ships) over the sea, the coastal regions appear to be considerable source of ozone precursors. The northern Adriatic Sea was identified also by (Kaiser et al., 2007) as a NO_x source for GAW stations and as an origin of ozone rich air masses for KV station. In addition, high ozone values measured at the coast in the northern Adriatic were reported by Cvitas et al. (1997). This northern Adriatic Sea phenomenon needs further investigation. In the first place the ozone as well as other pollutant measurements over the sea is needed to establish the actual degree of photochemical pollution. Secondly, further research is required to identify which processes (different vertical mixing, deposition, etc.) are responsible for formation of the eventual polluted air masses over the sea and over the coastal areas.

In the present chapter trajectories with final heights 50 m above ground level are presented and analyzed. Nevertheless, trajectories calculated for only one arrival height may not show all transport characteristics. To address this issue, we made an experiment in which we calculated and compared the trajectories with different final heights (50 m, 200 m, 100 m, 1500 m, 3000 m, 5500 m) for days with daily ozone maxima above 165 $\mu g/m^3$ in years 2004 and 2005 (altogether 32 days), while meteorological fields were calculated with identical configuration of ALADIN model. To take into account the uncertainty of each trajectory arising from the inaccuracy of PBL wind fields (hydrostatic model with rather coarse horizontal resolution etc.) and the fact that the air masses are not only transported, but also mixing takes place, in this experiment to each of the trajectory 10 additional trajectories with added random wind perturbations to the wind fields were calculated. The comparison of these "polluted trajectories" for different arrival levels showed very similar patterns for 50 m and 200 m trajectories, the patterns were slightly modified for 1000 m trajectories, while with further increment of trajectory arrival levels, westerly flow gradually predominated, resulting in trajectories originating above all from western directions (at heights of 3000 m and 5500 m). Results of this experiment for 50 m, 200 m and 1000 m trajectories confirmed the results presented so far, such as the Northern Adriatic region as a common origin of ozone rich air masses for Nova Gorica station. Although trajectories at higher levels (e.g. 3000 m) originated from west (for NG west means the area above Po River Basin) the air masses at these heights are (with occasional exceptions) likely to be disconnected from the near ground air.

The questions whether the high ozone concentrations are primarily caused by transport of ozone or transport of ozone precursors, as well as the contribution of ozone formation from local emissions, remain difficult to answer only with the methodology applied. The trajectory analysis cannot take into account processes like chemical reactions, wet and dry deposition, and the turbulence. To explain the ozone phenomenon over Slovenia, over the northern Adriatic Sea and its coastal regions accurately, all these processes must be considered. With the current

approach we are therefore not in a position to evaluate for example the "indirect impact" of the Po Basin emissions relative to the more local emissions (i.e. the Gulfs of Trieste and Kvarner) on ozone in Slovenia. To find the answers to these questions, a photochemical modeling was applied, presented in the following chapters.

Chapter 3

The WRF-Chem modeling System

The Weather Research & Forecasting model (WRF) is a meso-scale numerical weather prediction system designed to serve both operational forecasting and atmospheric research needs. It has been developed in a collaborative partnership of several USA institutions, principally among the National Center of Atmospheric Research (NCAR), the National Oceanic and Atmospheric Administration (NOAA), the National Center for Environmental Prediction (NCEP), the Forecast Systems Laboratory (FSL), the Air Force Weather Agency (AFWA), the Naval Research Laboratory, Oklahoma University, and the Federal Aviation Administration (FAA). It is a fully compressible and non-hydrostatic Euler model. The model physics includes bulk schemes, mixed-phase physics for cloud-resolving modeling, multi-layer land surface models ranging from a simple thermal model to full vegetation and soil moisture models, including snow cover and sea ice, turbulent kinetic energy prediction or non-local K schemes for planetary boundary layer calculation, and longwave and shortwave schemes with multiple spectral bands and a simple shortwave scheme. In a WRF-Chem modeling system a chemical model is fully on-line coupled with the WRF model (Grell et al., 2005).

A detailed description of the model can be found in the WRF and WRF-Chem User's Guides (Skamarock et al., 2005, 2008; Peckham et al., 2008) as well as on the WRF ARW and WRF-Chem user web sites (http://www.mmm.ucar.edu/wrf/users/, http://ruc.fsl.noaa.gov/wrf/WG11/). In my simulations WRF-Chem 2.2 beta version of the model was used.

3.1 Model dynamics

The compressible, non-hydrostatic Euler equations are formulated using a terrain-following hydrostatic-pressure vertical coordinate denoted by η and defined as:

$$\eta = (p_h - p_{ht})/(p_{hs} - p_{ht}). \tag{3.1}$$

p_h is the hydrostatic component of the pressure, and p_{hs} and p_{ht} refer to pressure values along the surface and top boundaries of the model domain, respectively. The flux form variables are defined as:

$$\mathbf{V} = \mu\mathbf{v} = (U, V, W), \qquad \Omega = \mu\dot{\eta}, \qquad \Theta = \mu\theta, \qquad \text{where} \quad \mu = p_{hs} - p_{ht}. \tag{3.2}$$

$\mu(x, y)$ presents the weight of the air per unit area within the column in the model domain at (x, y). $\mathrm{v} = (u, v, w)$ are the covariant velocities, while $\omega = \dot{\eta}$ is the contravariant vertical

velocity and θ the potential temperature. Using also $\phi = gz$ (geopotential) and p (pressure), the flux form equations are written as:

$$\frac{\partial U}{\partial t} + (\nabla \cdot \mathbf{V}u) - \frac{\partial}{\partial x}\left(p\frac{\partial \phi}{\partial \eta}\right) + \frac{\partial}{\partial \eta}\left(p\frac{\partial \phi}{\partial x}\right) = F_U \tag{3.3}$$

$$\frac{\partial V}{\partial t} + (\nabla \cdot \mathbf{V}v) - \frac{\partial}{\partial y}\left(p\frac{\partial \phi}{\partial \eta}\right) + \frac{\partial}{\partial \eta}\left(p\frac{\partial \phi}{\partial y}\right) = F_V \tag{3.4}$$

$$\frac{\partial W}{\partial t} + (\nabla \cdot \mathbf{V}w) - g(\frac{\partial p}{\partial \eta} - \mu) = F_W \tag{3.5}$$

$$\frac{\partial \Theta}{\partial t} + (\nabla \cdot \mathbf{V}\theta) = F_\Theta \tag{3.6}$$

$$\frac{\partial \mu}{\partial t} + (\nabla \cdot \mathbf{V}) = 0 \tag{3.7}$$

$$\frac{\partial \phi}{\partial t} + \mu^{-1}(\mathbf{V} \cdot \nabla\phi - gW) = 0 \tag{3.8}$$

The right-hand-side terms F_U, F_V, F_W and F_Θ represent forcing terms arising from model physics, turbulent mixing, spherical projections and the earth's rotation. Missing are the diagnostic relation for inverse density $\alpha = 1/\rho$:

$$\frac{\partial \phi}{\partial \eta} = -\alpha\mu = -\frac{\mu}{\rho} \tag{3.9}$$

and the equation of state:

$$p = p_0(R_d\theta/p_0\alpha)^\gamma. \tag{3.10}$$

$\gamma = c_{p_d}/c_{v_d}$ is the ratio of the heat capacities for dry air, $R_d = c_{p_d} - c_{v_d}$ is the specific gas constant for dry air and $p_0 = 10^5 Pa$ the reference pressure.

Equations (3.3) - (3.10) correspond to the dry air. Euler equations for moist air are formulated by the coupling of dry air mass to the prognostic variables (Eq. (3.3) - (3.6)), the conservation equation for dry air and by introducing source terms in the mass conservation equation (Eq. (3.7)).

With μ_d as mass of the dry air in the column and p_{dh} and p_{dht} as the hydrostatic pressure of the dry atmosphere, we redefine vertical coordinate:

$$\eta = (p_{dh} - p_{dht})/\mu_d \tag{3.11}$$

and the coupled variables:

$$\mathbf{V} = \mu_d\mathbf{v} = (U, V, W), \qquad \Omega = \mu_d\dot{\eta}, \qquad \Theta = \mu_d\theta. \tag{3.12}$$

With these definitions the moist Euler equations are rewritten (not shown here) and one new equation is added:

$$\frac{\partial Q_m}{\partial t} + \nabla \cdot (\mathbf{V}q_m) = F_{Q_m}, \tag{3.13}$$

where q_m stands for the mixing ratios for water vapor (q_v), ice (q_i), rain (q_r), cloud (q_c)... In addition, $Q_m = \mu_d q_m$, and $\theta_m \approx \theta(1 + 1.61q_v)$.

Before the governing equation are discretized, they are written again using the reference state ($\overline{p}$, $\overline{\theta}$, $\overline{\alpha}$, $\overline{\mu}_d$) and the perturbation variables (p', ϕ', α', and μ'_d), so that $p = \overline{p}(z)+p'$, $\phi = \overline{\phi}(z)+\phi'$, $\lambda = \overline{\lambda}(z)+\lambda'$ and $\mu_d = \overline{\mu}_d(x, y)+\mu'_d$. Consequently, the truncation errors arising from the horizontal pressure gradient calculations in the discrete solver and the machine rounding errors in the vertical pressure gradient and buoyancy calculations, are reduced. Reference state variables are a function of height only and satisfy the governing equations for the atmosphere at rest.

3.2 Discretization of governing equations

Time integration of governing equations is performed by a third order Runge Kutta (RK3) time integration scheme. The scheme is a predictor-corrector type and takes the form of 3 steps to calculate a solution $\Phi(t + \Delta t)$ from $\Phi(t)$:

$$\Phi^* = \Phi^t + \frac{\Delta t}{3} R(\Phi^t) \tag{3.14}$$

$$\Phi^{**} = \Phi^t + \frac{\Delta t}{2} R(\Phi^*) \tag{3.15}$$

$$\Phi^{t+\Delta t} = \Phi^t + \Delta t R(\Phi^{**}), \tag{3.16}$$

where Φ are prognostic variables ($\Phi = (U, V, W, \Theta, \phi', \mu', Q_m)$) and the $\Phi_t = R(\Phi)$ the model equations.

Inside the RK3 time step Δt sequence, the perturbation form of the governing equations are integrated using a smaller acoustic time steps with approach described in Wicker and Skamarock (2002). RK3 integration technique thus presents an outer loop for the large-time-step integration, inside which an inner loop for acoustic modes enables faster overall temporal integration.

Variables in the dynamic solver are spatially discretized in the form of an Arakawa C grid (Fig. 3.1), which means, that normal velocities are staggered one-half grid length from the thermodynamic variables (*mass* points). Not shown in the Fig. 3.1 are the column mass μ and the moisture q_m variables, defined at the mass points, the geopotential ϕ, defined at the w points, and the diagnostic pressure p and inverse density α variables, computed both at mass points.

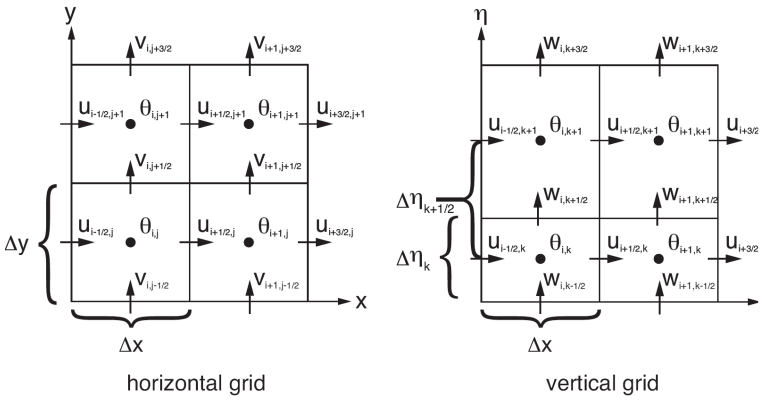

Figure 3.1: Spatial discretizatization of variables in dynamic solver.

3.3 Physical parameterizations

Many physical processes governing the larger-scale meteorology are fundamentally based on mechanisms rooted in the molecular and micro-scale, not resolved in a model. The impact of these sub-grid scale processes on the resolved-scale environment is represented in model in a simplified manner with parameterizations. Parameterizations generally contain assumptions and empirical relationships that allow complex processes to be calculated efficiently on the resolved-scale variables.

Physical processes are in the model classified into the following categories: microphysics, cumulus parametrization, planetary boundary layer, land surface model, radiation and diffusion. For each category a separate physics driver is responsible and several options for parameterizations are available. Physical packages compute tendencies for the velocity components, potential temperature and moisture fields (right terms in Eq. (3.3) - (3.6), and (3.13)).

Parameterizations of several physical processes in model may influence the simulated meteorological conditions (mixing heights, air temperatures, humidity, winds, stability...) and consequently the tropospheric ozone concentrations. In my research I decided to study the influence of two categories of physical processes, which seemed to be the most critical. These are the parametrization of surface processes (Land Surface Model, LSM) and the turbulent processes in the planetary boundary layer (PBL), the latter coupled with surface layer physics (SLP) parametrization.

The options for LSM, PBL and SLP parameterizations in WRF model are shortly presented below. For description of other model physical parameterizations, references can be found in Skamarock et al. (2005).

3.3.1 Land surface model

LSM estimates heat and moisture fluxes over land and sea-ice points. These fluxes provide a lower boundary condition for the vertical transport done in the PBL schemes. LSM can be very simple or sophisticated. The latter will use information about radiative forcing (from radiation scheme), precipitation forcing (microphysics and convective schemes), surface fluxes (surface layer scheme), as well as information about the land state's variables (skin temperature, soil temperature profile, soil moisture profile, snow cover, canopy properties) and land surface properties (albedo, soil moisture, roughness, emissivity, thermal inertia, vegetation...).

Two different options for LSM are described below.

3.3.1.1 5-layer thermal diffusion scheme

The 5-layer thermal diffusion scheme (Dudhia, 1996) uses five soil layers, which are 1, 2, 4, 8 and 16 cm thick. Below the bottom level, at 31 cm, the substrate temperature is kept constant during integration in a layer that is 32 cm thick.

The transfer of heat follows the one dimensional simple diffusion equation, as the heat flux, F ($\mathrm{Wm^{-2}}$), is linearly proportional to the temperature gradient:

$$F = -KC\frac{\partial T_s}{\partial z}. \tag{3.17}$$

K ($\mathrm{m^2 s^{-1}}$) is the soil's thermal diffusivity and C (J $\mathrm{m^{-3}K^{-1}}$) the volumetric heat capacity, the latter defined as product of soil density ρ_s (kg $\mathrm{m^{-3}}$) and soil specific heat capacity c_s (J $\mathrm{kg^{-1}}K^{-1}$), therefore $C = \rho_s c_s$. The flux convergence is proportional to the heating:

$$\frac{\partial T_s}{\partial t} = -\frac{1}{C}\frac{\partial F}{\partial z}. \tag{3.18}$$

In the model Eq. (3.17) is used to determine $F(z)$ within the soil, then Eq. (3.18) can be used given that $F(z = 0)$ is known at the surface, where it represents the net sensible, latent and radiative flux.

In the case of this very simple scheme soil moisture is determined and fixed with a landuse and season dependant constant value. There are no vegetation effects taken into account and snow cover is not considered.

3.3.1.2 Noah LSM

Noah LSM is a 4-layer soil temperature and moisture model with a canopy moisture and snow cover prediction (Chen and Dudhia, 2001). It includes root zone, evapotranspiration, soil drainage, and runoff. The model considers vegetation categories, monthly vegetation fraction, soil texture, surface emissivity properties and has an increased urban treatment. We initialized the temperature and soil moisture in layers with thickness of 7, 21, 72 and 155 cm from ECMWF (European Centre for Medium-Range Weather Forecasts) analysis fields.

a. Model thermodynamics

Similarly as in a simple 5-layer LSM the ground heat flux is controlled by the usual diffusion equation for soil temperature:

$$C(\Lambda)\frac{\partial T}{\partial t} = \frac{\partial}{\partial z}\left[K_t(\Lambda)\frac{\partial T}{\partial z}\right], \tag{3.19}$$

now written with the volumetric heat capacity, C (J m^{-3}K^{-1}), and the thermal conductivity, K_t (W m^{-1}K^{-1}). Both are formulated as functions of volumetric soil water content, Λ, which represents a fraction of unit soil occupied by water (Pan and Marth, 1987):

$$C = \Lambda C_{\text{water}} + (1-\Lambda_s)C_{\text{soil}} + (\Lambda_s - \Lambda)C_{\text{air}}, \tag{3.20}$$

$$K_t(\Lambda) = \begin{cases} 420\,\exp[-(2.7+P_f)], & P_f \leqslant 5.1 \\ 0.1744, & P_f > 5.1 < 0 \end{cases} \tag{3.21}$$

and

$$P_f = \log[\Psi_s(\Lambda_s/\Lambda)^b]. \tag{3.22}$$

C_{water}, C_{soil} and C_{air} are constant volumetric heat capacities, while Λ_s and Ψ_s are maximum soil moisture (porosity) and saturated soil potential (suction), respectively. Λ_s and Ψ_s depend on the soil texture.

b. Model hydrology

The prognostic equation used in model for the volumetric soil moisture content Λ is:

$$\frac{\partial \Lambda}{\partial t} = \frac{\partial}{\partial z}\left(D\frac{\partial \Lambda}{\partial z}\right) + \frac{\partial K}{\partial z} + F_\Lambda, \tag{3.23}$$

where both the soil water diffusivity, D, and hydraulic conductivity, K, are highly nonlinear functions of Λ. F_Λ represents sources and sinks for soil water: precipitation, evaporation and runoff. D is given by $D = K(\Lambda)(\partial\Psi/\partial\Lambda)$ (Hanks and Ashcroft, 1986), where Ψ is the soil water tension function. K and Ψ are computed by $K(\Lambda) = K_s(\Lambda/\Lambda_s)^{2b+3}$ and $\Psi(\Lambda) = \Psi_s/(\Lambda/\Lambda_s)^b$ (Cosby et al., 1984), where b is a curve-fitting parameter. K_s, Ψ_s and b depend on the soil type.

The procedure of numerical integration as well as detailed parametrization of canopy transpiration, precipitation, evaporation etc. is explained by Chen and Dudhia (2001). The snow and sea-ice model, not relevant for our simulations during the warm parts of the year, is also described there.

In WRF model the Noah LSM has two primarily variables upon which all the other secondary parameters are determined. These are vegetation type and the soil texture, both

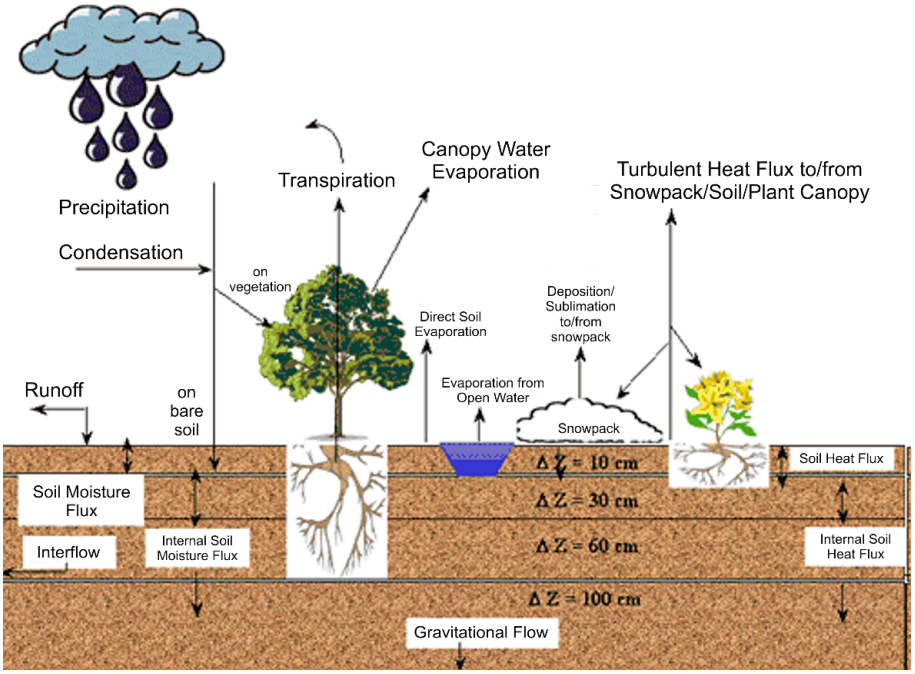

Figure 3.2: A schematic representation of the Noah LSM (Chen and Dudhia, 2001).

are derived from 1 km resolution U.S. Geological Survey (USGS) satellite land cover data. Consequently, secondary parameters such as albedo, roughness length, minimal stomatal resistance, soil moisture availability and others, are assumed to be land-cover dependant, they have constant values defined for different land-cover categories.

3.3.2 Planetary boundary layer schemes

The responsibility of PBL scheme is the representation of the sub-grid-scale turbulence in the PBL and in the free atmosphere. With determining the flux profiles, the PBL scheme provides atmospheric tendencies of temperature, moisture, and horizontal momentum. The schemes assume, that there is a clear scale separation between sub-grid and resolved eddies, which does actually not hold below the horizontal resolution of a few hundred meters. For simulations with horizontal resolution less than 1 km, when the model becomes to resolve the largest most energetic eddies (which scale to the PBL depth), PBL scheme should be turned off. Otherwise the energy of the largest eddies can be represented twice and serious errors can develop in model solutions.

3.3.2.1 YSU PBL scheme

The Yonsei University (YSU) PBL scheme is the first order non-local K scheme. It includes a so-called counter-gradient transports of heat and moisture in unstable conditions. The eddy diffusivity coefficient for momentum is a function of the friction velocity and the PBL height. It has an explicit treatment of the entrainment at the PBL top, where the entrainment is proportional to the surface buoyancy flux.

The turbulence diffusion equations for prognostic variables (U, V, Θ, Q, C) are in this

scheme expressed by:

$$\frac{\partial \Theta}{\partial t} = \frac{\partial(-\overline{w'\Theta'})}{\partial z} = \frac{\partial}{\partial z}\left[K_h\left(\frac{\partial \Theta}{\partial z} - \gamma_h\right) - \overline{w'\Theta'_h}\left(\frac{z}{h}\right)^3\right], \quad \text{for } z < h. \tag{3.24}$$

K_h is the eddy diffusivity for Θ and γ_h is the counter-gradient term representing the non-local mixing due to large convective eddies (Troen and Mahrt, 1986). K_h is computed as:

$$K_h = Pr^{-1} k w_s z \left(1 - \frac{z}{h}\right)^2, \tag{3.25}$$

where $k = 0.4$ is the von Kármán constant, z the distance from the surface and h the boundary layer height. The velocity scale w_s is represented by:

$$w_s = (u_*^3 + 7k w_*^3 z/h)^{1/3}, \tag{3.26}$$

where u_* is the surface friction velocity and $w_* = [(g/T_0)(\overline{w'\theta'_0}h)]^{1/3}$ the convective velocity scale. The Prandtl number, Pr, approximating the ratio of momentum (kinematic) and thermal diffusivity, varies within the boundary layer according the local stability and has profile similar to the case of eddy diffusivity:

$$Pr = 1 + (Pr_0 - 1)\exp[-\nu(z - \chi h)^2/h^2]. \tag{3.27}$$

Pr_0 is the Prandtl number at the surface layer, ν is an empirical constant, and χ the ratio of the surface layer height and the PBL height ($\chi = 0.1$).

The last term on the right side in the Eq. (3.24) presents the entrainment heat flux at the top of the PBL. It can be parameterized as:

$$\overline{w'\Theta'_h} = -A(w_*^3 + B u_*^3)/h, \tag{3.28}$$

A and B are numerically estimated constants.

The PBL top is calculated based on the critical bulk Richardson number Ri_b - where it has zero value ($Ri_b = 0$):

$$Ri_b(z) = \frac{g(\Theta_v(z) - \Theta_s)z}{\Theta_{va}(U(z)^2 + V(z)^2)}. \tag{3.29}$$

Under the stable regime K profile for free atmosphere is used.

3.3.2.2 MYJ PBL scheme

The Mellor-Yamada-Janjić (MYJ) PBL scheme parameterizes the turbulence with a nonsingular implementation of the Mellor-Yamada Level 2.5 turbulence closure model (Mellor and Yamada, 1982) through the range of the atmospheric turbulent regimes.

The Level 2.5 closure model is governed by the equation for turbulence kinetic energy e (Mellor and Yamada, 1982, see also Eq. (1.4)):

$$\frac{de}{dt} - \frac{\partial}{\partial z}\left[l q S_q \frac{\partial e}{\partial z}\right] = P_s + P_b - \epsilon. \tag{3.30}$$

S_q is an empirical constant ($S_q = 0.2$). Shear production, P_s, buoyant production, P_b, and model dissipation, ϵ, terms are further:

$$P_s = -\overline{w'u'}\frac{\partial U}{\partial z} - \overline{w'v'}\frac{\partial V}{\partial z}, \tag{3.31}$$

$$P_b = \beta g \overline{w'\Theta'_v}, \tag{3.32}$$

$$\epsilon = \frac{(2e)^{3/2}}{B_1 l}. \tag{3.33}$$

The average turbulent fluctuation terms are defined as:

$$\overline{u'w'} = K_m \frac{\partial U}{\partial z}, \quad \overline{v'w'} = K_m \frac{\partial V}{\partial z}, \quad \overline{\theta'w'} = K_h \frac{\partial \Theta}{\partial z}, \tag{3.34}$$

$$K_m = l(2e)^{1/2} S_m, \qquad K_h = l(2e)^{1/2} S_h, \tag{3.35}$$

where K_m and K_h are the vertical turbulent exchange coefficients for momentum and heat respectively. $B1$ is empirical constant, and $\beta = -(\partial\rho/\partial T)_p/\rho$ is the coefficient of thermal expansion. The momentum and heat stability functions , $S_M = S_M(G_M, G_H)$ and $S_H = S_H(G_M, G_H)$, are calculated as theoretical extensions from a base of neutral turbulent flow data, where:

$$G_M = \frac{l^2}{2e}\left[\left(\frac{\partial U}{\partial z}\right)^2 + \left(\frac{\partial V}{\partial z}\right)^2\right], \tag{3.36}$$

$$G_H = -\frac{l^2}{2e}\beta g \frac{\partial \Theta_v}{\partial z}. \tag{3.37}$$

S_M and S_H depend on numerous empirically determined constants, as well. Master length scale, l, is calculated as:

$$l = l_0 kz(kz + l_0)^{-1}, \quad l_0 = a_0 \frac{\int_0^\infty |z| e^{1/2} dz}{\int_0^\infty e^{1/2} dz}, \quad a_0 = \text{const.} \tag{3.38}$$

The differential equation for e production and dissipation is solved iteratively. The upper limit, PBL height, depends on the e, the buoyancy and shear of the driving flow, and is defined in the functional form separately for stable and unstable conditions. In the unstable conditions, the PBL height is derived from the requirements that the turbulent kinetic energy production is nonsingular in the case of growing turbulence. In the stable conditions, the upper PBL height is derived from the requirement that the ratio of the variance of the vertical velocity deviation and e cannot be smaller than that corresponding to the regime of vanishing turbulence.

The empirical constants of the scheme have been revised in Janjić (2002).

3.3.3 Surface layer physics parameterizations

Surface layer is defined as the layer near the earth's surface (usually 10 - 100 m thick) in which the turbulent fluxes are approximately constant with height. In this layer the mechanical (shear) generation of turbulence exceeds buoyant generation or consumption.

The SLP schemes in model calculate the stability dependant friction velocities and exchange coefficients that enable the calculation of surface heat and moisture fluxes by the LSMs and surface stress in the PBL scheme. Over water surfaces the surface fluxes and surface diagnostic fields are computed in the surface layer itself.

Two SLP schemes are available in 2.2 version of the WRF-Chem model, each option tied to particular PBL parametrization. Both SLP schemes use the similarity hypothesis of Monin and Obukhov (1954) as a basis for the description of mean wind speed and temperature as a function of height in the surface layer. In the Monin-Obukhov theory four dimensional scales for the surface layer are defined:

Friction velocity, a velocity scale: $u_* = (\tau_0/\rho)^{1/2}$
Surface layer temperature scale: $\Theta_* = F_{v0}/u_*$
Obukhov length, a length scale: $L = -u_*^3 \overline{\Theta_v}/k\, g\, F_{v0}$
Height about the ground scale: z

τ_0 is the turbulent stress at the surface, F_{v0} is a kinematic virtual heat flux at the surface, Θ_v virtual temperature, and k von Kármán constant. The key scales are used to express all surface layer flow properties as dimensionless functions of z/L. For example, the mean wind shear can be written as:

$$\frac{\partial \overline{V}}{\partial z} = \frac{u_*}{z} f\left(\frac{z}{L}\right), \tag{3.39}$$

where f is a universal function of the dimensionless height z/L. The forms of the f functions, which can be determined theoretically or empirically, differ between parameterizations. From equation (3.39) friction velocity, u_*, and further kinematic turbulent momentum flux, $u_*^2 = \overline{u'w'}$, can be expressed. Following the same procedure for flux temperature, Θ_*, and similar flux variables for water vapor, q_*, and other gases, χ_{m*}, and with the hypothesis that the fluxes in the surface layer are uniform with height, the sensible heat flux, and fluxes of water vapor and other gases can be calculated. References for description of exact expressions of flux variables and fluxes for different stability regimes above land and water can be for two model LSP schemes found in Skamarock et al. (2005).

3.4 WRF-Chem chemistry

The Eulerian continuity equation for chemical specie, i, describes the time dependency of the average species concentration, $C_i = m_i/m_{air}$, within each grid cell volume as a sum of all physical and chemical processes operating on that volume:

$$\begin{aligned}\frac{\partial C_i}{\partial t} &= -\nabla \cdot (\mathbf{v} C_i) + \nabla \cdot (K \nabla C_i) \\ &\quad + \left.\frac{\partial C_i}{\partial_t}\right|_{Chemistry} + \left.\frac{\partial C_i}{\partial_t}\right|_{Emission} + \left.\frac{\partial C_i}{\partial_t}\right|_{Removal}\end{aligned}$$

Terms on the right-hand side represent advection, turbulent diffusion, chemical transformations, sources of primarily pollutants (emissions) and removal by dry deposition and wet scavenging, respectively.

In WRF-Chem the Eulerian continuity equations for chemical species are written in the form of Eq. 3.13 for mixing ratios of water vapor, rain etc., thus for mixing ratio of specie i, as:

$$\frac{\partial \mu C_i}{\partial t} + \nabla \cdot (\mathbf{V} C_i) = F_{C_i}. \tag{3.40}$$

F_{C_i} includes terms for chemical transformations, turbulent mixing, sources from emissions, and deposition for pollutant i. In these equations similarly as in Eq. 3.13, μ is the weight of dry air per unit area within the column, and $\mathbf{V}$ are by μ multiplied covariant velocities. The prognostic equations are discretized in time and space in a finite volume formulation and calculated in every model time-step.

The calculation of turbulent mixing (diffusion) of pollutants depends on the selection of PBL parametrization scheme (described in Section 3.3.2). Description of model chemical mechanism, emissions, deposition, is given below.

3.4.1 Chemical mechanism

For the calculation of chemical transformations in the WRF-Chem model incorporated modified Regional Acid Deposition Model, version 2 (RADM2, Chang et al. (1989)), was used. RADM2 mechanism was originally developed by Stockwell et al. (1990). This mechanism is

widely used in atmospheric models and presents the compromise between chemical detail, accurate chemical predictions and computer resources. WRF-Chem model offers also some other options for calculations of chemical transformations, which were not used in our simulations.

In real world hundreds of different VOCs are emitted into the atmosphere. In model the complex organic chemistry is presented through a reactivity aggregated molecular approach. Organic species are grouped together into lumped species based on similarity in oxidation reactivity. Categories of VOC with large reactivity differences and complicated secondary chemistry are represented by larger number of intermediates and stable species. The aggregation of anthropogenic VOCs into lumped species for the purpose of our study, is described in Chapter 4).

RADM2 mechanism for anorganic species includes 14 stable species, 4 reactive intermediates (O^3P, O^3D, HO, HO_2) and 3 stable species (O_2, N_2, H_2O), while organic chemistry is represented by 26 stable species and 16 peroxy radicals.

Mechanism includes altogether 158 reactions among these species, 21 of them are photolysis reactions, such as:

$$\begin{aligned} NO_2 + h\nu &\rightarrow O(^3P) + NO, \\ O_3 + h\nu &\rightarrow O(^1D) + O_2, \quad \text{etc.} \end{aligned}$$

Photolysis frequencies for photolysis reactions are calculated at each grid point according to Mandronich (1987). In general, the photolysis frequency of the gas i, J_i, is given by the integral of the product of the actinic flux $I_A(\lambda)$, the absorption cross sections $\sigma_i(\lambda)$, and the quantum yields $\phi_i(\lambda)$ over the wavelength λ:

$$J_i = \int^{\lambda} I_A(\tau, \lambda) \cdot \sigma_i(\lambda) \cdot \phi_i(\lambda) d\lambda. \tag{3.41}$$

The rate constants k_r for majority altogether 124 thermal reactions are of the form $k_r = a \cdot \exp(-b/T)$, with coefficients a and b defined separately for each reaction. For example:

$$\begin{aligned} O(^3P) + NO_2 &\rightarrow NO + O_2 && a = 6.5 \cdot 10^{-12}, b = -120\,\mathrm{K} \\ O(^1D) + N_2 &\rightarrow O(^3P) + N_2 && a = 1.8 \cdot 10^{-11}, b = -110\,\mathrm{K} \\ O(^1D) + O_2 &\rightarrow O(^3P) + O_2 && a = 3.2 \cdot 10^{-11}, b = -70\,\mathrm{K}, \end{aligned}$$

and similarly for other thermal reactions the same form of k_r, where unit of a is cm^3 $\mathrm{molecule}^{-1}$ s^{-1}. The rate constants for the rest of RADM2 chemical mechanism reactions such as:

$$\begin{aligned} HO_2 + NO_2 &\rightarrow HNO_4, \\ NO + HO &\rightarrow HONO, \quad \text{etc.} \end{aligned}$$

and

$$\begin{aligned} O(^3P) + O_2 &\rightarrow O_3, \\ HO_2 + HO_2 &\rightarrow H_2O_2, \quad \text{etc.} \end{aligned}$$

are more complex functions of temperature and concentration of air [M] in molecules cm^{-3}. In general the reactions of RADM2 mechanism comprise chemical processes described in Introduction, Section 1.2.

3.4.2 Biogenic emissions

WRF-Chem version 2.2 has a biogenic emission module based on the description of Guenther et al. (1994); Simpson et al. (1995) and Schoenemeyer et al. (1997). The module on-line estimates emissions of isoprene, monoterpenes, other biogenic VOC and nitrogen emissions based on land cover category. These emissions are further disaggregated into RADM2 classes. The emission of isoprene by forests depends on both temperature and photosynthetic active radiation. The isoprene emissions of agricultural and grassland areas are considered to be functions of the temperature only. The emissions of monoterpenes, OVOC and nitrogen are also treated only as a functions of the temperature.

It must be noted, that by this approach the true nature of biogenic emissions can be only roughly estimated. For the Mediterranean area for example, biogenic emission fluxes from trees (e.g. holm oak, stone pine, aleppo pine) present significant addition to total VOC emissions. These emissions might not be presented accurately enough in the model, as well as biogenic emissions over the "green" Slovenia might be underestimated.

3.4.3 Anthropogenic emissions

There is no single tool for constructing the anthropogenic emissions data. Currently, only for United States, southern Canada and northern Mexico, anthropogenic emissions data and the necessary conversion tables are available for modeling the photochemistry with a WRF-Chem model. Consequently, I had to develop a method for preparing the anthropogenic emissions for our domain and for the RADM2 chemical mechanism used. As this was a rather big task, the construction of anthropogenic emissions is presented in a separate Chapter 4.

3.4.4 Dry deposition

Dry deposition is an important removal process for the gases in the lower layer of the atmosphere. It is calculated by multiplying concentrations C_l in the lowest model layer by the spatially and temporally varying deposition velocity, v_d:

$$v_d = \frac{1}{r_a + r_b + r_s}. \tag{3.42}$$

The aerodynamic resistance r_a represents bulk transport through the lowest layer by turbulent diffusion. The magnitude of r_a depends on surface roughness, wind speed, solar insolation, and atmospheric stability. r_b represents molecular diffusion through the thin layer of air directly in contact with surface, and depends only on the molecular diffusivity of each pollutant species. The surface resistance r_s depends upon the physical and chemical properties of the surface. It is derived from the resistances of the surfaces of the soil and the plants using seasonal land use data (Wesley, 1989).

3.5 Model setup and initialization

In our simulations the model was set up with three nested domains (D1, D2, D3) with horizontal resolution of 27 km, 9 km and 3 km, and 125×90, 124×88 and 112×88 horizontal grid points, respectively (Fig. 3.3). Domain D1 simulated synoptic scale meteorological conditions and was required because it provided chemical lateral boundaries for the inner D2 domain. The location of domain D2 enabled modeling of the industrialized Po Basin pollution and the eventual transport of polluted air masses to Slovenia in relatively good resolution. The inner

D3 domain was used to capture local scale features over Slovenia. Since the ozone exceedences most often occur at the Mediterranean part of the country, as well as trajectory analysis and model results show importance of Adriatic coastal regions, the center of D3 domain was shifted toward south-west from the center of Slovenia.

Simulations with different domain extensions, model resolutions (vertical and horizontal) and nesting strategies were performed, before the final configuration was chosen. For example, we started simulations with 81 vertical levels, without outer 27 km resolution domain and with additional 1 km domain centered in Ljubljana. Nevertheless, simulations of the extreme ozone events suggested, that chemical lateral boundary conditions at the 9 km domain (D2 in Fig. 3.3) needed to be provided more accurately and not just taken from the idealized profile specified in WRF-Chem chemistry routines. The outer D1 domain with 27 km resolution was thus added and consequently (because of large memory requirements) the inner most 1 km domain was excluded from regular simulations. To speed up the calculations of usually long lasting ozone episodes, we also decided to reduce the number of vertical levels from 81 to 51. But the high near ground vertical resolution with about 25 levels located within the lowest 2 km was retained. The comparison of the results of simulations performed with 81 and 51 vertical model levels for one of the high ozone episodes revealed no considerable deviations (results are not presented) in the near ground ozone fields. Nevertheless, the reduction of vertical levels may at least at higher altitudes (higher altitude sites, e.g. Krvavec) still to some extent influence the final results. The exact definition of 51 vertical levels in terms of η can be found in Appendix D under *eta_levels* namelist variable.

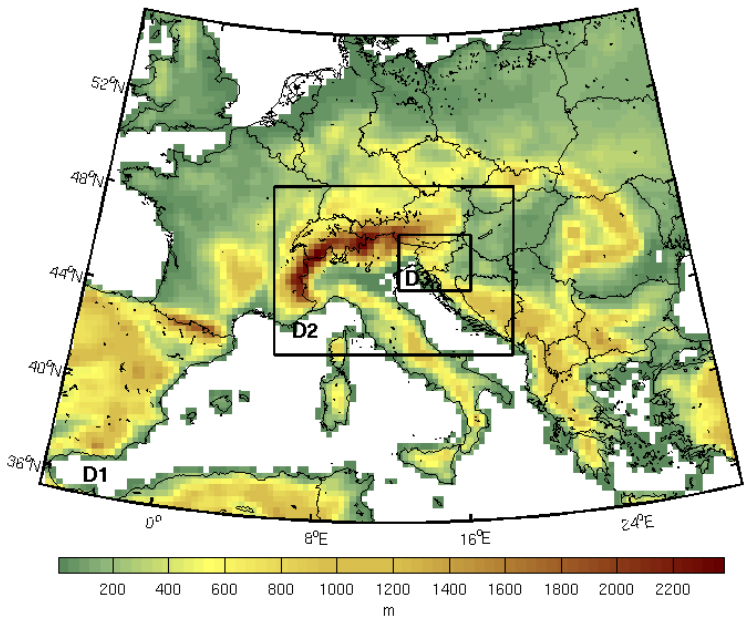

Figure 3.3: Modeling domains D1, D2 and D3 with horizontal resolution 27 km, 9 km and 3 km, respectively. Orography above 5 meters as represented in domain D1 (with 27 km resolution) is drawn in the background.

Simulations in 27 km, 9 km and 3 km domains were performed using a coupled one-way nesting strategy. The calculations on this three domains in this strategy were so performed simultaneously with feedback from the inner to outer domain turned off (option feedback set to zero in the namelist; Appendix D). The information thus propagated from outer to inner domain at every time step, but not in the opposite direction. In this way we avoided noise at boundaries in the outer domains and were able to compare results with different resolutions directly.

The initial and boundary meteorological conditions were taken from ECMWF analysis archive data with the horizontal resolution of 0.25° by 0.25° and the temporal resolution of 6 hours. We started the simulations a few days before the beginning of the high ozone episode (at least 3 to 4 days, usually even more), to allow the pollution to accumulate it the air masses. This output fields were then used for initialization of the chemistry on the first day of the episode simulation (meteorology was initialized again from the ECMWF analysis). In WRF-Chem version 2.2 data assimilation or observation-nudging is not supported. To stay close to the true meteorological conditions we re-initialized meteorology from ECMWF analysis typically every 2-5 days during the simulation. At each of these intermediate meteorology re-initializations we initialized chemistry from the previous run.

The simulations were performed with two different PBL options and two different land surface models, altogether thus with four different model configurations. Other model options, which were fixed in these simulations, can be seen in Appendix D. Table 3.1 summarizes some of them. In detail the meaning of these options (and the options not selected) is explained in Wang et al. (2007).

Table 3.1: Physical and chemistry options used in simulations.

Item	Selection
Cumulus option	Grell-Devenyi (D1 and D2), none for D3
Cloud effect in radiation scheme	Considered
Long wave radiation option	RRTM scheme
Short wave radiation option	Goddart scheme
Boundary layer option	Thermal diffusion or Noah land-surface scheme
Surface physics option	YSU or MYJ scheme
Microphysics scheme	Ferrier microphysics
Chemistry option	RADM2 mechanism, no aerosol
Subgrid convective transport	Turned on
Biogenic emission option	Guenther scheme
Photolysis option	Madronich photolysis

3.6 Monitoring sites used for model validation

Figure 3.4 shows locations of ground-level stations in D3 domain, measuring meteorological and ecological variables. These stations were used for model evaluation. For validation of vertical profiles of meteorological variables, radiosonde observations in Ljubljana, Udine and Zagreb were used. In Appendix A statistical scores, used in procedure of model evaluation, are presented and described.

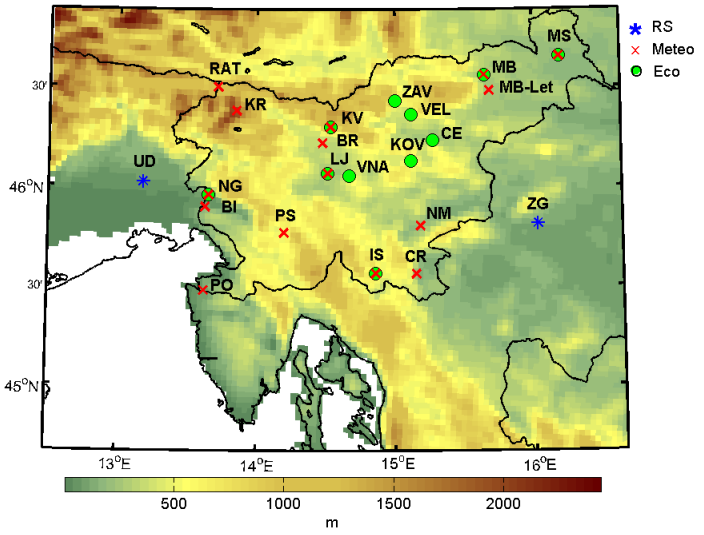

Figure 3.4: Orography as represented in the D3 domain. Denoted are stations, measuring ecological (Eco) and/or meteorological (Meteo) variables, used for model validation. Radiosoundings data (RS) from Udine, Zagreb and Ljubljana (location of the last presented with circle and cross, not with blue star) were used to validate upper level model results.

Chapter 4

Preparation of Anthropogenic Emission Database

Ozone modeling requires emission inventories of individual compounds with high temporal and spatial resolution. Significant modeling have been performed with more or less detailed inventories (e.g. Taghavi et al., 2005; Vautard et al., 2005; Mallet and Sportisse, 2005). These studies concluded that emissions are one of the crucial inputs required for running air quality models, as well as that the uncertainty of numerical results is a complex function of uncertainties of emissions of ozone precursors.

To be able to simulate ozone with a WRF-Chem model the emission database for the model domains had to be prepared, which at the same time had to meet the requirements of the RADM2 chemical mechanism, used in simulations. Since WRF-Chem model already offers an algorithm for calculating biogenic emissions online, I decided to prepare my method of inventory only for anthropogenic emissions.

In general, two different approaches for estimation of anthropogenic emissions exist. The *bottom-up* approach is based on collecting of detailed information about individual emission sources. Emissions are then calculated by multiplying an emission factor and the value of an associated activity indicator which is a quantitative parameter strictly related to the emission source (Francois et al., 2005). The *top-down* approach applies this concept to larger areas, where statistical data rather than detailed information about each source, are available. Emissions are subsequently distributed within the respective area using downscaling methods. For modeling applications on urban scale, the emission data provided by means of a bottom-up approach are required, while for mesoscale applications emissions can be estimated using a top-down methodology (Carnevale et al., 2006).

Emissions relevant for ozone processes originate from a broad spectrum of sources, such as many branches of industry, transport, agriculture and domestic sources. However, many of the data required for building a database with a bottom-up approach from "real data" were missing even for the whole Slovenia. A detailed inventory was constructed from real information about traffic, industrial and residential sources for the capital city, Ljubljana, for Zasavje region and some huge point sources, such as Šoštanj power plant. Remaining emissions for these two regions and emissions from all sources for the rest of Slovenia as well as for the neighboring countries, were estimated with the top-down approach with the temporal, spatial and chemical disaggregation of EMEP emissions (European Monitoring and Evaluation Programme; Vestreng et al., 2006).

Table 4.1: EMEP SNAP Categories.

SNAP	Description
S1	Combustion in energy and transformation industries
S2	Non-industrial combustion plants
S3	Combustion in manufacturing industry
S4	Production processes
S5	Extraction and distribution of fossil fuels and geothermal energy
S6	Solvent use and other product use
S7	Road transport
S8	Other mobile sources and machinery
S9	Waste treatment and disposal
S10	Agriculture
S11	Other sources and sinks

Based on the data available and the geographical area of interest, the emissions were separately prepared for three areas: with bottom-up approach for Ljubljana and Zasavje region (Database A), with top-down approach and higher resolution for the rest of Slovenia (Database B), and with top-down approach and lower resolution for the neighboring countries (Database C). To avoid the confusion and to enable the usage of all three databases at the same time, EMEP SNAP (Selected Nomenclature for Air Pollutants) classification of emissions from different sources (Table 4.1) was used.

A compendious description of the procedure of anthropogenic emission database construction:

Database A: ***Detailed inventory:*** For Ljubljana region emissions of primary pollutants such as CO_2, SO_2, NOx, CO, NH_3, CH_4, nmVOC (non-methan VOC), N_2O, PM10 and PM2.5 from traffic, industrial and residential sources (sectors S1, S2, S3 and S7 in Table 4.1) were inventoried from data on the yearly basis. In addition the emissions from industrial and residential sources (sectors S1, S2 and S3 in Table 4.1) for industrial Zasavje region and for thermal power plant in Šoštanj were calculated in the same way. For the temporal disaggregation of yearly accumulations to hourly emissions, the temporal profiles were calculated from real data and for each point source or road segment a corresponding temporal profile was used. For the further speciation of emitted nmVOC for chemistry simulations different profiles were used. They were selected separately for each point source, depending on the amount of different fuel types used, and for each road segment with regard to traffic density of different vehicle categories and their emission factors for average segment speed. This database was prepared in cooperation with the Energis Institute (http://www.ie-energis.si/).

Database B: ***Remaining emissions inside Slovenia:*** For sectors S1, S2, S3 and S7 yearly emissions of primary pollutants from detailed inventory (described in previous paragraph) were subtracted from corresponding EMEP grid cells. Emissions for each sector from S1 to S11 for each primary pollutant inside Slovenia were then spatially disaggregated with 100 meters resolution European Environment Agency (EEA) CORINE land cover and population density maps, always over area which was not included in the detailed inventory part (for sectors S1, S2 and S3 Slovenia without Ljubljana and Zasavje region, for sector S7 Slovenia without Ljubljana region). For road transport sector

spatial disaggregation was done considering the average annual road transport on state roads. Temporal profiles used were either the same as in detailed inventory, either were they adopted from other studies (for sectors other than S1, S2, S3 and S7). Profiles for nmVOC speciation were on the sector basis assigned according to the US Environmental Protection Agency (EPA) recommendations, except for traffic, where EEA speciation was used.

Database C: ***Emissions outside Slovenia:*** EMEP emissions were spatially disaggregated with 1 km EEA CORINE land cover and population density maps separately for each SNAP sector and each primarily pollutant. Seasonal and daily TNO-TROTREP/POET profiles (Olivier et al., 2003) were used for temporal disaggregation of sector emissions. Profiles for nmVOC speciation on the sector basis were the same as in Database B.

Databases B and C were constructed from gridded 50 km×50 km EMEP expert emissions for year 2003, while detailed A database was constructed from data for year 2005. Table C.1 in Appendix C summarizes the agreement between the sum of constructed emissions inside Slovenia (sum of databases A and B, described in detail in the following sections) and the total national emissions reported by Environmental Agency of Slovenia (ARSO, 2009). From year 2003 to 2005 SO_2 emissions from SNAP 1 sector changed significantly. This change was taken into account in simulations for episodes in year 2003. Except for higher values of CO, sum of A + B emissions for Slovenia match well with the reported national yearly emissions.

4.1 Spatial disaggregation of emissions

The EMEP emissions within a 50 km × 50 km grid square were spatially allocated based on EEA CORINE (Coordination of information on the environment) land cover data, EEA population density and average annual yearly traffic for Slovene state roads. Land cover, population density and traffic density data were used for calculation of the weighting factor maps (WFM), by which then original EMEP emission maps were multiplied for each pollutant (nmVOC, NOx, SOx, CO and NH3) from each SNAP sector separately. The resolution of final weighting factor maps was 1 km and 100 m for allocation to the 1 km and 100 m grid squares (database B and C), respectively. Geographic information system (GIS) was the main tool used in the allocation procedure.

Since the resolution of original land cover and population density maps was 100 m × 100 m (Fig. 4.1 - 4.2), maps with 1 km × 1 km resolution were calculated by aggregation of original maps into coarser grid. The values of each land cover category in aggregated 1 km resolution maps were calculated as percentage of 100 m squares of the same land cover category within the 1 km grid. With this approach as much information as possible was retained. Aggregation of population density to the 1 km grid was straightforward, aggregated map was obtained by averaging 100 m square values inside the 1 km squares.

It is evident from Fig. 4.3 - 4.4 that for some countries the land cover and population density data were missing. For these areas, as well as for regions outside the domain presented in Fig. 4.3 - 4.4 and for emissions from ships, downscalling of EMEP emissions was not applied. In these cases EMEP emissions with the original 50 km spatial resolution were used.

For each SNAP sector the decision about which information to consider at disaggregation, i.e. how to calculate the weighting factor map, was made separately. Tables 4.2 and 4.3 summarize the land cover categories to which different SNAP emissions were assigned, and for which sectors the population density was taken into account. For example, Table 4.2 shows,

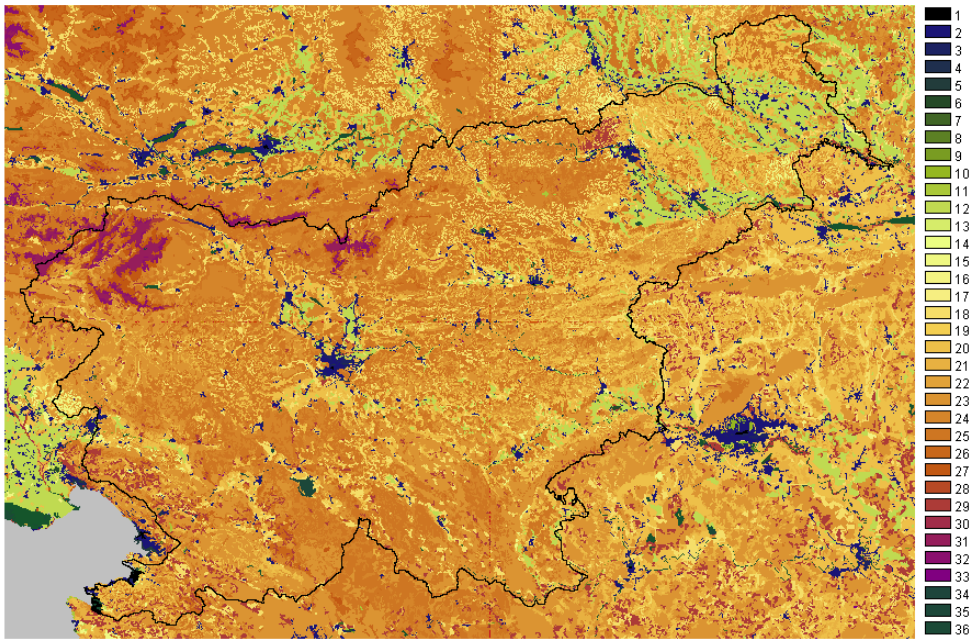

Figure 4.1: CORINE Land Cover 2000 with 100 m resolution, used for spatial disaggregation of EMEP emissions inside Slovenia. Values 1 - 11 indicate different artificial categories (urban, industrial, commercial etc.), values 12 - 22 indicate agricultural areas (arable land, permanent crops, pastures etc.), 23 - 34 different forest and semi natural areas, higher values indicate wetlands and water bodies. Detailed description of CORINE categories can be found in Appendix C.

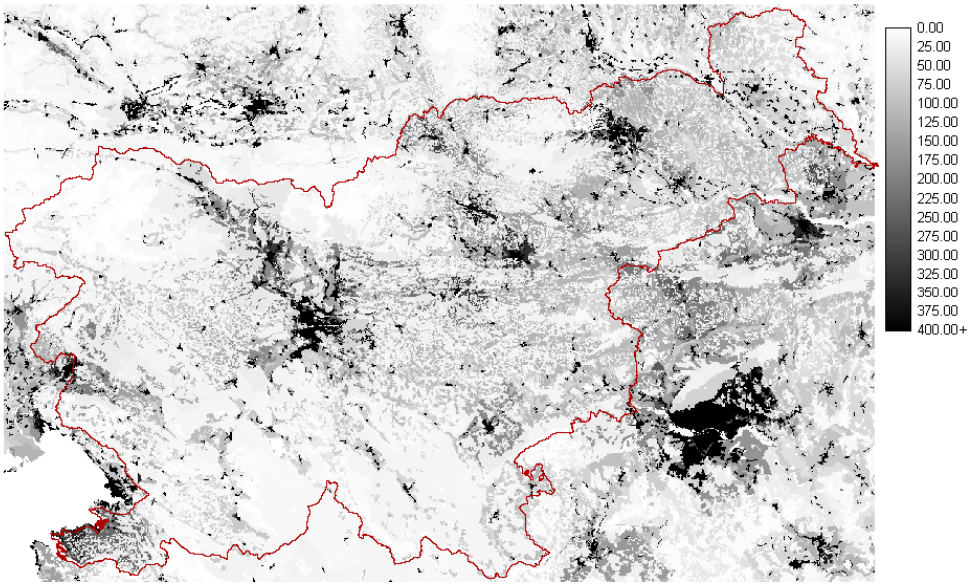

Figure 4.2: 100 m EEA population density of inhab/km^2, used for spatial disaggregation of EMEP emissions inside Slovenia.

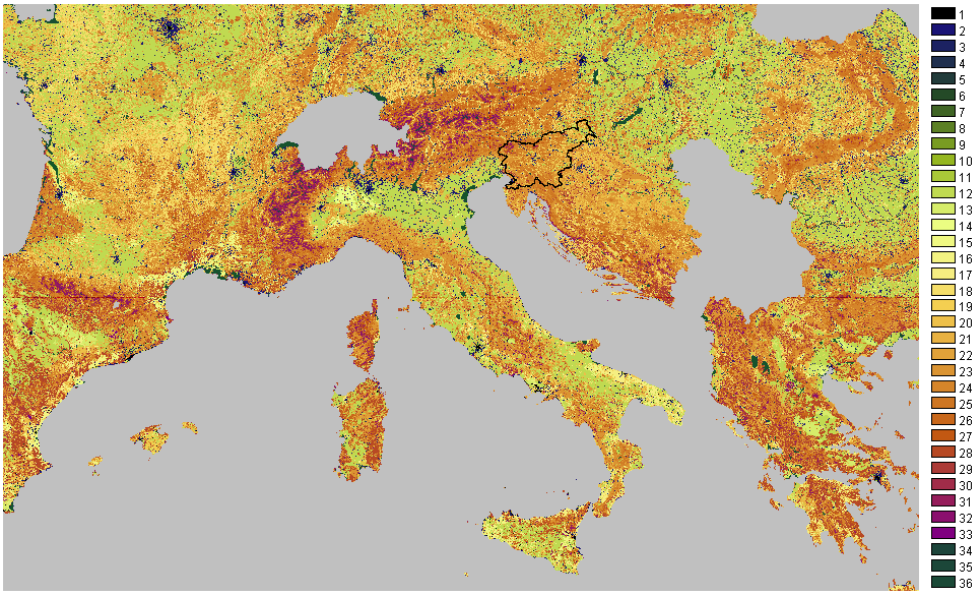

Figure 4.3: CORINE Land Cover 2000 with 100 m resolution, used for spatial disaggregation of EMEP emissions in neighboring countries. Missing are data for Switzerland, Serbia, Kosovo and Montenegro. Rough description of CORINE categories can be found in Fig. 4.1 caption.

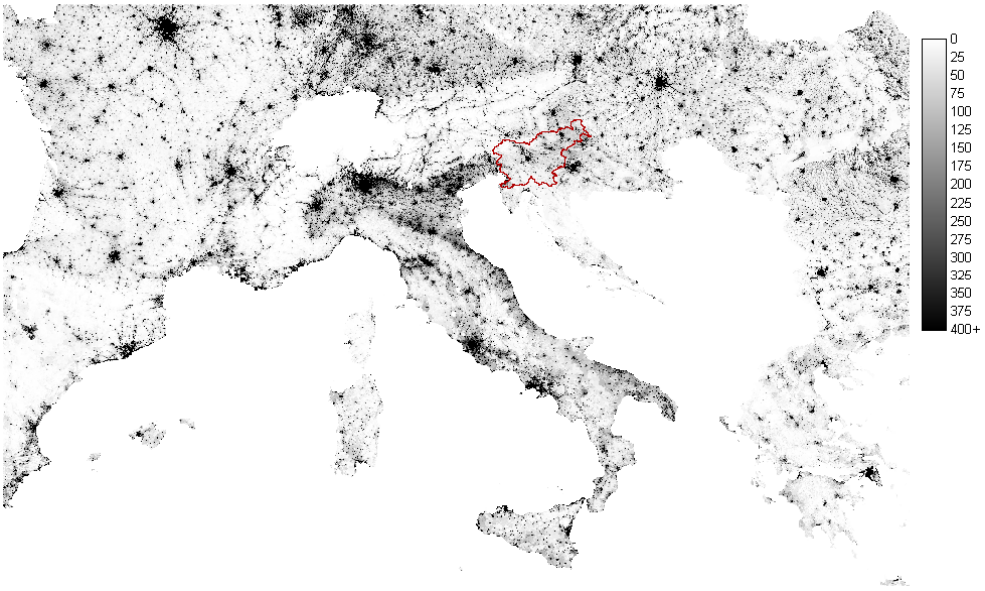

Figure 4.4: 100 m EEA population density of inhab/km2, used for spatial disaggregation of EMEP emissions in neighboring countries. Missing are data for Switzerland, Bosnia and Herzegovina, Serbia, Kosovo and Montenegro.

that the weighting factor map for SNAP 2 was calculated only from population density, while emissions from other sectors were in first place assigned to selected land cover categories (for example from SNAP 1 only to CORINE land cover categories 1 and 2). Population density was then considered in calculation of weighting factor fields for all sectors except SNAP 8 -

10. Inside Slovenia 6 different weighting factor maps were prepared, while disaggregation was performed with 3 different weighting factor maps.

The procedure for calculating the weighting factors maps was as follows:

- The first step was the preparation of the modified CORINE land cover maps for different SNAP sectors (MC^{SNAP}). These maps got value 1 at all 100 m squares with land cover categories specified in Tables 4.2, while zero values were assigned elsewhere. For example, for SNAP 8 inside Slovenia the modified CORINE land cover map was obtained by assigning value 1 to 100 m squares with original CORINE categories 5 or 6. This holds for 100 m resolution fields. In 1 km resolution outside Slovenia the percentage of selected land cover categories inside the 1 km square was assigned to each 1 km grid cell.

- For some SNAP sectors beside the CORINE land cover also the population density was used for emission disaggregation (SNAP 1, 3, 4, 5, 6, 7 inside Slovenia, Table 4.3). In that case the modified CORINE maps MC^{SNAP} from the previous step were multiplied by population density map (POP). Weighting coefficients for each 100 m grid square (WFM_{ij}^{SNAP}) were then calculated as the ratio between grid value of the multiplied field and the sum of all field values inside each EMEP grid cell. Consequently, the sum of weighting coefficients inside each EMEP grid cell was 1 (Equation 4.1 and Fig. 4.5);

$$WFM_{ij}^{SNAP} = \frac{MC_{ij}^{SNAP} \cdot POP_{ij}}{\sum_{S_E} MC_{ij}^{SNAP} \cdot POP_{ij}}, \tag{4.1}$$

  where MC_{ij}^{SNAP} and POP_{ij} are values of the modified CORINE land cover and population density in the ij-th grid cell, and WFM_{ij}^{SNAP} is the value of the SNAP weighting factor map in this grid cell. S_E is EMEP grid cell area into which falls the center of the ij-th 100 m grid square.

- If population density was not considered in the disaggregation procedure (inside Slovenia SNAP 8 - 10, outside Slovenia all except SNAP 2 and 7), then weighting factor maps were calculated as:

$$WFM_{ij}^{SNAP} = \frac{MC_{ij}^{SNAP}}{\sum_{S_E} MC_{ij}^{SNAP}}. \tag{4.2}$$

- If only the population density was considered in the disaggregation procedure (SNAP 2), then the weighting factor map was calculated as:

$$WFM_{ij}^{SNAP} = \frac{POP_{ij}}{\sum_{S_E} POP_{ij}}. \tag{4.3}$$

- Disaggregated emission maps were then calculated by multiplying EMEP maps by appropriate weighting factor maps. Examples of weighted factor maps for areas inside and outside Slovenia are shown in Appendix B. Special attention was devoted to EMEP grid squares with Slovenia state border crossings, to minimize errors at the edge of two databases.

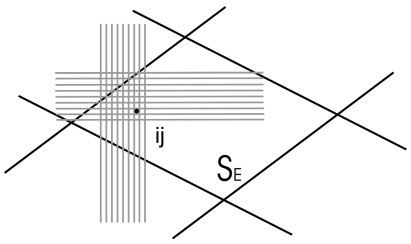

Figure 4.5: The fine scale spatial disaggregation. S_E is EMEP grid cell area and emissions from this area are then disaggregated into fine 100 m or 1 km grid, which cells are counted with ij.

Table 4.2: Data used for spatial disaggregation of individual SNAP sectors inside Slovenia. For sector 7 also traffic density at state roads was considered (not stated in table). Detailed description of CORINE categories can be found in Appendix.

SNAP	CORINE Categories	Population density
S1	1 - 2	Yes
S2	-	Yes
S3, S4, S5, S6, S7	1 - 4	Yes
S8	5 - 6	No
S9	8	No
S10	12 - 22	No

The procedure, described above, was more sophisticated for SNAP sectors 1, 2, 3, and 7 inside Slovenia. For these sectors we had to subtract the detailed database emissions from EMEP squared emissions first. Weighting coefficients were then calculated so that the sum of coefficients remained 1 inside each EMEP square, but only for area outside detailed emission database.

Road emissions for state roads inside Slovenia (SNAP 7) were estimated separately, so that average annual daily traffic for state roads in year 2005 was taken into account (Fig. 4.6). However, the ratio between different pollutant emissions and traffic density is not straightforward. It depends on the density of different vehicle types, their average speed, etc. For the purpose of this study the road emissions were estimated in a simplified manner. I calculated overall ratios between pollutant emissions and average annual traffic density for state roads inside Ljubljana region - for these roads I had emissions calculated from detailed data, considering vehicle types and average speeds on each road segment. These ratios presented empirical coefficients (K_{NO_x}, K_{VOC}, K_{NH_3}, K_{CO}, K_{SO_2}), by which average annual daily traffic was then multiplied for estimation of main pollutant emissions on state roads for the rest of Slovenia. Sum of state road emissions inside each EMEP grid was then finally subtracted from total EMEP grid for each pollutant separately, as well as were subtracted emissions from detailed emission database. The remaining EMEP traffic emissions were then finally disaggregated with appropriate weighting factor map to city centers (which are not included in the state roads database) and other urban areas. In Appendix B some examples of weighting factor maps for disaggregation inside Slovenia, as well as three maps for neighboring countries, are shown.

Table 4.3: Data used for spatial disaggregation of individual SNAP sectors outside Slovenia.

SNAP	CORINE Categories	Population density
S1, S3, S4, S5, S6, S8, S9	1 - 4	No
S2, S7	-	Yes
S10	12 - 22	No

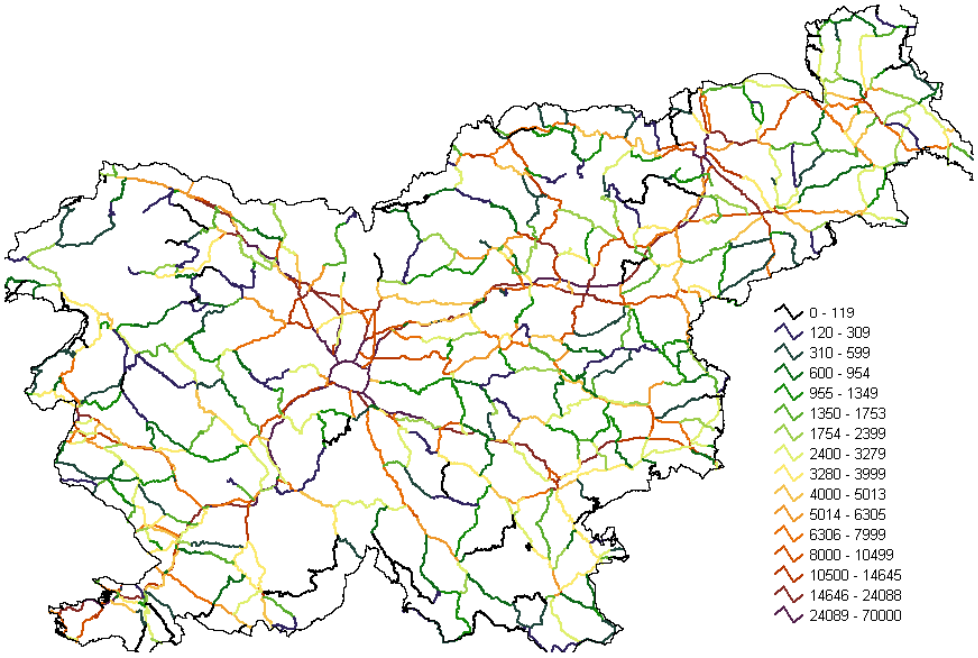

Figure 4.6: 2005 average annual daily traffic for Slovene state roads, the sum of all vehicle categories.

Approximations done so far may influence the quality of model results. But still we can hope, that emissions are estimated sufficiently well to help us understand the occurrence of high ozone phenomena and the circumstances leading to the highest measured ozone values all over the country.

Figures 4.7 - 4.10 show and example of original EMEP NO_x emissions from sector 7 (Fig. 4.7), disaggregated Database C NO_x emissions from this sector outside Slovenia (Fig. 4.8) and inside Slovenia (Fig. 4.9), and NO_x emissions from sector 7 for the Ljubljana and near surrounding region (Fig. 4.10). Note that emissions in Fig. 4.8 - 4.10 are expressed in different units (Mg year^{-1} per 1 km $\times$1 km or Mg year^{-1} per 100 m $\times$100 m).

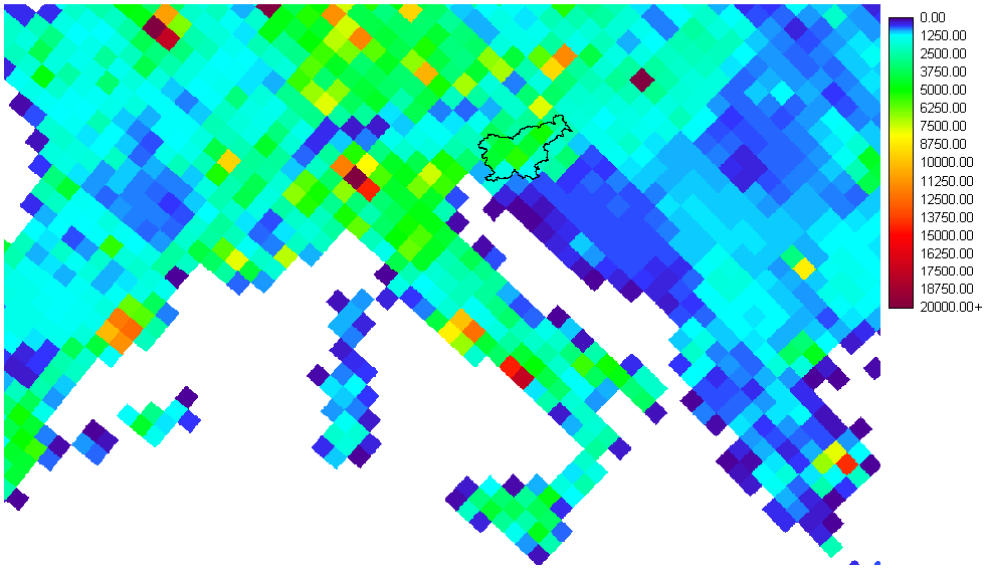

Figure 4.7: Gridded original 50 km ×50 km expert EMEP NO_x emissions for SNAP sector 7 in Mg year^{-1} for year 2003. Maximum value: 31675 Mg year^{-1} per 50 km ×50 km.

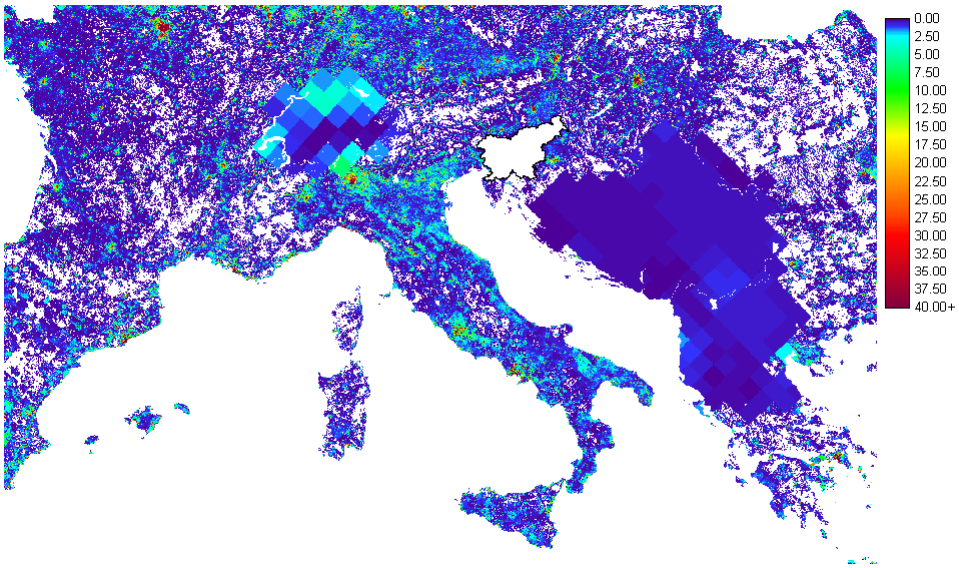

Figure 4.8: Disaggregated NO_x EMEP emissions from SNAP 7 outside Slovenia in Mg year^{-1} per 1 km ×1 km square with the horizontal resolution 1 km ×1 km. Maximum value: 4854 Mg year^{-1} per 1 km ×1 km.

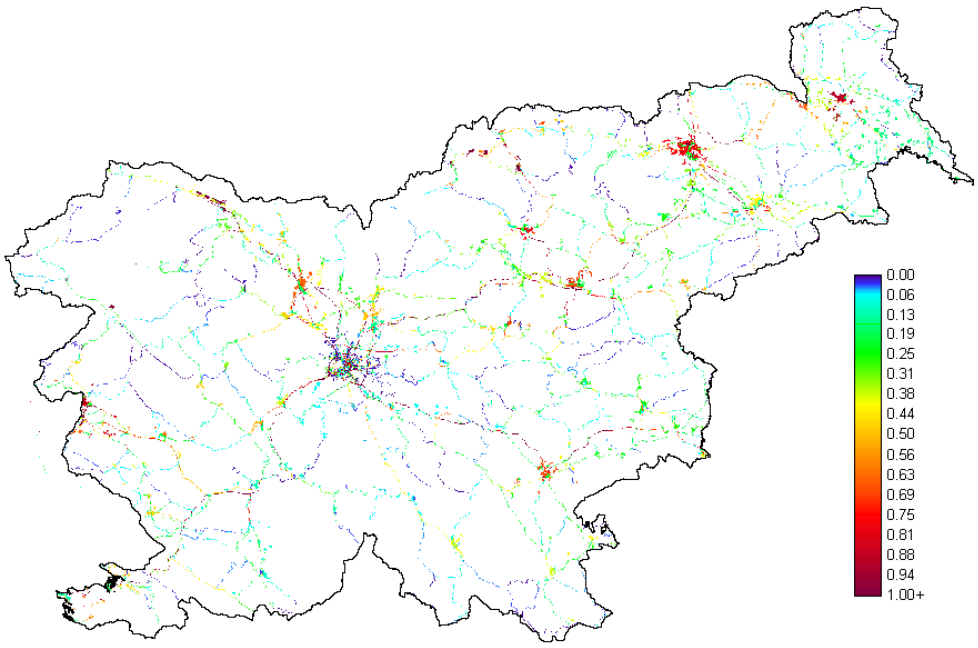

Figure 4.9: NO_x emissions inside Slovenia from sector 7. Map presents the sum of sector 7 NO_x emissions from detailed database A for Ljubljana, estimated state road emissions and disaggregated remaining EMEP emissions (database B). The spatial resolution is 100 m ×100 m, NO_x emissions are in Mg year^{-1} per 100 m ×100 m square. Maximum value: 12.8 Mg year^{-1} per 100 m ×100 m.

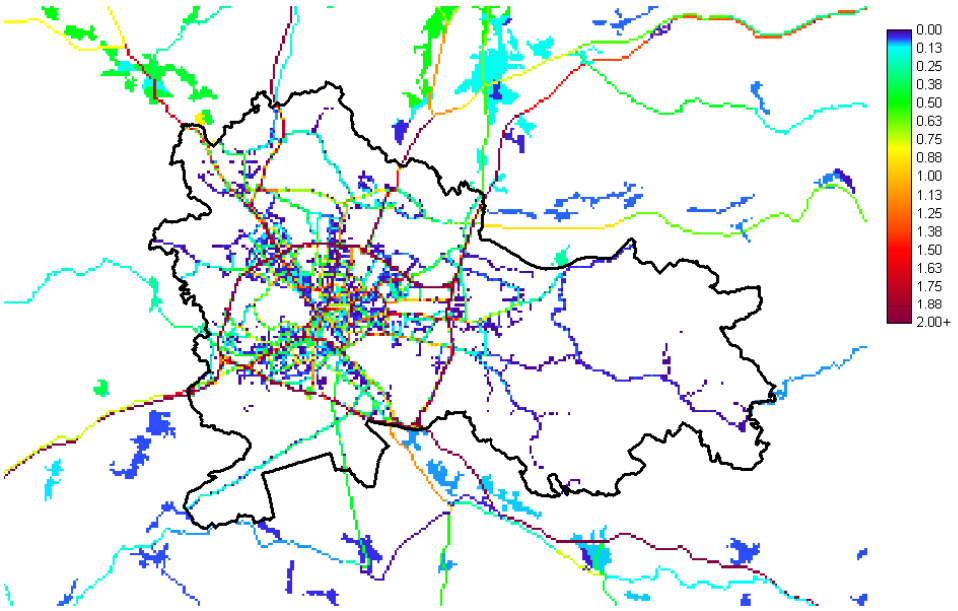

Figure 4.10: NO_x emissions in Mg year^{-1} per 100 m×100 m square from sector 7 for Ljubljana and near surrounding (zoom of Fig. 4.9).

4.2 Temporal disaggregation of emissions

Broadly speaking, the emissions can vary on three timescales: with season, with day of the week and with hour of day. A correct description of the seasonal dependence is important, because the photochemical conditions required for ozone formation occur during the summer months. The diurnal variations are also important, particularly for very reactive nmVOC which are rapidly oxidized during the daylight hours. The variation of emissions on time scales of a week, is believed to provide an explanation for the observed prevalence of photochemical ozone episodes on particular days of the week (Jenkin and Clemitshaw, 2000).

Temporal variations of emissions over all three corresponding timescales were considered for all three databases with different spatial resolution, separately for each SNAP sector. The daily and annual profiles for Ljubljana and Zasavje region for sectors S1, S2, S3 and S7 were calculated from the empirical data. These profiles are presented in Fig. 4.11 - 4.13. For each point source from sectors S1, S2 and S3 (industry and residential) in detailed database A the most reasonable yearly and daily profile was selected. For emissions outside Slovenia, e.g. for database C, temporal profiles estimated in POET project (Olivier et al., 2003) were used (Fig. 4.14 - 4.16). For disaggregated EMEP emissions inside Slovenia (database B) temporal profiles for sectors S1, S2, S3 and S7 were selected from detailed database profiles as shown in Table 4.4), and for the other sectors the same POET profiles as outside Slovenia (Fig. 4.14 - 4.16) were applied. The POET weekly profiles (Fig. 4.15) were used in all three databases.

Temporal profiles were used also for the regions were due to missing population and/or land cover data downscalling of EMEP emissions was not performed.

Table 4.4: Temporal profiles, selected for some sectors for database B - EMEP emissions inside Slovenia. Profile names correspond to Figures 4.11 - 4.13.

SNAP	Daily Profile	Yearly Profile
S1	Ind 1	Ind 2
S2	Res Summer	Res
S3	Ind 2	Ind 2
S7	Traff 3	Traff

Hourly emissions, E^p_{mdh}, of pollutant p for the month m, weekday d and hour of the day h, were calculated as:

$$E^p_{mdh} = E^p_{snap} \times \frac{Y_{snap}(m)}{12} \times \frac{W_{snap}(d)}{30.417} \times \frac{D_{snap}(h)}{24}, \tag{4.4}$$

where E^p_{snap} are yearly emissions of pollutant p from sector $snap$, while Y_{snap}, W_{snap} and D_{snap} are associated yearly, weekly and daily profiles, respectively.

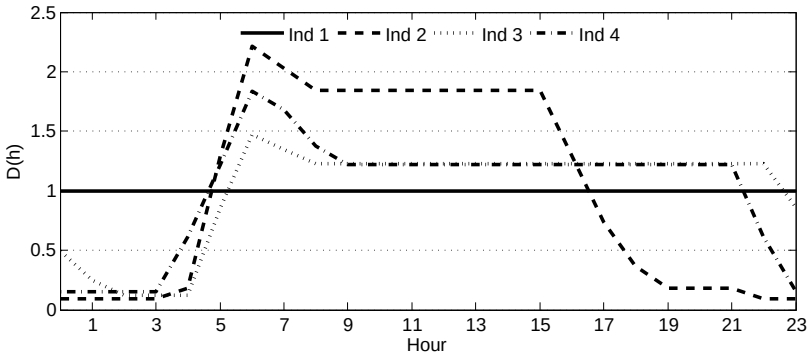

Figure 4.11: Daily profiles, calculated from data in detailed emission database for industrial sources (Ind 1: constant emission, Ind 2: one shift industry, Ind 3: two shifts industry, Ind 4: heat production industry).

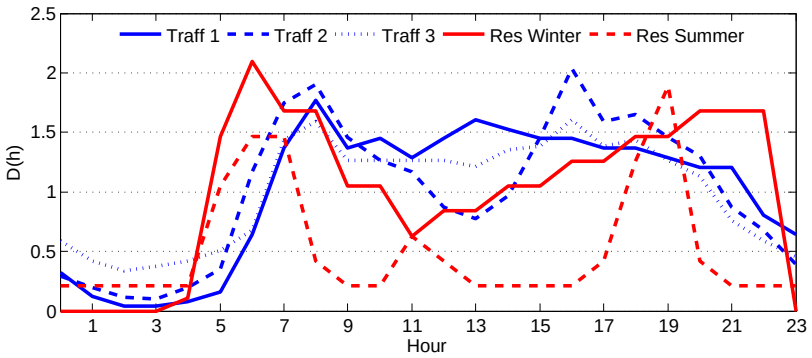

Figure 4.12: Daily profiles, calculated from data for detailed emission database for road transport (Traff 1: city centers, Traff 2: local traffic, Traff 3: motorways), summer and winter profiles for residential sources (Res Summer, Res Winter).

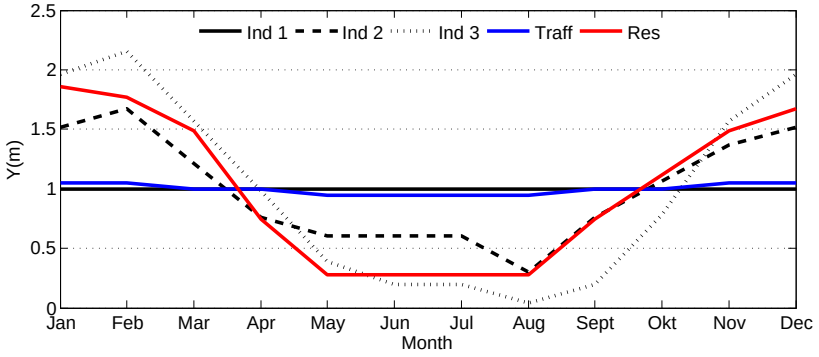

Figure 4.13: Annual profiles, calculated from data for detailed emission database for three different types of industrial sources (Ind 1: constant emission, Ind 2: ordinary industrial sources, Ind 3: heat production industry), for Road Transport (Traff) and residential sources (Res).

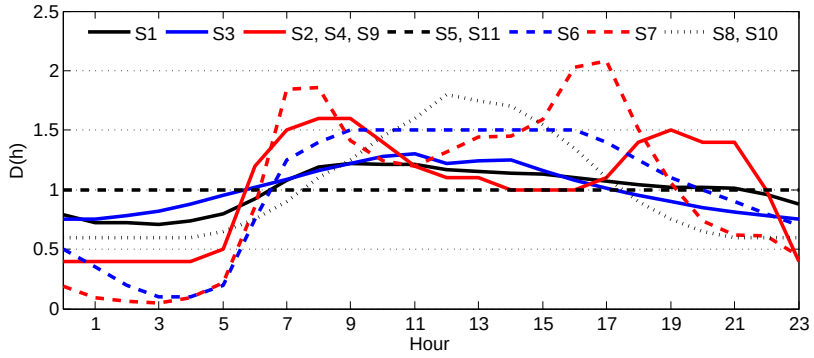

Figure 4.14: Daily profiles from POET project (Olivier et al., 2003), applied to disaggregated EMEP emissions outside Slovenia and partly also for disaggregated EMEP emissions inside Slovenia.

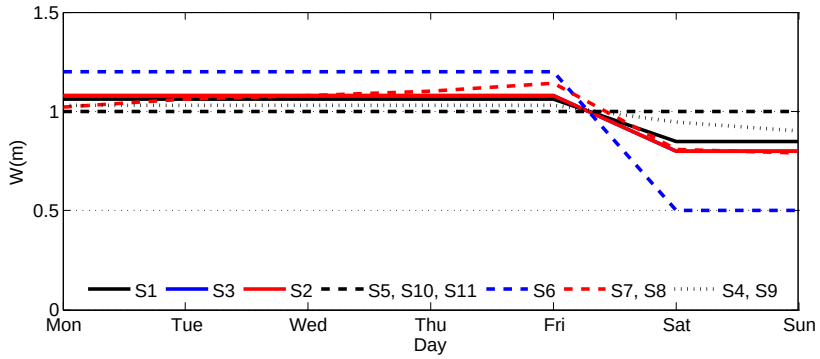

Figure 4.15: Weekly profiles from POET project (Olivier et al., 2003), applied to all three emission databases.

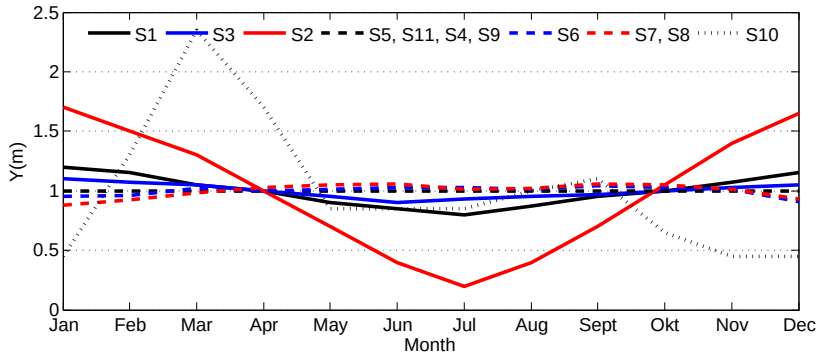

Figure 4.16: Monthly profiles from POET project (Olivier et al., 2003), applied to disaggregated EMEP emissions outside Slovenia and partly also for disaggregated EMEP emissions inside Slovenia.

4.3 Speciation of organic gases

Volatile organic compounds (VOCs) differ significantly in their effect on ozone formation, and these differences need to be represented appropriately in the models. Usually emissions of organic gases are typically reported in emission inventories only as aggregated organics, in our case as non-methane volatile organic compounds (nmVOC), which is in practice synonymous to reactive organic gases (ROG). For ozone modeling purpose, separate VOC compounds need to be speciated and in the next step the species need to be aggregated into groups with similar reactivities, determined by the chemical mechanism used in the model (in our case RADM2). At this procedure, we mainly follow EPA's CHIEF's emissions modeling clearinghouse (EMCH) website on VOC speciation. The exception were on-road emissions, where speciations for different vehicle types provided by EEA, were used. For final lumping of chemical species into RADM2 groups we used Carter's emitdb.xls Excell database (Carter, 2007). The speciation of nmVOC for modeling chemistry with RADM2 chemical mechanism implemented in WRF-Chem model for each source type in detailed database and for each SNAP sector in other two databases, thus consisted from the following steps:

1. The selection of the most appropriate source classification code (SCC) from EPA's SCC descriptions (www.epa.gov/ttn/chief/codes/scc_feb2004.xls).

2. The assignment of speciation profile based on selected SCC with the usage of EPA's Speciate version 4.0 (Hsu et al., 2006).

3. Conversion of nmVOC to total organic gases (TOG) and multiplication of the assigned profile's split factors times the TOG to estimate emissions of different compounds.

4. The assignment of different species to lumped RADM2 model species according to Carter (Carter, 2007).

For EMEP nmVOC speciation the procedure and profiles used are briefly presented here. For detailed database the methodology was similar. The main difference was that more profiles were used for different point sources according to different fuel types used, and that the speciation of road nmVOC emissions was done according to EEA CORINAIR profiles for different vehicle fuel types. Table 4.5 shows selected SCC assignments for major source types and the selected VOC profiles in Speciate database. For speciation of EMEP VOC emissions only these profiles were used. Table 4.6 shows VOC profile and corresponding VOCtoTOG conversion factor used for individual sectors. For sectors S2 (residential) and S3 (industry) the combination of three or four profiles was used according to mass proportion of different fuels used in sector. This fuel mass proportions were calculated on Ljubljana data.

With Table 4.6 the mass percentage of different VOC species in each snap sector is exactly defined. Namely, each of the VOC profiles in Table 4.6 has a known composition. An example for VOC profile number 2 shows Table 4.7, where the mass percentage of VOC species involved in this profile is presented. Similar tables are available also for other profiles, but since the number of species in some profiles is numerous, the tables are not shown here here. From the mass of total VOC emissions (in tons per year), E, the mass of each specie in profile is thus calculated as $E \times \mathrm{VOCtoTOG} \times \mathrm{Weight\,Percent}/100$. The final step is the calculation of *lumped RADM2 species* for modeling needs (from individual compounds to model species) with the help of Carter database (Carter, 2007). For profiles in Table 4.6 used for EMEP VOC speciation, Table 4.8 presents the final conversion table. This table summarizes results from all above described steps (step 1. to 4.).

Actually, in these final conversion factors (Table 4.8) all steps described so far are included: VOC toTOG conversion, mass decomposition like presented in Table 4.7, conversion from mass units (tons) to moles by dividing with specie molecular weight, and aggregation of individual species into RADM2 lumped species.

Input for the WRF-Chem model are chemical emissions of lumped species in units of mole per square kilometer per hour for all the gaseous chemical species - VOCs and other four main pollutants. Table C.2 in Appendix C collects the gaseous pollutants required by the model RADM2 mechanism and at the same time shows final splitting of two RADM2 lumped species for modeling purpose. Moles of VOC lumped species are calculated as descried above, moles of NH_3, CO, SO_2 are computed straightforward from mass and molecular weight. NOx emissions are first splitted into 90% of NO (in mass) and 10% of NO_2 and then converted to moles.

Table 4.5: Examples of classification of different source types according to EPA's SCC and selected speciation VOC profiles and VOC to TOG conversion factors from Speciate version 4.0 for those source types. The default profile assignment is "0" if the SCC is not found in the Speciation.

Source type	SCC	VOC Profile	VOC to TOG
Industry, Liquid petroleum gas	10201001 - 10201003	3	2.27
Industry, Natural gas	10200601 - 10200604	3	2.27
Industry, Wood	10200901 - 10200912	4642	1.385
Industry, Distillate oil	10200501 - 10200505	2	1.0
Industry, Residual oil	10200401 - 10200405	1	1.639
Electric Generation, Lignite	10100300 - 10100318	1178	1.021346
Cogeneration, Natural gas	20200203 - 20200204	7	3.333333
On - road emissions	2201001000 - 223007533	1314	1.193602
Agriculture	2805000000	203	12.5
Over All Average		0	1.157675

Table 4.6: Mass percentages of amount of VOCs being converted into different Speciate profiles (0, 1, 2,..., 1314) of final lumped VOC species (see Table 4.8).

SNAP/VOC Profile	0	1	2	3	4642	1178	203	1314
S1						1		
S2			0.55	0.24	0.2			
S3		0.04	0.36	0.55	0.05			
S4	1							
S5	1							
S6	1							
S7								1
S8	1							
S9	1							
S10							1	
S11	1							

Table 4.7: Example of the composition of Speciate profile number "2".

Specie ID	Molecular weight	Specie name	Percent by weight
465	30.02598	Formaldehyde	48.7
491	58.1222	Isobutane	4.1
592	58.1222	N-butane	12.2
600	100.20194	N-heptane	0.3
601	86.17536	N-hexane	10.8
605	72.14878	N-pentane	4.7
671	44.09562	Propane	1.2
2126	100.20194	Isomers of heptane	2.6
2127	86.17536	Isomers of hexane	5.2
2130	114.22852	Isomers of octane	4.7
2132	72.14878	Isomers of pentane	5.5

Table 4.8: Conversion factors from VOCs in Mg (tones) to moles of RADM2 lumped species for profiles used for speciation of EMEP organic gases. Factors include VOCto-TOG conversion, splitting the VOCs to different species, conversion from tons to moles for each specie and then aggregating moles of compounds into lumped RADM2 species. This table can be used for direct conversion of VOC SNAP emissions to model RADM2 input.

Field	0	1	2	3	4642	1178	203	1314
CH4	5360.82	11240.66	0.00	79334.91	18679.86	0.00	545427.57	10215.49
ETH	535.16	0.00	0.00	0.00	1035.31	709.90	83142.00	805.82
HC3	2274.31	3806.56	2844.71	4462.53	848.56	379.99	9475.30	2226.06
HC5	1187.88	909.32	1820.88	1806.87	16.87	1858.50	4472.08	2020.47
HC8	1848.53	0.00	28.29	255.20	199.38	144.48	5576.43	1017.45
OL2	1180.24	0.00	0.00	0.00	2903.91	0.00	0.00	2208.30
OLT	905.45	0.00	0.00	0.00	875.19	842.73	0.00	928.07
OLI	459.88	0.00	0.00	0.00	467.98	472.78	0.00	545.51
TOL	796.61	0.00	0.00	834.33	257.36	1705.26	0.00	1742.77
XYL	339.28	0.00	0.00	0.00	226.98	4607.19	0.00	1150.69
HCHO	597.61	22930.96	16219.29	6055.36	2822.12	0.00	0.00	596.43
ALD	442.54	0.00	0.00	0.00	4030.78	0.00	0.00	299.10
KET	272.61	1999.53	0.00	0.00	466.11	0.00	1089.03	50.64
ISO	67.98	0.00	0.00	0.00	43.78	0.00	0.00	0.02
CSL	111.84	0.00	0.00	0.00	1533.09	0.00	0.00	0.12
ORA1	105.64	0.00	0.00	0.00	0.00	0.00	0.00	0.07
ORA2	203.24	0.00	0.00	0.00	0.00	0.00	0.00	0.17
GLY	3.99	0.00	0.00	0.00	839.70	0.00	0.00	0.54
MGLY	0.00	0.00	0.00	0.00	1027.00	0.00	0.00	0.60
MACR	159.00	0.00	0.00	0.00	392.02	0.00	0.00	19.98
MVK	0.00	0.00	0.00	0.00	0.00	0.00	0.00	0.19
NR	3556.68	6087.76	2353.98	5137.97	2537.39	298.46	613.55	2000.14
NVOL	4.51	0.00	0.00	0.00	0.19	0.00	0.00	0.00

Chapter 5

Numerical Simulations of High Ozone Episodes

In the present chapter results of model simulations for three high ozone episodes in years 2003 - 2005 are presented and discussed. For each of the episode the synoptic situation, followed by episode weather characteristics over Slovenia and the evolution of the near ground ozone at Slovenian measuring sites, is described. The main purpose of the chapter is the presentation of model results and their evaluation.

Results of numerical simulations always include some errors. The numerical modeling of atmospheric photochemical pollution is from this point of view especially challenging because of numerous highly complex and nonlinear processes involved. There are many *a priori* known sources of uncertainties, which can significantly contribute to errors in simulated ozone levels. For example, the evolution of daytime and specially nocturnal PBL, thermal meso-scale winds and local circulations, are incompletely resolved by the model, but these certainly play a decisive role in determining the location of ozone plume and its concentrations. The problem becomes more pronounced over complex terrain and under hot summertime conditions with weak external dynamical forcing - both typical for high ozone episodes in Slovenia. Significant model errors can arise also from the uncertainties in initial chemical conditions, a regional transport of pollution accumulated in air masses over distant areas also can have important impact on ozone in local scales. Finally, the uncertainties in emissions are supposed to present a significant source of uncertainties as well. In our case, because of using a coupled meteorological-photochemistry model, we at least avoid the uncertainties that arise from the coupling of two different models.

To address the problem of uncertainties in model results a considerable number of simulations was performed for each of the episodes. The configuration of model among these simulations differed in selection of some of the meteorological parameterizations, boundary and initial conditions, and emissions. The advantage of a so obtained ensemble of solutions was twofold. First, a risk of basing an explanation of the episode on one uncertain deviant simulation was reduced. And secondly, from such an ensemble of solutions we could estimate the simulated ozone uncertainty and even compare the sensitivities of simulated ozone to different sources of uncertainties.

From the ensemble of numerical solutions it was usually not possible to choose one simulation, which could be denoted as the best one. For example, if the temperatures were simulated well in one simulation, then winds might be too strong or the PBL height unrealistically high, and if ozone was simulated relatively well in the interior of Slovenia, then its values might be

too low in the Mediterranean part.

Nevertheless, for each of the episode one simulation from the ensemble was selected as a *reference simulation*. Model namelist options used for all the reference simulations are shown in Appendix D, let us mention only that YSU PBL scheme and Noah land-surface model were used in these simulations. Emissions for reference simulations were calculated as explained in Chapter 4, and original model vegetation and landuse parameters (needed by different parametrization schemes) were used. Nesting strategy and distribution of vertical levels were the same in all (not only in reference) simulations. They are described in Section 3.5 and can also be deduced from namelist options in Appendix D. Other details about reference simulations, regarding frequency of re-initialization of meteorological fields and the time allowed for accumulation of pollutants in PBL, are separately for each of the episode described in the following Sections (e.g. in Section 5.1.2 for Episode I). Model configuration for reference simulations was chosen on the basis of preliminary experiments performed for hot summertime episodes, discussed in the present chapter. Although, as already mentioned, from the results of these experiments it was hard to select the best configuration, the purpose was to chose as optimal one as possible. But at the end the decision about the final reference model configuration was somehow subjective, as well. According to validation tests, made for measured meteorological and ecological variables, the results of reference simulations were pretty good, but like any other simulation from the ensemble have some deficiencies, as well. With having this in mind, results of the reference simulation, which are presented more in detail, must be considered. In the case of the first episode, Episode I, further the differences among the ensemble simulations are studied and ozone sensitivities to different changes applied are compared. As a confirmation to the findings from Episode I, results of similar comparisons are shown in Appendix G for Episode II. It is worth to make a brief discussion about the units in which ozone levels are expressed. Model calculates the concentrations of gases. Ozone (and other gases) in model output fields are thus expressed in ppm (parts per million). In Slovenia measured ozone levels are typically presented as densities, therefore in $\mu g/m^3$, as the legislation threshold values of air quality close to the ground are expressed in $\mu g/m^3$. To enable the comparison of simulated ozone levels and measurements, the model concentration values are converted to density values. The only exception, where model results for ozone are left in original ppm units, are vertical ozone profiles. The conversion factor between ozone concentration and ozone density depends on the meteorological conditions and is calculated as:

$$O_3(\mu g/m^3) = 1000 \cdot \frac{M_{O_3}}{M_{air}} \cdot \rho_{air} \cdot O_3(\text{ppm}). \tag{5.1}$$

The conversion factor between the concentration and density for the near ground ozone in standard atmosphere is almost exactly 2000 $\mu gm^{-3}/ppm$.

5.1 Episode I: 4 - 14 August 2003

5.1.1 Synoptic situation and ozone characteristics

The synoptic situation during the first half of August 2003 was governed by a blocking anticyclone which persisted over the western Europe. High pressure ridge at 500 hPa formed between 2 and 3 August over the Central Europe and Alps. On the 4 and 5 August the anticyclone extended from Scandinavia, over Western and Central Europe, and Mediterranean. It persisted over Europe until the cold front coming from the Atlantic Sea on 12 August started to push stagnant air masses toward East. Over Slovenia during the first part of the episode in the higher altitudes warm northwestern flow predominated, while between 10 and 13 August very warm and dry air flow was almost stagnant over the area. The episode was terminated by the cold front, passing Slovenia from northwest in the night between 14 and 15 August. The temperatures measured over Europe during this episode were extremely high, in Slovenia maximum of 39°C was recorded on 14 August at Črnomelj station.

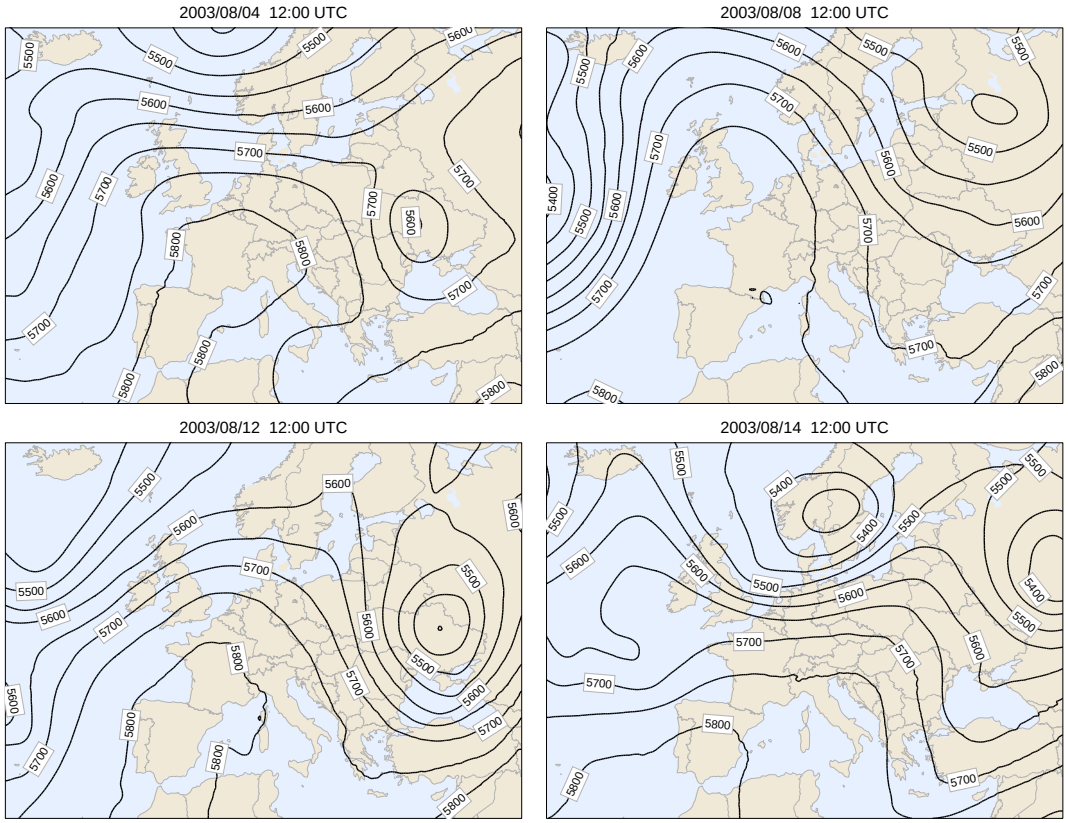

Figure 5.1: Geopotential height (gpm) at 500 hPa during the August 2003 episode.

High ozone values were measured all over Slovenia. For four measuring sites the ozone temporal evolution is shown in Fig. 5.2. The first exceedence of the hourly warning threshold value (180 μg/m^3) was recorded at Nova Gorica on August 5, after a few days of pollutants accumulation (August 1 - 4). On that day ozone concentrations almost reached the warning threshold value also at two other measuring sites (Krvavec and Kovk). On August 7 ozone values over Slovenia somewhat decreased. No station recorded maximum hourly value higher

than 165 μg/m^3 on that day. This ozone decrease coincide with a slightly lower measured near-ground temperatures. Also the atmosphere cleansing caused by showers and thunderstorms during the (late) afternoon of the previous day may contribute to lower ozone measured on August 7 (the atmospheric unstability on August 6 was caused by slightly cooler northwestern airflow and overheated near ground air).

Between August 8 and 11 the measured ozone values were again very high in the southwestern part of the country (Nova Gorica). Except on August 11 hourly values were occasionally close to warning threshold value also at sites Ljubljana, Iskrba, Krvavec and Kovk.

The highest ozone levels in the continental part of the country were during this episode measured from 12 to 14 August. More than 200 μg/m^3 hourly values were measured at background station Iskrba on 13 and 14 August, and exceedances of warning hourly values were recorded at Ljubljana, Murska Sobota, Velenje and Kovk.

Even worse were the 8 hourly ozone values (not shown, but can be for four sites deduced from Fig. 5.2). At Krvavec throughout the episode 8 hourly ozone levels were above the 120 μg/m^3 target value, while at other 3 sites 8 hourly ozone was above the target value every afternoon from August 3 onwards.

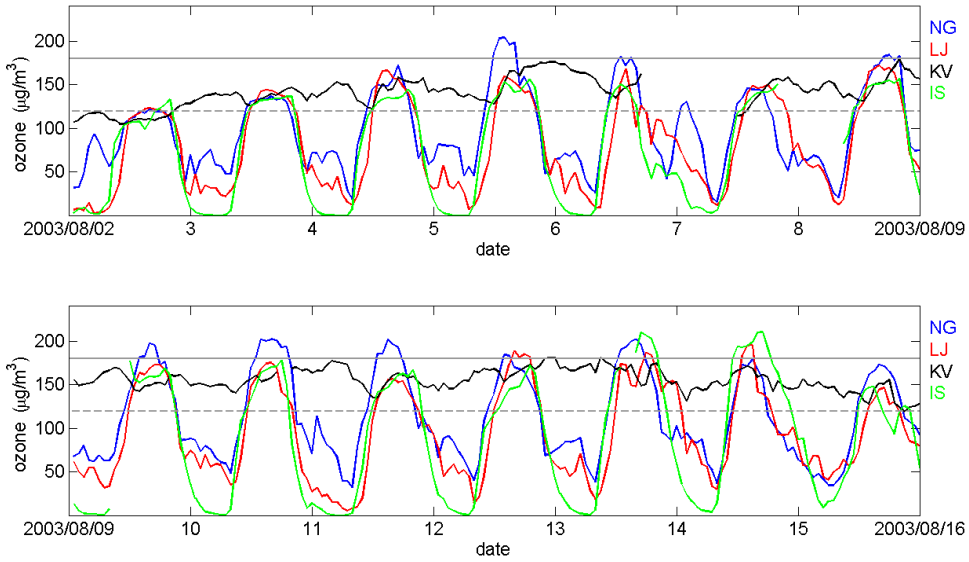

Figure 5.2: Measured average hourly values of ozone (in μg/m^3) for August 2003 episode at locations Nova Gorica (NG), Ljubljana (LJ), Krvavec (KV) and Iskrba (IS). Dotted red line: 1-hour warning ozone threshold value (180 μg/m^3). Dotted grey line: year 2010 8-hour target ozone value (120 μg/m^3).

The cold front passage in the night between August 14 and 15 did not entirely complete the high August 2003 ozone series. Specially at Nova Gorica station ozone was occasionally high also during the second part of the month (see Appendix E): for 6 days after August 15 daily ozone maxima at this station were higher than 165 μg/m^3, while hourly warning threshold value was exceeded once at Nova Gorica (on August 23) and once at Ljubljana (on August 28) station. The reason for smaller decline in ozone at Nova Gorica after the cold front passage was probably less efficient wet deposition in Mediterranean region - less precipitation were recorded there, specially on August 15. According to model results (presented below) the direction of front traveling (passing the Alpine barrier from north and thus pushing the

polluted air masses back to the south) may as well contribute to more polluted Mediterranean air on August 15 (the day after the cold passage), and consequently relatively high ozone at Nova Gorica on that day.

The ozone time evolution over Europe has for this episode already been studied by Vautard et al. (2005). They conclude that during the 2 week lasting episode ozone rich air masses were transported from place to place in an anticyclonic rotation over northwestern Europe (from southern Germany to North-central France and western France), while the southern areas (Marseille, the Po Basin and Genova) did not seem to be connected to this transboundary transport, and undergo more local episodes. To explain the dynamics of the high ozone measured over Slovenia, more detailed study as well as simulations with higher spatial resolution are needed.

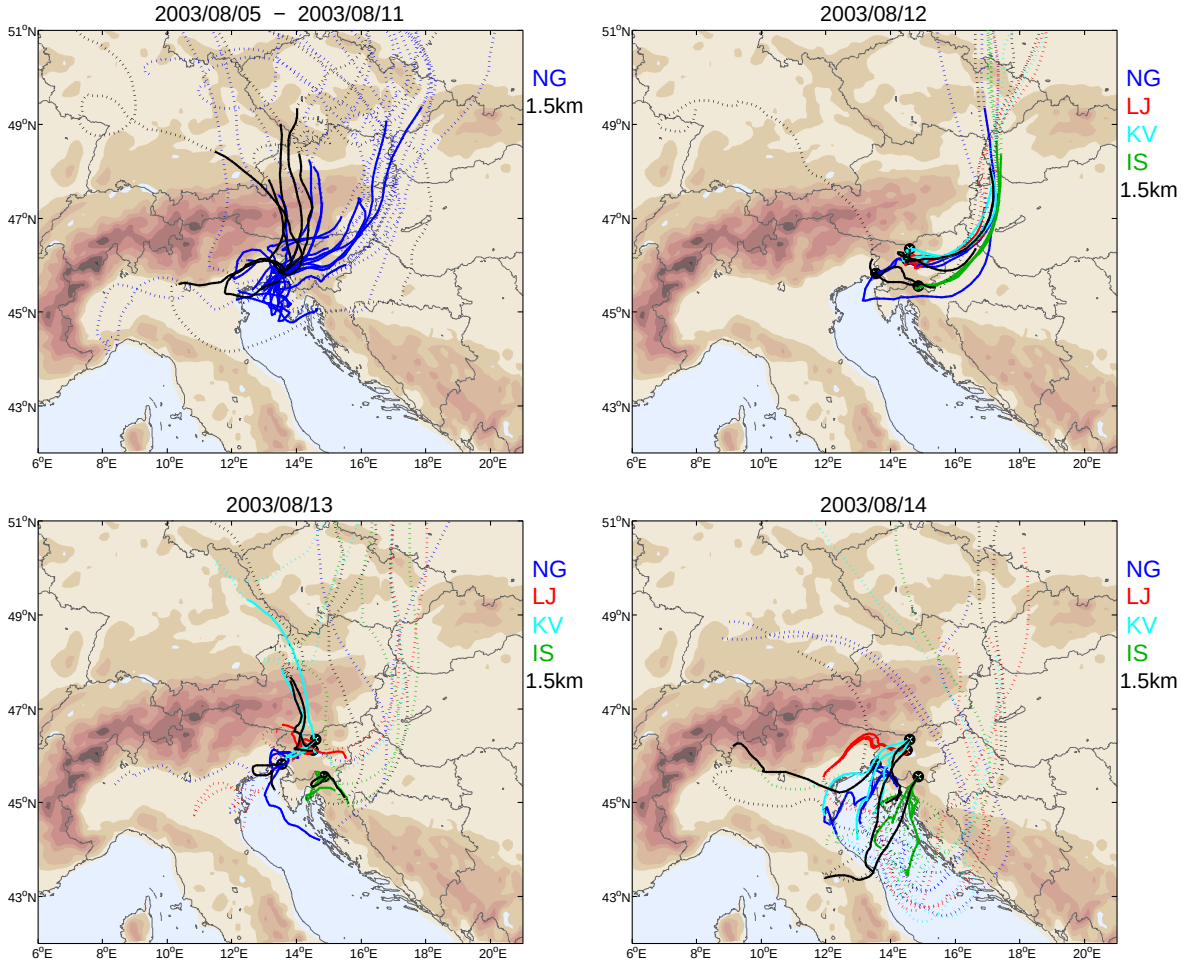

Figure 5.3: 3D backward trajectories for four measuring sites, calculated on Aladin fields for episode in August 2003. Trajectories have final points located 50 m agl (colored according to measuring site) or 1500 m amsl (black), and are calculated for different arrival times (9:00, 12:00 and 15:00 for 50 m agl, and 12:00 UTC for 1500 m amsl). Upper left: Nova Gorica trajectories for 5 - 11 August; Other: Nova Gorica, Ljubljana, Krvavec and Iskrba trajectories for a selected day. Details about calculation of the trajectories can be found in Chapter 2. The total length of trajectories is 96 hours. Solid line: the last 24 hours, dotted line: the rest of 96 hour trajectory.

3D backward trajectories calculated for four sites in Chapter 2 are presented in Fig. 5.3. For Nova Gorica it can be noted, that from 8 to 11 August (the days when only at this station ozone threshold hourly values were exceeded) most of the trajectories originated from central Europe and traveled over Slovenia. Most of them crossed Gulf of Trieste before they reached the measuring site. After August 12, when very high ozone was measured all over Slovenia, the flow direction over Slovenia changed from northeastern to southwestern. Most of the 96 hour trajectories still originated primarily from central Europe, but in the last 24 hours the air masses were slowly moving over the Slovenia or northern Adriatic sea and its coastal regions (mainly Gulf of Trieste and Kvarner Gulf). On the last day of the episode, the trajectories spent a significant time over Adriatic sea and the coastal regions before they reached the measurement sites from the southwest. It can be noted that these trajectories reveal no direct connection to the Po River Basin polluted air during this episode. Nevertheless, Po River Basin emissions still may cause a regional pool of pollution, which may extend towards the Adriatic and influence ozone levels on that area.

5.1.2 Reference simulation

The reference simulation was performed for the time period from 2 to 15 August 2003 inclusive. The meteorological fields were re-initialized on 8 and 13 August at midnight from ECMWF analysis fields. The model was first run for August 1 with the chemistry fields initialized from WRF-Chem idealized chemistry profile, to provide initial chemistry conditions for August 2. On 8 and 13 August, at re-initialization of meteorological fields, chemistry was initialized from previous run. YSU PBL scheme and Noah land-surface model were used in reference simulation, and the other namelist options were the same as shown in Appendix D.

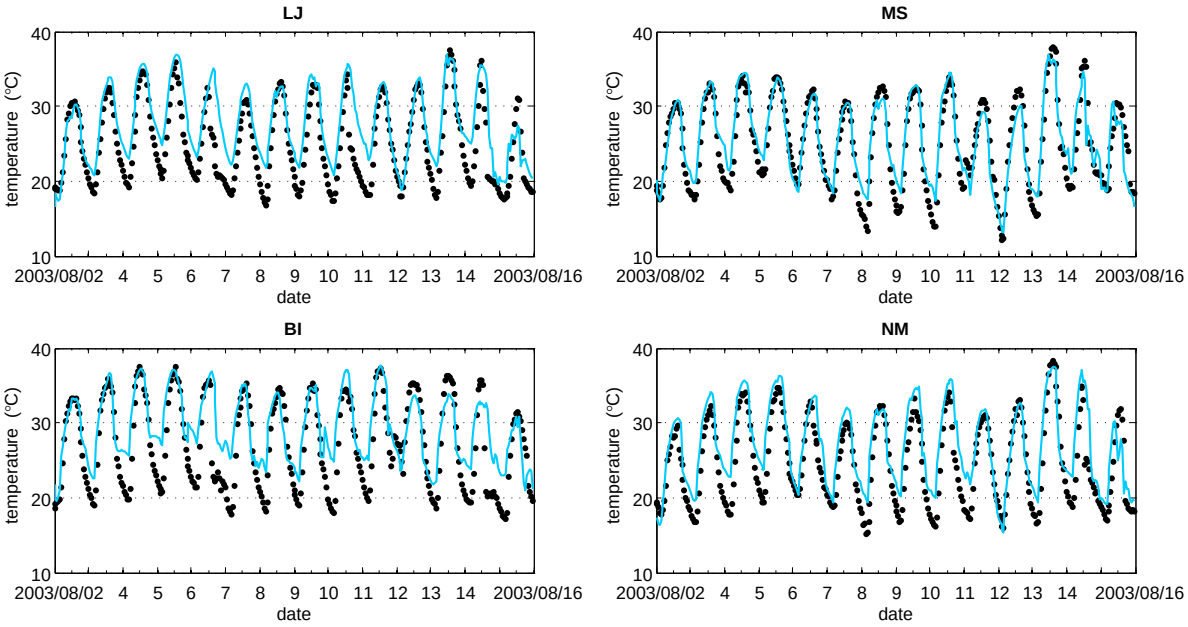

Figure 5.4: Simulated (blue line) and measured (black dots) temperatures for stations Ljubljana (LJ), Murska Sobota (MS), Bilje (BI) and Novo Mesto (NM).

First the model hourly outputs of the near ground temperature, water vapor mixing ratio, pressure and wind from D3 domain are compared to measurements of these variables at some

Slovenian stations. In Figure 5.4 the comparison of temperatures for four measuring sites located at different parts of Slovenia is shown. Diurnal values of modeled temperatures follow the observations well, while the nighttime coolings are systematically underestimated. Similar evolution of modeled and measured temperatures can be noticed also for other meteorological stations included in analysis (see also Fig. 3.4). The exceptions are stations Rateče with the underestimated simulated daytime temperatures and Kredarica with overestimated daily simulated temperature values.

The systematic errors in temporal courses of surface pressure arise from deviations between model and real relief. The temporal evolution of model surface pressure otherwise follows the measured values over Slovenia well (examples in Fig. 5.5 for two stations). Noticeably worse is the agreement between the modeled and observed water vapor mixing ratios. For most of stations model values of water vapor mixing ratios in reference simulation are systematically lower than measured. One of the highest underestimations among stations included in analysis can be noticed for Ljubljana (Fig. 5.5). But there are stations, for which the agreement between model and observations is good for water vapor mixing ratios, as well. One of such stations is Murska Sobota, presented in Fig. 5.5).

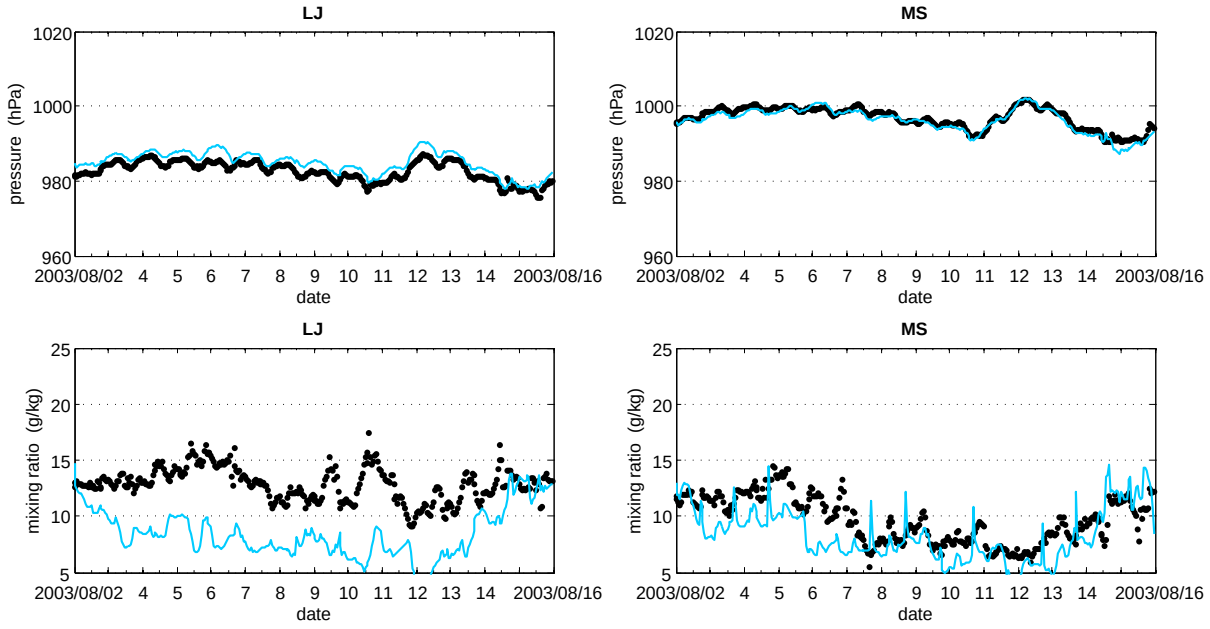

Figure 5.5: Simulated (blue line) and measured (black dots) surface pressure (upper panels) and water vapor mixing ratio (lower panels) for stations Ljubljana (LJ) and Murska Sobota (MS).

Specially challenging to simulate over complex terrain, but very important in modeling air pollution, is a wind field temporal evolution. The northwesterly flow, distinctive over Slovenia for the higher altitudes (in the middle of the troposphere) during the persisting synoptic situation, was at the lower altitudes blocked by the Alpine barrier. The analysis of simulated daytime wind fields at about 500 m above ground (20th model level) shows that the northeasterly flow pattern (as a consequence of weak air flow around Alps) prevailed over Slovenia at this height until August 12, when slowly southwesterly flow predominated. At close to the ground levels the wind field was highly influenced by the local topography. The

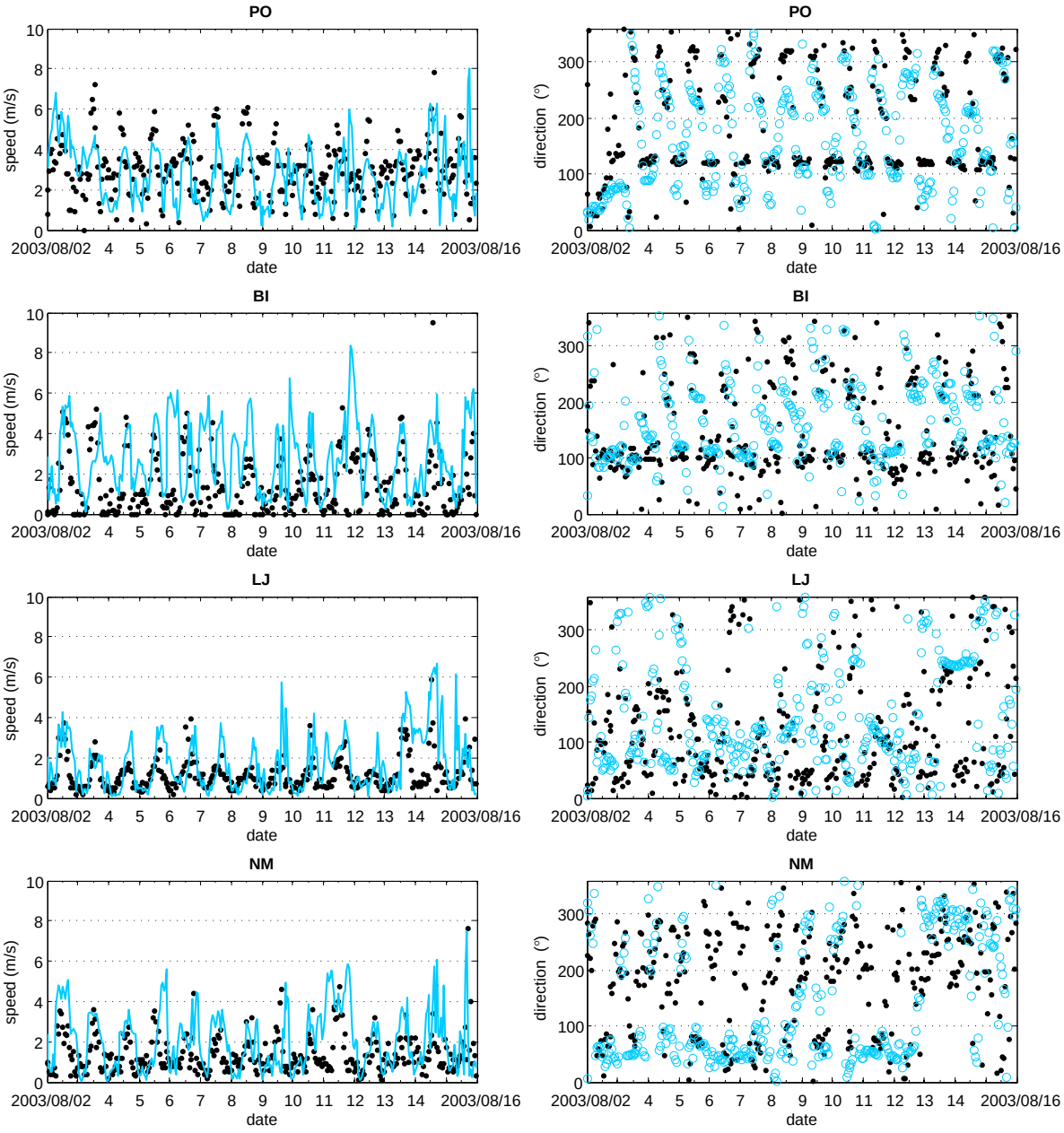

Figure 5.6: Simulated (blue) and measured (black dots) wind speed (left) and direction (right) for stations Portorož (PO), Bilje (BI), Ljubljana (LJ) and Novo Mesto (NM).

meso-scale (thermal) winds developed and governed the near ground air movements. Specially distinctive and at the same time detached from local circulations in the non-Mediterranean country, was the circulation of Mediterranean air masses. At the coastal region land and sea breezes developed and were considerably enhanced by the thermo-topographic effect of the Alps. Simulated winds show development of flow pattern in general perpendicular to the coast, with predominant southwesterly direction during the daytime in the area between Gulf of Trieste and the Alps (the sea breeze enhanced by the upslope winds), and the flow in the opposite direction (land breeze and the downslope winds) during the nighttime hours. This general circulation is further modified by the local topography, so the actual direction of the

night and daytime winds on the site depends on the site location. As an example are in Fig. 5.6 compared simulated and measured 10 m winds for some measurement sites located at different parts of Slovenia. For weaker winds in the interior of the country the discrepancies between simulated and measured wind directions are in general higher than for Mediterranean stations Portorož (PO) and Bilje (BI) with more pronounced circulation. If at these two stations the described circulation appears to persist through the entire episode, at the interior stations the local circulations were terminated on 13 and 14 August with the southwesterly flow.

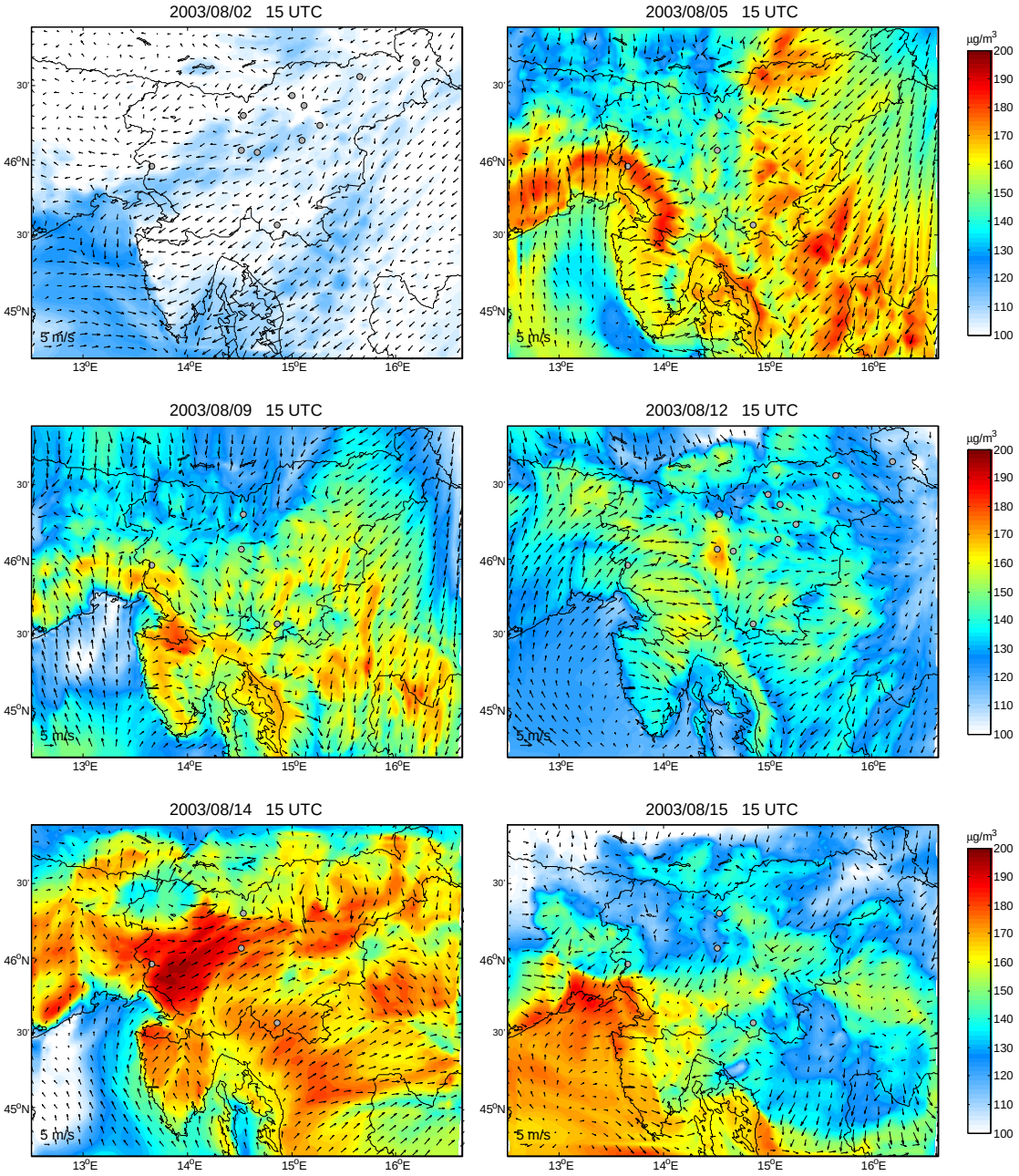

Figure 5.7: Examples of simulated near ground ozone field and surface winds. Results are from the reference simulation, shown for the D3 domain.

The temporal evolution of simulated near ground ozone together with 10 m wind field is briefly presented in Fig. 5.7. On August 2 the near ground air was mostly clean. After that day the pollution built up in the planetary boundary layer and on August 5 the simulated near ground ozone values were somewhere inside D3 domain already high. At the coasts of Gulf of Trieste the daytime sea breeze together with the Alpine upslope winds are well pronounced, while the central Slovenia is characterized by weak meso-scale winds with variable directions. In the northeastern part of the country, the air flow around Alpine barrier results in the northeastern winds. Similar daytime near ground wind patterns prevail till August 10 inclusive. On August 11 the northeastern flow predominated over the entire Slovenia, only at coasts of Gulf of Trieste and over the Friuli-Venezia Giulia region the circulation characteristic of the previous days persisted. Over the continental Slovenia to this northeastern flow somewhat lower measured and simulated temperatures are related, as well as decrease in the near ground daytime ozone levels can be noticed on August 11.

The comparison of simulated and measured ozone time series is for the majority of Slovenian stations presented in Fig. 5.8. In general model tends to overestimate nighttime ozone levels and underestimate the daytime ozone, which specially holds for stations with well pronounced measured diurnal ozone cycle (e.g. Iskrba, Ljubljana, Nova Gorica). Possible explanation for such behavior of simulated ozone (daytime underestimation, nighttime overestimation) may be the inaccuracies in simulated meteorology. For example, during the daytime temperatures are simulated well, but wind speeds are in general overestimated (see not only Fig. 5.6, but also Appendix F.2 for other measuring sites, where simulation D is reference). As it will be shown later, the simulated daytime PBL heights in the reference simulation are likely to be overestimated as well. Consequently, because of excessive mixing pollutants during the day are diluted too effectively, leading to the reduction (underestimation) of daytime ozone values. Similarly, during the night overestimated temperatures and overestimated wind speeds (the latter not for all stations, but for many of them) indicate that model has difficulty in simulating calm nighttime conditions. Since stable and calm nighttime boundary layer enable efficient reduction of nighttime ozone levels due ozone titration with fresh NO_x emissions being trapped in the near ground air, this may explain overestimated nighttime ozone levels. A typical example of station where such explanation could apply is Iskrba (meteorological variables for Iskrba are compared to measurements for the second part of the episode in Appendix F).

The highest deviations between model and measurements among stations are probably obtained for Nova Gorica, especially for the middle part of the episode. With model we are able to simulate the gradual accumulation of pollution over Slovenia in the beginning of the episode, (slight) ozone reduction after August 5, as well as ozone increase during the final part of the episode. More problematic to simulate seems to be the second part of the episode (after August 8), when the highest discrepancies are obtained for Nova Gorica, Ljubljana, Iskrba. Results of other simulations (with different timing of meteorology re-initialization, changed some of the model parameterizations - explained below) express similar behavior: with in general higher deviations between model and measurements in the second than in the first part of the episode. Consequently, I decided to study the contribution of different sources of uncertainties on model results for the second part of the episode more in detail. In the subsequent sections the results of different simulations for the period from 8 to 13 August 2003 are discussed with the aim to evaluate the effects of different model configurations on meteorological and ozone fields.

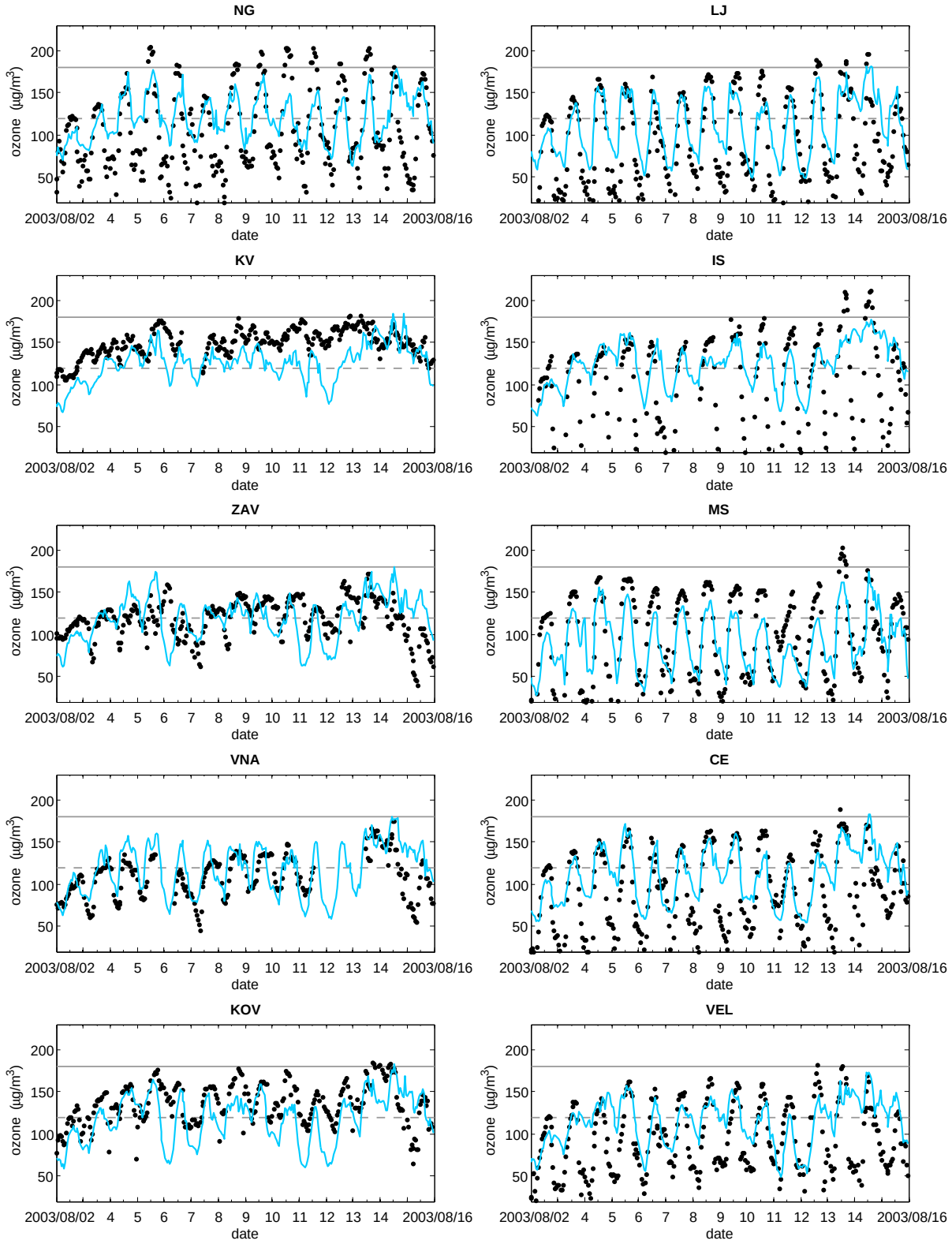

Figure 5.8: Simulated (blue) and measured (black) hourly ozone values for stations Nova Gorica, Ljubljana, Krvavec, Iskrba, Zavodnje, Murska Sobota, Vnajnarje, Celje, Kovk and Velenje. Grey solid line: 1-hour warning value; Grey dotted line: 8-hour target value.

5.1.3 Impact of different model PBL schemes and LSMs

Ozone production in the lower troposphere depends strongly on meteorological conditions. The described long lasting stagnating high pressure situation, characterized with hot weather, intensive solar irradiance, weak dynamics (light winds, little precipitation), presents conditions very favorable for ozone formation. When such conditions occur, the ozone levels are further influenced by meteorology in many ways. Variables such as temperature, water vapor mixing ratio, wind speed, cloud cover, precipitation and mixing height, affect the reaction rates, advection and dilution, as well as dry and wet deposition of pollutants.

The model simulations of such situations with weak dynamics, where turbulent motions can be of the same order as the wind speed, can thus be especially challenging. And the errors in model meteorological fields can contribute significantly to errors in simulated pollutant concentrations. As already explained in description of WRF-Chem model, the representation of boundary layer meteorology is closely related to PBL schemes and land surface models (LSMs), chosen for simulation. Turbulence (represented by the PBL scheme) is needed to transfer to the air the effects of surface inhomogeneities (represented by LSM), which drive these mesoscale phenomena, such as up- and down-slope winds, thermal heat island circulations, sea breezes and valley channeled winds.

It is thus worth to evaluate in the case of this episode how do the selections of the PBL scheme and the LSM in WRF-Chem model influence the representation of meteorological conditions of the PBL, and how do this changes in meteorological conditions influence the simulated ozone levels over Slovenia. The question as well arises: is there a combination of PBL scheme and LSM favorable to others?

Table 5.1: Experimental runs.

Experiment	PBL parametrization	LSM parametrization	Changed soil moisture availability
A	MYJ	Noah land surface	No
B	YSU	5-layer thermal diffusion	No
C	MYJ	5-layer thermal diffusion	No
C1	MYJ	5-layer thermal diffusion	Yes
D - reference	YSU	Noah land-surface	No

Additional reason why we studied the influence of selection of PBL schemes and LSMs in WRF-Chem model on the results is that WRF-Chem is a relatively new model, and there is a limited number of studies dealing with its performance. None of them focused on the ozone sensitivity to the selection of PBL schemes and LSMs in the model. At the same time there is also no existing study of the WRF model performance for the type of the episode we are interested in and/or for this geographical area. And it is well known, that the model performance depends on the area of the study and the meteorological situation. Further on, conclusions of previous studies (performed with other models) about this topic are diverse. Perez et al. (1987) for example concluded, that significant differences in simulated ozone may appear as result of different PBL parameterizations. But in study performed by Mao et al. (1987) the PBL schemes selected in MM5 meteorological model did not appreciably affect the CMAQ performance. And finally, it will be interesting to compare these results to simulated ozone sensitivity to emissions and boundary conditions.

As described in Section 3.3, there are two options for PBL scheme in WRF-Chem 2.2 (YSU and MYJ scheme, the third one, MRF, is going to be removed) and two options for land surface

model (thermal diffusion scheme and Noah LSM). There are for four possible combinations of these LSM and PBL schemes. These simulations are marked with letters from A to D, as indicated in Table 5.1. Actually, the simulation D is part of the reference simulation, presented above. To these four simulations an additional one was added, which is identical to C, except that the soil moisture availability is changed for 2 among 24 USGS land cover categories (see explanation is in the next paragraph). All five simulations are performed for the period from 8 to 14 August. The meteorology is similarly as in reference simulation initialized on August 8 at 0 UTC and re-initialized on August 13 at 0 UTC. Chemical initial conditions (for August 8) are taken from the reference simulation for August 8 at 0 UTC in all experiments. On August 13 at 0 UTC, when the meteorology is re-initialized, the chemistry is initialized from previous run of each simulation run. All other conditions (boundaries, emissions) are identical in all simulations

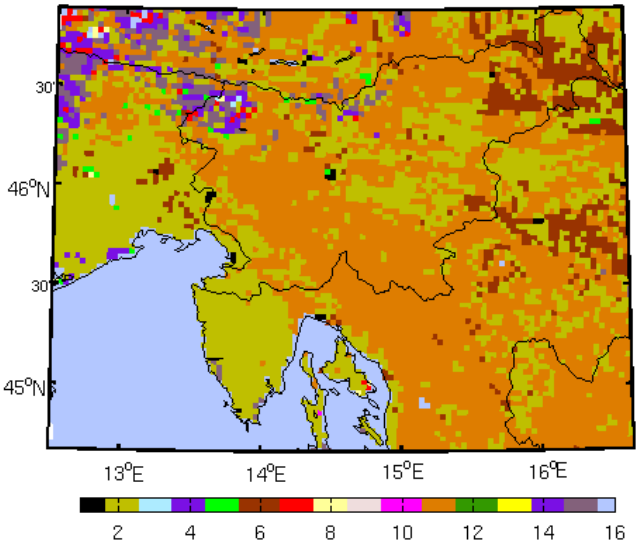

Figure 5.9: Dominant USGS landuse categories, as seen by D3 domain.

Figure 5.9 presents dominant USGS land cover categories, as seen by 3 km×3 km D3 domain. It can be noted, that categories 2 (dryland cropland and pasture) and 11 (deciduous broadleaf forest) are prevalent over Slovenia. It will be evident from the results presented in continuation of this Section, that in simulation C the near ground air moisture is systematically over-estimated, while daytime 2 m temperatures are significantly under-estimated. Similar behavior was found in simulations of type C performed for some other hot summertime episodes (results not presented). We performed numerous sensitivity tests with changed some of the landuse parameters (albedo, soil moisture, emissivity, roughness length), or with changed land cover data (we introduced Corine land cover instead of USGS, or changed the spread of the selected USGS category, e.g. urban, according to Corine land cover data), or with topography with higher than 1 km USGS resolution in simulations with horizontal resolution below 1 km. Probably the most interesting finding from these tests was, that drying the soil moisture significantly improves scores for the near ground temperatures in simulations type C. Namely, too high moisture availability in simulation C may cause too much latent heat flux at the expense of sensible heat flux resulting in the near ground air not warming enough. Although there are other possible reasons for erroneous temperatures in simulations type C

(like problems with PBL scheme coupling resulting in incorrect distribution of the heat in the surface layers, or insufficient radiative scheme), I decided to add the simulation C1 to the four A - D reference simulations. In C1 simulation the original 30% soil moisture availability for USGS land cover categories 2 and 11 was diminished to 10% value. Similar effect of drying the soil on the near ground temperatures was noticed also at applying the change in simulations A, B and D (not shown here).

A detailed comparison (time series) of simulated and measured values of meteorological as well as ecological variables, is shown in Appendix F. Here only statistical scores for simulated variables from different experiments and examples of vertical and horizontal cross-sections through atmosphere are presented.

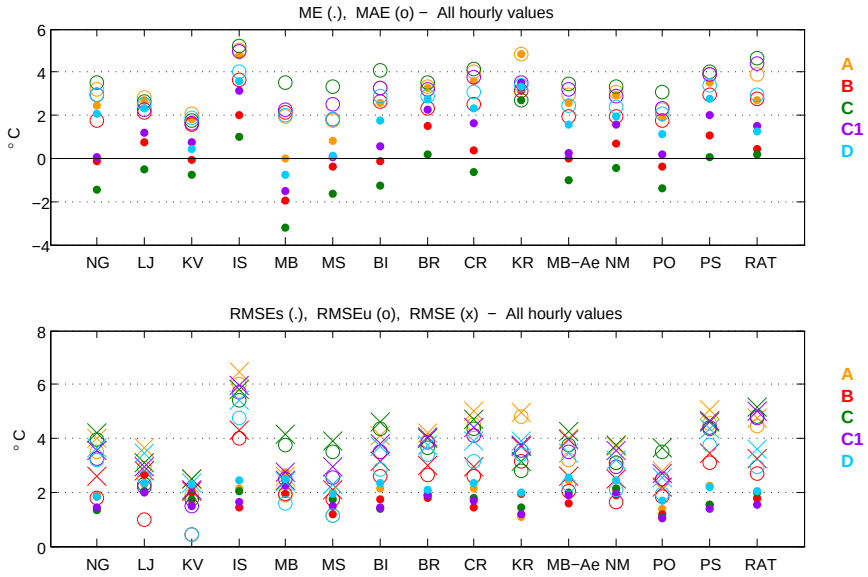

Figure 5.10: Statistical scores for 2m temperatures for experiments A, B, C, C1 and D at 15 stations during the second part of the August 2003 episode (8 -14 August). Mean error (ME): dots; mean absolute error (MAE): circles; root mean square error (RMSE): crosses; systematic RMSE (RMSEs): dots; unsystematic RMSE (RMSEu): circles. Definitions are in Appendix A.

Results show that simulated near ground air temperatures are highly influenced especially by model LSM. Maximum daily temperatures are very well simulated in experiments with Noah land surface model (simulations A and D), regardless the PBL scheme (Appendix, Fig. F.1). In simulations performed with the 5-layer thermal diffusion LSM parametrization, maximum daily temperatures are systematically underestimated (simulations B, C and C1), where with changed water vapor availability in C1 simulation the systematic daytime temperatures negative bias is reduced almost to the level of simulation B. On the contrary, the nighttime coolings tend to be underestimated in all experiments. The positive nighttime temperature bias is in general more pronounced for the simulations performed with the Noah land surface model (C and D), but further depends on the measuring site. With this in mind, we can discuss the statistical scores for the near ground temperatures in Fig. 5.10. Since in Fig. 5.10 all hourly values are taken into account, the result is bad outcome for all scores, with even worse taking's for simulations A and D on account on high nighttime bias. It is expected that accurate daytime temperatures play more important role in processes related

to ozone (nighttime processes are important as well, but are not that much influenced by temperatures). Statistical scores for daily maximum temperatures calculated over all stations included in Fig. 5.10 for 7 simulated days are presented in Table 5.2.

Table 5.2: Statistical scores for daily temperature maxima, wind speed (all hourly values) and water vapor mixing ratio (all hourly values) in experiments A - D, calculated over all stations included in Figures 5.10 - 5.12.

	$T_{max}(°C)$			v (m/s)			Q (g/kg)		
Exp	ME	MAE	RMSE	ME	MAE	RMSE	ME	MAE	RMSE
A	0.4	1.6	2.0	1.6	1.9	2.4	-1.6	2.3	2.9
B	-1.9	2.6	2.7	0.8	1.3	1.7	2.6	2.9	3.3
C	-5.1	5.3	5.6	0.9	1.4	1.8	3.6	3.7	4.3
C1	-2.7	3.2	3.3	1.1	1.5	2.0	2.8	3.0	3.5
D	-0.5	1.6	2.0	0.9	1.4	1.9	-1.9	2.5	3.1

The near ground water vapor mixing ratio is similarly as maximum daily temperatures usually best reproduced in simulations performed with more sophisticated Noah land surface model (simulations A and D), as shown in Fig. 5.11 and Table 5.2. Nevertheless, there are some exceptions, like Ljubljana and Postojna, where 5-layer thermal diffusion scheme proves better. In simulations A and D water vapor mixing ratio is systematically underestimated until the last two days of the episode, when simulated values begin to follow the observations well for most stations (Fig. F.4 in Appendix F). In other three experiments (5-layer thermal diffusivity scheme), mixing ratio has a positive bias for all the stations. The most is the water vapor mixing ratio overestimated in simulation C, followed by C1 and D.

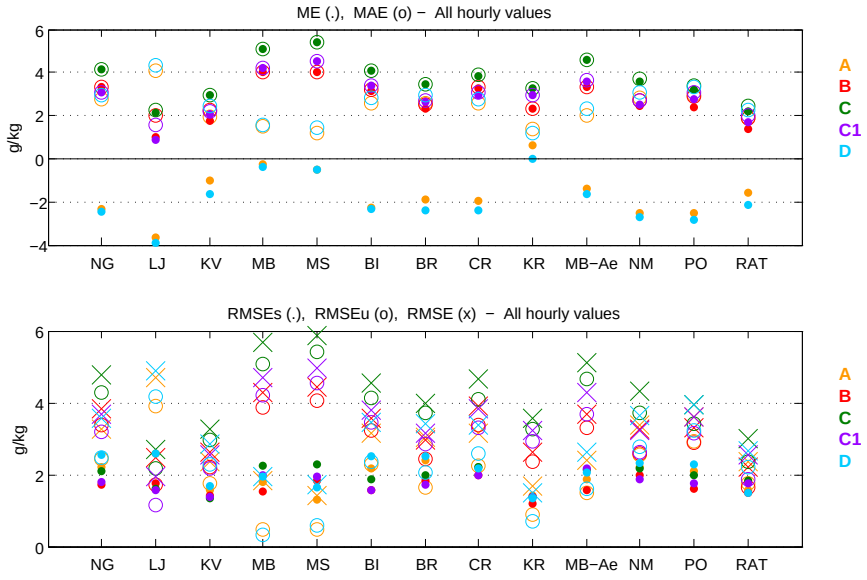

Figure 5.11: The same as Fig. 5.10, but for water vapor mixing ratio.

The comparison of hourly values of measured and simulated near ground winds (Appendix E, Fig. F.2, F.3) shows that some distinctive wind field characteristics are similar

in all simulations. For example, land-sea breeze at the coast (PO and also BI station), prevalent easterly or northeasterly winds on August 11 (LJ, IS, NM) and southwesterly or westerly on August 13 and 14 (LJ, MS, NM) are present in all simulations (Fig. F.3). Nevertheless, differences in simulated near ground winds among 5 simulations can be significant. This especially holds for days with the weakest external dynamical forcing (August 8 - 10). In these days wind characteristics especially for regions not influenced by distinctive dominant meso-scale winds, (developed at the coast or at high Alpine slopes) differ significantly among experiments (Fig. F.3, e.g. NG, LJ, IS, BR stations, and Figures 5.13 and 5.14).

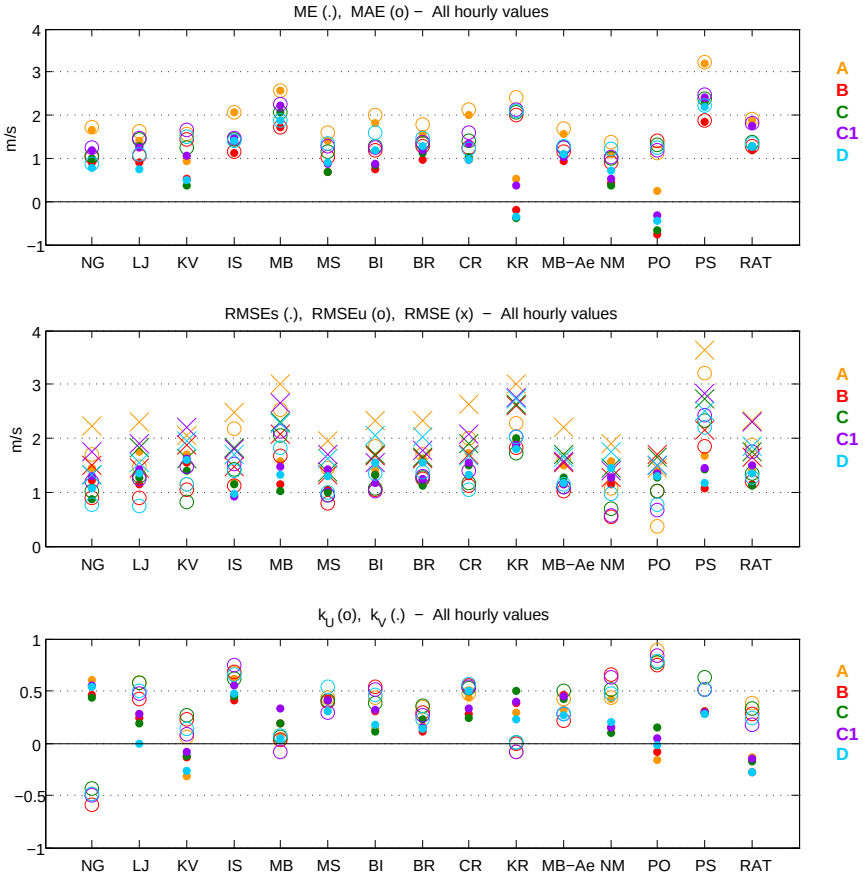

Figure 5.12: Upper two Figures are the same as in Fig. 5.10, but for 10 m wind speed. k_u and k_v are the correlation coefficient for u and v wind components.

Statistical scores for total wind speeds plus the correlation coefficients for meridional and zonal wind components (Fig. 5.12) vary among stations. The worse are scores for Postojna, followed by Maribor and Kredarica. For the wind speeds it can be noted, that with exception of Kredarica and Portorož simulated near ground winds are in average too strong. For almost all stations (except Portorož and Krvavec) the worst scores for wind speed are related to simulation A. The systematic overestimation of the near ground winds, again most distinct for simulation A, is clearly seen in Table 5.2, as well. The correlation coefficients for wind components (Fig. 5.12) express relatively poor agreement for most stations in all experiments. There is no favorite experiment according to these statistics.

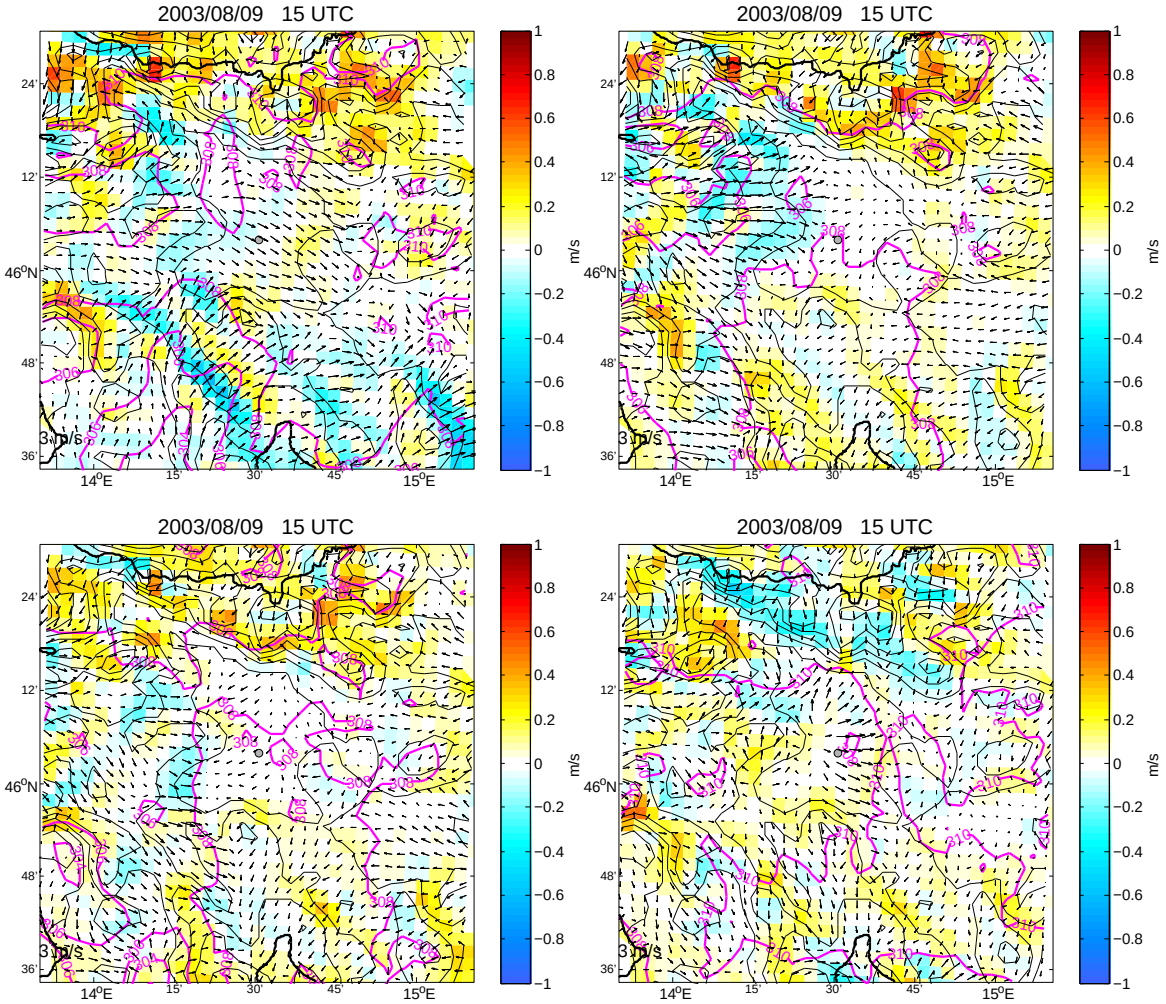

Figure 5.13: Comparison of near ground model outputs for experiments A, B, C1 and D (by turns) for August 9 at 15 UTC in an area within the D3 domain, 36×36 points, centered in Ljubljana (grey circle in the middle). Shown is horizontal wind field in every model grid point (arrows), vertical wind component (colored) and equivalent potential temperature (magenta contours). Thin black contours represent topography and bold black lines coast and borders.

The comparison of temporal courses for simulated PBL heights (Fig. F.5 in Appendix F) again shows significant differences between different experiments. Differences in PBL heights can be as high as 3 kilometers. Similar information bear Figures 5.13 and 5.14, where examples of comparison of the near ground and 1500 m 3D wind field and potential temperature is shown. Since dispersion of emitted pollutants is determined by advection (which is generally weak in our situation) and turbulent mixing of the air inside PBL (which is uncertain and in our case highly depends on the selection of parametrization schemes), significant differences in simulated ozone may exist between experiments. If this is a case, an important uncertainties in simulated ozone can arise from uncertainties in simulated meteorological conditions in PBL.

Since the near ground meteorological conditions and concentrations of pollutants (we are most interested in the near ground conditions, because we live there) are directly linked to the upper air conditions, it is important to evaluate the simulated vertical structure of the

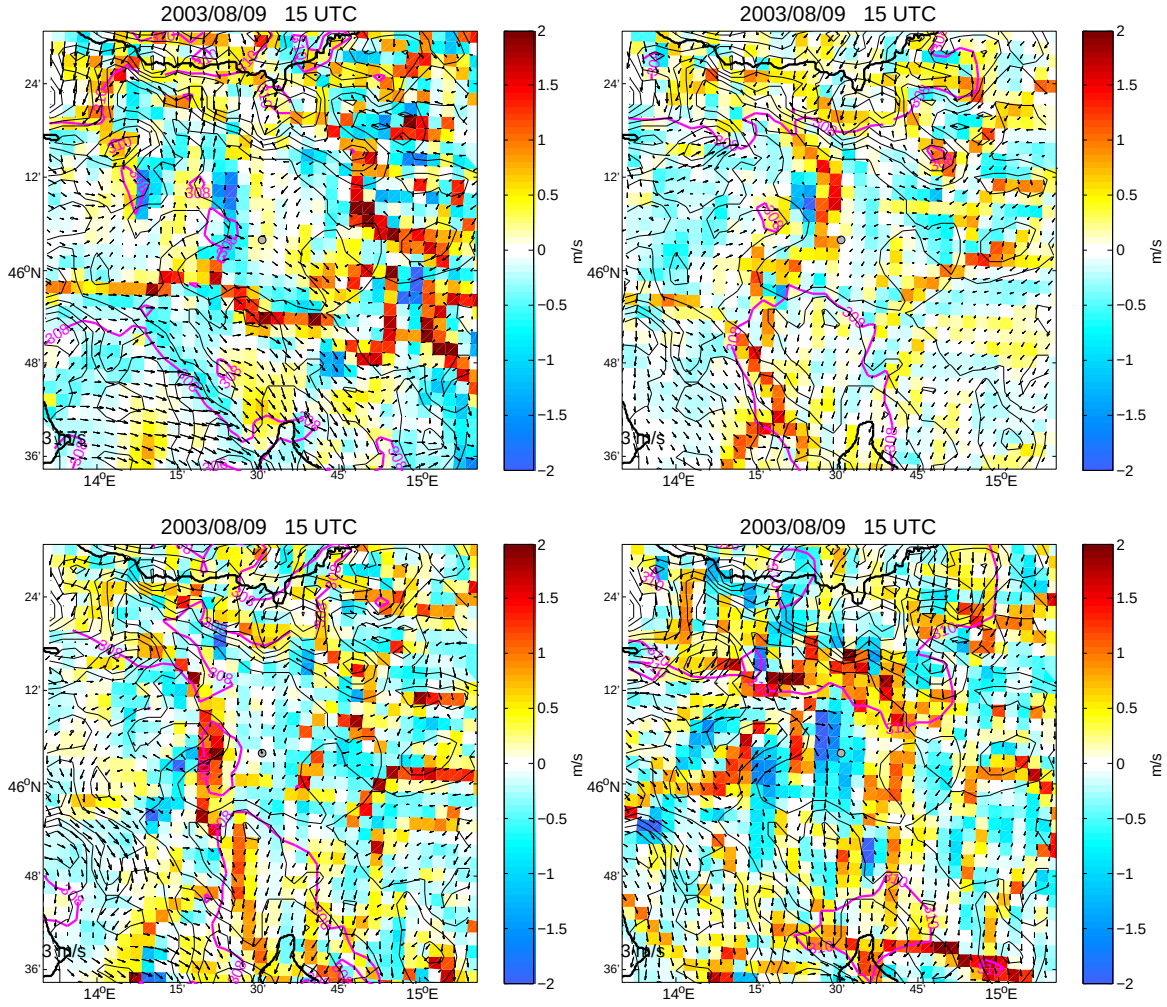

Figure 5.14: The same as Fig. 5.13 but for height 1500 m above mean sea level.

atmosphere as well. For this purpose the comparison of the model results with the Ljubljana, Udine and Zagreb radiosounding observations was done. In Figure 5.15 such comparison is made in the form of vertical profiles of ME and MAE for temperature, mixing ratio, wind speed and zonal wind component. Scores for temperature and potential temperature (the latter not shown, but is almost identical to profiles of temperature scores), clearly indicate the depth of the layer influenced by PBL and LSM parameterizations (the PBL height) - above 3 or 3.5 km differences among experiments became very small. Less pronounced, but as well present, is this characteristic with water vapor mixing ratio. The increase of MAE with height for winds (between 1 km and 3 km) could be partly explained by the fact, that radiosounde travels with winds and that consequently in higher altitudes the measurements are likely to be performed far away from the initial geographic location (where the model values are taken from). The wind field in the lee of the Alps varies with the geographic location much more that e.g. the temperatures. The scores for model winds are the worst around 3 km altitude (which is around the highest peaks in the model topography) and afterwards decrease with the height. Above 4 km the influence of Alpine barrier diminishes and so do the differences among wind scores for experiments A - D. The distinct profile of MAE for wind speed accounts mainly

on the meridional wind component (the vertical course of MAE, not shown, is very similar to the course of wind speed), while zonal wind components express the poorest agreement in the first 500 meters of the atmosphere.

The separate comparison of scores for radiosoundings performed at daytime and at nighttime (not presented here) showed, that in general the errors are more expressed in the daytime, while main course characteristics remain similar by day and night. Regardless the time of day vertical profiles of temperature and potential temperature are characterized by lower errors in simulations performed with Noah land surface model, while for mixing ratio in average the remainder simulations probably have proved better. Winds are problematic in all simulations and is almost impossible to expose the simulation that best approximates the wind field - at least on the basis of the available observations.

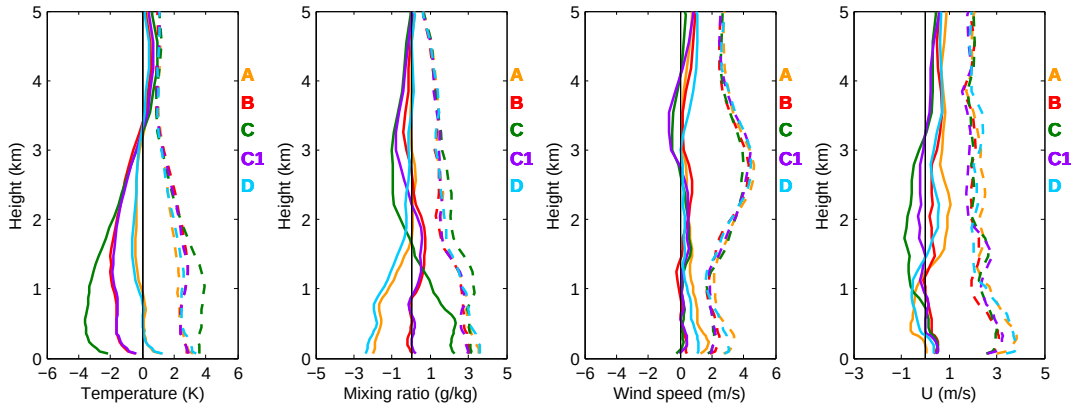

Figure 5.15: Mean error (solid lines) and mean absolute error (dotted lines) for temperature, water vapor mixing ratio, wind speed, and zonal wind component as a function of height. Simulated values are compared to sounding data for Ljubljana, Zagreb and Udine. Altogether 7 soundings per day were available for 7 days from 8 to 14 August 2003 (1/day for Ljubljana, 2/day for Zagreb, 4/day for Udine). Mean error is calculated as model minus observed value.

The comparison of simulated and measured temporal courses for the near ground ozone for most measurement stations is shown in Appendix F, Fig. F.6. The characteristic, that perhaps most strikes the eyes is, that ozone values in C simulation become markedly underestimated after the 3rd day of simulation (see temporal course for e.g. NG, LJ, KV, IS etc.). It is interesting that at least three days are needed for ozone in simulation C to become systematically underestimated and significantly lower that in other experiments. Since daytime temperatures are significantly underestimated in simulation C from the first day onwards, and at the same time daily temperatures correlate to daily ozone concentrations, one would expect the systematic ozone underestimations from the first simulated day onwards. One possible explanation why despite the low temperatures ozone concentrations in the first three days of simulation C are of the same order as in the remaining experiments could be the significantly lower PBL heights in simulation C (Fig. F.5) and consequently less efficient vertical mixing and dispersion of pollutants in simulation C.

Nevertheless, the comparison of ozone vertical cross-sections between experiment C and experiment C1 shows, that ozone concentrations in the lower atmosphere are lower in experiment C from the first day onwards, although the near ground values are of the same size order

for the first three days. An example of vertical cross-section through Nova Gorica station at constant longitude for experiment C is presented in Fig. 5.16 for August 9 at 15UTC. In this simulation maximum daily PBL height above Nova Gorica was less then 1500 m (Fig. F.5). The emitted pollutants of that day thus remain inside this layer. Ozone and other pollutants at higher levels are present as a consequence of chemistry initialization on August 8 from simulation type D. Simulations type D are characterized by high daytime temperatures and high daytime PBL heights resulting in ozone layer extending up to the altitudes of 3 kilometers. Since simulated PBL heights in experiment C are significantly lower (in general not above 1500 meters), ozone above this height gradually cleanses as a consequence of processes like chemical reactions, dispersion, etc. and absence of pollutant sources at these heights. At the same time conditions inside the PBL in simulation C appear to be inconvenient for ozone formation from fresh emissions, resulting in low ozone inside the PBL, as well (see example for August 12 in Fig. 5.16). After the third day of simulation this lower atmosphere ozone reduction results also in significant reduction of the near ground ozone values.

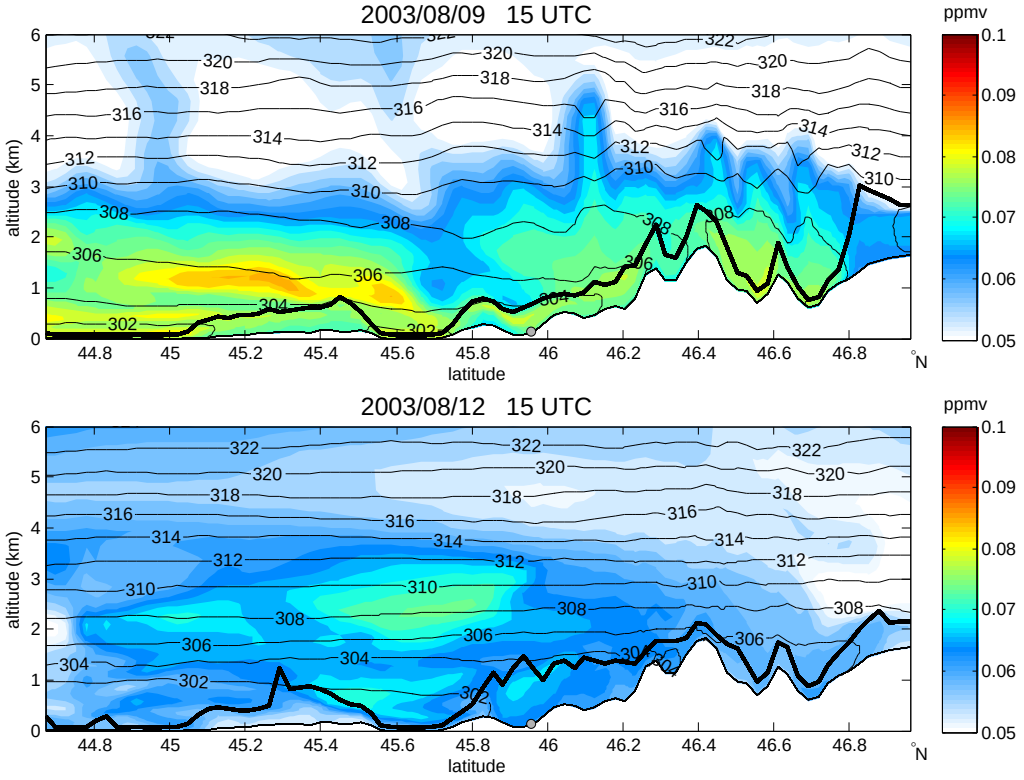

Figure 5.16: Vertical meridional (S-N) cross-section through Nova Gorica on August 9 and August 12 at 15 UTC for experiment C with strong underestimation of ozone production. Shaded: ozone concentrations in ppmv; contours: equivalent potential temperature; Bold black line: PBL height (calculated in model as explained in Section 3.3.2 for MYJ PBL scheme).

Figure 5.16 can be compared to Figures 5.17 and 5.18, where the same cross-sections are presented for experiments A, B, C1 and the reference experiment D. Since cross sections in all these experiments express markedly higher ozone values, closer to the measured ones, the effect of significantly under-predicted daytime temperatures in experiment C is clear.

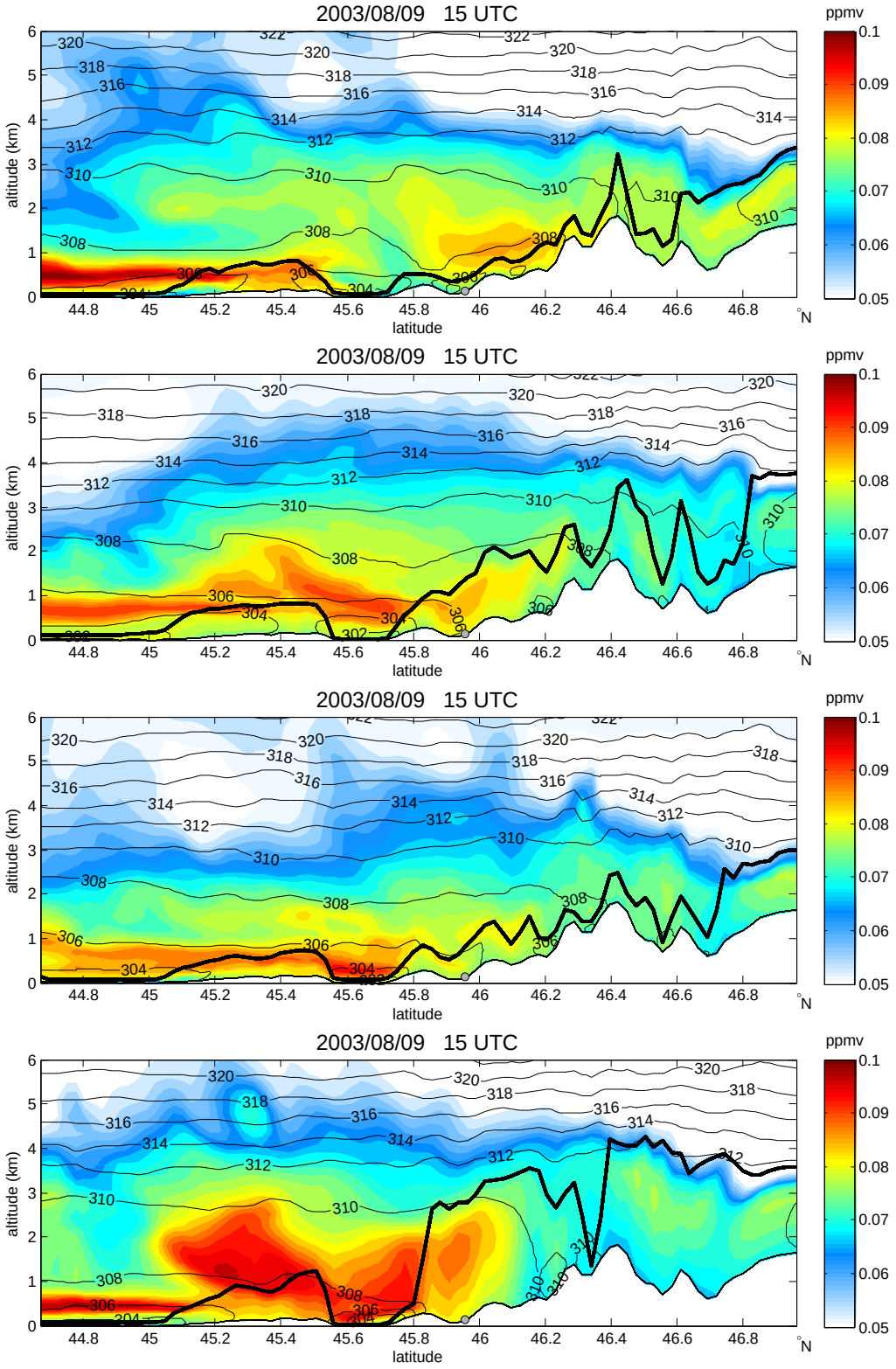

Figure 5.17: Vertical meridional (S-N) cross-section through Nova Gorica on August 9 at 15 UTC. From top to bottom results for experiments A, B, C1 and D (reference) are shown. Shaded: ozone concentrations in ppmv; contours: equivalent potential temperature; Bold black line: PBL height, calculated in model as explained in Section 3.3.2 for YSU (simulations B and D) or MYJ (simulations A and C1) PBL schemes.

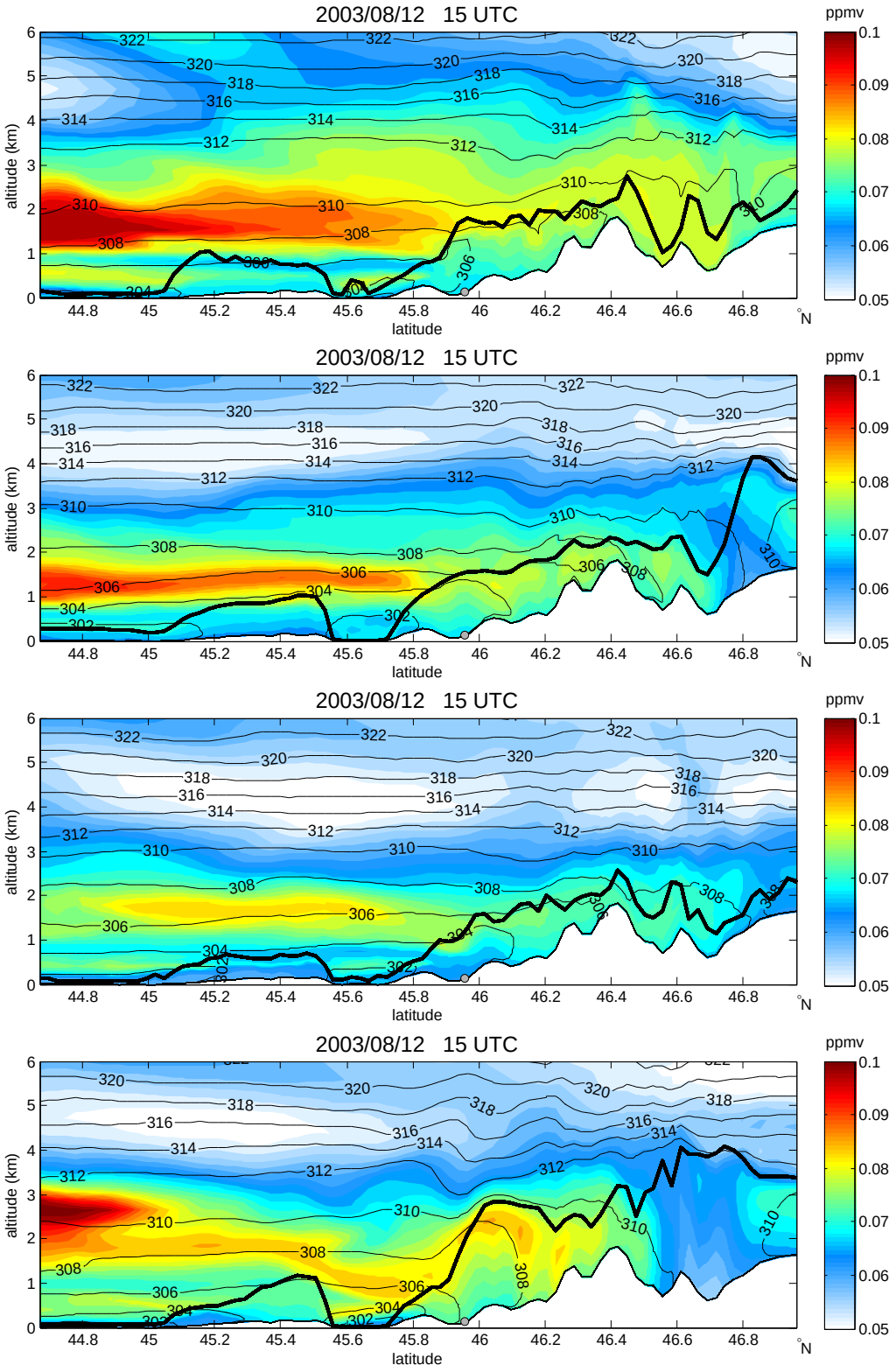

Figure 5.18: The same as Fig. 5.17, but for August 12 at 15 UTC.

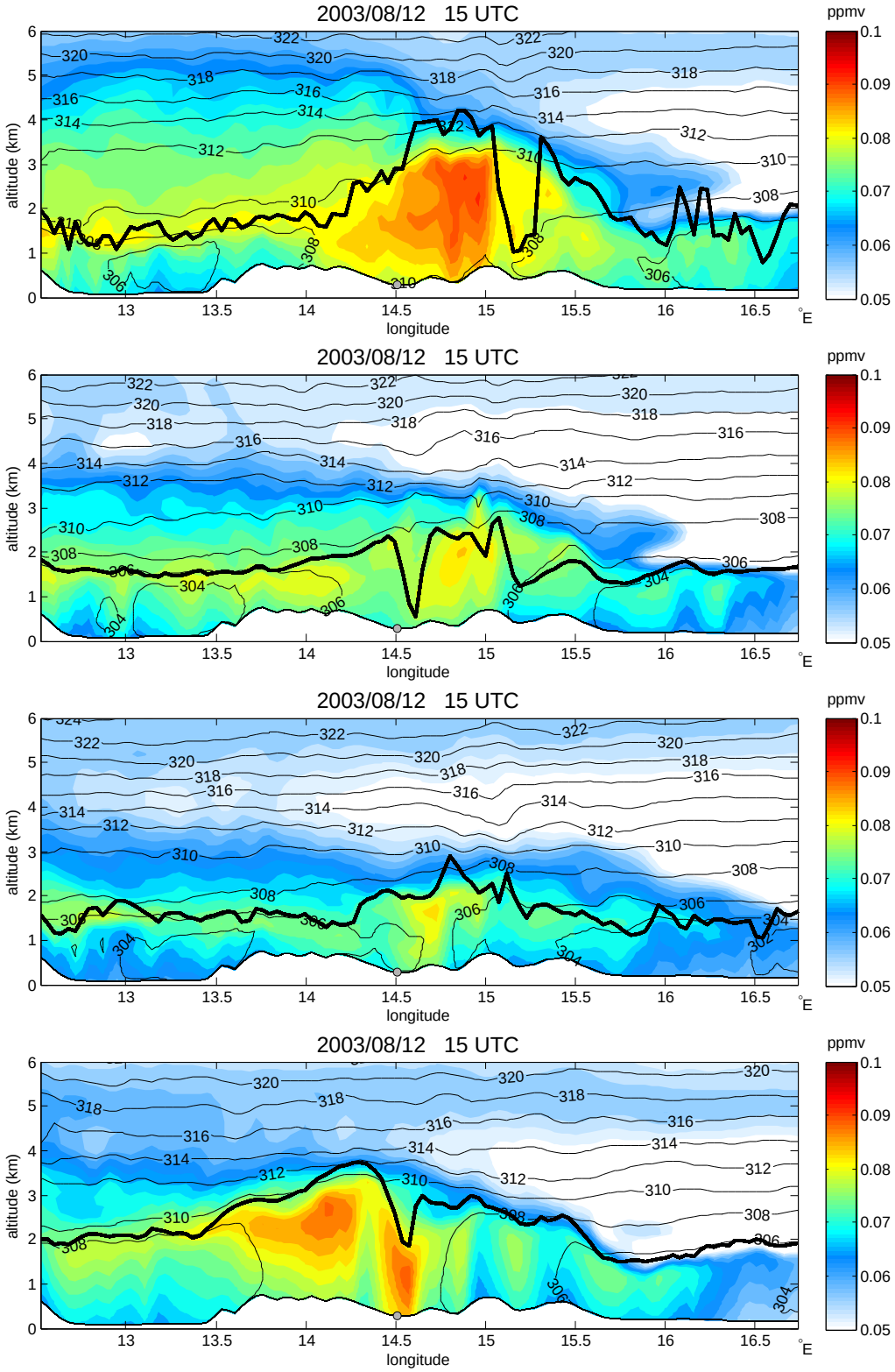

Figure 5.19: The same as Fig. 5.17, but for zonal (W-E) vertical cross-section through Ljubljana (marked with grey circle) for August 12 at 15 UTC.

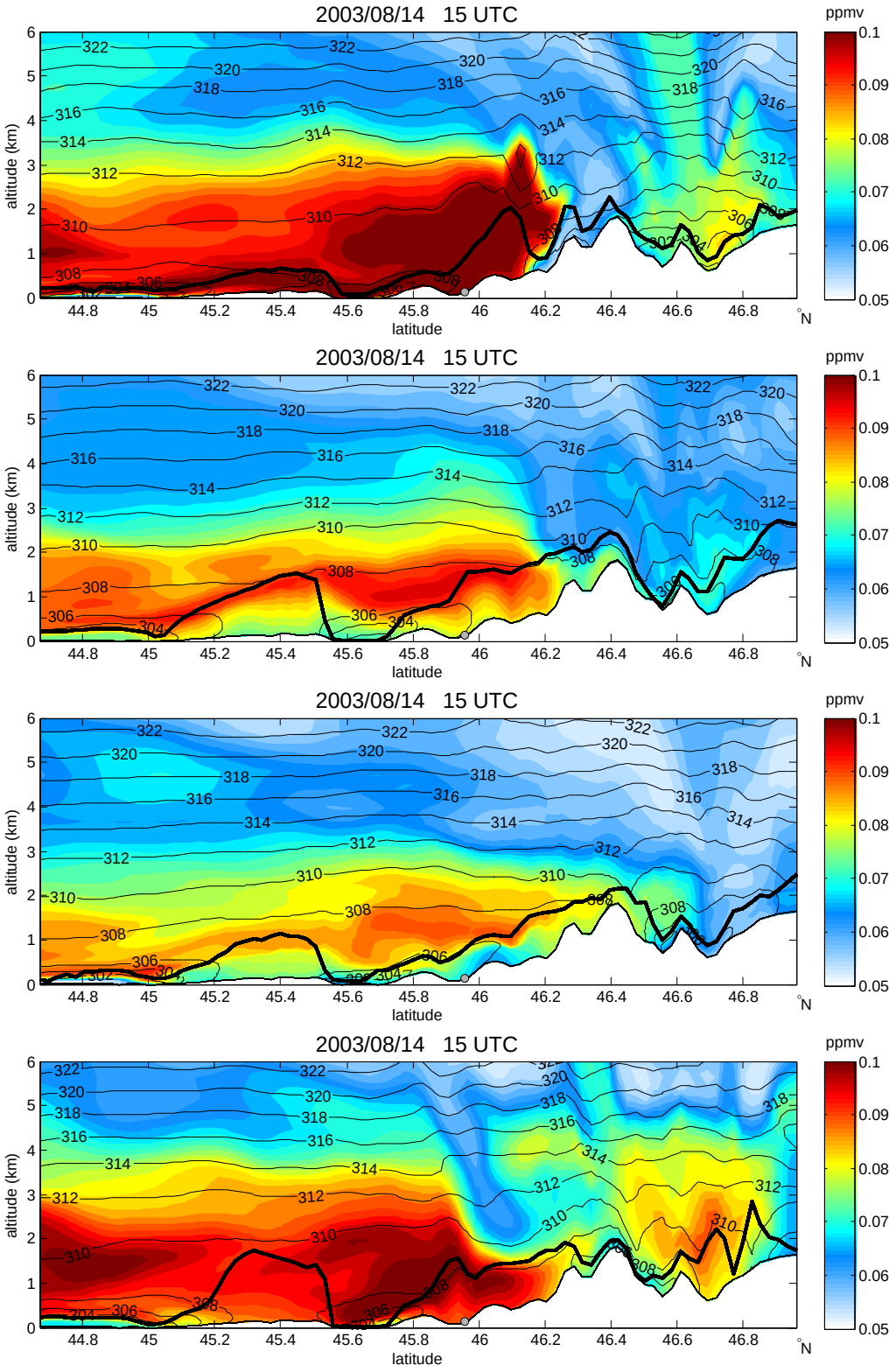

Figure 5.20: The same as Fig. 5.17, but for August 14 at 15 UTC.

For experiments A, B, C1 and D it is hard to make a conclusion about a value of simulated ozone, based on comparison of the near ground ozone time series in Fig. F.6. Perhaps there is some tendency for simulations B and C1 to produce lower near ground ozone at the end of the episode (during the last two days at e.g. IS, LJ), but this is not a rule. The vertical cross-sections for these experiments (examples are shown in Figures 5.17 - 5.20) reveal more features. As already explained, the height to which the increased levels of ozone occur, is related to the maximum PBL height of the present or previous days. It can be noticed from vertical cross-sections, that in simulations A and D the impact of the near ground emission sources (seen here as ozone) reaches higher altitudes, which is a consequence of higher thermal mixing related again to the higher daily near ground temperatures produced by Noah LSM. At the same time, inside this layer, influenced by emissions, the ozone production depends on meteorological conditions. It seems that again vertical temperature profile plays important role: in simulations A and D characterized by higher temperatures (Fig. 5.15) higher ozone concentrations at higher altitudes occur. Actually, differences in vertical ozone profiles among experiments seem to be even higher than in time series of the near ground ozone values. Sometimes these differences are observed mainly in the sense, that ozone maxima are diversely pronounced. For example, ozone layer above the Northern Adriatic area in Fig. 5.18 is resolved in all four experiments, although there are significant differences in its dimensions and the maximum height. Further, the intrusion of ozone rich air in Fig. 5.20 from southwest is as well suggested with all experiments, but its severity varies and sometimes the ozone reach layer does not reach the ground (in simulation C1 around Nova Gorica at 15UTC). Nevertheless, usually the differences among experiments prevent us to make some valuable concrete conclusions about the degree of ozone pollution for limited areas inside the model domain. For example, the air above Gulf of Trieste in Fig. 5.17 (latitudes between 45.5 and 45.7 degrees) can be almost clean (experiment A), almost clean near the sea level and polluted above (experiment B), polluted in the lowest level (experiment C1) and polluted up to almost 2 km (experiment D). Similarly, significant differences can exist among predictions of location and ozone levels in Ljubljana plume. In Figure 5.19 we show examples of vertical cross-section through Ljubljana at constant latitude on August 12, when in Ljubljana the highest ozone levels among all stations were measured. The elevated ozone as a consequence of production from Ljubljana emissions is resolved in all experiments, but the location and severity of maximum vary among the experiments. According to the near ground measurements again simulations A and D follow the observations better. In any case, for more accurate evaluation at least vertical ozone profiles, but better 3D structure measurements should be available.

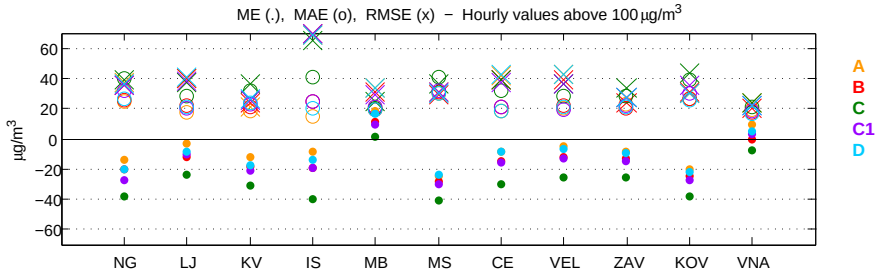

Figure 5.21: Statistical scores for ozone hourly values, only hours with measured hourly ozone above 100 μg/m^3 are taken into account. Statistical scores are explained in Appendix A.

How good are the simulated near ground simulated ozone values? Conventional scores for measurement stations are presented in Fig. 5.21. Only hourly values above 100 $\mu g/m^3$ are taken into account, because we are interested mainly in model ability to predict high (daily) ozone values. In average simulated ozone levels above 100 $\mu g/m^3$ have negative bias (se also Table 5.3), which is most pronounced in experiment C, and is the least in experiments A and D. The positive bias for Maribor was expected, because the station is located near the road and systematically measures low ozone levels on account of ozone titration with NO_x from road emissions. MAE and RMSE, calculated for hours with measured hourly ozone values above 100 $\mu g/m^3$, do not significantly differ among experiments (Table 5.3, Fig. 5.21), except that again the scores for experiment C are substantially poorer. These three statistical scores are calculated also for ozone daily maxima regardless the time of the observed and the modeled maximum. All stations from Fig. 5.21 are included in these calculations (7 days run is too short for statistical analysis of daily maxima for individual stations). Results expose the experiments A and D, as the best according to these scores, followed by experiments C1 and B, and finally with C as significantly worst experiment.

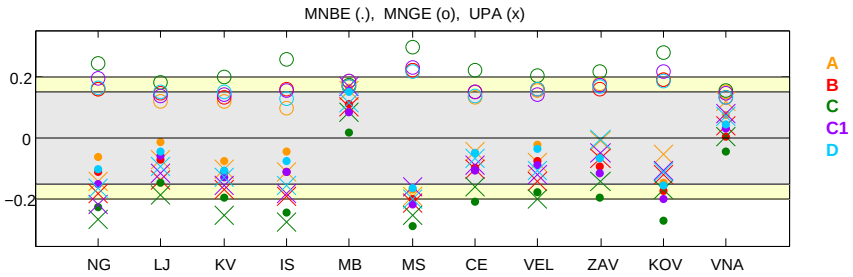

Figure 5.22: Statistical scores for ozone hourly values, only hours with measured hourly ozone values above 100 $\mu g/m^3$ are taken into account. Statistical scores are explained in Appendix A.

In Figure 5.22 MNBE, MNGE and UPA scores for ozone at different measurement stations are shown. According to US EPA recommendations the MNBE values should be less than $\pm$ 0.15 (inside the grey area in Fig. 5.22), MNGE should be less then 0.35 (inside the Fig. 5.22 area), and UPA less then $\pm$ 0.2 (less then the outer yellow edges in Figure). Except for Maribor, where the positive bias is explained by the influence of the nearby road, and for Kovk with negative bias from -0.15 (in exp. A and D) to -0.26 (in exp. C), MNBE values meet the recommendations. UPA values are within the $\pm$ 0.2 for all the stations in all except C experiment, while MNGE is less then the threshold for all the stations even in experiment C. MNBE, MNGE and UPA, calculated over all sites, are compared in Table 5.3, and these scores confirm that in general the best scores for the near ground ozone values are obtained in simulation A, followed by D, then by C1 and B, and the worst are scores for experiment C.

The question arises why do the simulated near ground ozone levels better match the observations in experiments A and D than in other experiments. The fact is that since daily ozone maxima tend to be underestimated by the model in all simulations, the better agreement between observations and experiments A and D is in a great deal a consequence of generally enhanced ozone production in the PBL in these two experiments (which can be observed e.g. in Figures 5.17 - 5.20). It has already been explained that ozone levels correlate significantly with temperature (e.g. Fig. 1.2 - 1.3), and daytime temperatures are higher in experiments A

Table 5.3: Statistical scores for ozone daily maxima (max) regardless the time of observed and modeled maximum, and for measured hourly values above 100 $\mu g/m^3$ (100), calculated over all stations included in Figures 5.21 and 5.22. Units for ME, MAE and RMSE are $\mu g/m^3$, while for UPA, MNBE and MNGE are percentages. Definitions are in Appendix A.

Stats / Exp	A	B	C	C1	D
ME_{max}	-9.4	-19.1	-28.6	-15.9	-14.0
MAE_{max}	19.9	24.0	33.7	23.2	20.5
$RMSE_{max}$	23.4	28.1	40.5	28.4	25.0
ME_{100}	-6.8	-13.8	-27.1	-15.2	-9.7
MAE_{100}	21.2	22.8	31.8	23.8	22.2
$RMSE_{100}$	26.1	26.9	37.9	28.8	27.0
UPA	-0.04	-0.10	-0.16	-0.08	-0.07
MNBE	-1.9	-7.0	-16.6	-8.1	-4.5
MNGE	15.1	15.0	20.7	15.9	15.0

and D with Noah land surface model, while they are systematically underestimated throughout the PBL in the remaining experiments (Fig. 5.15). Besides, water vapor mixing ratios are lower in experiments A and D (e.g. Figure 5.15, Appendix F), and as explained in Introduction (Eq. 1.20), reaction of ozone with water vapor presents important ozone sink. But, although the experiments A and D better reproduce the degree of ozone production, it is still possible that they worse represent the episode in terms of ozone spatial and temporal variability, location of maxima, extensiveness and duration of the highest ozone levels, etc.. The representation of the episode in these terms depends fundamentally on the evolution of the wind field.

As already shown (e.g. by examples in Fig. 5.13 - 5.14), on account on weak dynamical forcing and the prevalent meso-scale winds during the episode, it is very challenging for the model to accurately simulate the evolution of wind field. Consequently, it is hard to accurately simulate the ozone spatial distribution (e.g. the locations and extent of the maxima), specially over complex terrain with heterogeneous land surface characteristics, typical for Slovenia. It showed up that in the case of this episode the simulated near ground wind field was sensitive to almost any change being applied (beside choice of parameterizations also changes in timing of meteorology re-initialization, some soil parameters). Consequently, the direction of advection of emissions from sources and the near ground ozone spatial distribution vary among different simulations. The wind field unpredictability diminishes with the strengthening of external dynamical forcing, in our case with the occurrence of southwesterly flow in the last part of the episode. Figure 5.23 shows an example of the near ground ozone field around Ljubljana on August 8 for simulations A, B, C1 and D. Event hough the simulations started only 15 hours ago with the same boundary and initial conditions, significant differences in ozone field between the simulations can be noted. After 15 hours of simulation the highest near ground ozone values are still similar for all four simulations, but there are distinctive differences in the location of the ozone maxima. Since time is needed for ozone formation from emitted primarily pollutants, the maxima are usually not located over the main emission sources (Ljubljana). They are located in the downwind directions of emission areas, and thus depend on the temporal and spatial development of wind field in relation to the temporal and spatial variations of emissions. With the time elapsed from the beginning of the simulation, the differences in the near ground ozone between the simulations increase.

Finally an estimate of the uncertainties in simulated near ground ozone on account of

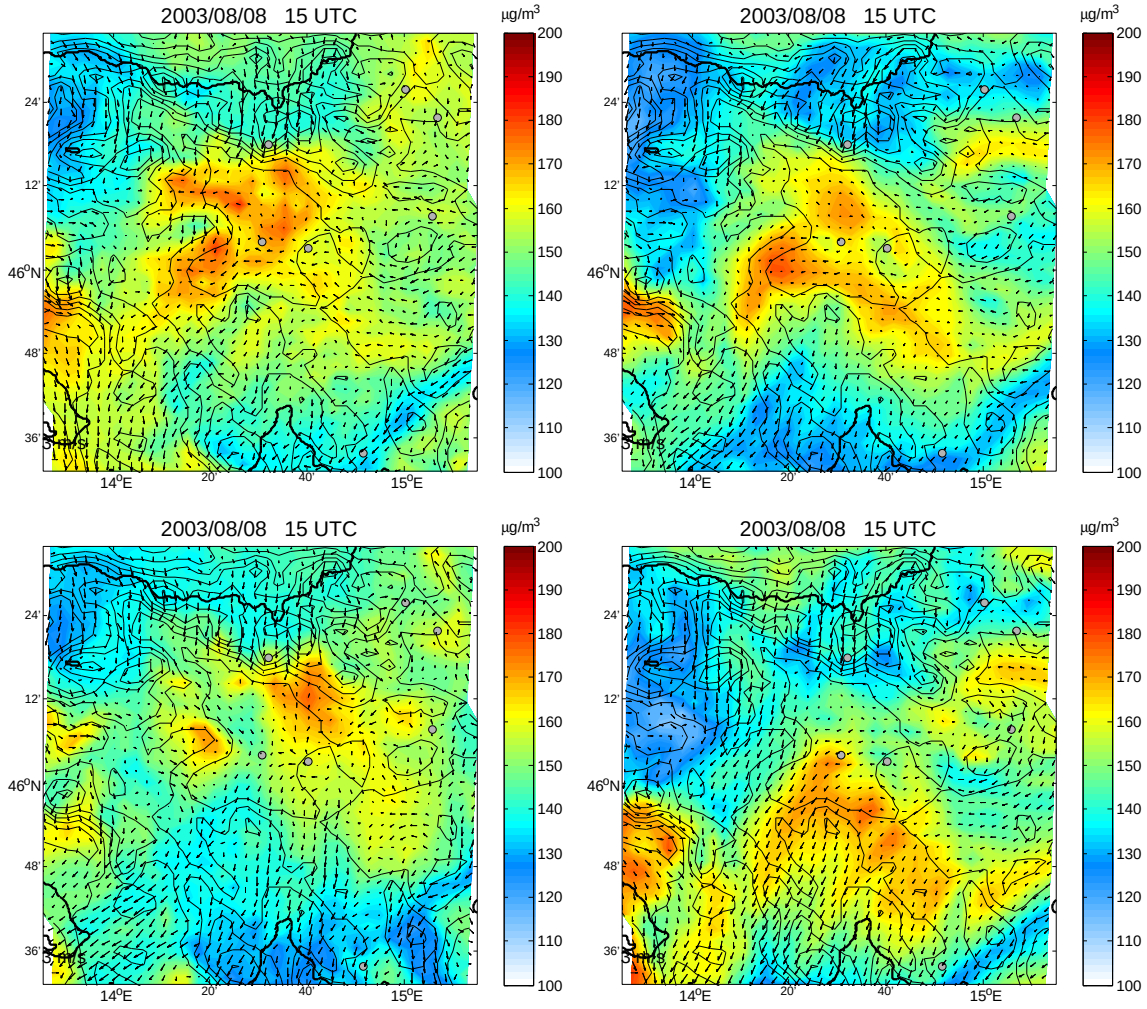

Figure 5.23: Comparison of the near ground ozone field for experiments A, B, C1 and D respectively for August 9 at 15 UTC in an area within the D3 domain, 36×36 points, centered in Ljubljana (grey circle in the middle). Horizontal wind field is shown in every model grid point by arrows. Thin black contours represent topography and bold black lines coast and borders.

uncertainties in PBL meteorological conditions is presented in Fig. 5.24, where for simulations A - C1 the deviations in ozone from reference simulation (run D) are calculated. Presented are results for all ozone hourly values and for daily maxima regardless the time of occurrence. Comparisons of all hourly values for Slovenian measuring sites (Fig. 5.24, left) confirm high sensitivity of ozone spatial distribution and temporal course to somewhat changed mixing, temperatures, winds etc. in the PBL. Differences in hourly values can be up to 60 μg/m^3, for simulation C even up to 80 μg/m^3. These results show again that because of ozone sensitivity to somewhat changed meteorological conditions it is hard to accurately predict the ozone course for individual points, as it is hard to accurately predict the locations and the time of occurrence of ozone maxima and minima over Slovenia. What we can probably expect from an accurate simulation is that it reasonably well estimates the overall Slovenian daily maxima and perhaps to some extent their extensions. But in general we cannot rely on details about temporal and spatial variability of the ozone field based on any of the simulations.

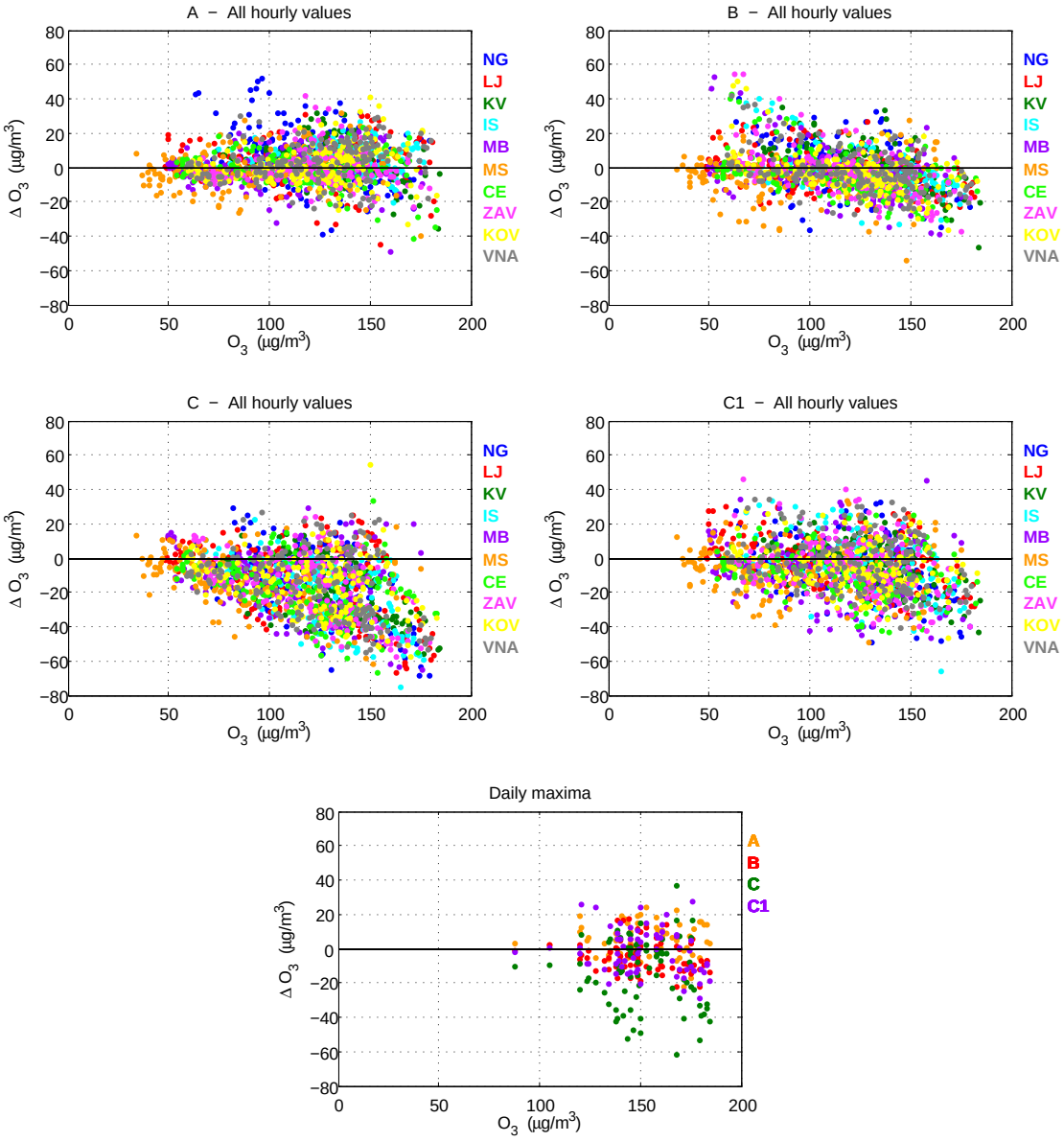

Figure 5.24: Deviations in ozone values from reference D simulation for simulations A, B, C, C1 with changed model LSMs and PBL schemes. Upper and middle panels: comparisons of all hourly ozone values for model points representing Slovenian ozone measuring sites. Lower panel: comparison of daily maxima only (for points representing measuring sites), regardless the time of daily maximum occurrence. Differences are calculated as experiment minus reference D simulation. Ozone values on x axis correspond to ozone value in reference simulation.

Even for ozone daily maxima (Fig. 5.24, right) differences among experiments can be rather high. Leaving the experiment C aside, differences in daily maxima are up to 30 μg/m^3. This value, as well as Fig. 5.24, will be used for relative comparisons of ozone sensitivity to uncertainties in simulated meteorological conditions to other sources of uncertainties (boundary and initial conditions, emissions, model resolution). In the sections that follow, we continue with the study of some of these influences on simulated ozone levels.

5.1.4 Impact of horizontal resolution

We further analyze the influence of reduced horizontal resolution on the simulated ozone by comparing the results of D2 domain with 9 km horizontal resolution to the results of D3 domain with 3 km resolution for reference D simulation. This comparison is possible, because by performing the simulations with one-way nesting strategy (with feedback from the internal D3 domain turned off) we have no noise in D2 from D3 domain.

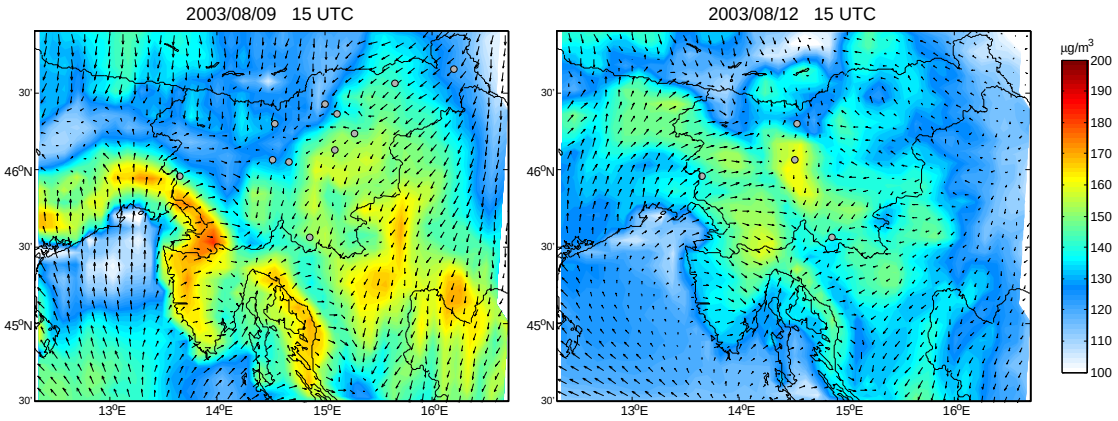

Figure 5.25: Examples of simulated near ground ozone field and surface winds from the coarse resolution simulation (reference simulation D but for domain D2 with 9 km resolution). Shown are results for an area inside the D2 domain, which approximately coincide with the D3 domain.

Figure 5.25 shows examples for the near ground ozone and surface wind fields in the area, extracted from the D2 domain with 9 km horizontal resolution. These fields can be directly compared to results from the 3 km resolution D3 domain for the same time (Fig. 5.7, the middle two panels). Coarser model resolution means coarser model topography, land surface data etc., and consequently smoother wind and ozone fields. As a consequence of somewhat changed winds in coarser domain (other meteorological variables probably have minor influence) the locations of ozone maxima and minima can be shifted, as well as some fine structures are lost. Nevertheless, in comparison with the changes obtained by selection of different model PBL scheme and LSMs, the coarser horizontal resolution appears to change surface ozone fields to a lesser extent. This conclusion is supported also by Fig. 5.26, where deviations between surface ozone obtained with 9 km and 3 km resolution are calculated for model points that represent the Slovenian measuring sites. If comparison of these results to Fig. 5.24 is made, it can be quickly noticed, that deviations in ozone are now less pronounced as they were on account on changed model schemes.

At certain locations ozone values in coarser domain can be coincidentally lower or higher than in domain with finer resolution. One of the reasons for that is a smoother coarser grid solution (compare e.g. Fig. 5.26 to Fig. 5.7), leading to enhanced or reduced ozone values on certain locations. Furthermore, a finer grid may sometimes over-emphasize flow adjustment to micro-terrain features (leading to more noise in solution) compared to the regional flow. This may explain why sometimes happens that coarse results are better then the fine ones.

With some rare exceptions, differences in ozone daily maxima between 9 km and 3 km simulation in Fig. 5.26 are not higher than $\pm$ 10 μg/m^3 (for Murska Sobota ozone is once reduced for 23 μg/m^3, and for two sites the ozone is reduced for 15 μg/m^3 in coarser resolu-

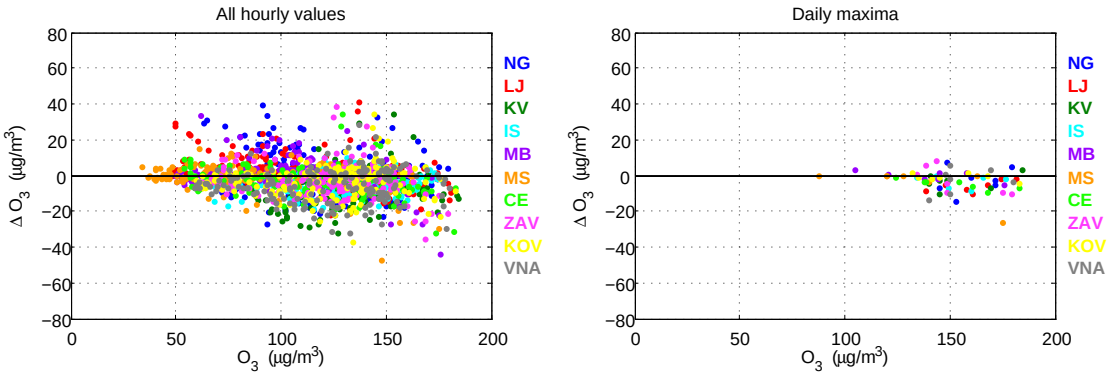

Figure 5.26: Deviations in the near ground ozone values in model points that represent the Slovenian measuring sites as a consequence of reduced horizontal resolution. Shown are differences for all hourly ozone values (left) and daily maxima regardless the time of maximum (right) between ozone in 9 km domain D2 and 3 km domain D3 in $\mu g/m^3$. Ozone on x axis correspond to 3 km resolution values in reference model run.

tion). The deviations are more pronounced in comparison of all hourly ozone values for the points representing Slovenian measuring sites, and are somewhat lower than in Fig. 5.24: the deviations caused by different horizontal resolutions are smaller than the ones resulting from different simulated PBL meteorology.

In the experiments presented in the subsequent sections we run the model only with two domains, D1 and D2, and compare the results obtained for domain D2 to the results of the reference simulation D for domain D2, analyzed in the present Section.

5.1.5 Impact of anthropogenic VOC speciation

The purpose of the next experiment is to study the near ground ozone sensitivity to uncertainties in anthropogenic VOC speciation. We perform a simulation, which is identical to experiment D presented so far, except that different speciation is applied to anthropogenic VOC emissions. The simulation is performed for both, D1 and D2 domains, and ozone values in D2 domain are then compared to ozone values in D2 domain from reference experiment D.

The VOC's emissions category contains hundreds of different compounds. According to e.g. Sillman (1999) the true impact of VOC on ozone chemistry is related more closely to the reactivity of the VOC species than to the total amount of VOC. Actually, the speciation is particularly important at considering biogenic VOC, because biogenic VOC are extremely reactive and their impact on ozone production is large relative to their ambient concentrations. Nevertheless, here we study only the impact of changes in anthropogenic emissions speciation.

The procedure used for VOC speciation for different emissions sources and the subsequent grouping of different VOC species into lumped species according to reactivity rates, is described in Section 4.3. Many approximations, as a consequence of insufficient data, had to be done in this procedure. To evaluate the impact of this uncertainties in VOC speciation, another VOC speciation, suggested by Passant (2002) for EMEP SNAP sector emissions, was used. The conversion factors for this alternative speciation (from tones of EMEP SNAP VOC emissions into moles of RADM2 lumped species) were calculated according to Carter (2007). These conversion factors are collected in Appendix C (Table C.4). For SNAP sectors 10 and 11, since VOC speciation by Passant (2002) for these sectors was not supplied, the speciation from Section 4.3 for these sector emissions was used.

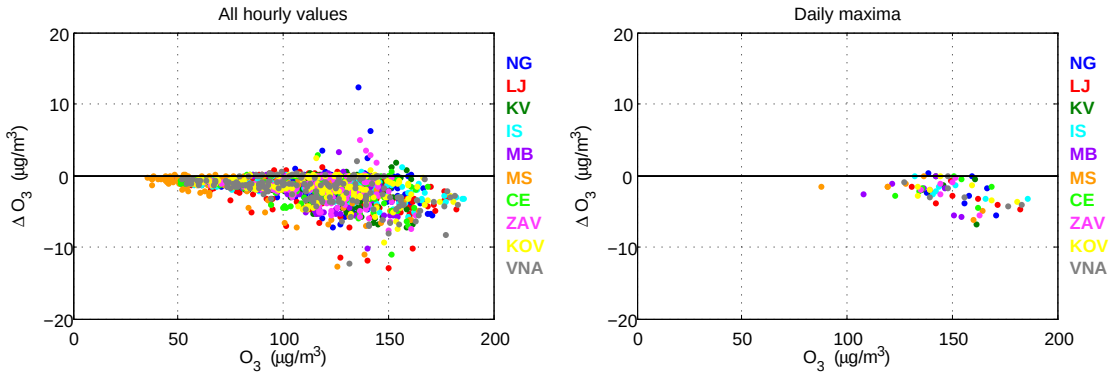

Figure 5.27: Differences in simulated ozone values in D2 domain, obtained with two different VOC speciations for 8 - 14 August 2003. Left: comparison of all hourly ozone values for model points that represent the Slovenian ozone measuring sites. Right: the same, but for daily maxima. Differences correspond to simulation with changed VOC speciation minus reference simulation, while ozone values on x axis are the reference simulation values.

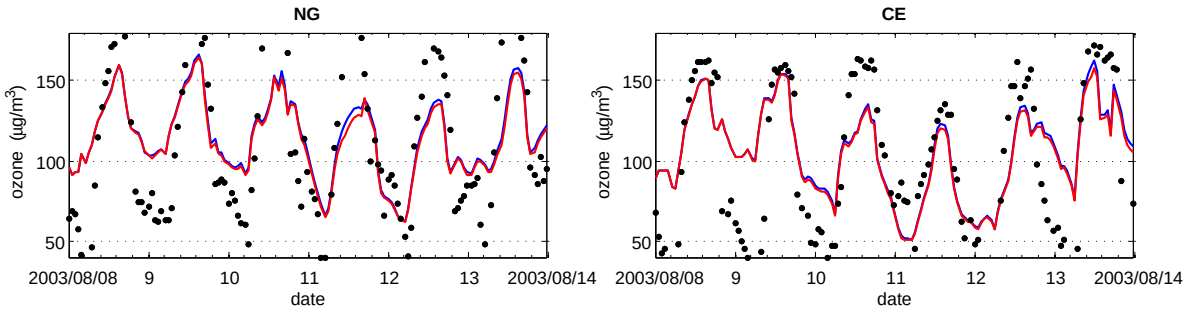

Figure 5.28: Ozone time series for Nova Gorica and Celje station. Blue line: experiment D, ozone values from D2 domain; Red line: the same but with different VOC speciation; Black dots: hourly measurements.

Figure 5.27 presents deviations in simulated surface ozone as a consequence of different anthropogenic VOC speciation (note that y-axis scale is changed according to Figures 5.24 and 5.26). The ozone sensitivity on the applied changes in VOC speciation is significantly smaller than it is when meteorological schemes and horizontal resolution are tested. Daily maxima now differ only up to about 5 μg/m^3, while comparison of all hourly values for model points representing the measuring sites, exhibits slightly higher sensitivity. There are some exceptions, but in general these differences are up to 10 μg/m^3.

Comparison of temporal courses between the two simulations reveal only minor differences between the two runs. Example for two sites is shown in Fig. 5.32, and the influence of different anthropogenic VOC speciation on ozone time series for the other measuring sites is very similar.

On the basis of these results we can conclude, that model results seem not to considerably depend on the details in these two different anthropogenic VOC speciations. Discrepancies between model and measurements are likely to originate from other more dominant sources of uncertainties.

5.1.6 Impact of bulk ±30% changes in VOC and NO_x emissions

Since the uncertainties in emission database prepared for the purpose of our study might be significant, in the present Section the NO_x and VOC emissions and their impact on simulated ozone is studied. With the experiments presented here we try to find the answers on the following questions:

1. What is the impact of emission uncertainties on simulated ozone?
2. Can be systematic errors in simulated ozone for some locations explained by under- (over-) estimation of specific pollutant emissions?
3. Is ozone at Slovenian measuring sites more sensitive to changes in VOC or maybe to changes in NO_x emissions?

These questions must be studied in the light of the complex nature of the O_3 - NO_x - VOC relations. As briefly explained in Introduction, Section 1.2.3, for some conditions (in Fig. 1.7 for VOC/NO_x>15) the process of ozone production is almost entirely controlled by NO_x and is largely independent of VOC (NO_x sensitive conditions). For other conditions (in Fig. 1.7 for VOC/NO_x<4) ozone production increases with increasing VOC and does not increase (or sometimes even decreases) with increasing NO_x (VOC sensitive conditions). Consequently, in our experiments in some locations ozone is more likely to be sensitive to uncertainties (errors) in VOC emissions (its production will not change significantly by changing NO_x), while the opposite may hold for other locations. In addition, these characteristics are influenced by meteorological conditions, as well. If we want to study the impact of the changed NO_x and VOC emissions, it is thus crucial to study this impact together with the ozone sensitivity for that time and place.

Typically, but not always, freshly emitted pollutants are characterized by VOC sensitive chemistry. As the air parcels age, the VOC/NO_x ratios increase and the chemistry changes from the VOC sensitive to NO_x sensitive conditions (e.g. Milford et al., 1994; Sillman, 1999). In real world this idealized pattern is modified by the complex spatial variability of emissions. Beside VOC/NO_x ratio there are also other factors affecting the O_3 to VOC and NO_x sensitivity. According to Sillman (1999) the VOC or NO_x sensitivity in models is influenced also by:

- VOC reactivity: Locations with highly reactive VOC (xylenes, isoprene,...) are more likely to have NO_x sensitive chemistry.
- Biogenic hydrocarbons: Biogenic VOC are extremely reactive relative to most anthropogenic VOC, consequently their impact on ozone production is large relative to their ambient concentrations.
- Photochemical aging: Close to the emission sources a polluted air is likely to have VOC sensitive chemistry. As the air mass ages, chemistry shifts to NO_x sensitive. The shift is often accelerated by the biogenic emissions.
- Severity of pollution: Events with higher overall ozone concentrations are likely to have peak ozone sensitive to VOC chemistry, while events with lower precursors are more likely to have peak ozone sensitive to NO_x.
- Meteorological conditions: Decreased sunlight, increased cloud cover and decreased water vapor cause a shift toward VOC sensitive chemistry, as a consequence of a reduction

in the source of radicals. Stronger winds and more rapid dispersion act toward NO_x sensitive chemistry, while stagnant events with light winds cause a shift toward VOC sensitive chemistry by allowing air to go under photochemical aging for a longer period before it is advected out of the area of emission sources. Lower temperatures correlate with lower biogenic emissions, which favors VOC sensitive conditions.

Our strategy was as follows. The experiment with reference configuration D (boundary and initial conditions, meteorology) was run with four different (± 30 % VOC and ± 30 % NO_x) emissions. A 30 % bulk emissions change was applied for all anthropogenic sectors over all European emissions. Model was in these experiments run on D1 and D2 domain. Changes in simulated ozone as a consequence of emission changes were then analyzed together with simulated afternoon O_3/NO_y ratio. The values of afternoon O_3/NO_y ratio can be (similarly as the values of initial morning VOC/NO_x ratio) used as indicator for NO_x or VOC sensitive conditions. According to Sillman (1995, 1997) O_3/NO_y ratio over 8 (ratio with median 11) indicates NO_x sensitive conditions, O_3/NO_y ratio below 6 (ratio with median 5) indicates VOC sensitive conditions, while conditions with O_3/NO_y ratio between 6 and 8 are transitional. NO_y we calculated as a sum of volume parts per million of the following simulated compounds: NO, NO_2, HNO_3, PAN, NO_3, N_2O_5 and HONO. O_3 values were left in ppmv units in calculations of the O_3/NO_y ratio.

In Figure 5.29 deviations in the near ground ozone levels caused by 30 % bulk changes of NO_x or VOC emissions are shown. The response to NO_x reduction may be either ozone reduction or enhancement, depending on the type of conditions (NO_x or VOC sensitive) of the place and time. On the contrary, the reduction of VOC generally leads to ozone reduction, and vice versa. Surprisingly, although the reduction/increase of emissions is considerable the comparison shows differences usually less than 10 $\mu g/m^3$ for all hourly values. Most of daily maxima change for less than 5 $\mu g/m^3$. The exception is Nova Gorica station, where applied differences in emissions have higher influences on ozone, up to 20 $\mu g/m^3$ for all hourly values and up to 10 $\mu g/m^3$ for daily maxima.

Results in Fig. 5.29 can be further explained by Fig. 5.30, where afternoon ozone deviations caused by emission changes for the model points representing measuring sites are shown as a function of O_3/NO_y ratio. In Fig. 5.30 the transition zone suggested by Sillman (Sillman, 1995; Sillman et al., 1997), $6 \leq O_3/NO_y \leq 8$, between VOC and NO_x sensitive conditions is marked with grey. In our results the transition zone seems to be slightly moved towards higher O_3/NO_y ratios (ratio value somewhere between 8 and 10). For ratio values higher than transitional sites experience NO_x sensitive conditions. In such conditions ozone is more sensitive to changes in NO_x than VOC emissions. Another characteristic of NO_x sensitive conditions is, that NO_x increment always leads to ozone increment as well. The site with the most pronounced NO_x sensitive conditions (Fig. 5.30) in the afternoons during the episode is the rural station Iskrba. On the other hand the O_3/NO_y ratios below the transition zone indicate the VOC sensitive conditions, where ozone is more sensitive to changes in VOC emissions. Moreover, in these conditions NO_x reduction leads to the ozone increment. Such conditions during the episode prevailed at the Mediterranean station Nova Gorica.

It can be now explained why in Fig. 5.29 at the point representing Nova Gorica station ozone was occasionally significantly more sensitive to emission changes than the points representing other stations. If in the afternoon Nova Gorica experienced the VOC sensitive conditions, the conditions in Nova Gorica are expected to be even more VOC sensitive for the rest of the day and during the night. (We explained how the meteorological conditions cause shift towards VOC sensitive chemistry.) In the "highly VOC sensitive hours" the emission

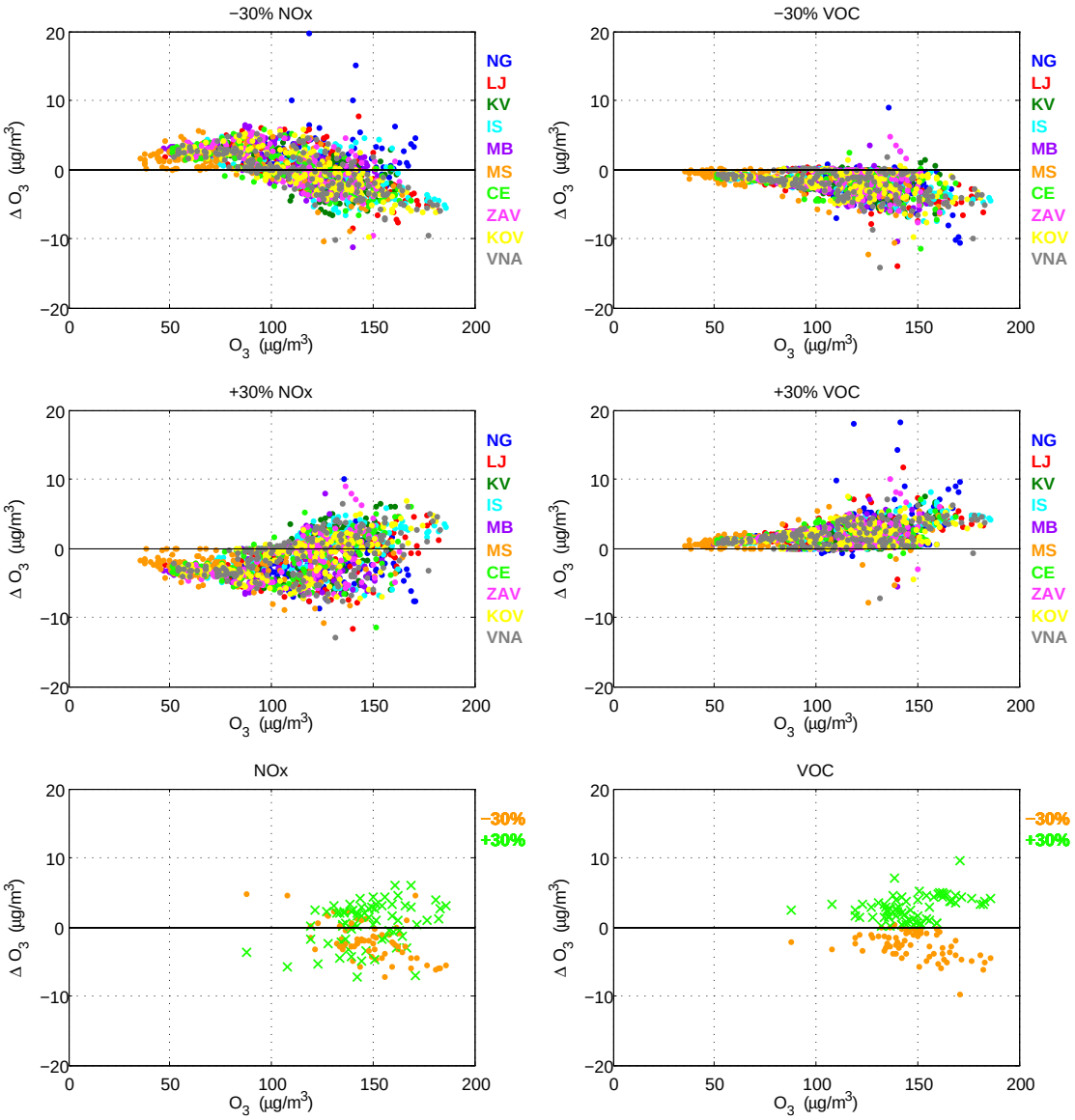

Figure 5.29: Influence of ±30% NO_x or VOC bulk emission changes on simulated ozone. Shown are differences in ozone according to reference run for model points representing measuring sites over Slovenia for 8 - 14 August 2003. Left: run with ±30% NO_x emissions, Right: ±30% VOC. Upper and middle panels: all hourly ozone values. Bottom panels: daily maxima only. Ozone values on x axis correspond to values in reference simulation.

changes had even more pronounced impact on the near ground ozone levels at this site.

It is worth to explain how the Nova Gorica in simulations experiences the VOC sensitive conditions. In reality there are only some moderate emission sources near the site (mainly from traffic), and no major NO_x sources (like a power plant). Why does then air appear to be "saturated" with NO_x? We suspect, that the simulated VOC sensitive conditions, which often appear at this station is arise from errors in spatial disaggregation of anthropogenic emissions outside Slovenia. Since we had no data about the locations of major point sources outside Slovenia (we downscaled the area emissions), the emissions were distributed according to population density and land cover. Many of large point sources in this area are located

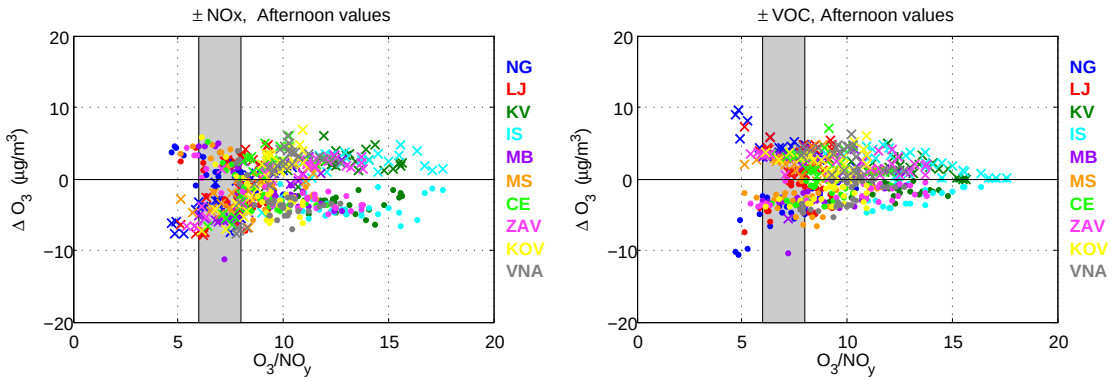

Figure 5.30: Afternoon ozone changes (for hours 12 - 16 UTC throughout the simulation) for four emission scenarios (+30%:crosses, −30%: dots) as function of O_3/NO_y ratio. Left: ±30% NO_x, Right: ±30% VOC. Grey patch denotes the transition area between VOC and NO_x sensitive conditions, according to Sillman (1995).

near the coast, and since the method based on the population density can not deal with them appropriately, small towns inside 50 km×50 km square were assigned significantly higher emissions on account of huge points sources inside the same square. Nova Gorica is located in the border between Slovenia and Italy, in fact the town is connected with Italian Gorizia into one urban agglomeration. The effect of artificially enlarged (NO_x) emissions in Gorizia, as well as in other small towns in Friuli-Venezia Giulia region on account on coastal point sources, may cause the ozone VOC sensitivity conditions in model at Nova Gorica station. Similar phenomena was noticed in northern Slovenia, when at the beginning the Šoštanj power plant was not considered as a point source. The problem was not solved well in the areas outside the country, and probably affects simulated ozone mainly at the near border Slovenian measuring sites. For Nova Gorica station it is important to point out, that this problem may explain the systematic underestimations of daily simulated ozone at this station. Additional reason for simulated daytime ozone underestimations (in Mediterranean and non-Mediterranean Slovenia) may as well present underestimated biogenic emissions.

The relation in Fig. 5.30 between the O_3/NO_y ratio and the effect that have emission changes on the near ground ozone can now be more widely used. From the O_3/NO_y ratios we can get the estimate for O_3 sensitivity to ±30% emission changes for other simulations without additional model runs. For example, we can compare the ozone sensitivity to ±30% changes in emissions for experiments A-D (from Section 5.1.3) on the basis on O_3/NO_y fields. For August 9 at 15 UTC the near ground O_3/NO_y ratios are shown in Fig. 5.31. It can be seen, that in this case all simulations have some common VOC sensitive areas (like blue areas around Ljubljana, Zasavje, downwind area of the Šoštanj Power Plant, Maribor, coast in Gulf of Trieste, Rijeka etc.). In simulations A and D otherwise the NO_x sensitive conditions over Slovenia predominate in widespread red areas, while in simulations B and C1 transitional conditions (green) are dominant over the majority of the area. Marked differences in simulated ozone sensitivity are for these runs obtained above the Adriatic Sea. Consequently, in e.g. simulation B the near ground ozone above the Adriatic Sea would increase with the increased NO_x, while would increase only with increased VOC and decrease with increased NO_x in other three cases.

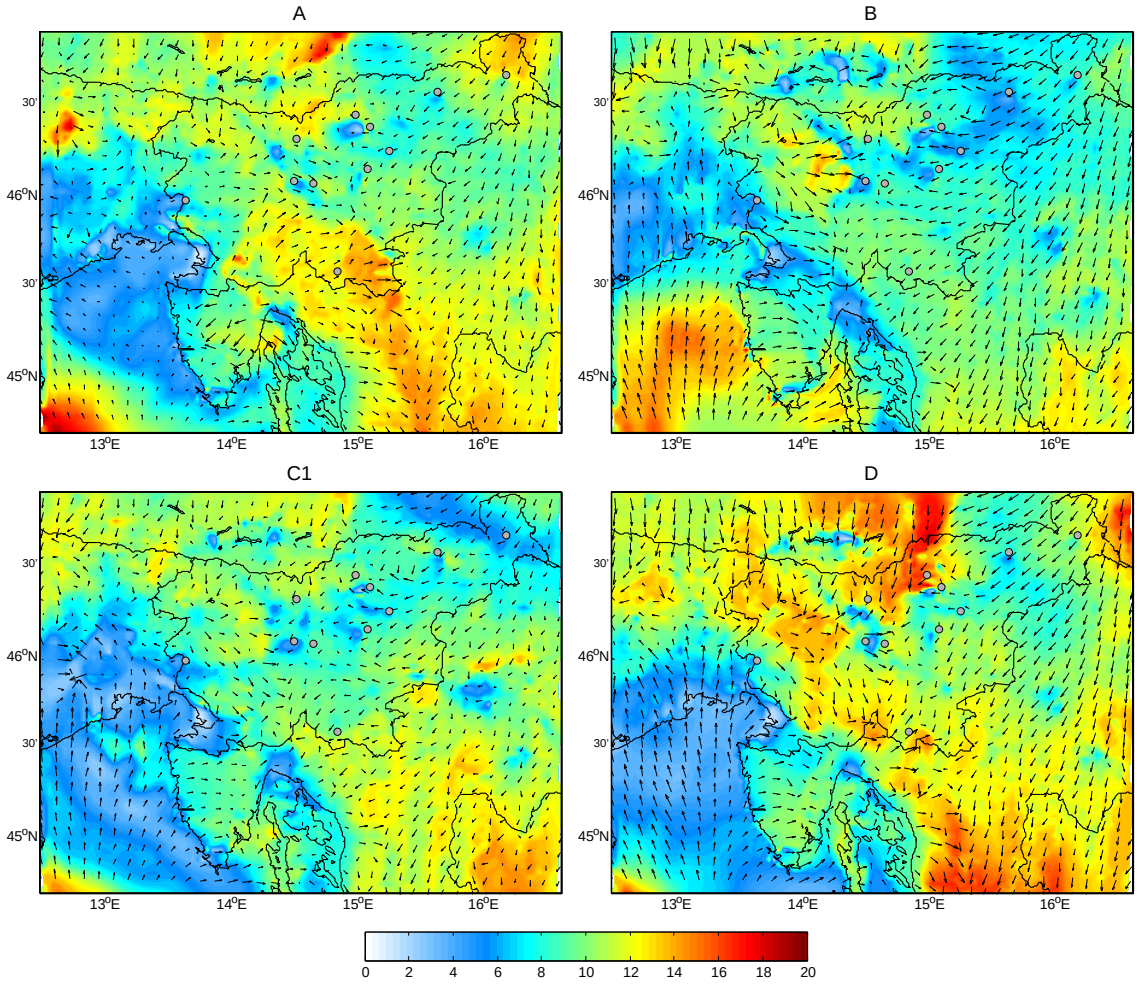

Figure 5.31: O_3/NO_y ratios for experiments A, B, C1 and D from Section 5.1.3, calculated for August 9 at 15 UTC, D3 domain.

We can expect, that the estimate of the degree of changes in modeled ozone values as a consequence of 30 % changes in VOC/NO_x emissions, is for different O_3/NO_y ratios representative also for other (meteorologically) similar episodes. Actually, the same experiment with 30 % emission changes, performed for the episode presented in the next Section 5.2 (June 2004), showed similar relation between O_3/NO_y ratio and the response in simulated ozone (results of this experiment can be found in Appendix G).

Figure 5.32 shows examples of temporal courses for the emission experiments. Differences in ozone among the experiments are mainly in the form of more or less pronounced maxima and minima. More variability among the experiments would be obtained, if some spatial variability would be introduced to the emission fields (instead of the simple bulk rate reduction/increment), while the size order of changes would probably remain similar also in that case. The latter is important, because errors in emissions are certainly not evenly spread in space, while the actual total amount of emissions is likely to be within ± 30 % of the current estimates.

At the end we can conclude, that ozone deviations as a consequence of the applied 30 % bulk emission changes are even in the most sensitive conditions significantly less pronounced than

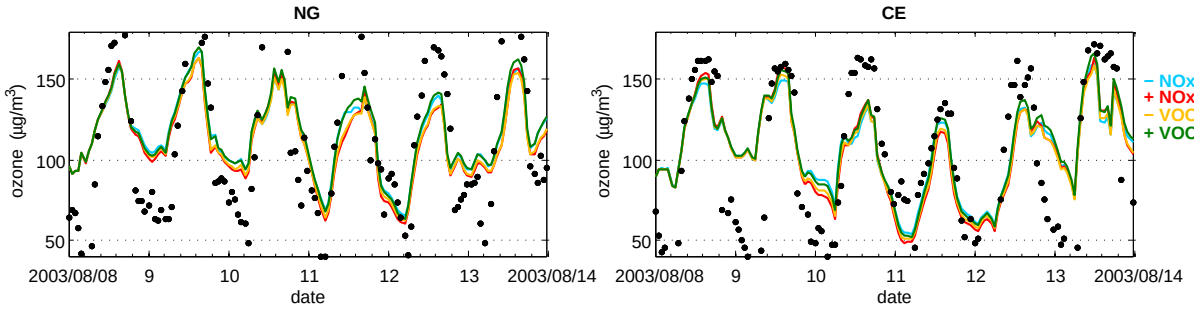

Figure 5.32: Ozone time series for Nova Gorica and Celje station. Shown are simulated ozone values (from D2 domain) for four experiments with ± 30 % bulk changes in VOC or NO_x emissions. Measured hourly values are marked with m.

they were due to the changed PBL meteorology. With the exception of the near border stations (Nova Gorica, Murska Sobota), for which discrepancies between model and measurements may be to some extent explained by the emission errors, for the interior of Slovenia this is less likely to be the case.

5.1.7 Impact of chemical initial and lateral boundary conditions

To minimize the uncertainties in simulated ozone, arising from the uncertainties in initial chemical conditions, chemistry was always initialized from previous runs. We analyze the model results after at least 3 or 4 days of simulation, but usually we wait even longer. The question arises whether such a long model adaptation is really necessary. And further, to which extent does the state of the previous day(s) influence the today's ozone levels?

In the present experiment the chemistry on August 8 is initialized with the WRF-Chem idealized routines and the results of this simulation are compared to the reference D simulation, where chemistry is initialized from previous run. On the first day of simulation differences in ozone are enormous (Fig. 5.33 and 5.34). The differences for the near ground ozone values then diminish with each additional day of simulation. On the fourth day the near ground ozone levels over Slovenia are identical in both simulations. Nevertheless, there are still considerable differences in the near ground ozone over Italy and over the Adriatic Sea, which are even more pronounced in the higher model levels. On the fifth day of simulation results for the near ground ozone over Slovenia from both simulations further remain the same. But, at the end of the episode, on August 13 and 14, the differences between the two simulations become evident over Slovenia again. The reason for such development is, that with the south-westerly flow the pollution accumulated over a longer time period over Adriatic Sea and over Italy and Ligurian Sea in previous days (weeks), is now advected towards Slovenia. Different time available for the accumulation of pollutants over these areas (in reference simulation the accumulation began on August 1, while in experimental run on August 8), results in different influence of (with southwesterly winds) advected pollution to the simulated ozone over Slovenia.

For initial conditions we can conclude, that they are extremely important. Specially on the first and on the second day of simulations with different initial conditions, differences in ozone over Slovenia were as high as 60 $\mu g/m^3$. Although in the consequent days these differences over Slovenia diminish, they become visible again when the regional transport of polluted air became important at the end of the episode. This experiment so at the same time confirms,

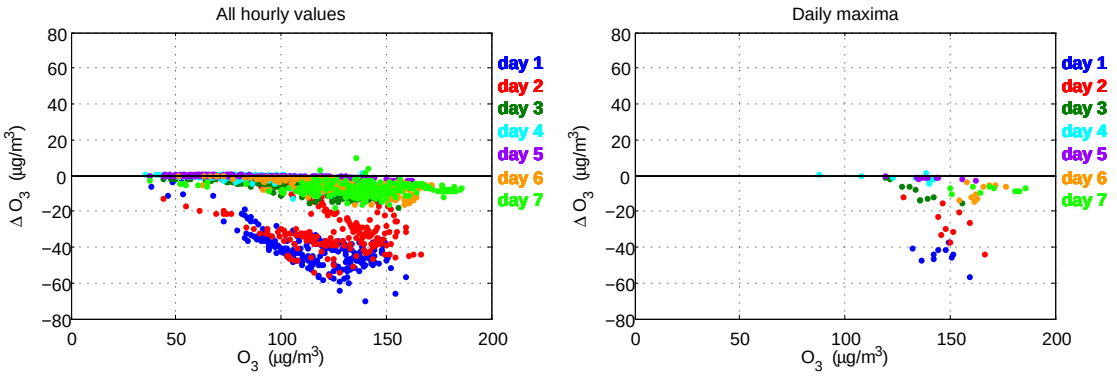

Figure 5.33: Differences in simulated ozone values near to the ground, obtained with two different chemical initial conditions for 8 - 14 August 2003. The reference simulation is compared to the run with chemistry initialized on August 8 from the WRF-Chem idealized routines. Left: all hourly ozone values, points corresponding to Slovenian ozone measuring sites. Right: the same, but for daily maxima only. Differences are calculated as experimental run minus reference simulation. Ozone values on x axis are from the reference simulation.

that in the last part of the August 2003 episode, the pollution accumulated during a longer time period over Mediterranean (with Po Basin emissions as the main source), contributed to very high ozone levels over Slovenia. Even 7 days of simulations appears to be in this case not enough to get the actual degree of accumulated Mediterranean pollution.

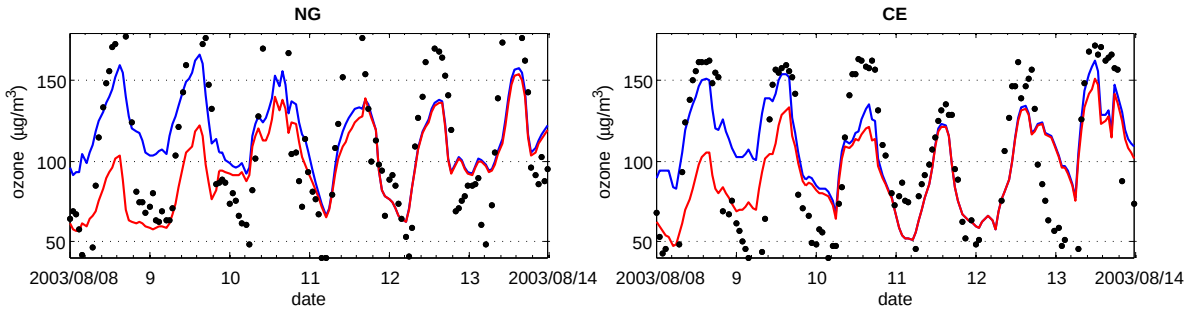

Figure 5.34: Ozone time series for Nova Gorica and Celje station from D2 domain for two different initial chemistry conditions. Blue: reference simulation, initialized from previous run; Red: initialized from the WRF-Chem idealized chemistry profile.

In other words, to simulate the today's ozone levels accurately, it is crucial to start with accurate initial conditions. Due to a continuous transport and accumulation of ozone and precursors in the broad region, it is difficult to accurately define initial conditions. Consequently, initial conditions can lead to considerable uncertainties in model results.

To test the influence of chemical lateral boundary conditions, we performed an experiment, where emissions in D1 domain (outside the D2 domain) were set to zero. The purpose of comparing the results of this experiment to otherwise identical reference simulation was to determine whether the inclusion of D1 domain is unavoidable, as well as to study to what extent the regional transport from central Europe contributes to ozone levels over Slovenia.

The stronger is the advection, the greater is the importance of the proper specification of

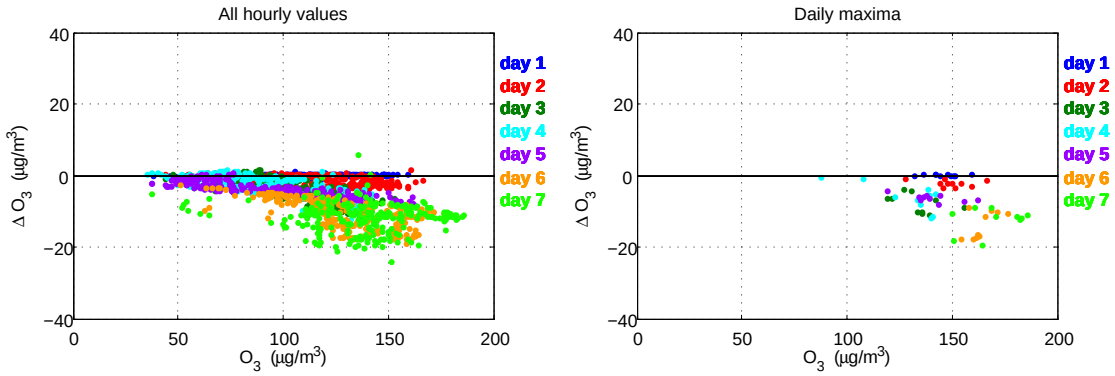

Figure 5.35: Differences in simulated ozone values, obtained with two different chemical lateral boundary conditions for domain D2 for 8 - 14 August 2003. The reference run is compared to the run with emissions set to zero outside the D2 domain. Left: all hourly ozone values, points corresponding to Slovenian ozone measuring sites. Right: the same, but for daily maxima only. Differences are calculated as experimental run minus reference simulation. Ozone values on x axis are from the reference simulation.

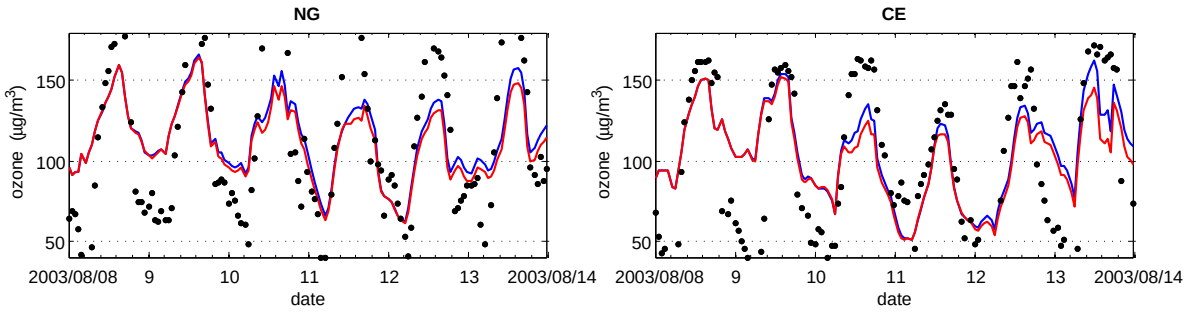

Figure 5.36: Ozone time series for Nova Gorica and Celje station from D2 domain for two different lateral chemical boundary conditions in domain D2. Blue: reference simulation, lateral chemical conditions calculated online from D1 domain every time step; Red: the same, but emissions in D1 domain are set to zero.

lateral boundary conditions. The influence of changed chemical lateral boundary conditions on the near ground ozone levels above Slovenia in the present experiment is shown in Fig. 5.35 and 5.38. From the third day onwards the influence of the chemical lateral boundaries is of the order of 10 - 20 μg/m^3. This values can be taken as estimate for the influence of regional transport on Slovenia ozone from areas outside domain D2. Results confirm, that the inclusion domain D1 is required. Otherwise at the lateral boundaries of domain D2 the levels of chemical species may not be specified accurately enough for runs over longer time intervals.

If concentrations of species at relatively distant lateral boundaries of domain D2 are important, it is even more clear, that Slovenian ozone is a part of the overall pollution over a much wider area. Setting the emissions to zero everywhere except in Slovenia (not tested) would dramatically reduce the pollution over Slovenia: Slovenia is a small country and as such is under the significant impact of transport of pollution from neighboring countries.

5.1.8 Impact of meteorology re-initialization

According to the results of experiments presented so far in 5.1.3 - 5.1.7 the planetary boundary layer meteorology and the transport and accumulation of pollution during previous days present the most important, but the least manageable source of uncertainties in simulated ozone. I thus decided to complete the series of sensitivity tests with the final experiment, where the frequency of re-initialization of meteorological fields is increased.

In the previous simulations were meteorological fields re-initialized on August 8 and August 13. The evaluation of the near ground meteorological variables confirmed, that from the "weather" point of view this was sufficient. However, this may not hold true as regards transport and dispersion of pollutants. With more frequent re-initializations of meteorological fields specially the air flow at higher altitudes (still inside daytime PBL heights) might be better represented, which may further affect the pollution transport and finally the near ground ozone levels.

In this final test a simulation with re-initialization of meteorological fields every 2 days was performed, that is on August 10, 12 and 14 at 00 UTC. Otherwise the simulation was again identical to reference experiment D in Section 5.1.3. All three domains (D1, D2, D3) were included in simulation, to make the comparison to experiment D possible. The evaluation (statistical and comparison of time series) of the near ground meteorological variables showed no significant differences between the two simulations (results not shown). Even the vertical profiles of statistical scores for meteorological variables (like in Fig. 5.15) are similar (not shown).

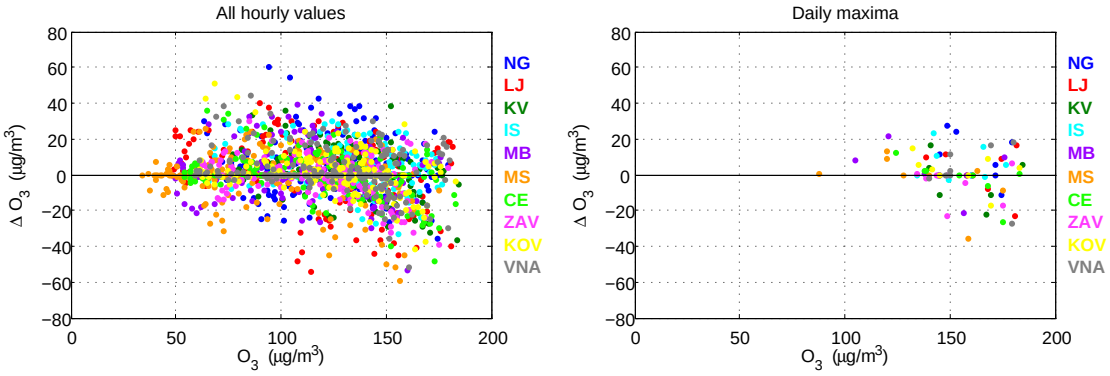

Figure 5.37: Differences in simulated ozone values, obtained from simulations with different frequency of re-initialization of meteorological fields. The reference simulation is compared to the run with every 2-days re-initialization.

However, the analysis of the near ground ozone values reveals differences of the same order as were obtained by changing PBL scheme or LSM in model. Differences in daily maxima are within ± 30 % and for comparison of all hourly values are within ± 60 % (Fig. 5.37). In average there is somewhat better agreement with measurements for simulation with every 2-days re-initialization. Average statistical scores for ozone daily maxima are now 10.0, 19.9 and 23.7 μg/m^3 for ME, MAE and RMSE respectively, compared to slightly worse scores for experiment D in Table 5.2.

Looking at individual stations, the largest improvement can be seen for Nova Gorica, here results from the reference simulation were (specially between August 8 and 13) the worst of all measuring sites. On August 10 and 11 in the present experiment the ozone rich zone formed

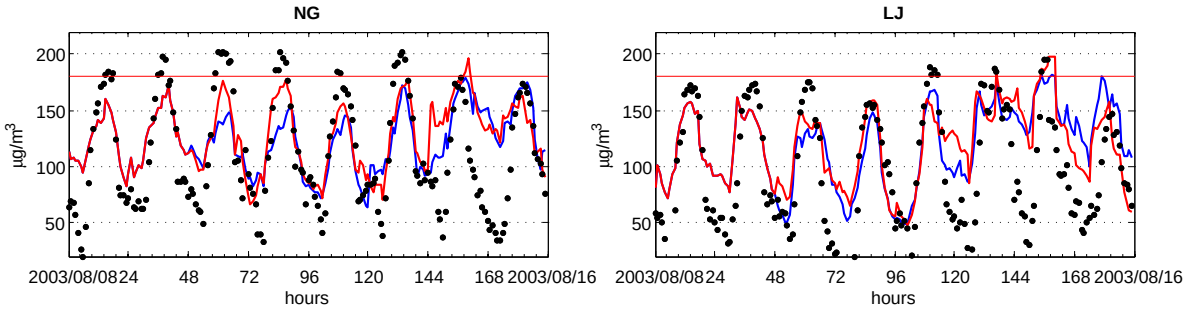

Figure 5.38: Ozone time series for Nova Gorica and Ljubljana station. Blue: reference experiment D. Red: the same but with every 2-days re-initialization of meteorology. For the first two days the simulations are identical.

along the coastline. This zone spread towards interior with the sea-breeze and the upslope Alpine winds (Fig. 5.39). Since measurements confirm significant differences in ozone between Mediterranean part and interior of Slovenia, this simulation is likely to be close to the true episode evolution for these two days.

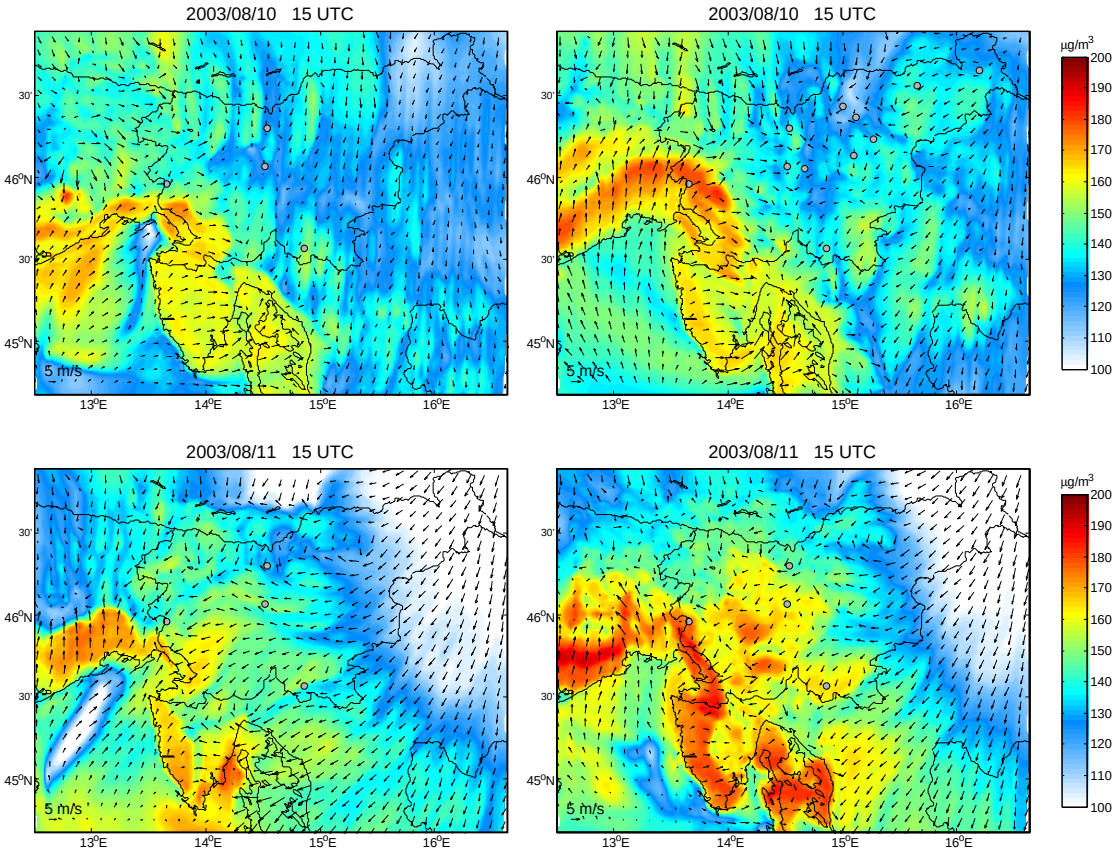

Figure 5.39: Examples of simulated near ground ozone field and surface winds comparison for two consecutive days. Left panels: simulation D. Right panels: simulation of type D with meteorology re-initialized every 2-days.

5.2 Episode II: 10 - 11 June 2004

5.2.1 Synoptic situation and ozone characteristics

In the first days of June 2004 a shallow area of low air pressure extended over the southern and eastern Europe. Weather in Slovenia was characterized by local rain showers and thunderstorms, cloudy sky and relatively low daily temperatures (up to 25°C at the coastal area). At the same time anticyclone formed over the western Europe and from June 6 onwards slowly moved and expand towards East.

From June 7 to 9 the area of high air pressure extended over central and southern Europe. Warm northwestern winds over Slovenia at higher levels were related to the high pressure ridge located west of Slovenia (Fig. 5.40). The sky over Slovenia was mostly clear and daily temperatures increase from day to day, but have not reach 30°C, yet.

On the June 10 and 11 the anticyclone slowly began to weaken, while in altitudes the strengthened westerly flow was bringing warm and moist air. In the afternoons and evenings over Slovenia local rain showers and thunderstorm occurred, and the highest daily measured near ground temperatures finally exceeded 30°C.

On the June 12 the cold front reach the Alps from west and passed Slovenia in the night between June 12 and 13.

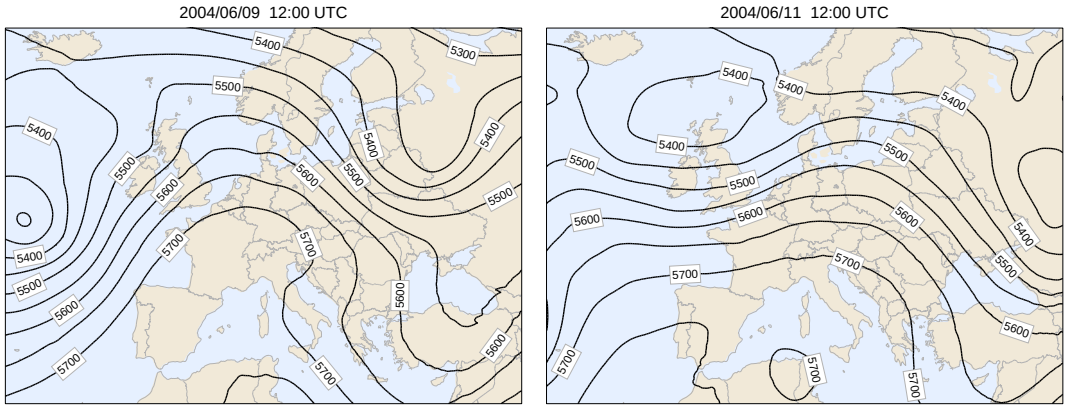

Figure 5.40: Geopotential height (gpm) at 500 hPa during the June 2004 episode.

From the ozone point of view this episode was very short but with extremely high measured ozone values. Up to and including the June 9 ozone over Slovenia was relatively low. Hourly values were below the legally permitted levels, only the 8 hour averages were occasionally above the 120 $\mu g/m^3$ target value at Nova Gorica station. Finally, on the 10 and 11 June ozone values over Slovenia markedly increased (Fig. 5.41). At some stations daily maximum exceeded 200 $\mu g/m^3$ on the first day (Nova Gorica, Vnajnarje, Kovk, Krvavec), while at some other stations hourly warning values were exceeded (Ljubljana, Iskrba) on that day. For some of this stations, the highest ozone values were measured over the night (Vnajnarje, Kovk). On the next day, June 11, ozone values somewhat decrease, but daily maxima at some stations were still above 180 $\mu g/m^3$. The 8 hour ozone values highly above the 120 $\mu g/m^3$ target value were during these two days at all four stations.

According to trajectories (Fig. 5.42) the regional transport of photochemical pollution accumulated over the Mediterranean (including the Po Basin pollution) could explain the

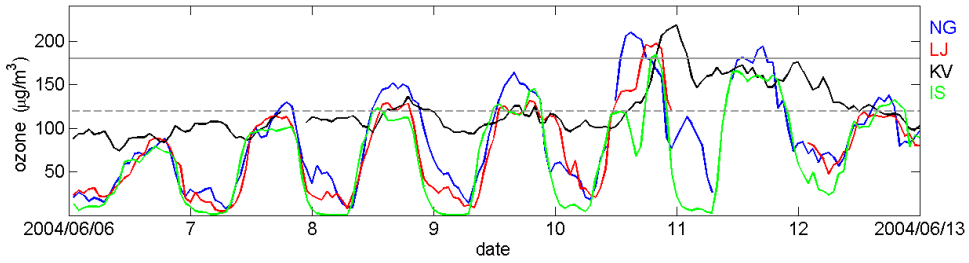

Figure 5.41: Measured average hourly values of ozone (in μg/m^3) for June 2004 episode at locations Nova Gorica (NG), Ljubljana (LJ), Krvavec (KV) and Iskrba (IS).

"ozone jump". Actually, this is one of a few episodes in years 2003 - 2005, for which trajectories suggest a direct connection between the Po Basin emission areas and high ozone measured over Slovenia. The temporal sequence of the highest measured ozone at Slovenian measuring sites confirms as well the invasion of polluted air from southwest. For the four measuring sites can be the temporal sequence noticed in Fig. 5.41. Ozone values above 200 μg/m^3 are first measured in Nova Gorica between 12 and 15 UTC. A couple of hours later ozone increased in the interior of Slovenia: in Ljubljana and Iskrba values above 180 μg/m^3 were measured in late afternoon (16 to 19 UTC). Extremely high ozone values above 200 μg/m^3 were then measured at Krvavec (18 to 24 UTC) and Kovk (June 11, at 1 to 6 UTC). On the contrary to the sites characterized by generally low nighttime ozone values, as a consequence of different local factors (local traffic emissions: Ljubljana, Nova Gorica; surpressed vertical mixing, local biogenic emissions, no ozone replenishment from above: Iskrba) ozone at Vnajnarje retained the very high values throughout the night (from June 10 at 16 UTC to June 11 at 5 UTC).

5.2.2 Model results

Similarly as for the August 2003 episode a considerable number of simulations for this episode was performed as well. Again a simulation type D was chosen as a reference simulation. We do not analyze and describe step by step the results of different simulations as we did for the previous episode. However, the comparisons of the near ground ozone sensitivities to different changes applied for this episode confirm the outcome of the previous episode. The latter can be evident from Appendix G, where Figures, presenting the results of sensitivity tests for this episode in the same manner as for the August 2003 episode, are shown.

The reference simulation is again of type D, which means that the model was run with the Noah land surface model and YSU PBL scheme. The simulation started on June 1 at midnight, so that after 6 days of simulation valuable chemical initial conditions were prepared for June 7. On June 7 the meteorological fields were re-initialized and chemistry was initialized from the previous run. The meteorology was re-initialized on June 11 and 12 at 00 UTC as well.

Figures 5.43 and 5.44 show the evolution of the ozone episode, as seen by the reference simulation. In Figure 5.43 the near ground ozone values are shown for D3 domain, while in Fig. 5.44 ozone and winds at 8th model level (270 meters above ground) in D2 domain are presented. On June 7 ozone was low over Slovenia as well as over the entire D2 domain. On June 8 the simulated ozone was still low over Slovenia, somewhat higher ozone over southwestern

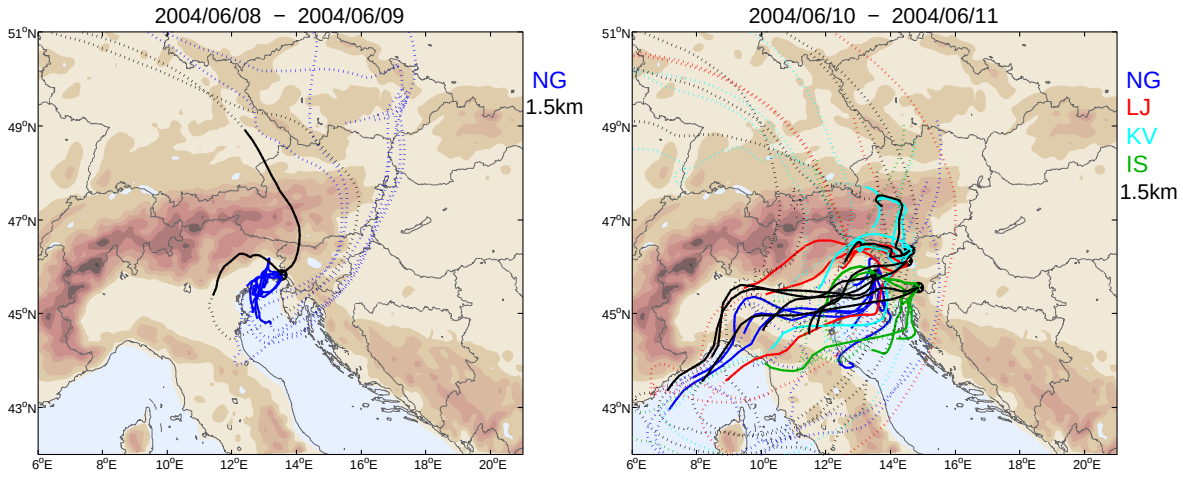

Figure 5.42: 3D backward trajectories for four measuring sites, calculated on Aladin fields for episode in June 2004. Trajectories have final points located 50 m agl (colored according to measuring site) or 1500 m amsl (black), and are calculated for different arrival times (9:00, 12:00 and 15:00 for 50 m agl, and 12:00 UTC for 1500 m amsl). Left: Nova Gorica trajectories for June 8 - 9; Right: Nova Gorica, Ljubljana, Krvavec and Iskrba trajectories for June 10 - 11. The total length of trajectories is 96 hours. Solid line: the last 24 hours, dotted line: the rest of 96 hour trajectory.

Slovenia was probably a part of the northern Adriatic "ozone cloud": the highest ozone levels inside D2 domain appeared over the northern Adriatic Sea. On the next day, June 9, ozone values over the sea further increased as a consequence of pollution advected from the Po River Basin area. The influence of the northern Adriatic Sea ozone maximum on that day extended even deeper into the interior of Slovenia, but according to model results it has not reached Ljubljana and other more eastern measuring sites yet. This coincides with higher measured ozone at Nova Gorica station on June 8 and 9 than at other interior stations. On June 10 and 11 this highly polluted air with southwesterly winds traveled over Slovenia toward east. From the ozone and wind fields for June 12 we can gather about the locations of the cold front at Alpine north-western ridges, which in model simulation passed Slovenia at the end of that day.

The point-by-point comparison of reference simulation with simulations with different frequency of meteorology re-initializations and different PBL scheme indicates some differences in the near ground ozone levels again. Nevertheless, in general the results of simulations are similar to each other. The characteristics described above on the basis of results of reference simulation, are common to all simulations.

In Figure 5.45 the near ground ozone values from the reference simulation, as well as from some other ensemble simulations, are compared to the measured hourly values. The spread of the ensemble presents an estimate about the uncertainty of the simulated near ground ozone. Similarly as in the earlier episode, model systematically overestimates nighttime ozone levels. Daytime levels surprisingly well follow the measurements during the first 4 presented days. On the days with the highest measured ozone maxima (10 - 11 June), the simulated ozone levels are the highest as well. However, the true location and the exact timing of the maximum ozone levels do not exactly coincide with the measurements. The model persistently underestimates the height of extreme maxima - no simulation predicts hourly ozone levels above 200 $\mu g/m^3$.

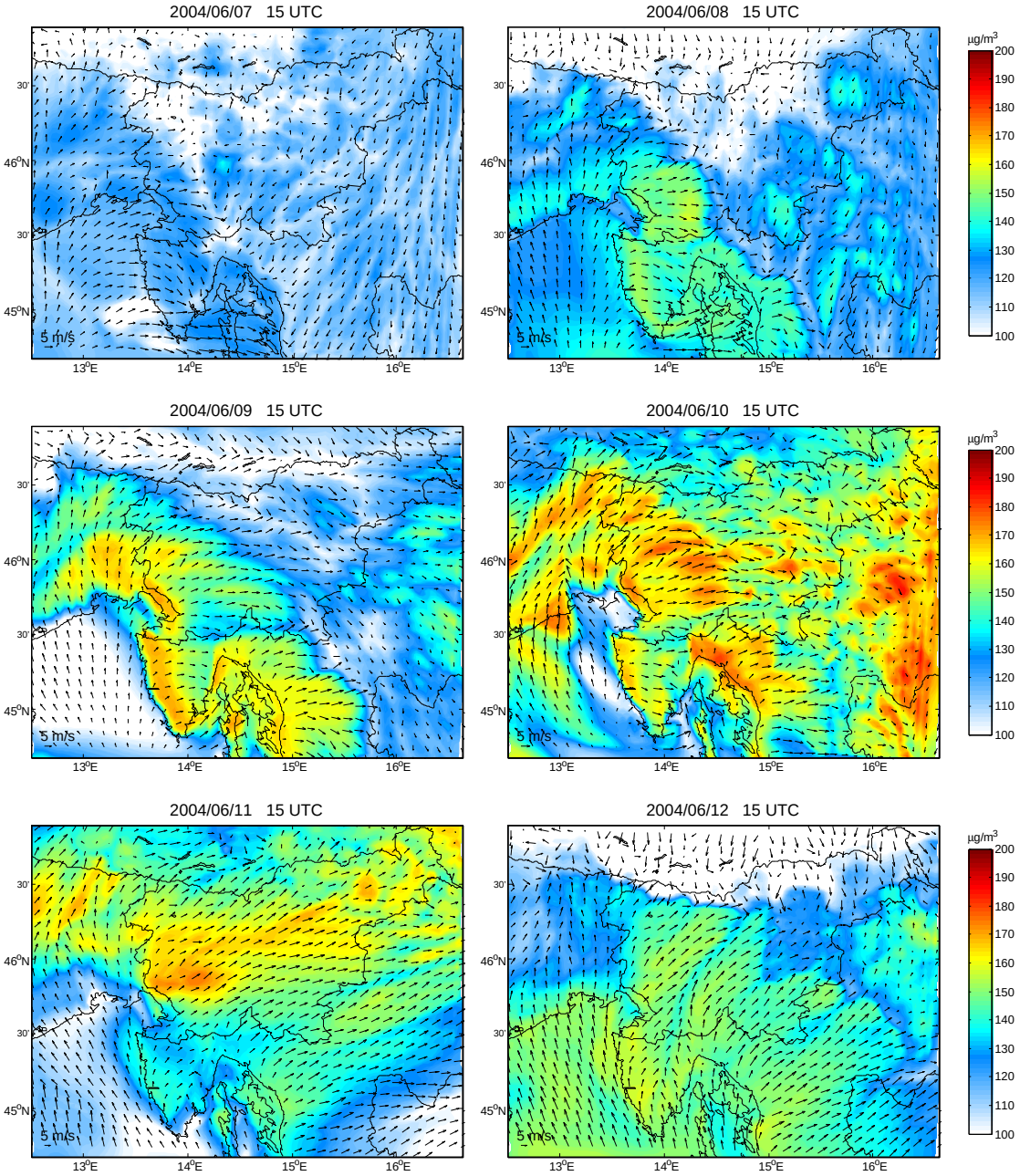

Figure 5.43: Simulated near ground ozone values and 10 m model winds in D3 domain for episode in June 2004. Results are from the reference simulation.

Figure 5.46 further compares the measured and simulated NO_x near ground values for the same simulations. In Maribor the simulated NO_x values are underestimated, which is because of the measuring site, located near substantial road emissions. In other stations the size order of simulated values is reasonable, the model fairly well predicts the time of two daily maxima (the morning and the evening one).

The comparison of the measured and simulated near ground meteorological variables (not

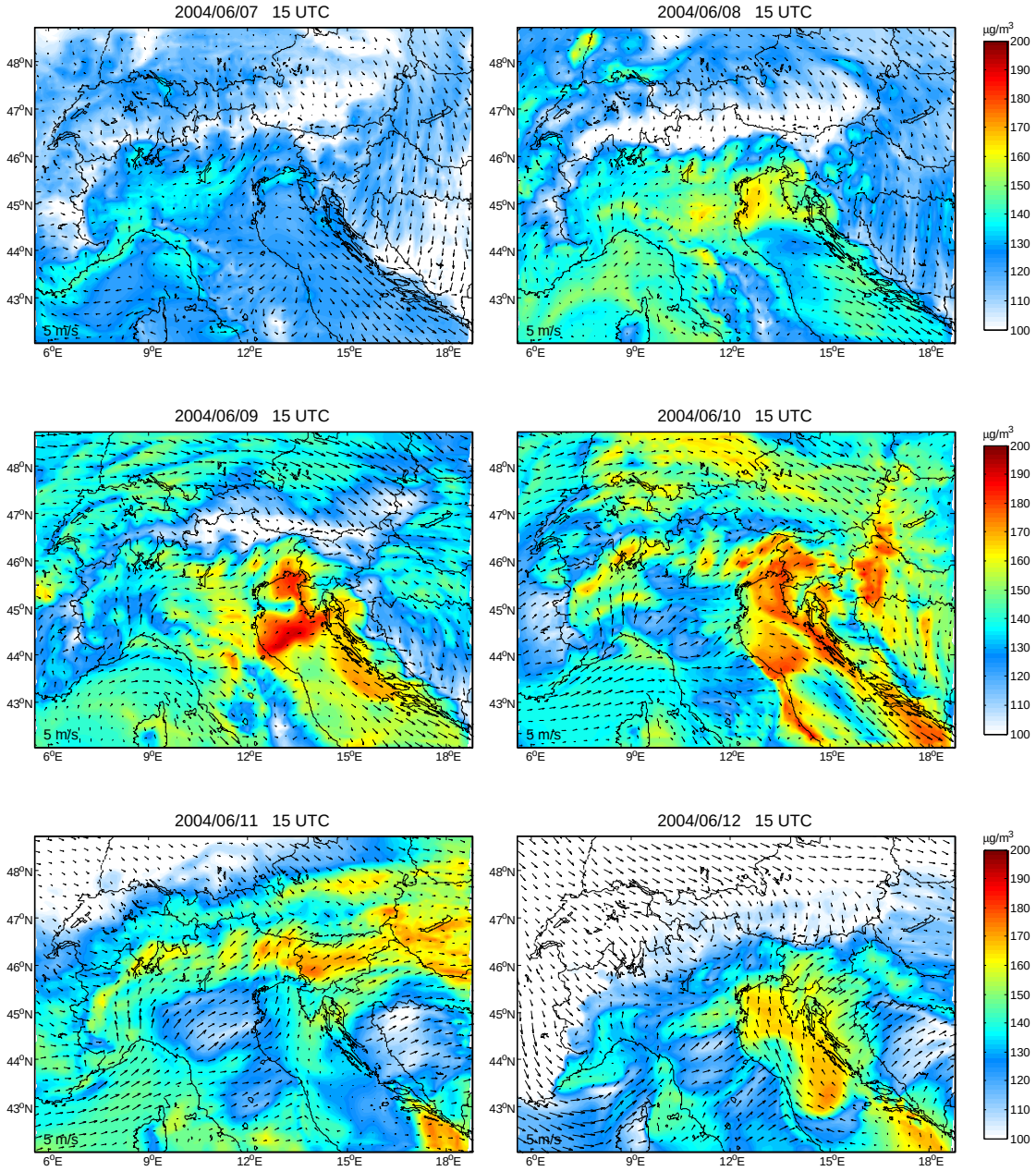

Figure 5.44: Ozone values at 8th model level (≈ 270 m above ground level) and model winds at this level in D2 domain for episode in June 2004. Results are from the reference simulation.

included here) showed that similarly as in simulation D of the earlier episode the nighttime temperatures are overestimated by the model, while daytime temperatures have a positive bias. Wind speed for the daytime 10 m winds is systematically overestimated, but some significant characteristics of the day-night winds are well resolved by the model (e.g. sea-land breeze and southern wind in the last 2 days Portorož, up and down slope winds in Bilje and Nova

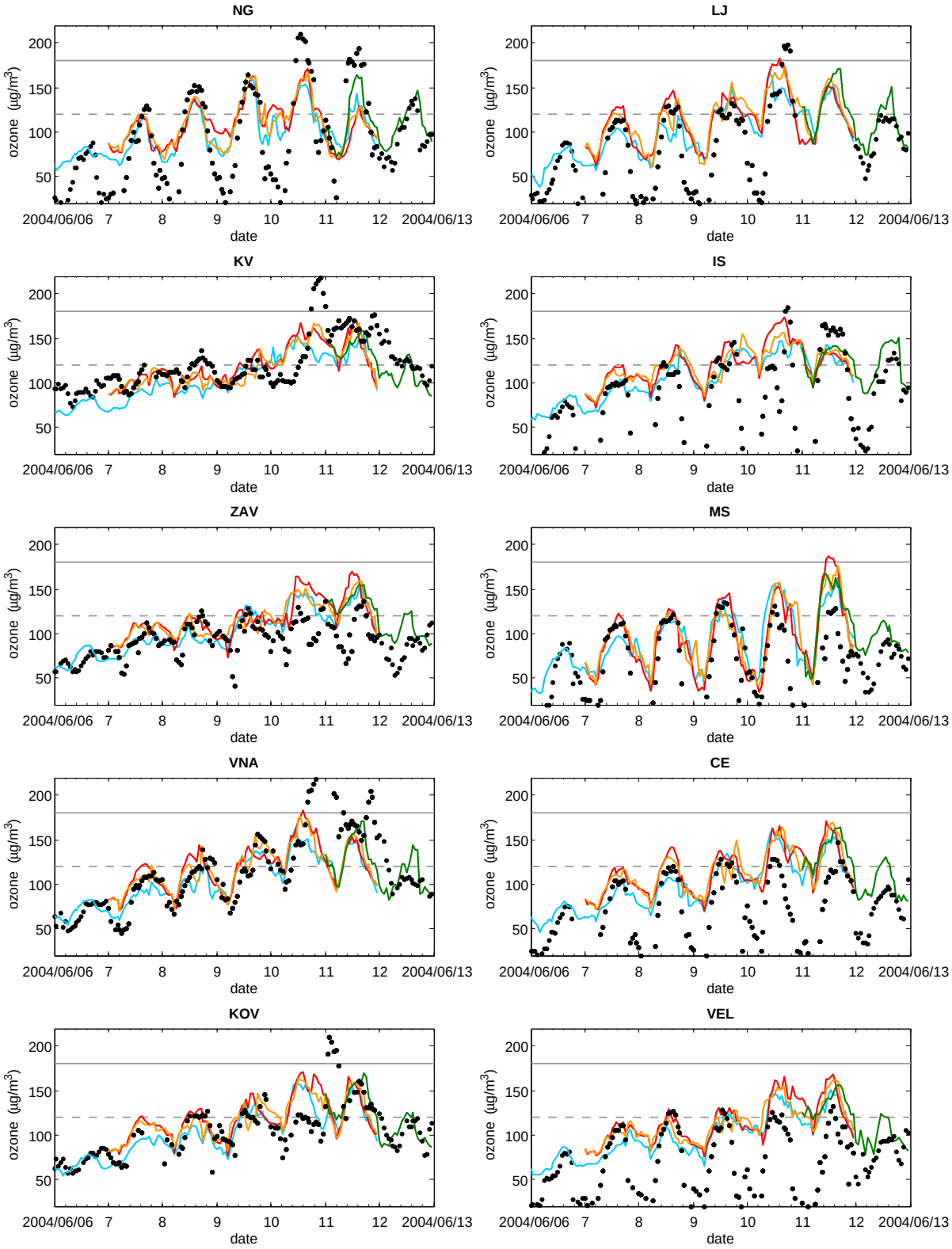

Figure 5.45: Measured (black dots) and simulated hourly ozone values for measuring sites. Blue: reference simulation; Red: different PBL scheme; Green, orange: different frequency of meteorology re-initialization.

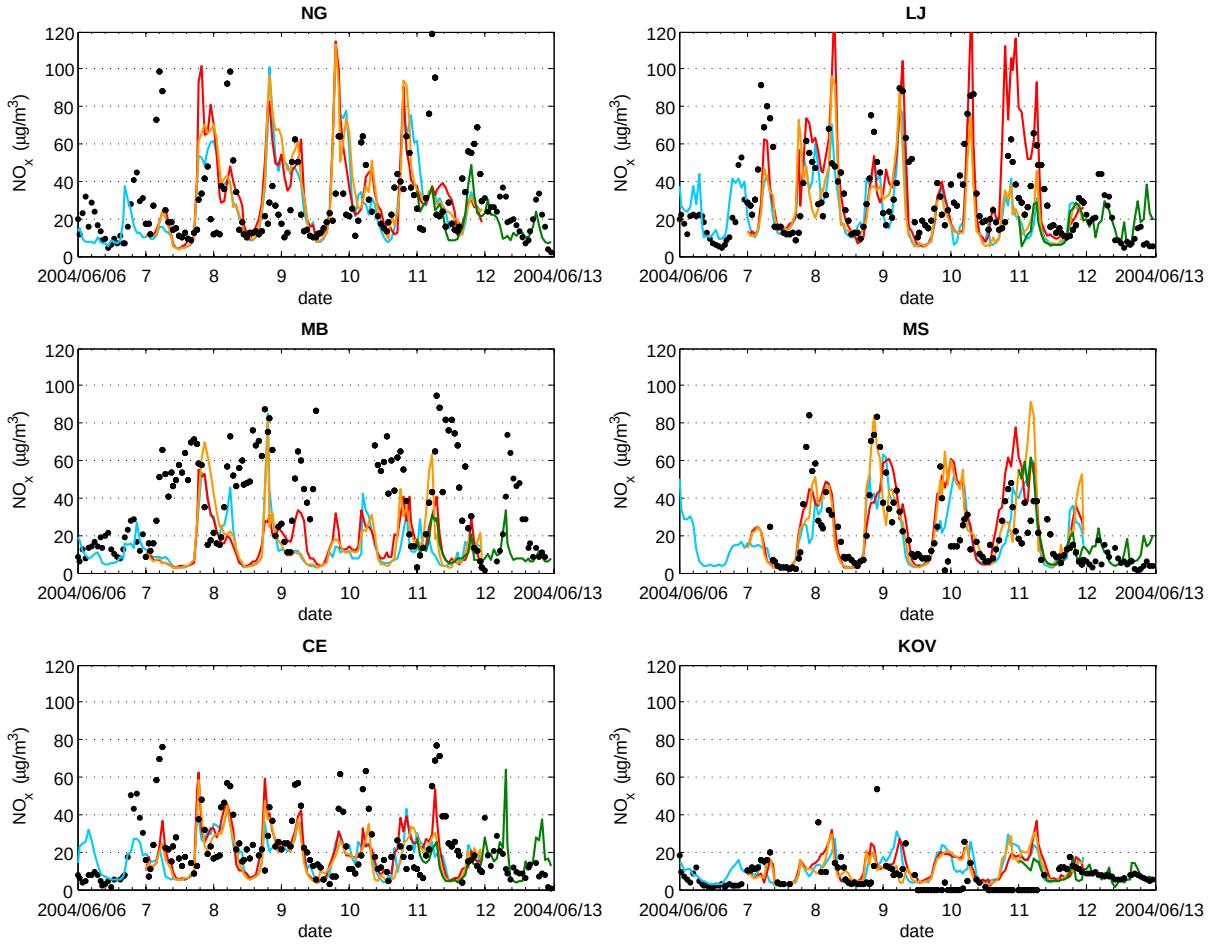

Figure 5.46: The same as Fig. 5.46, but for NO_x.

Gorica, western daytime winds and southern nighttime in Postojna etc.). For many stations the water vapor mixing ratio is underestimated during this simulations, while for some of them the agreement is well.

5.3 Episode III: 19 - 26 June 2005

5.3.1 Synoptic situation and ozone development

The third episode to some extent contained the characteristics of the two episodes presented so far. Again the development of the high ozone episode was associated with the formation of the anticyclone, which extended over western and central Europe from the 17 up to the 23 June 2005 and over the southern and eastern Europe in the next 2 days, respectively. The high pressure ridge at 500 hPa was stagnating over western Europe, so that until about the 23 June Slovenia was located on its western slope. The northwestern flow over Slovenia then after June 23 slowly turned into the western flow of June 25, when the high pressure ridge slightly moved towards East (Fig. 5.47) and persisted at this location until June 29.

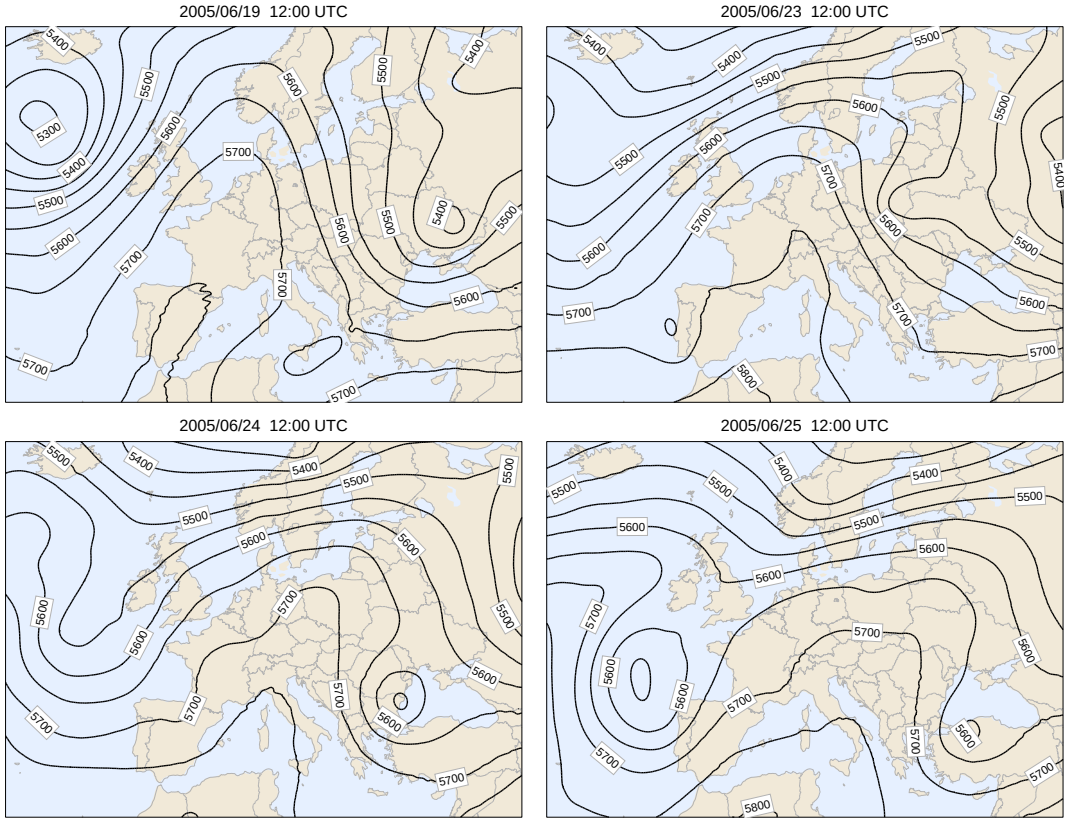

Figure 5.47: Geopotential height (gpm) at 500 hPa during the June 2005 episode.

The near ground air temperatures at Slovenian coast exceeded 30 °C from the 16 June onwards, while in the continental Slovenia measured temperatures were slightly lower. The afternoons of the 22, 23 and 25 June were characterized by local showers and thunderstorms. Otherwise the mostly clear weather was prevalent up to and including June 25. From the 26 June onwards frequent rain showers and thunderstorms (occasionally with hail and heavy winds) were occurring throughout the days, as a consequence of atmosphere instability caused by moist and warm air at higher altitudes.

Ozone hourly threshold values were from the 22 June onwards exceeded at Nova Gorica, as well as 8 hour averages at Krvavec were slightly above the 120 μg/m^3 target value. At

other stations until June 25 ozone daily maximum values were relatively low. On the 25 June in Ljubljana, Krvavec, Vnajnarje, Zavodnje and Celje the maximum hourly values were above 180 $\mu g/m^3$ and the 8 hour averages were significantly above the target level (Fig. 5.48). After June 25 ozone levels over Slovenia decreased, the only exception was Nova Gorica, where on June 28 hourly daily maximum 181 $\mu g/m^3$ was measured.

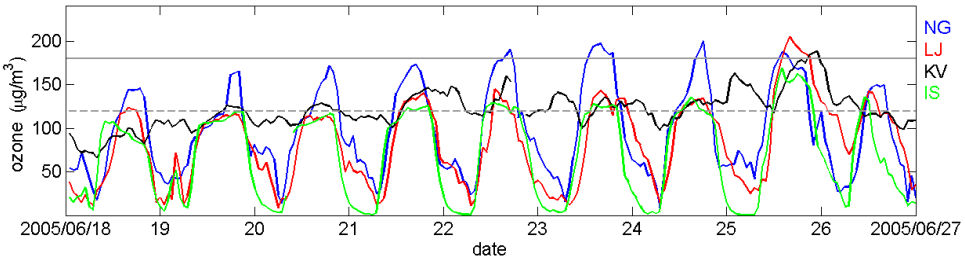

Figure 5.48: Measured average hourly values of ozone (in $\mu g/m^3$) for for June 2005 episode at locations Nova Gorica (NG), Ljubljana (LJ), Krvavec (KV) and Iskrba (IS).

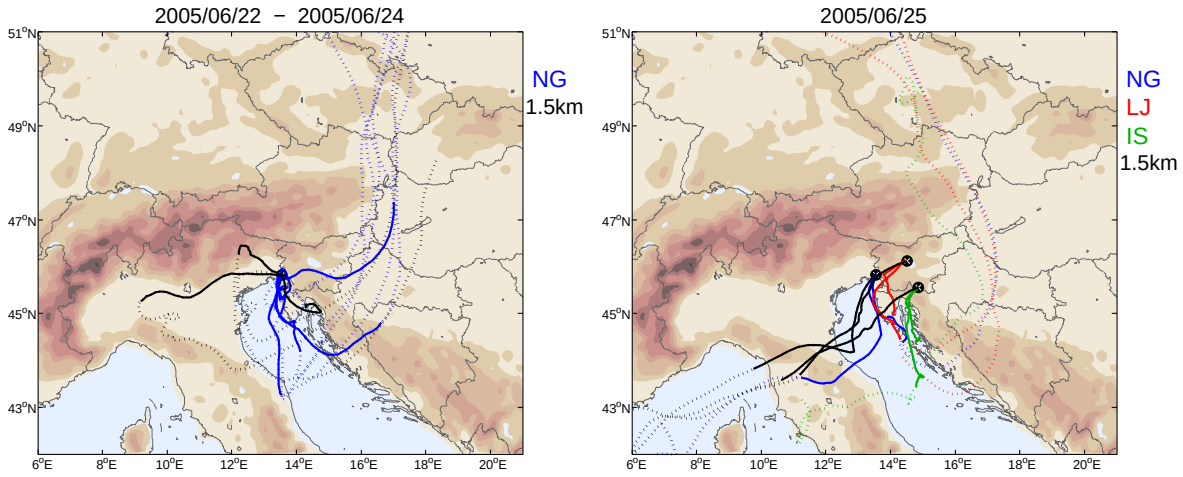

Figure 5.49: 3D backward trajectories for three measuring sites, calculated on Aladin fields for episode in June 2005. Trajectories have final points located 50 m agl (colored according to measuring site) or 1500 m amsl (black), and are calculated for different arrival times (12:00 and 15:00 for 50 m agl, and 12:00 UTC for 1500 m amsl). Left: Nova Gorica trajectories for June 22 - 24; Right: Nova Gorica, Ljubljana and Iskrba trajectories for June 25. The total length of trajectories is 96 hours. Solid line: the last 24 hours, dotted line: the rest of 96 hour trajectory.

3D backward trajectories calculated for the 50 m and 1500 m final heights for the days, when among the lower altitude stations ozone was high only at Nova Gorica, are similar to the trajectories, calculated for the same situation in the previous two episodes. According to trajectories, the air masses originated from the central Europe. With the northeastern flow in lower altitudes they traveled around Alps (usually over southeastern regions of Slovenia), rounded over the northern Adriatic Sea and the coastal regions and finally reached Nova Gorica from south or west (Fig. 5.49). One of the trajectories, calculated for June 23 with

final point at 1500 m, rounds over Po Basin before it reaches the Nova Gorica station. In Fig. 5.49 all of the trajectories for the June 25 with final points located 1500 m amsl originate from southwest. They cross Apennines south of Po River Basin and Adriatic Sea before they reach the measuring site. While all except one of the trajectories for that day with final point 50 m above the station originate still from central Europe and spend the last 24 hours over the Adriatic coast before they reach the station.

5.3.2 Model results

The simulations were started on the 14 June 2005 to enable the accumulation of pollutants in the planetary boundary layer. The results of simulations are shown and analyzed between 19 and 26 June. In the reference simulation the model run with Noah LSM and YSU PBL scheme (type D), and meteorological fields were re-initialized every 48 hours from the 19 June onwards. Again, additional simulations with changed frequency of meteorology re-initialization and one simulation with different LSM (simulation type B) were performed to get some estimate about the ensemble spread of simulated ozone (uncertainty of simulated ozone).

Figure 5.50 shows daytime near ground ozone fields and 10 m winds for reference simulation in D3 domain between June 21 and 26. Figure 5.51 is similar, except that ozone and winds are shown at 8th model level in D2 domain.

On June 21 the simulated ozone levels over Slovenia were low (Fig. 5.50). Some isolated "ozone clouds" with maximum near ground levels not higher than 150 μg/m^3 occurred inside Slovenia (for example Ljubljana plume south of the city) and over eastern edges of Slovenian Mediterranean. The highest ozone levels in D2 domain were simulated south of the Po Basin (Fig. 5.51).

On the next day simulated near ground hourly ozone reached 180 μg/m^3 levels on the west coast of Istria and at coast of the Gulf of Trieste. The daytime sea-breeze and upslope Alpine winds were carrying the ozone rich air toward the interior land, but at least is Slovenia the maximum simulated ozone over Mediterranean did not exceed the hourly warning value. The rest of Slovenia was on that day cut off from the Mediterranean ozone rich air. Again some isolated plumes (Ljubljana, Zasavje) with maxima not above the warning value formed during the day. On the contrary to Slovenia, the simulated ozone levels over the Po River area in D2 domain on June 22 were already very high. For that day the highest ozone values on the 8th model level were simulated over the western part of northern Adriatic Sea. This "over the sea" pollution appears to originate mainly from the northern Italy.

On June 23 the situation was similar as during the previous day, except that the maxima over Mediteranean Slovenia, Istria, Gulf of Rijeka and it coastal regions, Friuli-Venezia Giulia region, as well as over Adriatic Sea and parts of Po River Basin on the 8th model level, were more pronounced. The interior of Slovenia was still cut off the Mediterranean air in which the simulated ozone values exceeded the warning levels.

On the next day the influence of Mediterranean pollution extented somewhat deeper into Slovenia. This and somewhat higher simulated PBL heights for that day may to some extent explain lower simulated ozone levels during that day over the Mediteranean Slovenia, Istria, Gulf of Rijeka and its coastal regions, Friuli-Venezia Giulia region. However, over these regions the near ground ozone were still higher than over the rest of D3 domain area - the only exception was Ljubljana plume. Ozone over the Po Basin and Adriatic Sea was still high during this day, but similarly a little lower than on the previous day.

On June 25 with the southwesterly flow the pollution accumulated over the Adriatic Sea traveled over Slovenia. The time series of ozone and wind fields at higher levels (not shown)

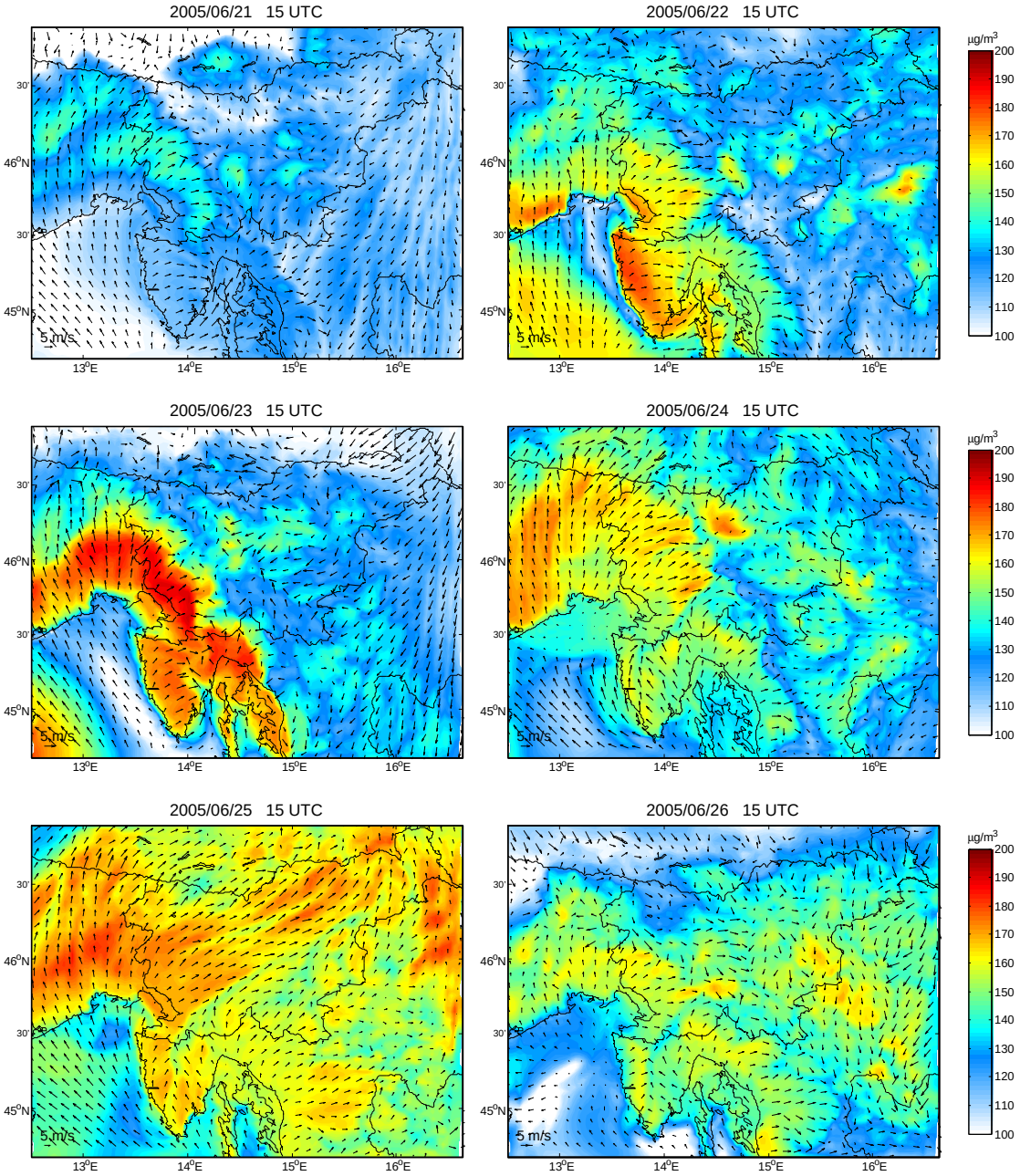

Figure 5.50: Simulated near ground ozone values and 10 m model winds in D3 domain for episode in June 2005. Results are from the reference simulation.

suggest, that the Po Basin pollution directly influenced the air quality in Slovenia during this day, when high near ground ozone levels were measured at many stations.

On the last day of simulation, June 26, the flow over Slovenia changed toward northeastern, and it seems that this flow pushed the rest of polluted air back towards the Adriatic Sea. The temperatures decreased and the extensive showers and thunderstorms cleaned the air over the continental Slovenia. The simulated daytime ozone on that day was lower over Slovenia again.

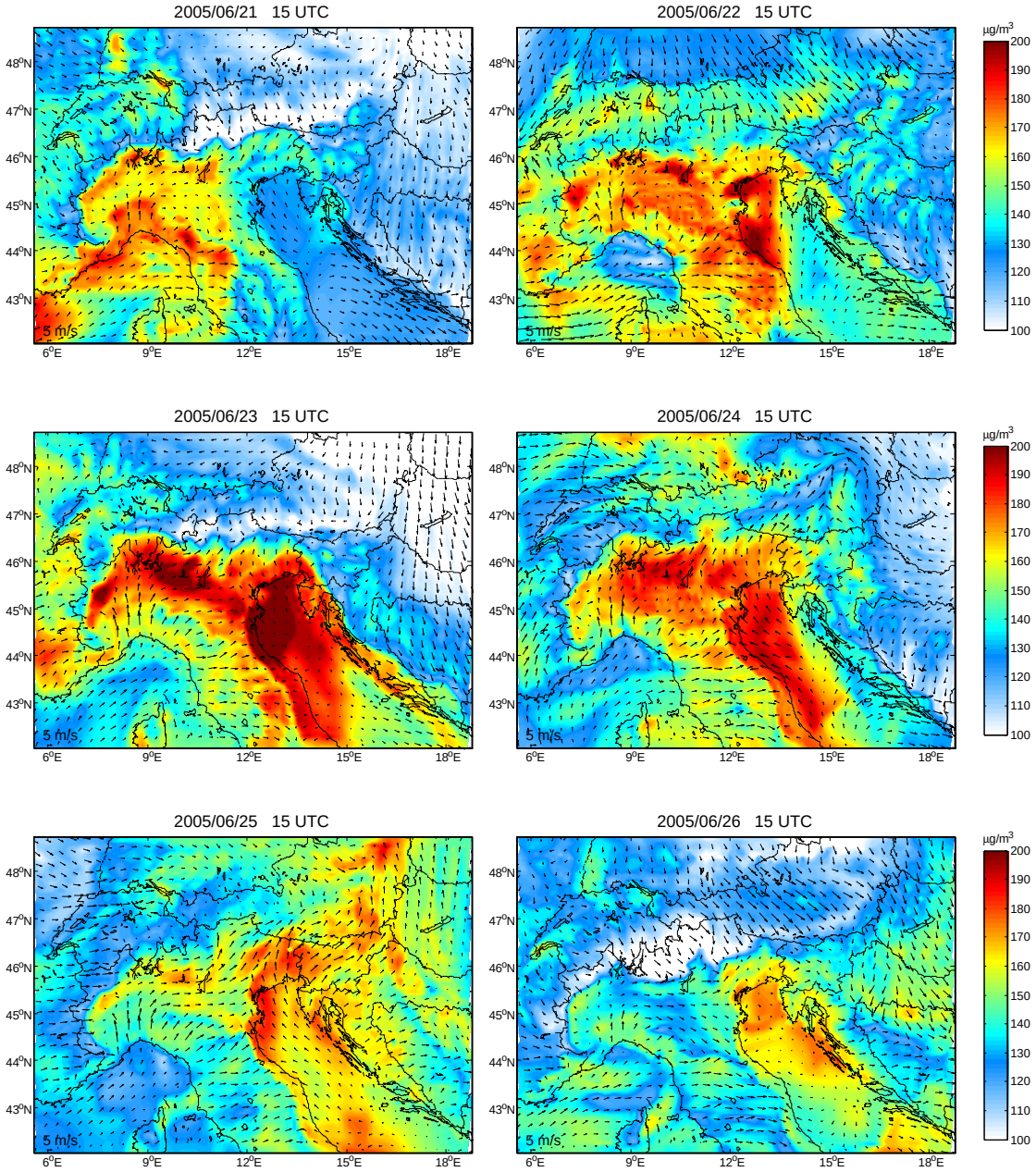

Figure 5.51: Ozone values at 8th model level (≈ 270 m above ground level) and model winds at this level in D2 domain for episode in June 2005. Results are from the reference simulation.

The polluted air over the Adriatic Sea persisted for a few another days and contributed to occasionally high ozone levels in the Mediterranean land (not shown). While over the interior of Slovenia ozone levels remained low.

The comparisons of measured and simulated ozone levels for Slovenian stations are shown in Fig. 5.52. The gradual increase of ozone levels as well as the ozone jump on June 25 is well

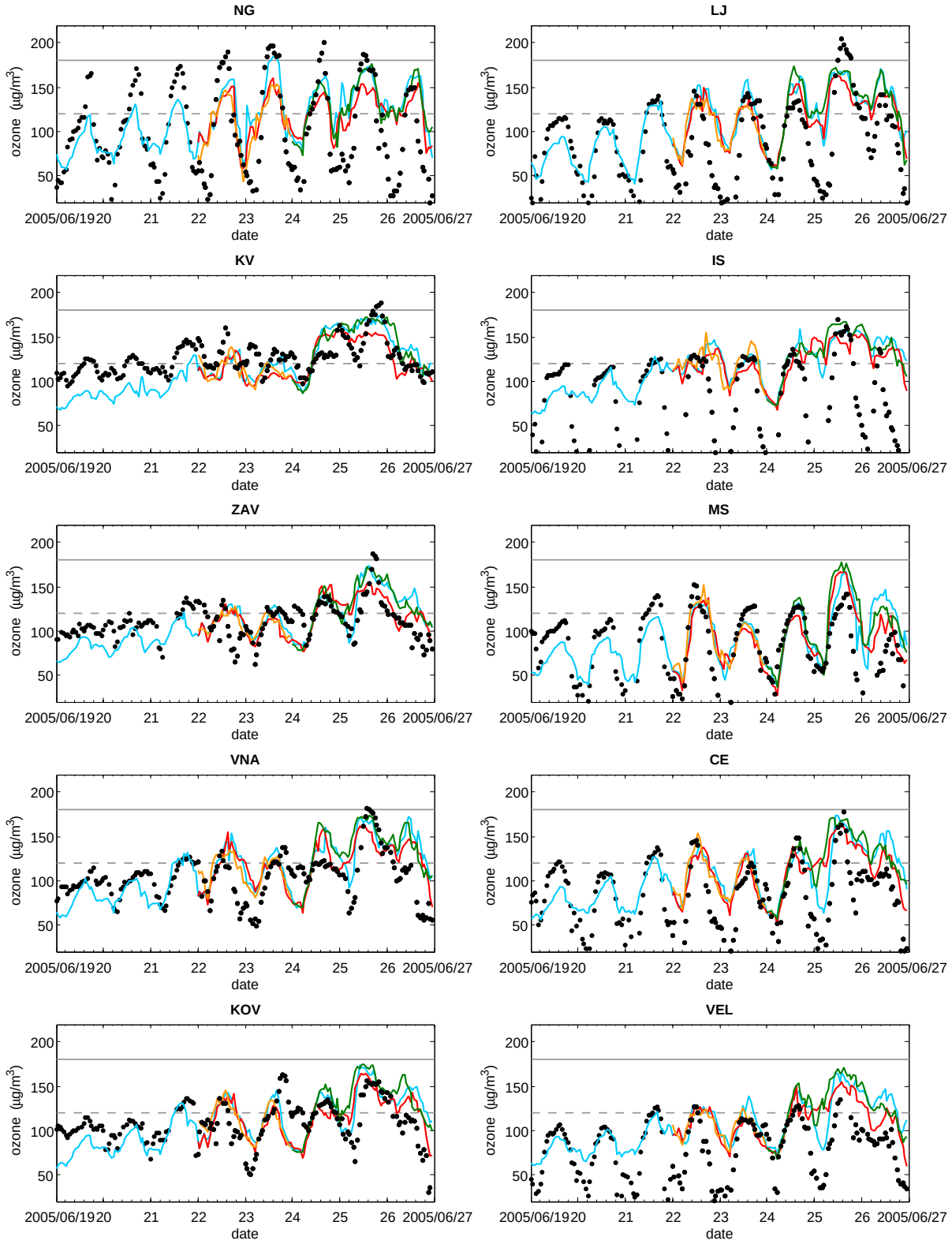

Figure 5.52: Measured (black dots) and simulated hourly ozone values for measuring sites. Blue: reference simulation; Red: different PBL scheme; Orange, green: different frequency of meteorology re-initialization.

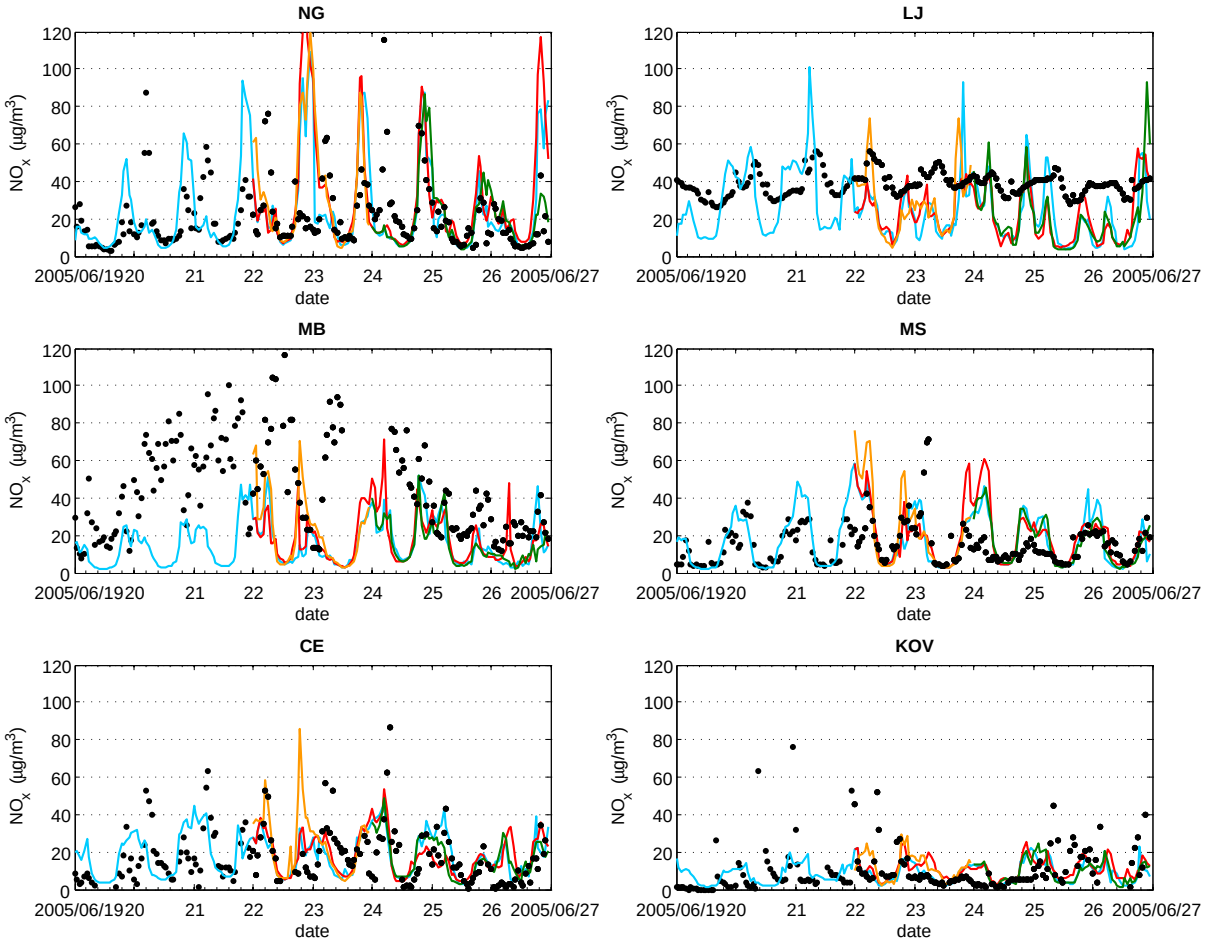

Figure 5.53: The same as Fig. 5.52, but for NO_x.

represented by the model. Similarly as in the earlier episodes model hardly represents the exact locations of the maxima. For example, significantly higher ozone levels were on June 25 measured (but not simulated) in Ljubljana, and were simulated (but not measured) in continental Murska Sobota at the NE of the country. However, there are many stations, where high ozone was measured and simulated for that day (Krvavec, Iskrba, Zavodnje, Vnajnarje, Celje). Although simulations confirm that the areas influenced by Mediterranean air over the first part of the episode (June 22 - 24) experienced higher ozone than the rest of Slovenia, the agreement between model and measurements for Nova Gorica station is poor again. These discrepancies at Nova Gorica may originate either in inaccurately spatially distributed anthropogenic emissions outside Slovenia (as explained for this station in Section 5.1.6) or in complexity of air circulation, which develops during these episodes over the northern Adriatic Sea and its coastal regions and may be not accurately enough represented by the model. Underestimation of biogenic VOC emissions may as well contribute to ozone discrepancies. But it must be noted, that as shown in Section 5.1.6 simple bulk increment of VOC emissions would result in increased ozone during daytime and nighttime (though specially for Nova Gorica station according to Fig. 5.29 significantly smaller ozone enhancement is expected during the nighttime), while ozone during nighttime is already overestimated by the model.

In Figure 5.53 simulated NO_x levels are compared to the measured values. Again for Maribor NO_x values are systematically underestimated, as expected (local effect of the nearby road). In Nova Gorica the heights of simulated maxima correspond to the measured maxima, except that in model results morning maxima (while in reality afternoon maxima) are dominant. Measured NO_x in Ljubljana during this episode expresses less diurnal variability than usual, which is not represented by the model. Better during this episode is the agreement for Murska Sobota, Celje and Kovk, where except the exact maxima heights model resolves NO_x courses reasonably well.

Chapter 6

Discussion

The study of the near ground ozone characteristics in Slovenia started with basic statistical approaches. Results of these analysis showed, that a significant part of ozone temporal variability for separate measuring sites can be explained merely by terms of basic meteorological variables (Žabkar et al., 2006, 2008). Such result was to some extent expected, because concentrations of air pollutants depend highly on meteorological conditions. For ozone it is generally known, that high near ground levels are usually related to hot, calm and clear sky summertime conditions, resulting in high correlation coefficients between ozone and temperatures, solar irradiance and ozone levels of the previous day. This particularly holds for urban areas, where specific conditions enable effective ozone production from local emissions. In areas not directly influenced by local emissions the actual ozone levels depend further on the air mass origins and on processes to which the air masses have been subjected on their way (chemical transformations, wet and dry deposition, diffusion).

According to the trajectory analysis results for warm part of the years 2003 and 2004, the air masses origin has a certain influence on ozone levels even at stations, where this was less expected (e.g. Ljubljana with considerable local emissions). The main discovery of the trajectory analysis presented in Chapter 2 is that a common source for most with ozone polluted air masses at four Slovenian stations appears to be the area over the northern Adriatic Sea and its coastal regions. The most common path for polluted air masses appears to be through the Gulf of Trieste for Nova Gorica and through the Gulf of Rijeka for Iskrba station. Ozone levels in the air masses with the south-western origin are usually higher even in Ljubljana. The elevated Krvavec site experiences completely different behavior with high ozone levels throughout the day. During the warmest hours of the day, when the well mixed layer formed above the Ljubljana basin reaches this station, Krvavec can be under direct influence of Ljubljana basin pollution. During the rest of the day the station is under the influence of polluted layers intruded into the lower free troposphere during previous days either from daytime PBL or maybe occasionally even from the stratosphere. The Po River Basin was despite the expectations not identified as a direct common source of polluted air, some pattern toward Po River area was identified only with the concentration weighted trajectory (CWT) field for Nova Gorica station.

It was not possible to fully explain the role of Po River Basin and the relation between Slovenian ozone and the northern Adriatic Sea air mass origin with the methodology, which only considered trajectories. In addition, the statistical approaches could only be used for selected stations with a sufficiently long time series of measurements. With a meteorological-photochemistry model is on the other hand simulated the evolution of the specific episodes with the purpose to explain the circumstances that lead to the high near ground ozone levels.

Nevertheless, simulating ozone with a deterministic model has significant deficiencies, and consequently limitations, as well. If with statistical approaches we do not have to take care about the details regarding the underlaying processes, in deterministic model all the decisive mechanisms must be well presented in the model to enable the valuable simulations.

Among many *a priori* known sources of model uncertainties, is according to the results for WRF-Chem simulations of high ozone episodes in Slovenia, the meteorological representation of the planetary boundary layer the most problematic. If the weather characteristics favorable for high ozone episodes (hot anticyclonic summertime situations) are usually the least challenging to predict, the opposite holds for the accurate and detailed representation of the PBL (especially the wind field in PBL) and it's dynamics. Namely, as a consequence of weak synoptic dynamical forcing, the local physical processes determine the thermally driven air circulations and consequently the directions of advection of polluted air from local sources, the diffusion and dilution of pollutants, as well as the air cleansing with precipitation and dry deposition. These for ozone formation critical physical processes are fundamentally based on mechanisms rooted in the subgrid scale, and are thus in model represented in a simplified manner with parameterizations. The parameterizations generally contain different assumptions and empirical relationships, that allow complex processes to be calculated efficiently based on the resolved-scale variables. In addition, these processes depend on terrain and different land surface characteristics, which are again only roughly resolved by the model.

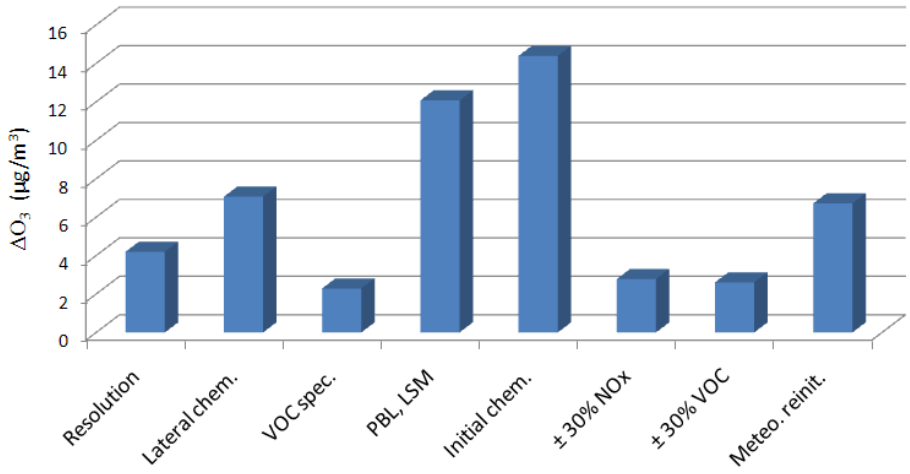

Figure 6.1: The sensitivity of the simulated ozone values to different model configurations. Shown is the comparison of the mean absolute deviations from reference D simulation in simulated daily ozone maxima (regardless the time of occurrence) averaged over all Slovenian ozone stations. The figure compare the results of different sensitivity tests applied for the second part of the August 2003 episode. The sensitivity tests are described in Chapter 5. Resolution: mean absolute deviation in daily ozone maxima in the run with the reduced model horizontal resolution (9 km instead of 3 km); Lateral chem.: changed chemical boundary conditions; VOC spec.: VOC speciation; PBL, LSM: different model parametrization schemes; Initial chem.: initial chemistry conditions; ±30% VOC and NO_x: bulk changes in emissions; Meteo. reinit.: frequency of meteorology re-initialization.

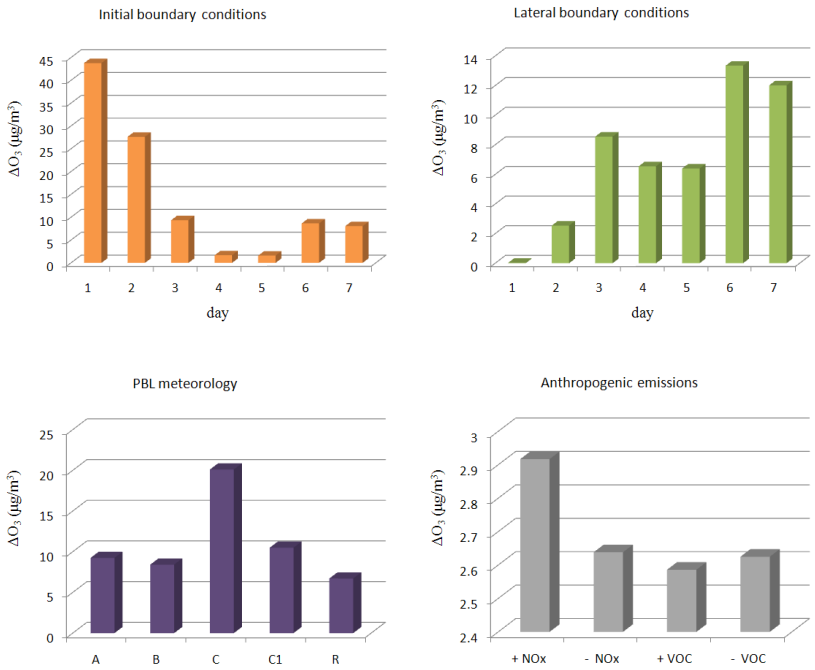

Figure 6.2: The same as Fig. 6.1, except that results are presented more in detail. For initial and boundary chemical conditions mean absolute deviations in ozone daily maxima are shown separately for each day of simulation. The influence of PBL meteorology is shown separately for simulations with changed meteorological representation of PBL, letters correspond to different type of model run (A - D, Table 5.1), and different frequency of meteorology re-initialization (R). Influences of bulk emission changes are represented separately for 30% reduced (−) and 30% enhanced emissions (+).

The simulated ozone levels are most sensitive to the chemistry initialization and to selected PBL and land surface model (LSM). Figures 6.1 and 6.2 compare the average influence that have different sources of uncertainties on maximum daily simulated ozone levels (regardless the time of occurrence). In Figures 6.1 and 6.2 average deviations in ozone daily maxima from the reference simulation D for different sensitivity tests (presented in Chapter 5) are averaged over all model points representing Slovenian ozone stations. The highest column in Fig. 6.1 represents the influence of initial chemical conditions, i.e. the accumulation of pollution in air masses during previous days. Any change applied to anthropogenic emissions (VOC speciation, ±30% bulk changes) has significantly smaller impact on the simulated daily near ground ozone maximum.

Results from Fig. 6.1 are again, but now more in detail, presented in Fig. 6.2, where influence on ozone daily maxima is shown separately for each day of simulation for initial and boundary chemical conditions, and separately for each type of change that affects the simulated meteorological conditions. It is evident, that after three days of simulation initial chemistry conditions become almost negligible (on the 4th and 5th day of simulation) if the episode is dominated by the ozone production from local emissions. At the end of the episode, after 6 to 7 days of simulation, when Slovenia is influenced by the pollution accumulated over longer time period in air masses over Mediterranean (also Po River Basin), initial chemical conditions became more important again. Obviously, even 7 days of pollutant accumulation

is in this case not enough.

Also very important influence on the simulated meteorological conditions in PBL, and consequently on the spatial patterns and the maximum levels of simulated ozone, have parameterizations of **surface processes** (different LSMs) and **turbulence** (different PBL schemes). The column in Fig. 6.1 representing the influence of these parameterizations on simulated ozone is the second highest. Similar effect may have the representation of other physical processes in the model, which was not systematically studied. For example, the **radiation** flux divergence at the surface has a direct impact on the surface fluxes of heat and moisture, and on temperature. **Sub-grid shallow clouds** and **deep convection** also play important role in turbulent mixing and vertical distribution of chemical species. In our case the modeling of PBL meteorology is additionally challenging, because of the very complex terrain in the area we are interested in. Complex terrain plays significant role in the development of these meteorological processes, but can only roughly be represented in meteorological model with affordable resolution. Chemical boundary conditions in Fig. 6.2 have from the 3rd day onwards influence that is comparable to the influence of PBL meteorology (simulations A, B, C1, D, R, the latter refers to more frequent meteorology re-initialization). The prominent simulation type C has ozone underestimated as a consequence of unrealistically represented meteorological conditions (significantly underestimated temperatures, lower PBL heights, higher water vapor mixing ratios).

It is worth to note that enhanced/reduced emissions, as well as changed chemical boundary and initial conditions (changes that affect ozone through chemistry) result in somewhat enhanced or reduced ozone fields, while otherwise the overall appearance of ozone fields remains similar. This is quite different than with the meteorology, where the appearance of ozone fields can significantly change just as a consequence of somewhat changed meteorological conditions.

According to model results all three discussed episodes express a similar temporal evolution, which in general consists of three phases, closely related to the synoptic situation. The duration and significance of each phase vary among the episodes. In the **first phase** the 500 hPa geopotential ridge is located west of Slovenia. Slovenia is during this phase in the area of subsidence and heating at upper levels. For the higher altitudes (e.g. Krvavec station) due to the descending air the probability of influence of stratospheric ozone intrusions during this phase increases, while stratospheric ozone is unlikely to contribute to ozone levels at lower altitude stations. Alpine barrier blockades the northwestern flow which prevails in the higher altitudes. In model a weak flow around Alps can occur at the lower levels, but in general in the PBL local meso-scale winds develop and govern the pollutant dispersion over Slovenia. The coastal area at the Mediterranean side of the Alpine-Dinaric mountain ridge is in this phase of the episode included in the wider air circulation over the Northern Adriatic Sea. This coastal air circulation (described below) separate the Mediterranean and central and NE Slovenian air masses and that explains why at coastal regions often significantly higher ozone mixing ratios are measured. During this phase occasionally high ozone levels are recorded also in the central and NE parts of Slovenia, but their location, extension and duration is hard to predict according to hardly predictable local scale circulations. In the **second phase** of the episodes the southwestern flow related to the shift of 500 hPa geopotential ridge toward east predominates over Slovenia. With the southwestern flow, in the cases of all three discussed episodes, the accumulated Mediterranean pollution is advected over Slovenia, resulting in very high measured ozone at some interior stations. The episodes are terminated by the **third phase**. Ozone decrease during this phase is often related to the atmosphere cleansing by frontal precipitation (in case of widespread rain - scattered showers do not produce enough precipitation to completely eliminate ozone). The processes that contribute to ozone decrease

are also cooling of the lower troposphere and changes in flow strength and direction.

In the Mediterranean area during the first phase of the episodes the characteristic diurnal cycles of meso-scale flow regime develop and enable the formation of pollutant layers. This diurnal cycle consists of morning sea-breeze development at Northern Adriatic Sea coasts, subsequent coupling of sea-breezes with Alpine mountain upslope winds and nighttime katabatic drainage. If this air circulation above the area of Adriatic Sea, its coasts and inland mountain ridges persists for days, accumulation of pollutants in re-circulating air masses can be significant. Similar processes have been observed to enable the formation and transport of pollutant layers for example at Athens (Lalas et al., 1987), Los Angeles (Lu and Turco, 1994), over Northern (Millan et al., 1984) and Eastern (Millan et al., 1992) coasts of Spain etc. Since the thermo-topographic circulation is characteristic for the area above the Po Basin and the Alps (e.g. Baertsch-Ritter et al., 2003), the question arises how the Po Basin and the Northern Adriatic Sea circulations are connected. To answer this question more detailed investigation is still needed.

Despite the complexity of the processes interacting with each other, large model uncertainties in initialization of chemistry, in physical parameterizations, representation of surface parameters and complex terrain, we were able to simulate the flow regimes, which at least according to the near ground measurements, appear to be valuable. More measurements, especially daily vertical profiles and three-dimensional wind measurements would be needed to evaluate the model results more in detail, especially to study the actual air masses circulations and maybe even re-circulations above the Adriatic sea, its coastal regions and the Alpine slopes. These measurements would enable the more detailed evaluation of different model schemes as well, which was now limited almost entirely to the near ground variables.

Reasons for the relatively weak model results obtained with the combination of MYJ PBL scheme and 5-layer thermal diffusion scheme (simulation of type C) have not been discussed yet. Since the unofficial beta version of the model was used in simulations, additional simulations with the official WRF-Chem 3.0 version of the model (released in 2008) are needed to exclude the possibility of trouble in coupling of the two schemes, related to WRF-Chem 2.2 model version. In our case with the changed values of parameter for soil moisture availability the simulations with these two schemes became as reliable as the simulation with any other combination of LSM and PBL scheme.

Table 6.1: Statistical scores calculated for the near ground ozone densities (μg/m^3). Results are from three reference simulations (three ozone episodes) and for 11 model points representing the most reliable ozone measuring sites. Except in the case of UPA, MNBE and MNGE, which are non-dimensional, values are expressed in μg/m^3. ME, MAE and RMSE are calculated separately for daily maxima (regardless the time of occurrence) and hours with measured values above 100 μg/m^3

ME_{max}	MAE_{max}	$RMSE_{max}$	ME_{100}	MAE_{100}	$RMSE_{100}$	UPA	MNBE	MNGE
-1.5	20.6	25.8	-2.1	20.5	26.2	0.06	1.2	15.6

Table 6.1 shows statistical scores for ozone, calculated from all three reference simulations for Slovenian ozone measuring sites. Values of UPA, MNBE and MNGE, calculated for hours with ozone above 100 μg/m^3, fall inside the ranges suggested by EPA for acceptable levels of model performance (Appendix A). The scatter plots of simulated and measured ozone hourly values for three reference runs (for three episodes) for Slovenian measuring sites are shown

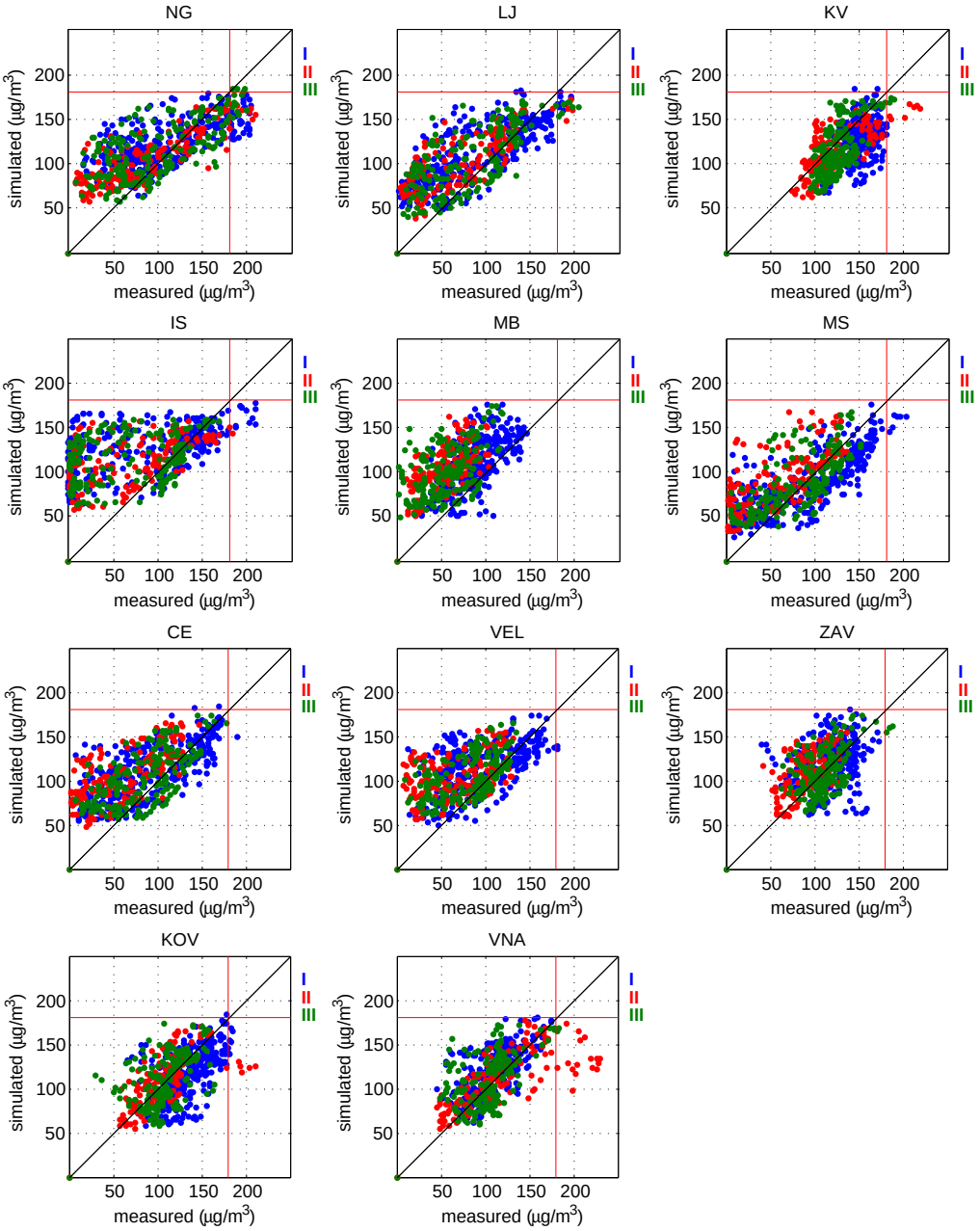

Figure 6.3: Scatter plots compare simulated (reference run only) and measured hourly ozone values for Slovenian measuring sites during the three episodes. Dots are colored according to the episode (I, II or III). NG - Nova Gorica, LJ - Ljubljana, KV - Krvavec, IS - Iskrba, MB - Maribor, MS - Murska Sobota, CE - Celje, VEL - Velenje, ZAV - Zavodnje, KOV - Kovk, VNA - Vnajnarje.

in Figure 6.3. Similarly, in Fig. 6.4 simulated and measured ozone daily maxima for three reference runs are compared. At some stations model performs better than at the others. For example, at Iskrba model significantly overestimates nighttime ozone values, which can be explained with the nighttime ozone characteristics at this site (very low measured ozone are

consequence of the very stable near ground layer and local biogenic NO_x emissions, as explained in Chapter 2). Model often underestimates the extreme ozone value, such as during Episode II at Vnajnarje, Krvavec and Kovk (this underestimation is less significant in simulation with different PBL scheme). Nevertheless, scatter plots for daily maxima show in spite of the underestimation of the highest values relatively good agreement (Fig. 6.4).

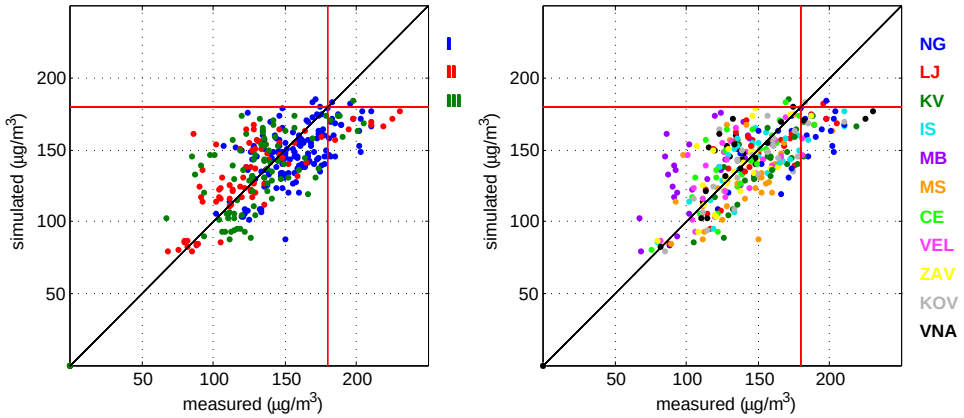

Figure 6.4: Scatter plots compare simulated and measured ozone daily maxima for Slovenian stations for all three reference runs. Dots are colored according to the Episode (left) or measuring site (right). Site notations are the same as in Fig. 6.3

Although with the model we were able to represent the principal ozone characteristics during the high ozone episodes, is the forecast (determination) of the accurate location, extension and duration of the highest ozone levels over the complex terrain of Slovenia not possible. The model could thus be used as a tool in suggesting the cases of ozone exceedances. The best solution for ozone forecasting would probably be the use of deterministic model in combination with a post processing, including statistical methods and experiences. Statistical approaches are namely, although primitive, sometimes able to implicitly take into account some processes which can be meaningful but are hardly well represented (or maybe biased) in deterministic model. The latter specially holds for the processes related to local site characteristics.

Chapter 7

Conclusions

The results of the trajectory analysis, performed for the warm parts of the years 2003 and 2004, show that ozone levels for four analyzed measuring sites in Slovenia were significantly higher in short trajectory clusters with a southwestern origin. Moreover, from the results of additional trajectory analysis we can conclude that a common origin of ozone rich air masses for the analyzed stations appears to be the area over the Northern Adriatic Sea.

Model simulations performed for three selected episodes confirm that during the first phase of the episodes in the area of the Adriatic Sea, its coastal areas and Alpine slopes, typical air circulations develop and enable the accumulation of pollutants in air masses re-circulating above that area. The accumulated pollutants together with meteorological conditions, favorable for ozone formation (high temperatures, clear sky, lack of precipitation) explain significantly higher frequency of ozone exceedances at Mediterranean Slovenia during the first phase of the episodes. The continental Slovenia during this phase generally experienced somewhat lower ozone levels with rarely recorded exceedances.

During the second phase of the episode the pollution accumulated over the Northern Adriatic sea, its western and eastern coasts and also over more interior land (also Po River Basin) is with southwesterly flow advected towards and over Slovenia, resulting (in the case of the discussed episodes) in ozone exceedances measured at continental Slovenian stations. This explains the influence of the pollution with northern Adriatic Sea origin on ozone levels measured in central Slovenia indicated by trajectory analysis.

Ozone in planetary boundary layer at lower altitudes is over continental Slovenia during the first phase of the episode formed primarily from local emissions under hot and calm meteorological conditions. Nevertheless, the experimental simulation with changed lateral chemical boundary conditions for D2 domain showed the contribution of regional transport from distant areas up to 10 $\mu g/m^3$ for ozone daily maxima during this phase.

To the pool of pollution, formed over the northern Adriatic Sea and the coastal areas during the first phase, contribute the Friulian plain emissions and coastal emissions (along wider area of northern, western and eastern coasts). The direct role of the Po River Basin emissions to this ozone rich air masses was not empirically estimated, but it is likely that the Po River Basin emissions also contribute to this accumulated pollution. There were some rare occasions (Episode 2), when according to trajectories and WRF-Chem model results Slovenia was under a direct influence of polluted air masses advected from the Po River Basin.

Ozone at high altitude station Krvavec has some distinctive characteristics. Average daily course expresses only slight minima at about 10:00 UTC when well mixed boundary layer formed above Ljubljana basin reaches the site. With the exception of a few daytime hours the site is located above the Ljubljana basin mixed layer. During the remainder of the day

(including nighttime) the site is under influence of elevated ozone layers inserted to the lower free troposphere from the daytime PBL and being then further a subject of regional transport. Occasionally also ozone layers intruded from the stratosphere may present a contribute to the high ozone levels at this site. A case by case study would be needed to confirm influence of stratospheric intrusions. A clear conclusion about reasons for relatively high ozone levels at elevated Krvavec and rural Iskrba site during spring can not be done on the basis of performed research and is left for the further research.

The comparison of impacts that have different sources of model uncertainties showed that simulated ozone is most sensitive to the initial chemical conditions, confirming the importance of accumulation of pollutants on final photochemical pollution. After three days of simulation (in the case of Episode I) the influence of initial conditions became almost negligible, indicating that three days were needed for the pollution to reach the sufficient levels during the first phase of the discussed episode. The finding, that at the end of the episode (after 6 to 7 days of simulation, when Slovenia is influenced by the Mediterranean pool of pollution) the initial chemical conditions became more important again, indicates that accumulation over a rather long time period contributes to the final level of Mediterranean pool of pollution.

The second highest influence to simulated ozone levels has been shown to have the representation of the PBL meteorology. If the problem of chemical initial conditions can be somehow handled by starting the simulation early enough (many days before the start of the episode), the problem of uncertainties in PBL meteorology remains without a concrete solution. Additional 3D measurements of PBL structure would be needed to verify different model solutions and/or nudge model toward more accurate solution over the limited areas.

Lateral chemical boundary conditions showed to be the next important contribution to simulated ozone levels (almost as important as PBL meteorology) showing that regional transport contributes to Slovenian ozone levels also in days (during the first phase) when production from local emissions predominates. In must be noted, that the influence of chemical boundaries generally depends on the distance between the boundaries and the area of interest, and the location of main emission source areas. In our case chemical boundaries were tested for the D2 domain, which covered also all the main expected impact sources of emissions. As already explained, the contribution of lateral boundary conditions increases during the second phase, when influence of regional transport increases.

According to the results of experiments for bulk emission changes the uncertainties in emissions are not expected to contribute to simulated ozone levels in central Slovenia in a higher degree. The exception is Nova Gorica station (perhaps also other near border regions), where simulated ozone levels were not only more sensitive to the bulk emission changes then elsewhere, but Nova Gorica also rather unexpectedly experienced VOC limited conditions, which may be explained by the inaccurately spatially disaggregated emissions outside Slovenia (huge costal point sources distributed according to population density and land cover).

The simulated NO_x/VOC ozone sensitivity depends on the meteorological conditions. In the experiment performed for Episode I the majority of Slovenia during the daytime experienced NO_x sensitive conditions. The exceptions were some urban regions (Ljubljana, Maribor etc.), huge sources (power plants) and, as already mentioned, the Mediterranean near border regions (Nova Gorica, coastal area).

On account of various sources of uncertainties the model was not able to represent the true locations of ozone plumes and the exact time of ozone maxima occurrence. The model as well generally underestimated the highest ozone levels which also applies to the ozone exceedances. Nevertheless, the results of model simulations helped to recognize and explain some important characteristics of temporal and spatial dynamics of high ozone episodes in Slovenia.

Bibliography

ARSO (2008). Kakovost zraka v sloveniji v letu 2007, *Technical report*, Ministrstvo za okolje in prostor, Agencija RS za okolje, Vojkova 1b, Ljubljana.

ARSO (2009). `http://www.arso.gov.si/`.

Baertsch-Ritter, N., Prevot, A. S. H., Dommen, J., Andreani-Aksoyoglu, S. and Keller, J. (2003). Model study with UAM-V in the Milan area (I) during PIPAPO: simulations with changed emissions compared to ground and airborne measurements, *Atmospheric Environment* **37**: 4133 – 4147.

Balzhanov, V. (1994). Surface ozone at mount areskutan: Connection with ozone in the free troposphere, *ITM report, Stockholm* .

Bernard, S. M., Samet, J. M., Grambsch, A., Ebi, K. L. and Romieu, I. (2001). The potential impact of climate variability and changes on air pollution-related health effects in the United States, *Environmental Health Perspectives* **109**: 199 – 209.

Carnevale, C., Gabusi, V. and Volta, M. (2006). POEM-PM: An emission model for secondary pollution control scenarios, *Environmental Modelling and Software* **21**: 320–329.

Carter, W. P. L. (2007). Development of an improved chemical speciation database for processing emissions of volatile organic compounds for air quality models, `http://pah.cert.ucr.edu/~carter/emitdb/`.

Carter, W. P. L. (2008). Development of the saprc-07 chemical mechanism and updated ozone reactivity scales, final report to the california air resources board contract no. 03-318, `www.cert.ucr.edu/~carter/SAPRC`.

Case, J. L., Manobianco, J., Dianic, A. V., Wheeler, M. W., Harms, D. E. and Parks, C. R. (2002). Verification of high-resolution RAMS forecasts over East-Central Florida during the 1991 and 2000 summer months, *Weather Forecast* **17**: 1133–1151.

Chang, J. S., Binkovski, F. S., Seaman, N. L., McHenry, J. N., Samson, P. J., Stockwell, W. R., Walcek, C. J., Mandronich, S., Middleton, P., Pleim, J. and Lansford, H. (1989). The regional acid deposition model and engineering model, *Technical report*, Stat-of-Science/Technology, Report 4 National Acid Precipitation Assesment Program, Washington, DC.

Chen, F. and Dudhia, J. (2001). Coupling an Advanced Land Surface-Hydrology Model with the Penn State-NCAR MM5 Modeling System. Part I: Model Implementation and Sensitivity, *Monthly Weather Review* **129**: 569 – 585.

Cosby, B. J., Hornberger, G. M., Clapp, R. B. and Ginn, T. R. (1984). A statistical exploration of the relationships of soil moisture characteristics to the physical properties of soils, *Water Resources Research* **20**: 682 – 690.

Cristofanelli, P., Bonasoni, P., Carboni, G., Calzolari, F., Casarola, L. and et al., S. S. (2007). Anomalous high ozone concentrations recorded at a high mountain station in italy in summer 2003, *Atmospheric Environment* **41**: 1383–1394.

Cvitas, T., Kezele, N. and Klasinc, L. (1997). Boundary-layer ozone in croatia, *J. Atmos. Chem.* **28**: 125 – 134.

Dawson, J. P., Adams, P. J. and Pandis, S. N. (2007). Sensitivity of ozone to summertime climate in the eastern USA: A modeling case study, *Atmospheric Environment* **41**: 1494 – 1511.

Derwent, R. and Davies, T. (1994). Modelling of the impact of nox or hydrocarbon control on photochemical ozone in europe, *Atmospheric Environment* **28**: 2039–2052.

Dodge, M. C. (1977). Combined use of modeling techniques and smog chamber data to derive ozone precursor relationships.

Dudhia, J. (1996). A multi-layer soil temperature model for MM5, *Preprints, 6th Annual MM5 Users Workshop,* Boulder, CO .

EPA (1991). Guideline for regulatory application of the urban airshed model. us epa report no. epa-450/4-91-013, *Technical report*, Office of Air and Radiation, Office of Air Quality Planning and Standards, Technical Support Division, Research Triangle Park, North Carolina, US.

Finlayson-Pitts, B. J. and Pitts, J. N. (1999). *Chemistry of the Upper and Lower Atmosphere; Theory, Experiments and Applications*, Academic Press.

Francois, S., Grondin, E., Fayet, S. and Ponche, J. L. (2005). The establishment of the atmospheric emission inventories of the ESCOMPTE program, *Atmospheric Research* **74**: 5–35.

Galvez, O. (2007). Synoptic-scale transport of ozone into southern ontario, *Atmospheric Environment* **41**: 8579–8595.

Geleyn, J. F. (1987). Use of a modified Richardson number for parameterizing the effect of shallow convection, J. Meteor. Soc. Japan, Special NWP symposium issue.

Giard, D. and Basil, E. (2000). Implementation of a New Assimilation Scheme for Soil and Surface Variables in a Global NWP Model, *Monthly Weather Review* **128**: 997 – 1015.

Grell, G. A., Peckham, S. E., Schmitz, R., McKeen, S. A., Frost, G., Skamarock, W. and Eder, B. (2005). Fully coupled "online" chemistry within the WRF model, *Atmospheric Environment* **39**: 6957 – 6975.

Guenther, A. B., Zimmerman, P. R. and Wildermuth, M. (1994). Natural volatile organic compound emission rate estimates for US woodland landscapes, *Atmospheric Environment* **28**: 1197 – 1210.

Hafner, W., Solorzano, N. and Jaffe, D. (2007). Analysis of rainfall and fine aerosol data using clustered trajectory analysis for national park sites in the western us, *Atmospheric Environment* **41**: 3071–3081.

Hanks, R. J. and Ashcroft, G. L. (1986). Applied Soil Physics, Springer-Verlag.

Heck, W. W., Taylor, O. C., Adams, R., Bingham, G., Miller, J., Preston, E. and Weinstein, L. (1982). Natural volatile organic compound emission rate estimates for US woodland landscapes, *Journal of the Air Pollution Control Associationt* **32**: 353 – 361.

Hobbs, P. V. (1998). *Introduction to Atmospheric Chemistry; A Companion Text to Basic Physical Chemistry for the Atmospheric Sciences*, John Wiley & Sons.

Hochberg, Y. and Tamhane, A. (1987). *Multiple Comparison Procedures*, John Wiley & Sons.

Hollander, M. and Wolfe, D. (1973). *Nonparametric Statistical Methods*, John Wiley & Sons.

Holton, J. R. (1992). *An Introduction to Dynamic Meteorology*, Academic Press, UK.

Hough, A. M. (1988). An intercomparison of mechanisms for the production of photochemical oxidants, *Journal of Geophysical Research* **93**: 3789 – 3812.

Hsu, Y., Strait, R., Roe, S. and Holoman, D. (2006). SPECIATE 4.0, Speciation Database Development Documentation, Final Report, EPA Contract No. EP-D-06-001, Work Assignment Numbers 0-03 and 68-D-02-063, WA 4-04 and WA 5-05, `http://www.epa.gov/ttn/chief/software/speciate/speciate4/documentation/speciatedoc_1206.pdf`.

Janjić, Z. I. (2002). Nonsingular Implementation of the Mellor–Yamada Level 2.5 Scheme in the NCEP Meso model, *NCEP Office Note* **437**: 61.

Jenkin, M. E. and Clemitshaw, K. C. (2000). Ozone and other secondary photochemical pollutants: chemical processes governing their formation in the planetary boundary layer, *Atmospheric Environment* **43**: 2499–2527.

Kaiser, A., Scheinfinger, H., Spangl, W., Weiss, A., Gilge, S. and et al., W. F. (2007). Transport of nitrogen oxides, carbon monoxide and ozone to the alpine global atmosphere watch stations jungfraujoch (switzerland, zugspitze and hohenpeissenberg (germany), sonnblick (austria) and mt. krvavec (slovenia), *Atmospheric Environment* pp. 9273–9287.

Kalabokas, P. D., Volz-Thomas, A., Brioude, J., Thouret, V., Cammas, J. P. and Repapis, C. C. (2000). Mediterranea rural ozone characteristics around the urban area of Athens, *Atmospheric Environment* **34**: 5199 – 5208.

Kessler, E. (1969). On the distribution and continuity of water substance in atmospheric circulations, *Meteorological Monographs* **10**: 1 – 84.

Klaic, Z. B., Belusic, D., Bulic, I. H. and Hrust, L. (n.d.). Mesoscale modeling of meteorological conditions in the lower troposphere during a winter stratospheric ozone intrusion over zagreb, croatia, *J. Geophys. Res.* **108**.

Lalas, D. P., Tombrou-Tsella, M., Petrakis, M., Asimakopoulos, N. D. and Helmis, C. (1987). An experimental study of the horizontal and vertical distribution of ozone at Athens, *Atmospheric Environment* **21**: 2681 – 2693.

Lefohn, A., Shadwick, D., Feister, U. and Mohnen, V. (1992). Surface level ozone: climate change and evidence for trends, *Journal of Air and Waste Management Association* **42**: 136–144.

Leighton, P. A. (1961). *Photochemistry of Air Pollution*, Academic Press. New York.

Levy, I. J., Carrothers, T. J., Tuomisto, J. T., Hammitt, J. K. and Evans, J. S. (2001). Assesing the publich health benefits of reduced ozone concentrations, *Environmental Health Perspectives* **109**: 1215 – 1226.

Lisac, I., Marki, A., Tiljak, D., Klasinc, L. and Cvitaš, T. (1993). Stratospheric ozone intrusion over zagreb, croatia, on february 6, 1990, *Meteorol. Z.* **2**: 224–231.

Liu, K. Y. and Hsiao, Z. W. L. F. (2002). A modelling of the sea breeze and its impacts on ozone distribution in northern Taiwan, *Environmental Modelling & Software* **17**: 21 – 27.

Logan, J. (1985). Tropospheric ozone: seasonal behaviour, trends, and anthropogenic influence, *Journal of Geophysical Research* pp. 10463–10482.

Logan, J. (1989). Ozone in rural areas of the united states, *Journal of Geophysical Research* **94**: 8511–8532.

Louis, J. F., Tiedke, M. and Geleyn, J. F. (1982). A short history of the PBL parameterizationas at ECMWF, Proc. of the ECMWF workshop on planetary boundary parameterization, Reading, 25–27 Nov. 1981.

Lu, R. and Turco, R. P. (1994). Air pollutant transport in a coastal environment. Part I. Two-dimensional simulations of sea-breeze and mountain effects, *Journal of the Atmospheric Sciences* **51**: 2285 – 2308.

Mallet, V. and Sportisse, B. (2005). A comprehensive study of ozone sensitivity with respect to emissions over Europe with a chemistry-transport model, *Journal of Geophysical Research* **110**: D22302, doi:10.1029/2005JD006234.

Mandronich, S. (1987). Photodissociation in the atmosphere, 1, Actinic flux and the effects of ground reflections and clouds, *Journal of Geophysical Research* **92**: 9740 – 9752.

Mao, Q., Gautney, L. L., Cook, T. M., Jacobs, M. E., Smith, S. N. and Kelsoe, J. J. (1987). Interaction between soil hydrology and boundary-layer development, *Boundary Layer Meteorology* **38**: 185 – 202.

Mellor, G. L. and Yamada, T. (1982). Development of a Turbulence Closure Model for Geophysical Fluid Problems, *Review of Geophysics and Space Physics* **20**: 851 – 875.

Milford, J., Gao, D., Sillman, S., Blossey, P. and Russell, A. G. (1994). Total reactive nitrogen (NO_y) as an indicator for the sensitivity of ozone to NO_x and hydrocxarbons, *Journal of Geophysical Research* **99**: 3533–3542.

Millan, M. M., Alonso, L., Legarreta, J. A., Albizu, M. V. and Ureta, I. (1984). A fumigation episode in an industrialized estuary: Bilbao, November 1981, *Atmospheric Environment* **18**: 563 – 572.

Millan, M. M., Artinano, B., Alonso, L., Castro, M., Fernandez-Patier, R. and Goberna, J. (1992). A Meso-Meteorological Cycles of Air Pollution in the Iberian Peninsula, (MECAPIP), Air Pollution Research Report 44, EUR No. 14834, European Commision DG XII/E'1, Rue de la Loi, 200, B-1040, Brussels, *Technical report*.

Millan, M. M., Salvador, R., Mantilla, E. and Artinano, B. (1996). Meteorology and photochemical air pollution in southern Europe: experimental results from EC research projects, *Atmospheric Environment* **30**: 1909 – 1924.

Monin, A. S. and Obukhov, A. M. (1954). Basic laws of turbulent mixing in the surface layer of the atmosphere, *Contrib. Geophys. Inst. Acad. Sci.,* USSR **151**: 163 – 187.

Monks, S. (2000). A review of the observations and origins of the spring ozone maximum, *Atmospheric Environment* **34**: 3454–3561.

Moody, J. and Galloway, J. (n.d.). Quantifying the relationship between atmospheric transport and the chemical composition of precipitation on bermuda, *Tellus* **40**.

Olivier, J., Peters, J., Granier, C., Pétron, G., Müller, J. F. and Wallens, S. (2003). Present and future surface emissions of atmospheric compounds, POET Report N.2, EU project EVK2-1999-00011, `http://www.oma.be/TROPO/POET_emissions_report.pdf`.

Ollinger, S. V., Aber, J. D. and Reich, P. B. (1996). Predicting the effects of tropospheric ozone on forest productivity in the Northeastern U.S., Proceedings 1995 meeting of the northern global change program; Gen. Tech. Rep. NE-214. Radnor, PA: U.S. Department of Agriculture, Forest Service, Northeastern Forest Experiment Station pp. 217 – 225.

Pan, H. L. and Marth, L. (1987). Interaction between soil hydrology and boundary-layer development, *Boundary Layer Meteorology* **38**: 185 – 202.

Pasquill, F. and Smith, F. B. (1983). *Atmospheric Diffusion*, Ellis Horwood Ltd.

Passant, N. R. (2002). Speciation of UK emissions of NMVOC, AEAT/ENV/0545 report,London, *Technical report*.

Peckham, S. E., Grell, G. A., Fast, J. D., Gustafson, W. I., Ghan, S. J., Zaveri, R., Easter, R. C., Barnard, J., Chapman, E., Schmitz, R. and Salzmann, M. (2008). WRF/Chem Version 3.0 User's Guide, `http://ruc.fsl.noaa.gov/wrf/WG11/Users_guide_22jul08.pdf`.

Perez, C., Himenez, P., Jorba, O., Sicard, M. and Baldasano, J. M. (1987). Influence of the PBL scheme on high-resolution photochemical simulations in an urban coastal area over the Western Mediterranean, *Atmospheric Environment* **40**: 5274 – 5297.

Pilegaard, K., Skiba, U., Ambus, P., Beier, C., Bruggemann, N., Butterbach-Bahl, K., Dick, J., Dorsey, J., Duyzer, J., Gallagher, M., Gasche, R., Horvath, L., Kitzler, B., Leip, A., Pihlatie, M. K., Rosenkranz, P., Seufert, G., Vesala, T., Westrate, H. and Zechmeister-Boltenstern, S. (2006). Factors controlling regional differences in forest soil emission of nitrogen oxides (NO and N2O), *Biogeosciences* **3**: 651 – 661.

PORG (1997). Ozone in the United Kingdom. Fourth Report of the UK Photochemical Oxidants Review Group. Department of the Environment, Transport and the Regions, *Technical report*, Department of the Environment, Transport and the Regions, London.

Ricco, A., Giunta, G. and Chianese, E. (2007). The application of a trajectory classification procedure to interpret air pollution measurements in the urban area of naples (southern italy), *Science of the Total Environment* **376**: 198–214.

Ritter, B. and Geleyn, J. F. (1992). A comprehensive radiation scheme for numerical weather prediction models with potential applications in climate studies, *Monthly Weather Review* **120**: 303 – 325.

Rosenthal, J. S., Helvey, R. A., Battalino, T. E., Fisk, C. and Greiman, P. W. (2003). Ozone transport by mesoscale and diurnal wind circulations across southern California, *Atmospheric Environment* **37**: 51 – 71.

Scheel, H., Areskoug, H., Geiss, H., Gomiscek, B., Granby, K. and et al., L. H. (1997). On the spatial distribution and seasonal variation of lower-troposphere ozone over europe, *Journal of Atmospheric Chemistry* **28**: 11 – 28.

Schoenemeyer, T., Richter, K. and Smiatek, G. (1997). Vorstudie uber ein raumlich und zeitlich aufgeschlostes Kataster anthropogener und biogener Emissionen fuer Bayern mit Entwicklung eines Prototyps und Anwendung fur Immissionsprognosen. Abschluss bericht an das Bayerische Landesamt fur Umweltschutz. Fraunhofer-Institut fuer Atmosphaerische Umweltforschung, Garmisch-Partenkirchen.

Schuepbach, E., Davies, T. D. and Massacand, A. C. (1999). An unusual springtime ozone episode at high elevation in the swiss alps: Contribution both from cross-tropopause exchange and from the boundary layer, *Atmospheric Environment* **33**: 1735 – 1744.

Seaman, N. L. (2000). Meteorological modeling for air-quality assessments, *Atmospheric Environment* **34**: 2231 – 2259.

Seibert, P., Kromp-Kolb, H., Baltensperger, U., Jost, D., Schwinkowski, M. and et al., A. K. (1994). Trajectory analysis of aerosol measurements at high alpine sites, *Transport snd transformation of pollutants in the troposphere* pp. 689–693.

Seibert, P., Kromp-Kolb, H., Kasper, A., Puxbaum, M. K. M. and et al., D. J. (1997). Transport of polluted boundary layer air from the po valley to high alpine sites, *Atmospheric Environment* pp. 3953–3965.

Seinfeld, J. H. and Pandis, S. N. (1998). *Atmospheric Chemistry and Physics; From Air Pollution to Climate Change*, Cambridge University Press.

Sillman, S. (1995). The use of no_y, h_2o_2 and hno_3 as in dicators for o_3-no_x-rog sensitivity in urban locations, *Journal of Geophysical Research* **100**: 14175–14188.

Sillman, S. (1999). The relation between ozone, no_x and hydrocarbons in urban and polluted rural environments, *Atmospheric Environment* **33**: 1821–1845.

Sillman, S., He, D., Cardelino, C. and Imhoff, R. E. (1997). The use of photochemical indicators to evaluate ozone-nox-hydrocarbon sensitivity: Case studies from atlanta, new york and los angeles, *Journal of the Air and Waste Management Association* **47**: 642–652.

Sillman, S. and Samson, P. J. (1995). Impact of temperature on oxidant photochemistry in urban, polluted rural and remote environments, *Journal of Geophysical Research* **100**: 11497–11508.

Simpson, D., Guenther, A., Hewitt, C. N. and Steinbrecher, R. (1995). Biogenic emissions in Europe. 1. Estimates and uncertaintes, *Journal of Geophysical Research* **100D**: 22875 – 22890.

Skamarock, W. C., Klemp, J. B., Dudhia, J., Gill, D. O., Barker, D. M., Huang, X. Z., Wang, W. and Powers, J. G. (2008). A Description of the Advanced Research WRF Version 3, *Technical report*, Mesoscale and Microscale Meteorology Division, NCAR, Boulder, Colorado.

Skamarock, W. C., Klemp, J. B., Dudhia, J., Gill, D. O., Barker, D. M., Wang, W. and Powers, J. G. (2005). A Description of the Advanced Research WRF Version 2, Last revision: January 2007, *Technical report*, Mesoscale and Microscale Meteorology Division, NCAR, Boulder, Colorado.

Staehelin, J. and Smith, W. (1991). Trend analysis of tropospheric ozone concentration utilizing the 20 year data set of ozone ballon soundings over Payerne (Switzerland), *Atmospheric Environment* **25**: 1739 – 1757.

Staff, H. and Tyler, G. (1996). Effects of acid deposition and tropospheric ozone on forest ecosystems in Sweden, *Biological Conservation* **75**: 1739 – 1757.

Stockwell, W. R., Middleton, P., Chang, J. S. and Tang, X. (1990). The second-generation regional acid deposition model chemical mechanism for regional air quality modeling, *Journal of Geophysical Research* **95**: 16343 – 16367.

Stohl, A. and Seibert, P. (1998). Accuracy of trajectories as determined from the conservation of meteorological tracers, *Q. J. Roy. Met. Soc.* **124**: 1465–1484.

Stohl, A., Wotawa, G., Seibert, P. and Kromp-Kolb, H. (1995). Interpolation errors in wind fields as a function of spatial and temporal resotluion and their impact on different types of kinematic trajectories, *Journal of Applied Meteorology* **34**: 2149–2165.

Stull, R. B. (2000). *Meteorology for Scientists and Engineers,*, Brooks/Cole.

Taghavi, M., Cautenet, S. and Arteta, J. (2005). Impact of a highly detailed emission inventory on modeling accuracy, *Atmospheric Research* **74**: 65–88.

Team, A. I. (2003). The aladin project, mesoscale modeling seen as a basic tool for weather forecasting and atmospheric research, *WMO Bull.* **46**: 317–324.

Tov, D. A.-S., Peleg, M., Matveev, V., Mahrer, Y., Seter, I. and Luria, M. (1997). Recirculation of polluted air masses over the East Mediterranean coast, *Atmospheric Environment* **31**: 1441 – 1448.

Troen, I. and Mahrt, L. (1986). A Simple Model of the Atmospheric Boundary Layer: Sensitivity to Surface Evaporation, *Boundary-Layer Meteorology* **37**: 129 – 148.

Vautard, R., Honore, C., Beekmann, M. and Rouil, L. (2005). Simulation of ozone during the August 2003 heat wave and emission control scenarios, *Atmospheric Environment* **39**: 2957–2967.

Vestreng, V., Rigler, E., Adams, M., Kindbom, K., Pacyna, J. M., Gon, H. D., Reis, S. and Travnikov, O. (2006). Inventory review 2006, Emission data reported to LRTAP and NEC Directive, Stage 1, 2 and 3 review and Evaluation of inventories of HM and POPs. EMEP/MSC-W Technical Report 1/2006 ISSN 1504-6179, `http://www.emep.int`.

Volz, A. and Kley, D. (1988). Evaluation of the Montsouris series of ozone measurements made in the nineteenth century, *Nature* **323**: 240 – 242.

Žabkar, J., Žabkar, R., Vladušič, D., Čemas, D., Suc, D. and Bratko, I. (2006). Q^2 Prediction of ozone concentrations, *Ecological Modelling* **191**: 68 – 82.

Žabkar, R., Rakovec, J. and Gaberšek, S. (2008). A trajectory analysis of summertime ozone pollution in Slovenia, *Geofizika* **25**: 179–202.

Wakamatsu, S., Uno, I., Ueda, H., Ueharra, K. and Tateishi, H. (1989). Observational study of stratospheric ozone intrusions into the lower troposphere, *Atmospheric Environment* **23**: 1815 – 1826.

Wang, W., Barker, D., Bray, J., Bruyere, C., Duda, M., Dudhia, J., Gill, D. and Michalakes, J. (2007). User guide for advanced research wrf (arw) modelling system version 2.2, *Technical report*, Mesoscale & Microscale Meteorology Division National Center for Atmosphere Research.

Wesley, M. L. (1989). Parameterization of surface resistance to gaseous dry deposition in regional numerical models, *Atmospheric Environment* **16**: 1293 – 1304.

Wicker, L. J. and Skamarock, W. C. (2002). Time splitting methods for elastic models using forward time schemes, *Monthly Weather Review* **130**: 2088–2097.

Wotawa, G., Kroeger, H. and Stohl, A. (2000). Transport of ozone towards the Alps - result from trajectory analyses and photochemical model studies, *Atmospheric Environment* **9**: 1367–1377.

Wotawa, G. and Kromp-Kolb, H. (2000). The research project VOTALP - general objectives and main results, *Atmospheric Environment* **34**: 1319 – 1322.

Zhong, S. Y., In, H. J., Bian, X. D., Charney, J., Heilman, W. and Potter, B. (2005). Evaluation of real-time high-resolution MM5 predictions over the Great Lakes Region, *Weather Forecast* **20**: 63–81.

Appendices

Appendix A

Statistical scores used for model evaluation

To quantitatively evaluate the model's performance, some standard statistical measures were computed over space and time for meteorological parameters and ozone concentrations. We decided to choose conventional measures which are simple and have physical meaning clearly defined. All of them are easy to understand and enable direct comparison to the results from other studies.

Mean Error :

$$\mathrm{ME} = \frac{1}{N}\sum_{i=1}^{N}(M_i - O_i), \tag{A.1}$$

where M is a modeled (simulated) variable and O is a corresponding observed (measured) value of the same variable. i counts the total sampling $N = m \times n$ over time and space, where m in number of spatial points and n number of temporal points (e.g. hours, days). If $m = 1$ or $n = 1$, statistical measures are computed only over temporal or spatial domain, respectively. ME represents systematic errors, usually caused by consistent misrepresentation of local properties.

Mean Absolute Error :

$$\mathrm{MAE} = \frac{1}{N}\sum_{i=1}^{N}|M_i - O_i|. \tag{A.2}$$

Root Mean Square Error :

$$\mathrm{RMSE} = \sqrt{\frac{1}{N}\sum_{i=1}^{N}(M_i - O_i)^2}. \tag{A.3}$$

Systematic Root Mean Square Error :

$$\mathrm{RMSEs} = \sqrt{\frac{1}{N}\sum_{i=1}^{N}(\hat{M}_i - O_i)^2}. \tag{A.4}$$

Unsystematic Root Mean Square Error :

$$\mathrm{RMSEu} = \sqrt{\frac{1}{N}\sum_{i=1}^{N}(M_i - \hat{M}_i)^2}. \tag{A.5}$$

$\hat{M}_i = n + kO_i$, where n and k are calculated by the least squares regression. If RMSE emphasizes extreme differences between modeled and observed values, the systematic and unsystematic RMSE (RMSEs and RMSEu) quantify the type of error. In theory systematic errors should account for processes that the model does not routinely simulate well, whereas unsystematic errors could be attributed to random model or/and observation uncertainties. RMSEu also contains a component of natural subgrid-scale variability, because the model value is an average over a grid volume, while the observed value is a point measurement (Case et al., 2002; Zhong et al., 2005). For an unbiased variable RMSEu and RMSE are equal. The measures presented so far share the same physical unit as the variable being evaluated.

Pearson Correlation Coefficient :

$$r = \frac{\sum_{i=1}^{N}(M_i - \overline{M})(O_i - \overline{O})}{\sqrt{\sum_{i=1}^{N}(M_i - \overline{M})^2(O_i - \overline{O})^2}}, \tag{A.6}$$

where $\overline{M}$ and $\overline{O}$ are average modeled and observed variable values. r indicates the strength of a linear relationship between two variables.

Some additional dimensionless statistical measures were used for evaluating the modeled ozone concentrations. A skillful model should be able to simulate accurately both the concentration of a species and its temporal and spatial variability. We decide to use by the EPA (1991) provided set of useful statistical measures.

Mean Normalized Bias Error :

$$\text{MNBE} = \frac{1}{N}\sum_{i=1}^{N}\frac{M_i - O_i}{O_i} \times 100. \tag{A.7}$$

Mean Absolute Normalized Gross Error :

$$\text{MNGE} = \frac{1}{N}\sum_{i=1}^{N}\frac{|M_i - O_i|}{O_i} \times 100. \tag{A.8}$$

A cut-off value of 100 μg/m^3 for measured ozone concentration was used for calculating MNBE and MNGE to avoid excessive weighting of relative means by low values. If MNBE measures the model'a ability to replicate observed patterns, the MNGE is a measure of model precision. EPA (1991) suggested that for model simulations of O_3 used for regulatory applications MNBE should be within $\pm$15% and the MNGE should be less than 35% for an acceptable level of model performance.

Unpaired Peak Prediction Accuracy :

$$\text{UPA} = \frac{M_{MAX} - O_{MAX}}{O_{MAX}} \times 100. \tag{A.9}$$

UPA quantifies the difference between the highest observed 1-hour daily concentration at a given location and modeled 1-hour daily maximum at this location, regardless the time of observed and modeled maximum. The US EPA suggestion is that UPA should be less than $\pm$20%.

Index Of Agreement :

$$\text{IOA} = 1 - \frac{\sum_{i=1}^{N}(M_i - O_i)^2}{\sum_{i=1}^{N}(|M_i - \overline{O}| + |O_i - \overline{O}|)^2}. \tag{A.10}$$

The range of IOA is 0 - 1, with score 1 indicating perfect model agreement with the observations.

Appendix B

Weighting factor maps for spatial disaggregation of EMEP emissions

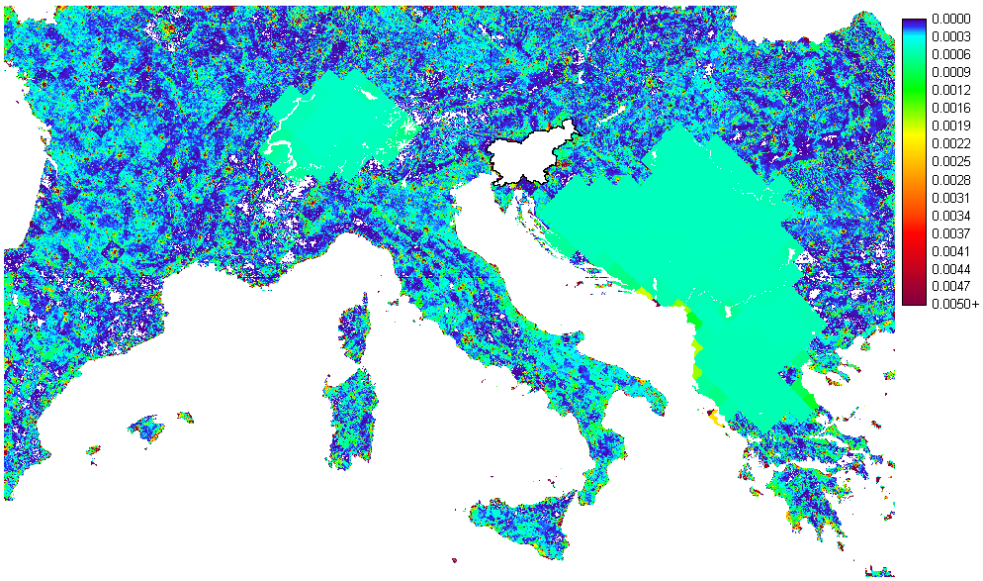

Figure B.1: Weighting factor map with the horizontal resolution 1 km, calculated from population density.

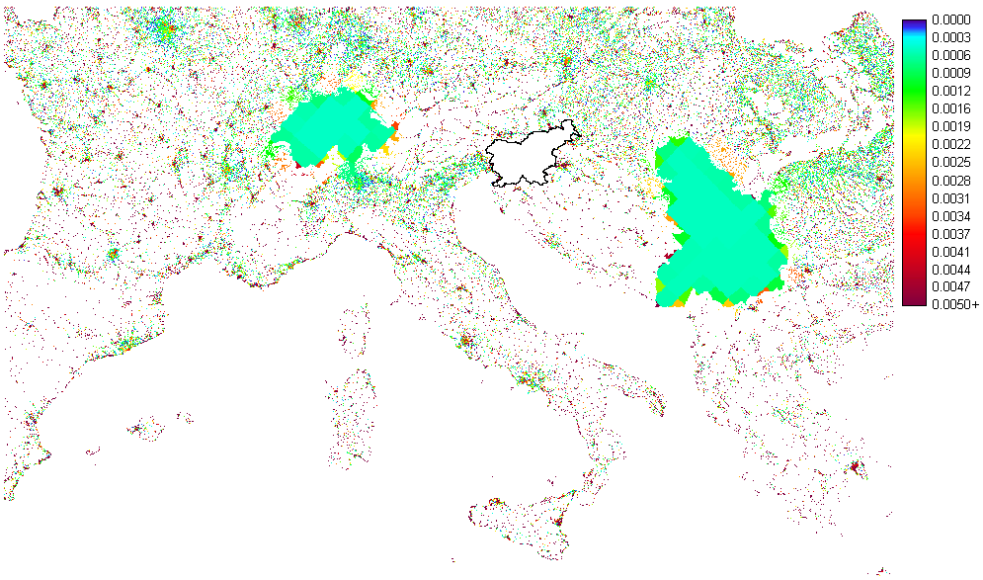

Figure B.2: Weighting factor map with the horizontal resolution 1 km, calculated from urban 1-4 CORINE categories. Used for disaggregation of sectors S1, S3, S4, S5, S6, S7 and S9 emissions outside Slovenia.

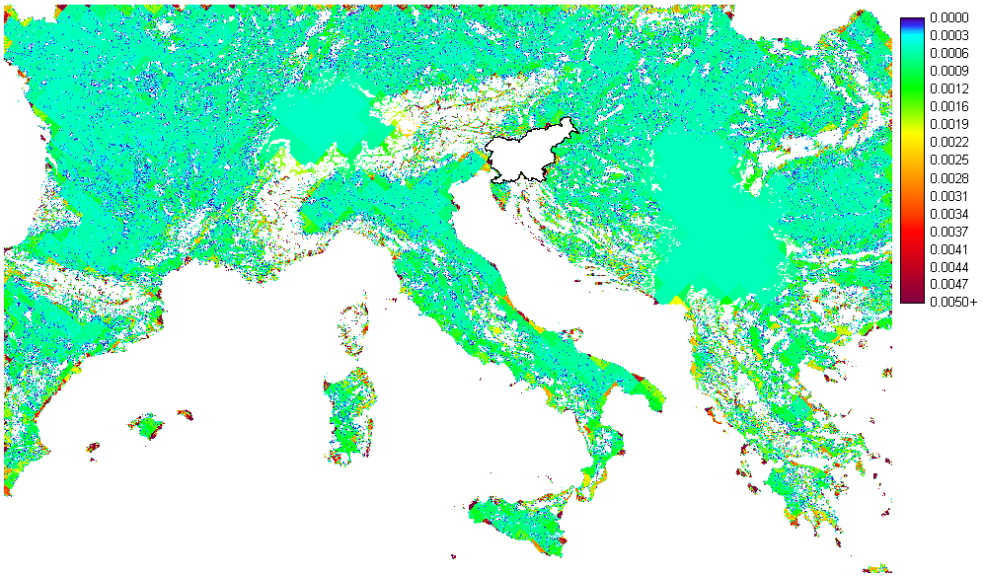

Figure B.3: Weighting factor map with the horizontal resolution 1 km, calculated from 12-22 vegetation CORINE categories. Used for disaggregation of sector S10 emissions outside Slovenia.

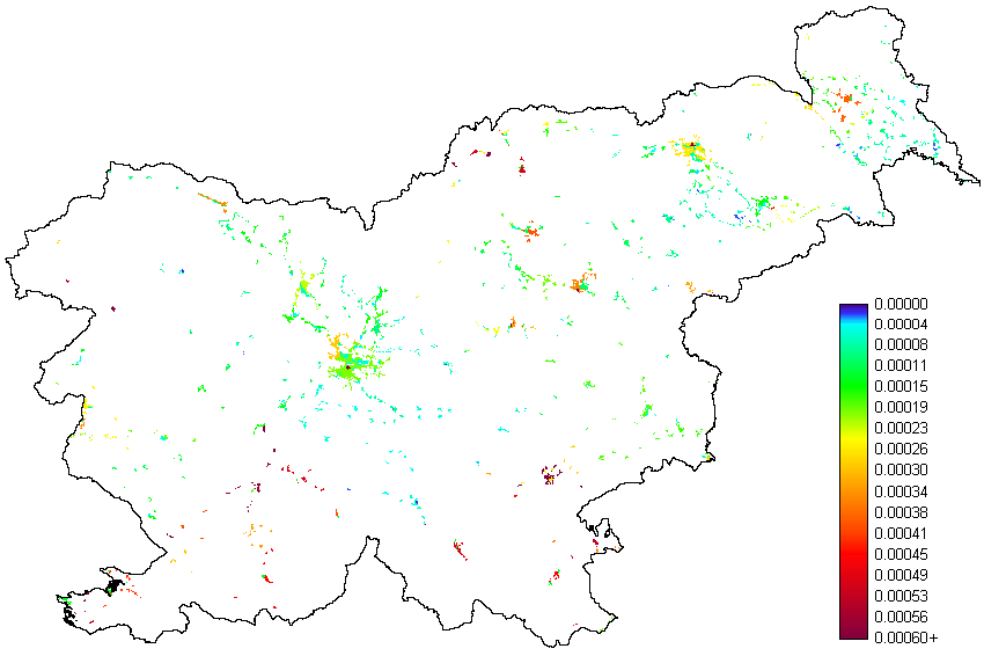

Figure B.4: Weighting factor map with the horizontal resolution 100 m, calculated from urban 1-4 CORINE categories inside Slovenia.

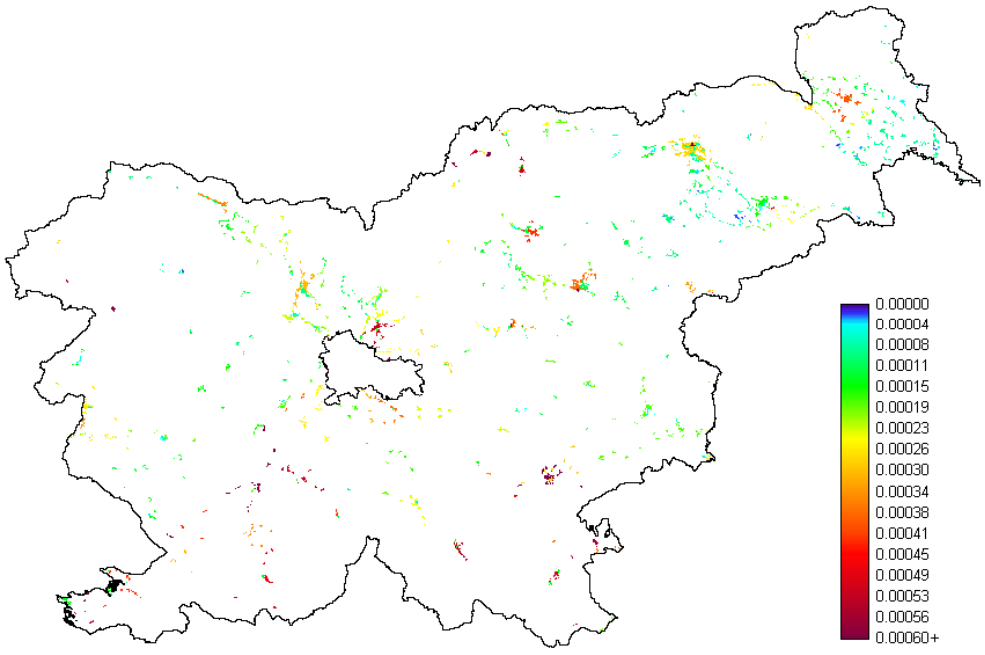

Figure B.5: Weighting factor map with the horizontal resolution 100 m, calculated from urban 1-4 CORINE categories inside Slovenia without Ljubljana region. Used for disaggregation of emissions inside Slovenia from which the detailed emissions from Ljubljana region have already been subtracted.

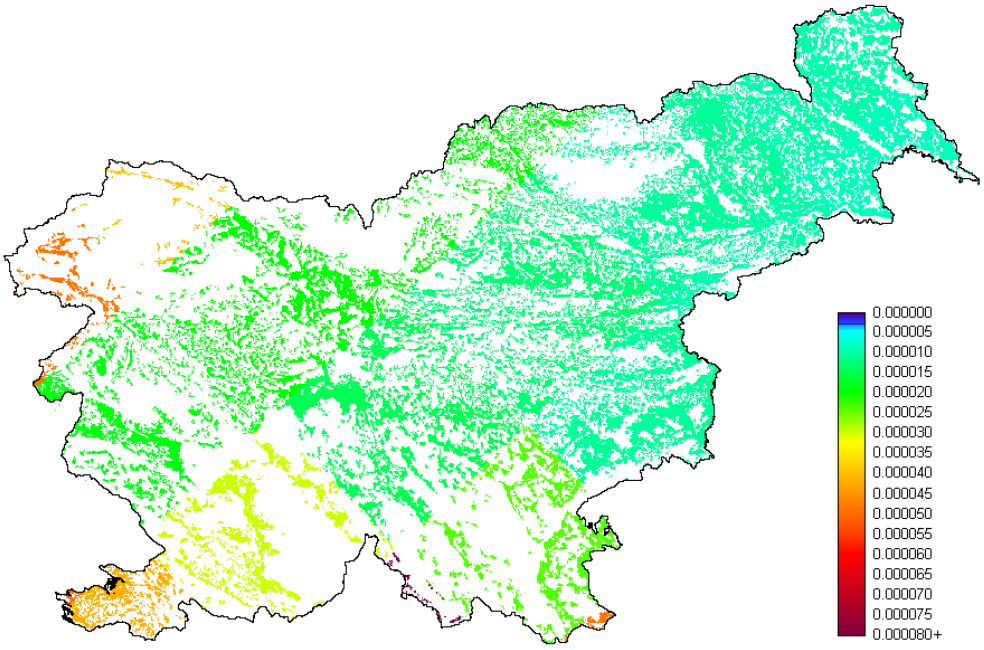

Figure B.6: Weighting factor map with the horizontal resolution 100 m, calculated from 12-22 vegetation CORINE categories. Used for disaggregation of sector S10 emissions inside Slovenia.

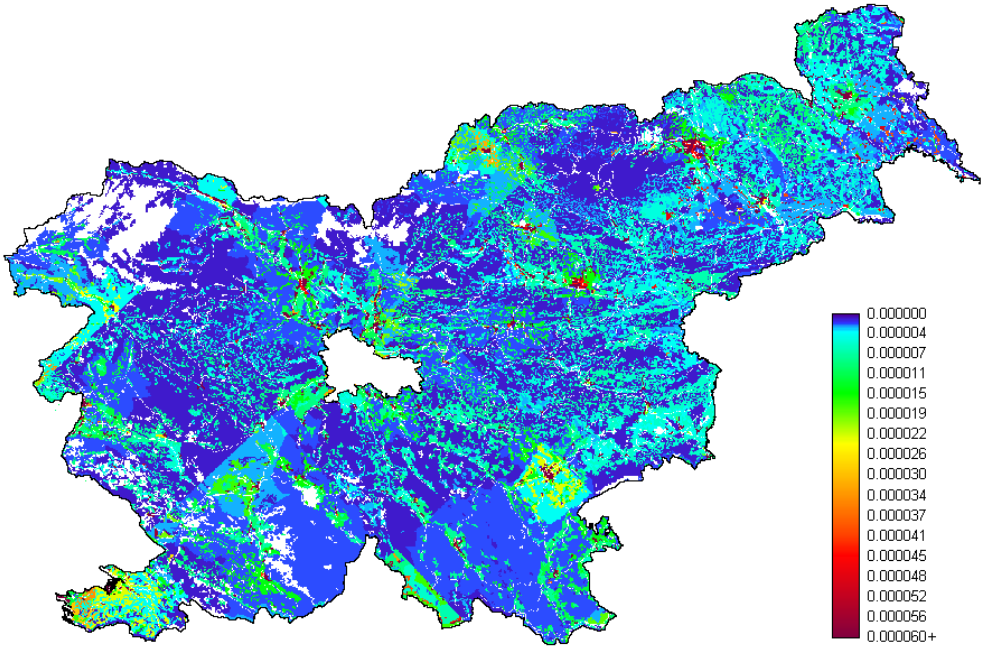

Figure B.7: Weighted factor map with the horizontal resolution 100 m, calculated from population density inside Slovenia.

Appendix C

Tables associated with preparation of anthropogenic emissions

Table C.1: The comparison of national emissions for years 2003 and 2005 (in Gg), reported by the Environmental Agency of the Republic of Slovenia, and calculated as a sum of Databases A + B. For the latter, emissions for years 2003 and 2005 are the same, except for SO_x from SNAP 1.

Reported by Environmental Agency for years 2003/2005					
SNAP	SO_x	NO_x	NH_3	nmVOC	CO
S1	51.0/32.5	16.4/15.0		1.6/1.8	0.98/1.3
S2	3.3/2.5	3.6/3.5		8.5/8.4	29.9/29.7
S3	6.2/3.7	4.3/4.8		2.0/1.3	2.3/1.9
S4	4.3/2.4			4.5/6.4	
S5				5.5/2.6	
S6				11.2/11.8	
S7	0.65/0.75	31.5/34.0	0.85/0.9	13.4/12.0	47.5/49.2
S8	-/0.01	0.48/0.50		0.05/0.06	0.50/0.46
S9					
S10			18.4/17.3		
S11					
Total	65.6/41.8	56.3/57.7	19.2/18.3	46.7/43.5	81.3/82.5

Sum of databases A + B for years 2003/2005					
SNAP	SO_x	NO_x	NH_3	nmVOC	CO
S1	50.4/30.6	14.5		1.6	1.5
S2	3.3	3.6		7.9	37.4
S3	6.9	5.4		1.1	4.3
S4	2.8			1.5	
S5				4.8	
S6				14.5	
S7	0.9	32.1	0.8	14.3	62.2
S8	0.4	1.1		0.2	0.9
S9			0.2		2.0
S10			21.2		
S11					
Total	64.7/44.8	56.8	22.2	45.7	108.2

Table C.2: Conversion table used to produce input emissions data for WRF-Chem simulations. This table lists the input chemical field (from emission inventory), the emission field name used in WRF-Chem model, the weight factor applied to the chemical field and the full chemical species name.

Field	Name	Weight	Species name
CO	e_co	1.00	
NOX	e_no	1.00	
SO2	e_so2	1.00	
NH3	e_nh3	1.00	
ETH	e_eth	1.00	Ethane
HC3	e_hc3	1.00	Alkane 500<kOH<5000
HC5	e_hc5	1.00	Alkane 5000<kOH<10000
HC8	e_hc8	1.00	Alkane kOH>10000
OL2	e_ol2	1.00	Ethylene
OLT	e_olt	1.00	Alkene kOH<20000 /ppm/min
OLI	e_oli	1.00	Alkene kOH>20000 /ppm/min
TOL	e_tol	1.00	Toluenes
XYL	e_xyl	1.00	Xylenes
HCHO	e_hcho	1.00	Formaldehyde
ALD	e_ald	1.00	Aldehides
KET	e_ket	1.00	Ketones
ISO	e_iso	1.00	Isoprene
CSL	e_csl	1.00	Cresols
ORA1	e_hc3	1.00	
ORA2	e_ora2	1.00	
GLY	e_ald	1.00	Glyoxal
MGLY	e_ald	1.00	Methylglyoxal
MACR	e_ald	0.50	Methacrolein
MACR	e_olt	0.50	Methacrolein
MVK	e_ket	0.50	Methylvinyl ketone
MVK	e_olt	0.50	Methylvinyl ketone

Table C.3: CORINE land cover Categories.

1	Artificial surfaces	Urban fabric	Continuous urban fabric
2	Artificial surfaces	Urban fabric	Discontinuous urban fabric
3	Artificial surfaces	Industrial, commercial, transport	Industrial or commercial
4	Artificial surfaces	Industrial, commercial, transport	Road and rail networks
5	Artificial surfaces	Industrial, commercial, transport	Port areas
6	Artificial surfaces	Industrial, commercial, transport	Airports
7	Artificial surfaces	Mine, dump, construction sites	Mineral extraction sites
8	Artificial surfaces	Mine, dump, construction sites	Dump sites
9	Artificial surfaces	Mine, dump, construction sites	Construction sites
10	Artificial surfaces	Artificial, non-agricultural veget.	Green urban areas
11	Artificial surfaces	Artificial, non-agricultural veget.	Sport and leisure facilities
12	Agricultural areas	Arable land	Non-irrigated arable land
13	Agricultural areas	Arable land	Permanently irrigated land
14	Agricultural areas	Arable land	Rice fields
15	Agricultural areas	Permanent crops	Vineyards
16	Agricultural areas	Permanent crops	Fruit trees, berry plantations
17	Agricultural areas	Permanent crops	Olive groves
18	Agricultural areas	Pastures	Pastures
19	Agricultural areas	Heterogeneous agricultural areas	Annual crops
20	Agricultural areas	Heterogeneous agricultural areas	Complex cultivation
21	Agricultural areas	Heterogeneous agricultural areas	Principally agriculture land
22	Agricultural areas	Heterogeneous agricultural areas	Agro-forestry areas
23	Forest, semi natural	Forests	Broad-leaved forest
24	Forest, semi natural	Forests	Coniferous forest
25	Forest, semi natural	Forests	Mixed forest
26	Forest, semi natural	Scrub and/or herbaceous veget.	Natural grasslands
27	Forest, semi natural	Scrub and/or herbaceous veget.	Moors and heathland
28	Forest, semi natural	Scrub and/or herbaceous veget.	Sclerophyllous vegetation
29	Forest, semi natural	Scrub and/or herbaceous veget.	Transitional woodland-shrub
30	Forest, semi natural	Open spaces, little/no veget.	Beaches, dunes, sands
31	Forest, semi natural	Open spaces, little/no veget.	Bare rocks
32	Forest, semi natural	Open spaces, little/no veget.	Sparsely vegetated areas
33	Forest, semi natural	Open spaces, little/no veget.	Burnt areas
34	Forest, semi natural	Open spaces, little/no veget.	Glaciers and perpetual snow
35	Wetlands	Inland wetlands	Inland marshes
36	Wetlands	Inland wetlands	Peat bogs
37	Wetlands	Maritime wetlands	Salt marshes
38	Wetlands	Maritime wetlands	Salines
39	Wetlands	Maritime wetlands	Intertidal flats
40	Water bodies	Inland waters	Water courses
41	Water bodies	Inland waters	Water bodies
42	Water bodies	Marine waters	Coastal lagoons
43	Water bodies	Marine waters	Estuaries
44	Water bodies	Marine waters	Sea and ocean

Table C.4: Conversion factors from VOC in Mg (tones) to moles of RADM2 lumped species, computed for SNAP sectors for VOC speciation reported by Passant (2002). Lumping was performed according to Carter (2007). Molecular weights were assigned to species by the help of ChemFinder (*http://chemfinder.cambridgesoft.com/result.asp*).

RADM2 Specie / SNAP	1	2	3	4	5	6
CH_4	897.9	3824.5	1031.0	698.4	2793.5	0
ETH	1107.0	3249.1	3237.0	8475.3	7430.5	4787.4
HC3	579.8	3108.6	1979.5	1160.5	2847.6	1169.7
HC5	0	985.5	101.1	444.6	993.7	1759.4
HC8	570.3	2602.2	3136.9	1532.8	0	0
OL2	513.6	1421.1	392.1	1043.9	64.2	0
OLT	0	228.1	0	37.0	309.5	41.0
OLI	301.8	580.7	712.3	187.4	36.7	781.8
TOL	518.1	15.6	53.3	101.4	0	883.7
XYL	18450.6	1332.2	5894.9	0	0	
HCHO	0	0	0	22.7	0	0
ALD	21.8	0	34.8	47.9	0	668.3
KET	0	0	0	0	0	0
ISO	0	0	0	21.3	0	0
CSL	0	0	0	0	0	0
ORA1	0	0	0	50.0	0	0
ORA2	0	0	0	0	0	0
GLY	0	0	0	0	0	0
MGLY	0	0	0	0	0	0
MACR	0	0	0	0	0	0
MVK	1709.9	1810.5	3131.0	2456.6	2107.7	2674.1
NR	0	0	0	0	0	0

RADM2 Specie / SNAP	7	8	9	10	11
CH_4	465.6	266.0	8713.2	83142.0	535.2
ETH	2290.2	924.2	3781.4	9475.3	2274.3
HC3	2508.9	690.3	284.9	4472.1	1187.9
HC5	523.1	187.0	653.6	5576.4	1848.5
HC8	2174.4	2423.9	0	0.0	1180.2
OL2	980.3	750.9	74.3	0.0	905.5
OLT	1250.9	311.9	195.3	0.0	459.9
OLI	1608.0	759.5	272.5	0.0	796.6
TOL	956.7	623.6	113.0	0.0	339.3
XYL	732.7	832.6	5828.2	0.0	597.6
HCHO	238.7	257.2	0	0.0	442.5
ALD	13.1	26.1	0	1089.0	272.6
KET	0	0	0	0	68.0
ISO	0	0	0	0	111.8
CSL	0	0	0	0	105.6
ORA1	0	0	0	0	203.2
ORA2	0	34.5	0	0	4.0
GLY	0	0	0	0	0
MGLY	82.04	0	0	0	159.0
MACR	0	0	0	0	0
MVK	1658.9	5008.4	3604.7	613.6	3556.7
NR	0	0	0	0	4.5

Appendix D

WRF-Chem model namelist options used for reference simulations

&time_control
run_days = 5,
run_hours = 0,
run_minutes = 0,
run_seconds = 0,
start_year = 2003, 2003, 2003, 2003, 2005,
start_month = 08, 08, 08, 08, 08,
start_day = 08, 08, 08, 08, 08,
start_hour = 00, 00, 00, 00, 00,
start_minute = 00, 00, 00, 00, 00,
start_second = 00, 00, 00, 00, 00,
end_year = 2003, 2003, 2003, 2003, 2005,
end_month = 08, 08, 08, 08, 08,
end_day = 13, 13, 13, 13, 13,
end_hour = 00, 00, 00, 00, 00,
end_minute = 00, 00, 00, 00, 00,
end_second = 00, 00, 00, 00, 00,
interval_seconds = 21600,
input_from_file = .true., .true., .true., .true., .true.,
fine_input_stream = 0, 0, 0, 2, 2,
history_interval = 60, 60, 60, 60, 60,
frames_per_outfile = 24, 24, 24, 24, 24,
restart = .false.,
restart_interval = 1440,
auxinput5_interval = 60, 60, 60, 60, 60,
io_form_auxinput5 = 2
io_form_history = 2
io_form_restart = 2
io_form_input = 2
io_form_boundary = 2
io_form_auxinput4 = 2
debug_level = 0

history_outname = ”/media/meteo1/junij2005/wrfout_d<domain>_<date>”
/
&domains
time_step = 90,
time_step_fract_num = 0,
time_step_fract_den = 1,
max_dom = 3,
s_we = 1, 1, 1, 1, 1,
e_we = 125, 124, 112, 76, 88,
s_sn = 1, 1, 1, 1, 1,
e_sn = 90, 88, 88, 88, 88,
s_vert = 1, 1, 1, 1, 1,
e_vert = 51, 51, 51, 51, 51,
num_metgrid_levels = 22
eta_levels = 1, 0.995, 0.99, 0.985, 0.98, 0.975, 0.97, 0.965, 0.96, 0.955, 0.95, 0.945, 0.938, 0.931, 0.924, 0.915, 0.906, 0.897, 0.888, 0.879, 0.867, 0.855, 0.843, 0.831, 0.819, 0.803, 0.787, 0.771, 0.755, 0.739, 0.719, 0.699, 0.679, 0.654, 0.629, 0.604, 0.574, 0.544, 0.514, 0.479, 0.444, 0.409, 0.374, 0.339, 0.299, 0.259, 0.219, 0.169, 0.119, 0.069, 0
dx = 27000, 9000, 3000, 1000, 333.3333,
dy = 27000, 9000, 3000, 1000, 333.3333,
grid_id = 1, 2, 3, 4, 5,
parent_id = 0, 1, 2, 3, 4,
i_parent_start = 1, 43, 65, 41, 28,
j_parent_start = 1, 30, 34, 40, 27,
parent_grid_ratio = 1, 3, 3, 3, 3,
parent_time_step_ratio = 1, 3, 3, 3, 3,
feedback = 0,
smooth_option = 1
/
&physics
mp_physics = 5, 5, 5, 5, 5,
ra_lw_physics = 1, 1, 1, 1, 1,
ra_sw_physics = 2, 2, 2, 2, 2,
radt = 27, 9, 3, 1, 0.3,
sf_sfclay_physics = 1, 1, 1, 1, 1,
sf_surface_physics = 2, 2, 2, 2, 2,
bl_pbl_physics = 1, 1, 1, 1, 1,
bldt = 0, 0, 0, 0, 0,
cu_physics = 3, 3, 0, 0, 0,
cudt = 9, 5, 5, 5, 5,
isfflx = 1,
ifsnow = 1,
icloud = 1,
surface_input_source = 1,
num_soil_layers = 4,
num_land_cat = 24,
ucmcall = 0,
cu_rad_feedback = .true.,

```
maxiens = 1,
maxens = 3,
maxens2 = 3,
maxens3 = 16,
ensdim = 144,
/
&fdda
/
&dynamics
dyn_opt = 2,
rk_ord = 3,
w_damping = 0,
diff_opt = 1,
km_opt = 4,
mix_full_fields = .true.,
damp_opt = 1,
zdamp = 5000., 5000., 5000., 5000., 5000.,
dampcoef = 0.01, 0.01, 0.01, 0.01, 0.01,
khdif = 0, 0, 0, 0, 0,
kvdif = 0, 0, 0, 0, 0,
smdiv = 0.1, 0.1, 0.1, 0.1, 0.1
emdiv = 0.01, 0.01, 0.01, 0.01, 0.01,
epssm = 0.1, 0.1, 0.1, 0.1, 0.1,
non_hydrostatic = .true., .true., .true., .true., .true.,
time_step_sound = 4, 4, 4, 4, 4,
h_mom_adv_order = 5, 5, 5, 5, 5,
v_mom_adv_order = 3, 3, 3, 3, 3,
h_sca_adv_order = 5, 5, 5, 5, 5,
v_sca_adv_order = 3, 3, 3, 3, 3,
pd_moist = .true., .true., .true., .true., .true.,
pd_scalar = .true., .true., .true., .true., .true.,
pd_chem = .true., .true., .true., .true., .true.,
/
&bdy_control
spec_bdy_width = 5,
spec_zone = 1,
relax_zone = 4,
specified = .true., .false., .false., .false., .false.,
periodic_x = .false., .false., .false., .false., .false.,
symmetric_xs = .false., .false., .false., .false., .false.,
symmetric_xe = .false., .false., .false., .false., .false.,
open_xs = .false., .false., .false., .false., .false.,
open_xe = .false., .false., .false., .false., .false.,
periodic_y = .false., .false., .false., .false., .false.,
symmetric_ys = .false., .false., .false., .false., .false.,
symmetric_ye = .false., .false., .false., .false., .false.,
open_ys = .false., .false., .false., .false., .false.,
open_ye = .false., .false., .false., .false., .false.,
```

```
nested = .false., .true., .true., .true., .true.,
/
&grib2
/
&namelist_quilt
nio_tasks_per_group = 0,
nio_groups = 1,
/
&chem
kemit = 11,
chem_opt = 1, 1, 1, 1, 1,
bioemdt = 60, 60, 60, 60, 60,
photdt = 30, 30, 30, 30, 30,
chemdt = 1.5, 0.5, 0.17, 0.17, 0.17,
frames_per_emissfile = 24,
io_style_emissions = 2,
chem_in_opt = 1, 0, 0, 0, 0,
phot_opt = 1, 1, 1, 1, 1,
drydep_opt = 1, 1, 1, 1, 1,
bio_emiss_opt = 1, 1, 1, 1, 1,
gas_bc_opt = 1, 1, 1, 1, 1,
gas_ic_opt = 1, 1, 1, 1, 1,
aer_bc_opt = 1, 1, 1, 1, 1,
aer_ic_opt = 1, 1, 1, 1, 1,
have_bcs_chem = .false., .false., .false., .false., .false.,
gaschem_onoff = 1, 1, 1, 1, 1,
aerchem_onoff = 0, 0, 0, 0, 0,
wetscav_onoff = 1, 1, 1, 1, 1,
cldchem_onoff = 0, 0, 0, 0, 0,
vertmix_onoff = 1, 1, 1, 1, 1,
chem_conv_tr = 1, 1, 1, 1, 1,
/
```

Appendix E

Days in years 2003 - 2005 with maximum daily measured ozone above 165 μg/m^3 at least at one station

Table E.1: Maximum hourly measured ozone and local time of measured daily maximum values for days with ozone above 165 μg/m^3 at least at one of four stations (Nova Gorica, Ljubljana, Iskrba, Krvavec). Colored episodes are analyzed in thesis.

day	month	year	NG	NG$_{hour}$	LJ	LJ$_{hour}$	IS	IS$_{hour}$	KR	KR$_{hour}$
7	5	2003	175	15	156	19	143	15	168	19
31	5	2003	173	17	132	12	124	15	134	15
4	6	2003	**182**	17	134	14	119	13	140	19
9	6	2003	**206**	14	163	14	147	14	170	19
10	6	2003	**187**	15	146	16	140	15	163	18
11	6	2003	**243**	15	**187**	12	143	15	168	15
12	6	2003	**182**	15	153	14	143	17	172	14
13	6	2003	**195**	14	161	14	145	11	171	14
20	6	2003	166	15	143	12	148	18	136	13
21	6	2003	172	18	93	17	90	17	86	19
23	6	2003	171	14	163	14	137	12	155	14
25	6	2003	**208**	15	158	14	160	15	127	14
26	6	2003	178	17	133	14	130	15	142	16
27	6	2003	170	15	133	14	132	17	139	19
8	7	2003	**181**	18	144	17	115	17	115	16
10	7	2003	165	18	143	15	131	16	125	14
16	7	2003	166	16	161	15	152	12	169	16
21	7	2003	**196**	14	**190**	16	175	17	**183**	19
22	7	2003	**188**	17	174	19	178	15	166	19
26	7	2003	**191**	19	151	19	130	19	137	19
27	7	2003	**196**	17	177	19	170	18	153	19
28	7	2003	**182**	14	161	12	**188**	16	156	14

Table E.1: Continued.

day	month	year	NG	NG_{hour}	LJ	LJ_{hour}	IS	IS_{hour}	KR	KR_{hour}
4	8	2003	173	16	166	14	145	18	158	16
5	8	2003	**204**	13	160	13	156	18	172	19
6	8	2003	**182**	12	168	13	151	12	162	16
8	8	2003	**184**	17	172	15	157	19	179	19
9	8	2003	**198**	15	173	17	178	11	162	10
10	8	2003	**202**	13	175	15	178	17	169	19
11	8	2003	**202**	14	157	15	167	19	163	16
12	8	2003	**184**	13	**189**	15	172	18	173	18
13	8	2003	**203**	15	**186**	17	**210**	16	174	19
14	8	2003	179	14	**196**	14	**210**	16	171	13
15	8	2003	173	15	146	16	148	14	156	17
17	8	2003	179	15	167	15	169	17	153	18
18	8	2003	166	12	163	13	152	16	152	15
22	8	2003	173	15	155	16	154	18	155	19
23	8	2003	**187**	18	166	15	162	14	169	19
24	8	2003	177	18	160	15	162	15	159	19
28	8	2003	168	19	**189**	15	172	14	172	16
19	9	2003	**206**	16	126	17	118	13	114	15
20	9	2003	**219**	14	163	16	126	18	164	19
21	9	2003	**211**	16	135	16	116	15	134	19
10	6	2004	**210**	14	**198**	19	**184**	19	**184**	19
11	6	2004	**194**	16	-1	-2	165	11	172	12
28	6	2004	170	13	158	15	147	15	126	16
6	7	2004	**188**	15	173	14	164	16	154	10
17	7	2004	173	14	170	17	150	13	173	18
19	7	2004	173	17	144	17	146	17	136	18
20	7	2004	**195**	17	168	19	144	16	152	19
21	7	2004	**199**	15	173	15	154	13	152	13
22	7	2004	**209**	17	172	14	145	12	139	10
23	7	2004	177	14	162	13	121	13	143	14
1	8	2004	177	12	151	14	134	18	129	13
2	8	2004	173	15	120	14	110	12	112	17
3	8	2004	174	14	115	13	99	12	109	16
19	6	2005	166	19	116	18	119	19	126	16
20	6	2005	172	18	115	13	117	18	129	16
21	6	2005	174	16	140	18	126	19	147	19
22	6	2005	**190**	16	145	12	129	12	160	15
23	6	2005	**197**	15	143	15	127	13	136	16
24	6	2005	**200**	17	134	17	136	14	132	16
25	6	2005	**186**	13	**205**	15	169	13	179	18
28	6	2005	**181**	14	116	14	99	13	120	14
29	6	2005	172	15	143	13	149	14	154	18
15	7	2005	167	13	173	17	130	14	174	16
16	7	2005	175	12	**185**	17	166	18	167	17
17	7	2005	**200**	16	161	16	158	11	143	11
18	7	2005	168	14	158	11	149	19	152	16
27	7	2005	**191**	18	153	16	124	12	151	18
28	7	2005	**199**	18	**184**	18	170	16	154	19
29	7	2005	**199**	17	172	16	119	13	165	19
30	7	2005	166	15	151	13	103	18	154	17

Appendix F

Time series of near ground variables for experiments with different model PBL schemes and LSMs for Episode I

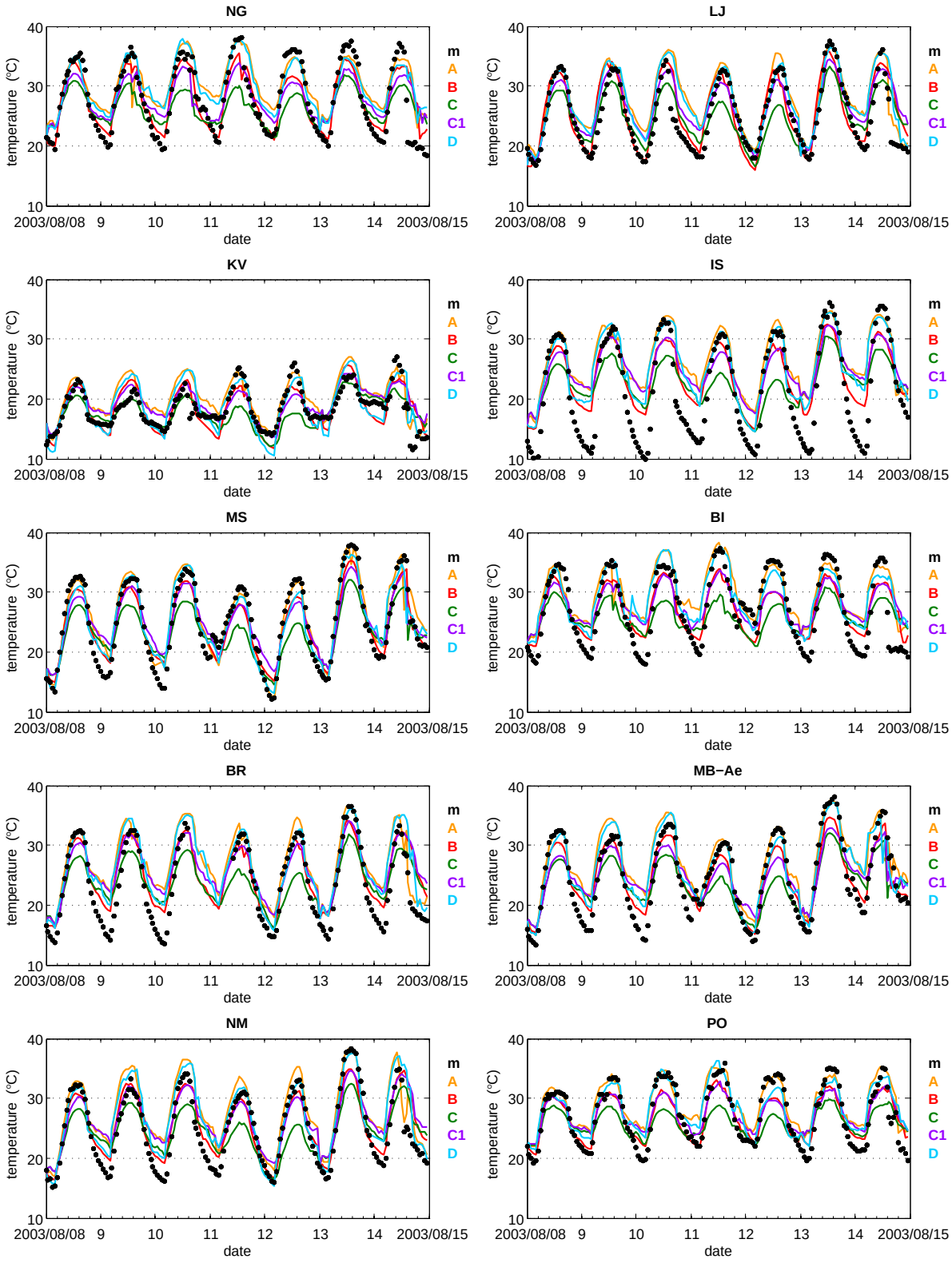

Figure F.1: Measured (black dots) and simulated near ground temperature for stations NG (Nova Gorica), LJ (Ljubljana), KV (Krvavec), IS (Iskrba), MS (Murska Sobota), BI (Bilje), BR (Brnik), MB-Ae (Maribor letališče), NM (Novo Mesto) and PO (Postojna). Experiments (A, B, C, C1, D) are described in Table 5.1.

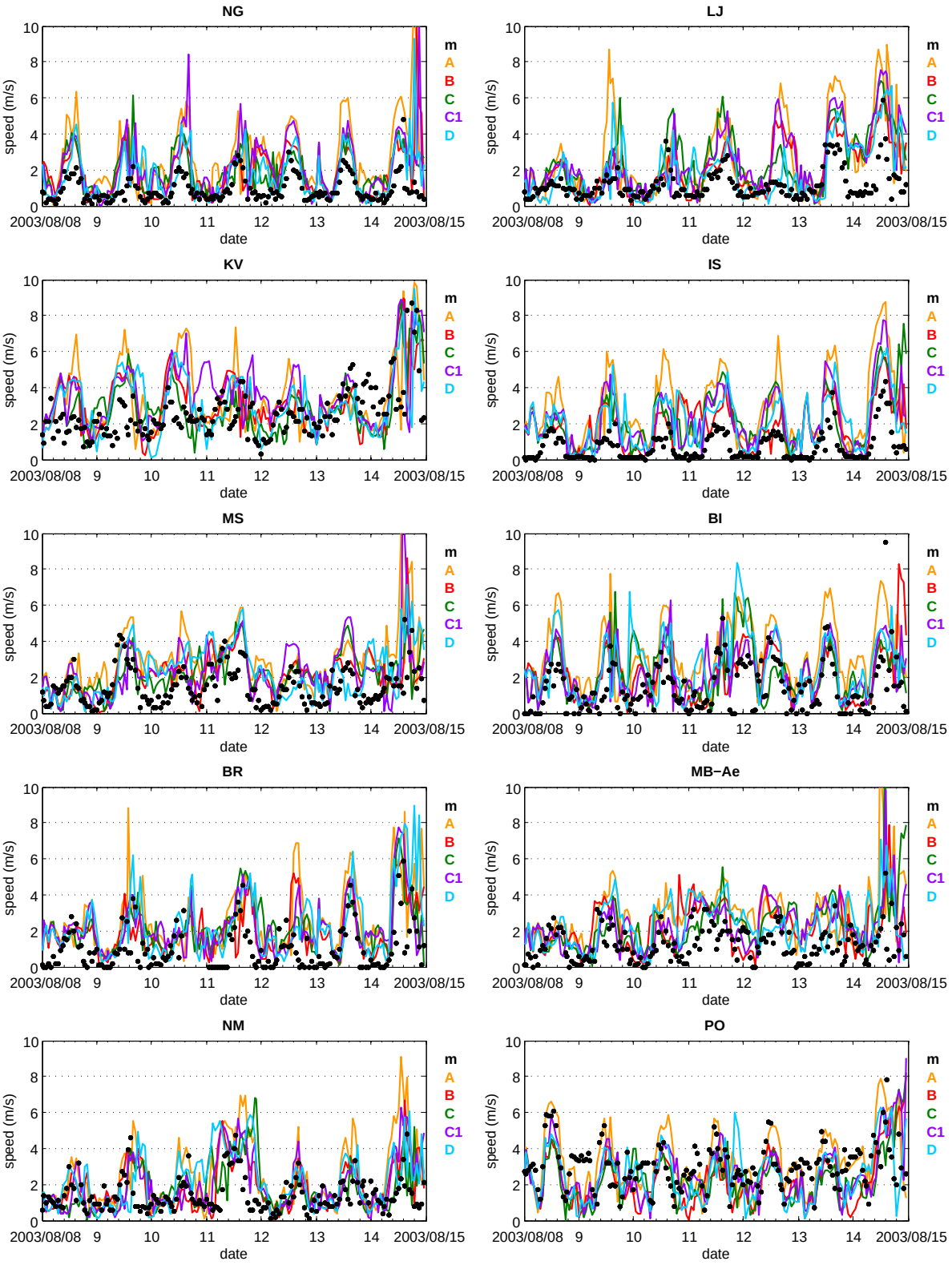

Figure F.2: The same as Fig. F.1, but for wind speed.

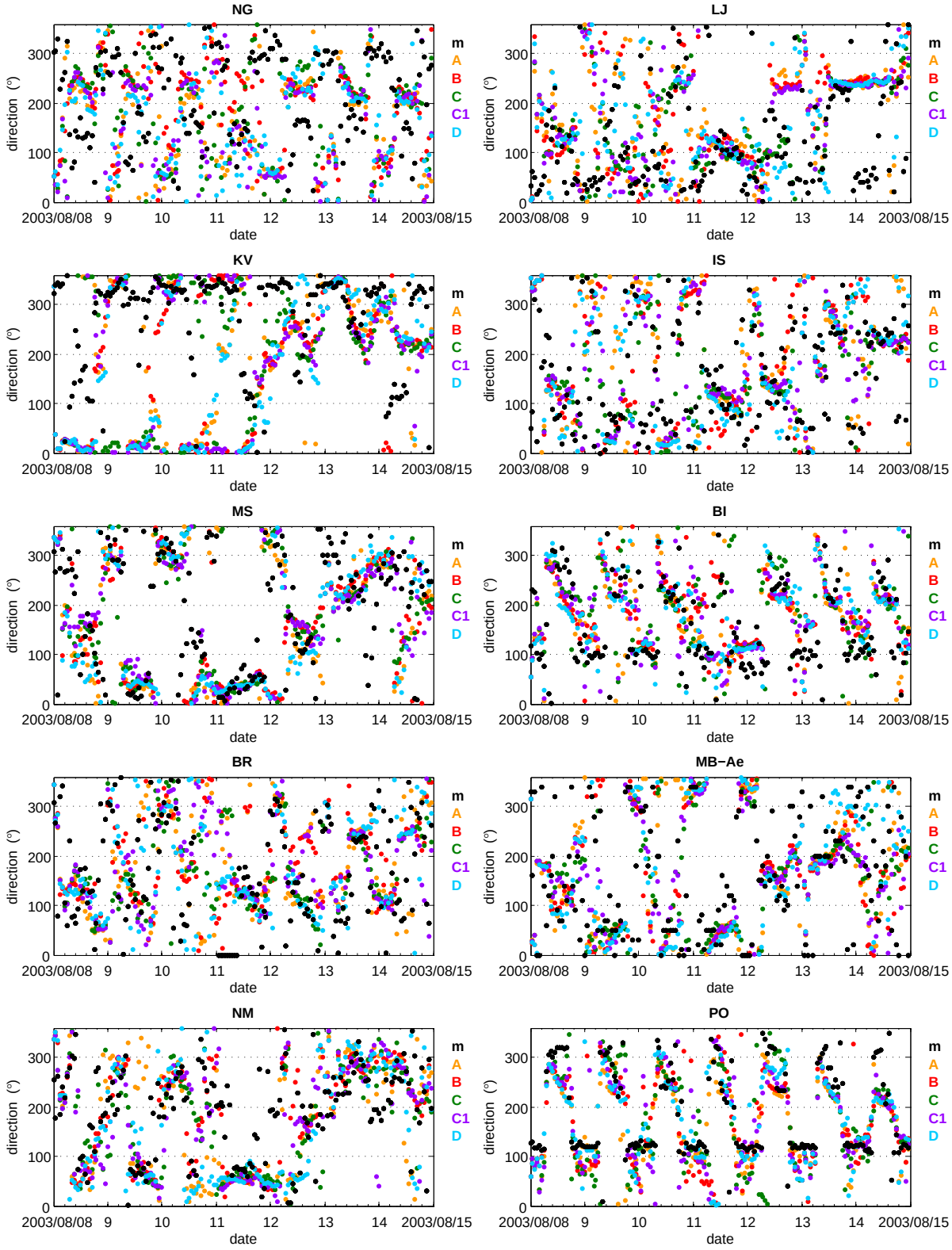

Figure F.3: The same as Fig. F.1, but for wind direction.

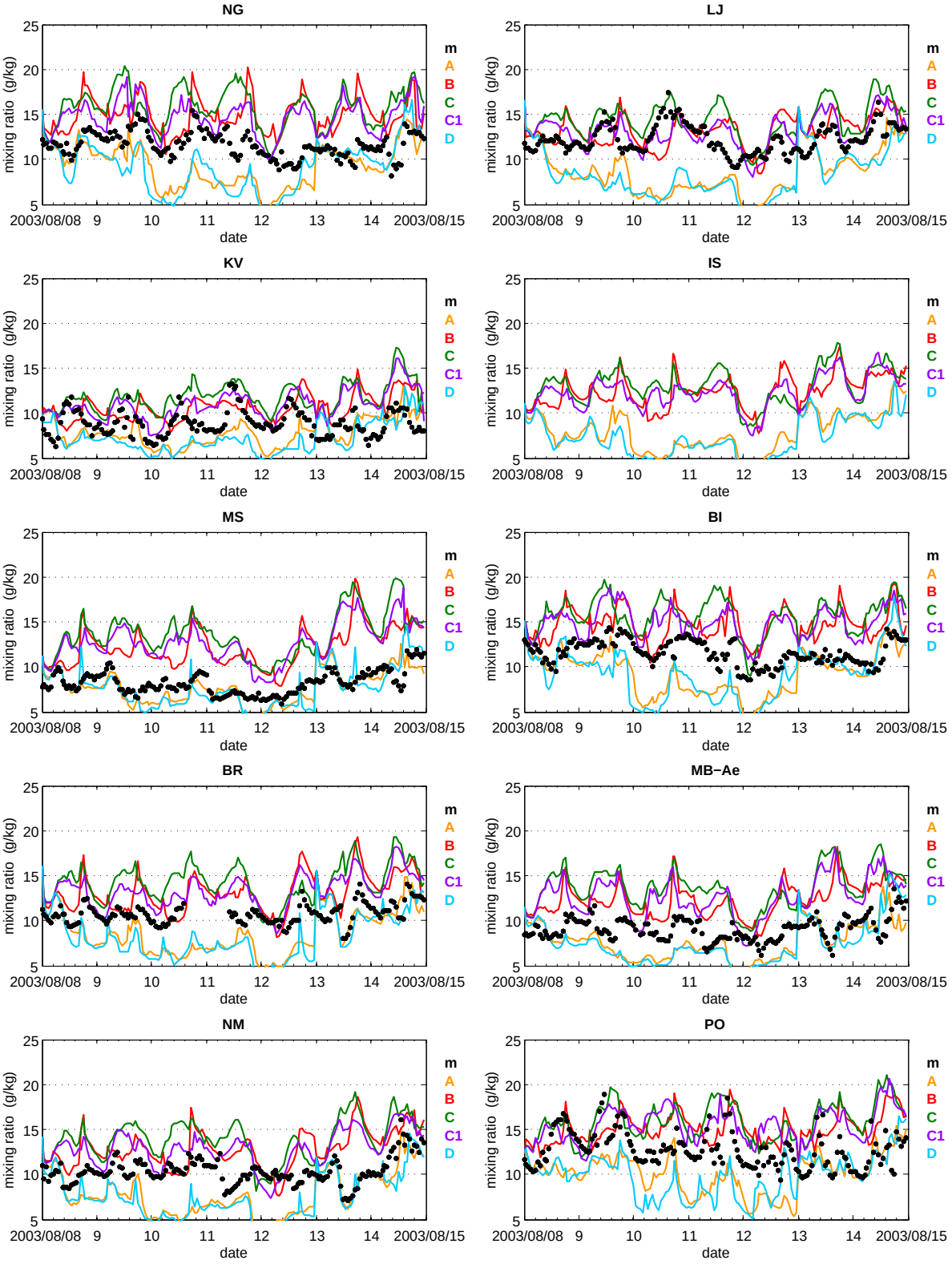

Figure F.4: The same as Fig. F.1, but for water vapor mixing ratio.

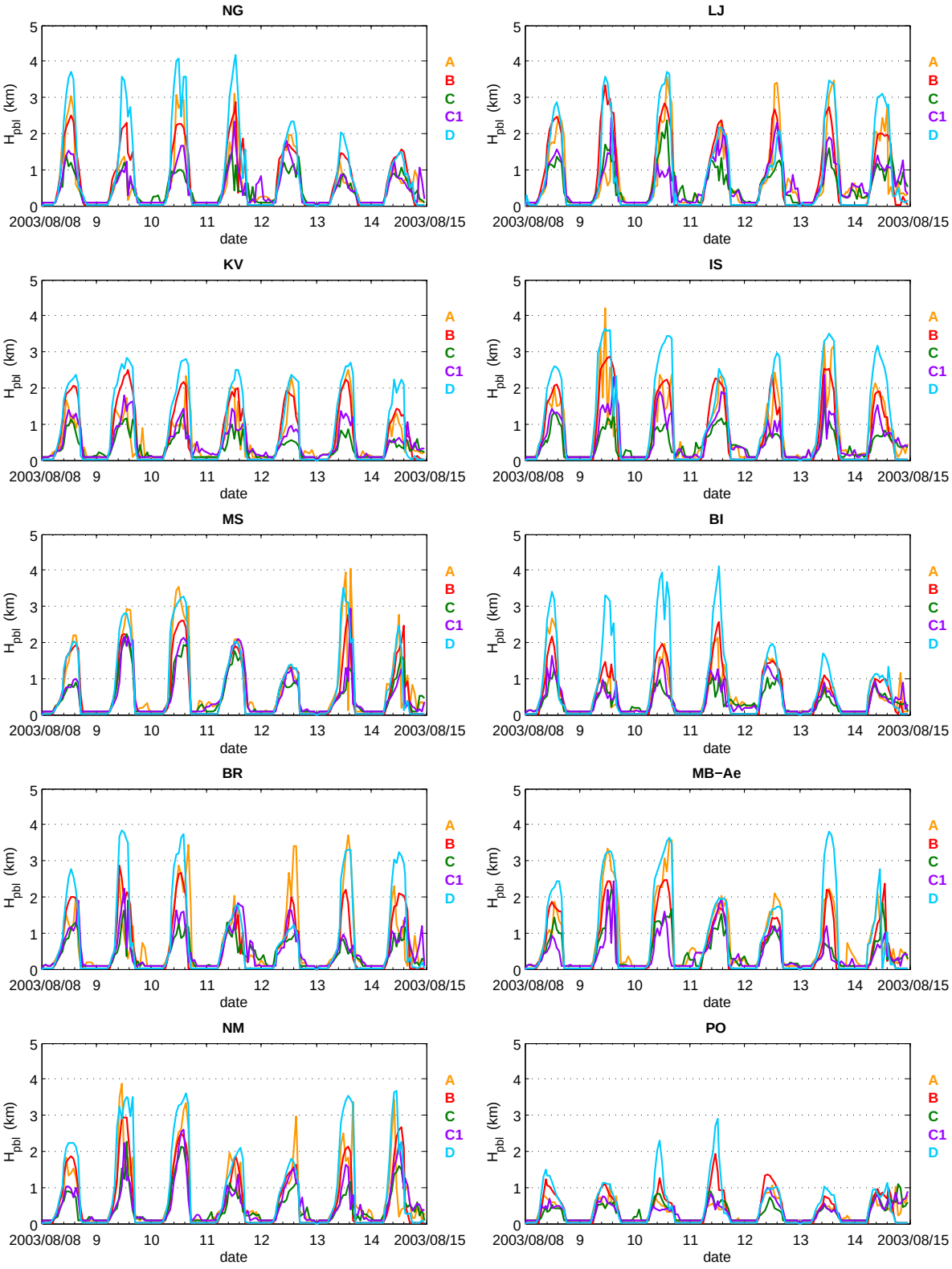

Figure F.5: The same as Fig. F.1, except that we do not have measured values, but for PBL height.

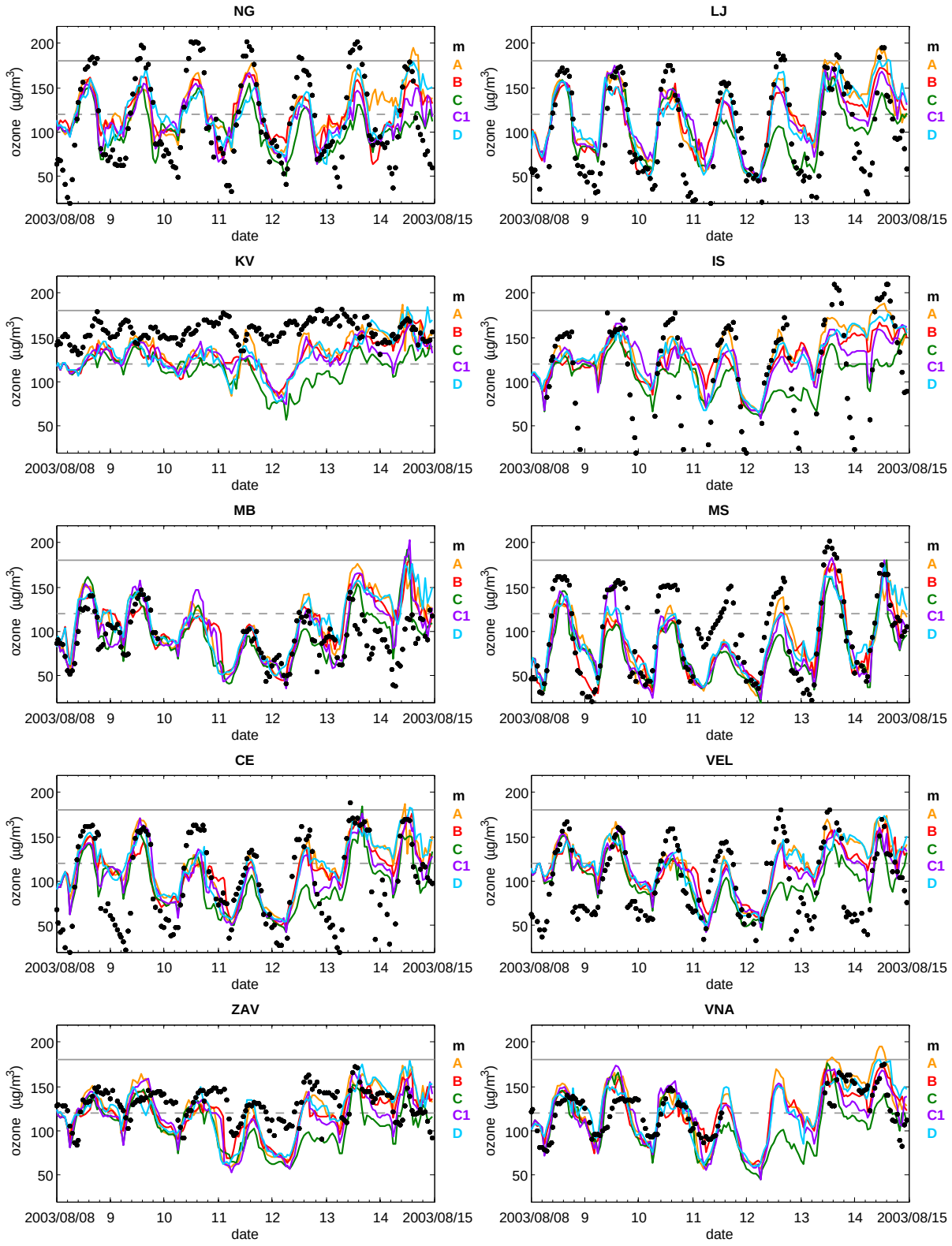

Figure F.6: Measured (black dots) and simulated hourly near ground ozone values for stations NG (Nova Gorica), LJ (Ljubljana), KV (Krvavec), IS (Iskrba), MB (Maribor), MS (Murska Sobota), CE (Celje), VEL (Velenje), ZAV (Zavodnje) in VNA (Vnajnarje). Experiments (A, B, C, C1, D) are described in Table 5.1.

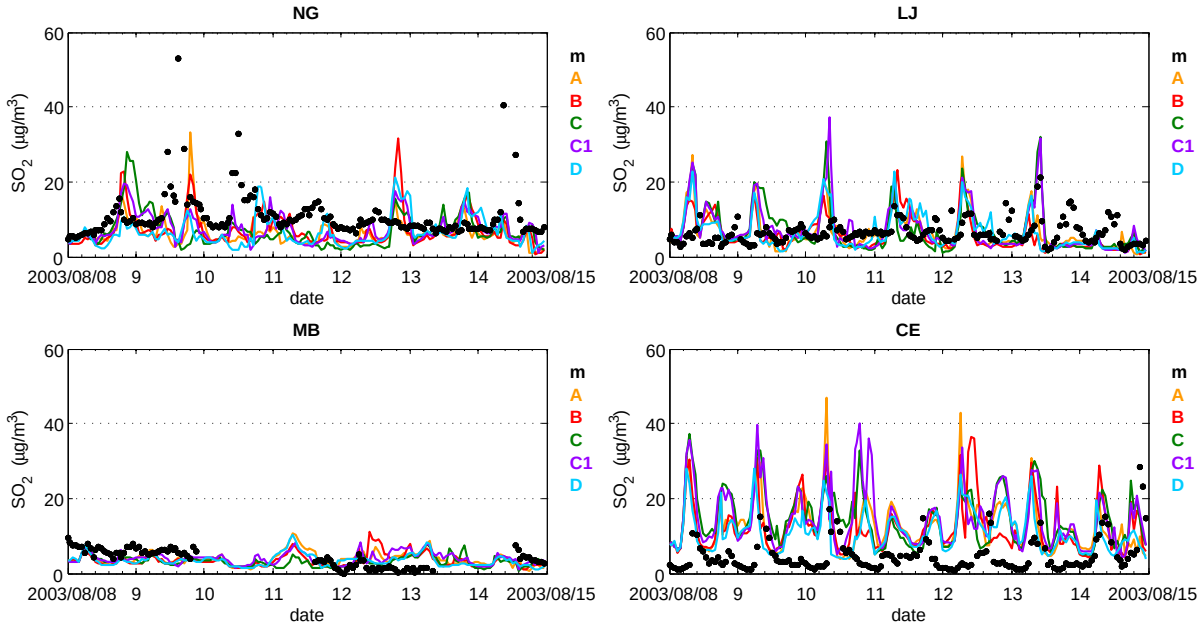

Figure F.7: The same as Fig. F.6, but for SO_2 hourly values.

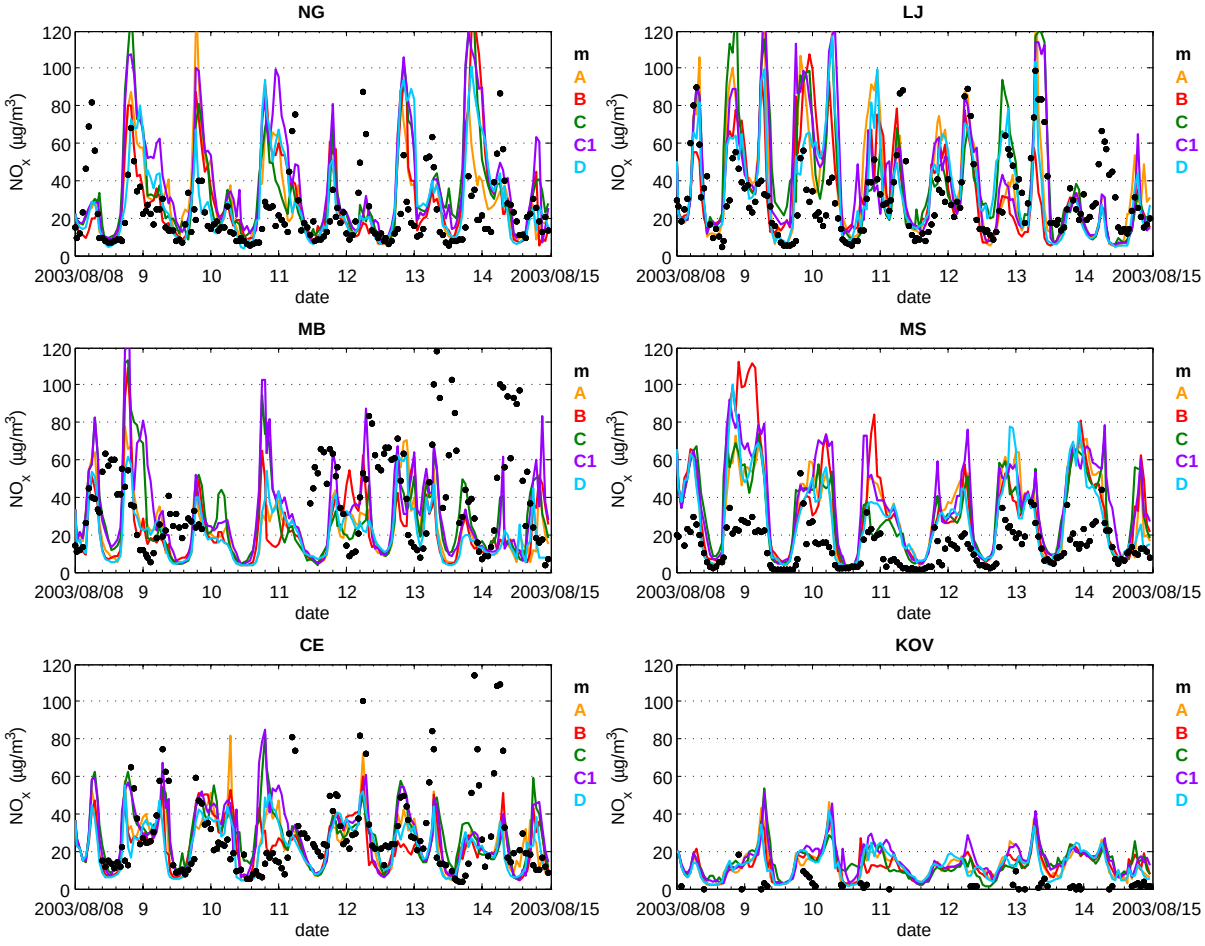

Figure F.8: The same as Fig. F.6, but for NO_x hourly values.

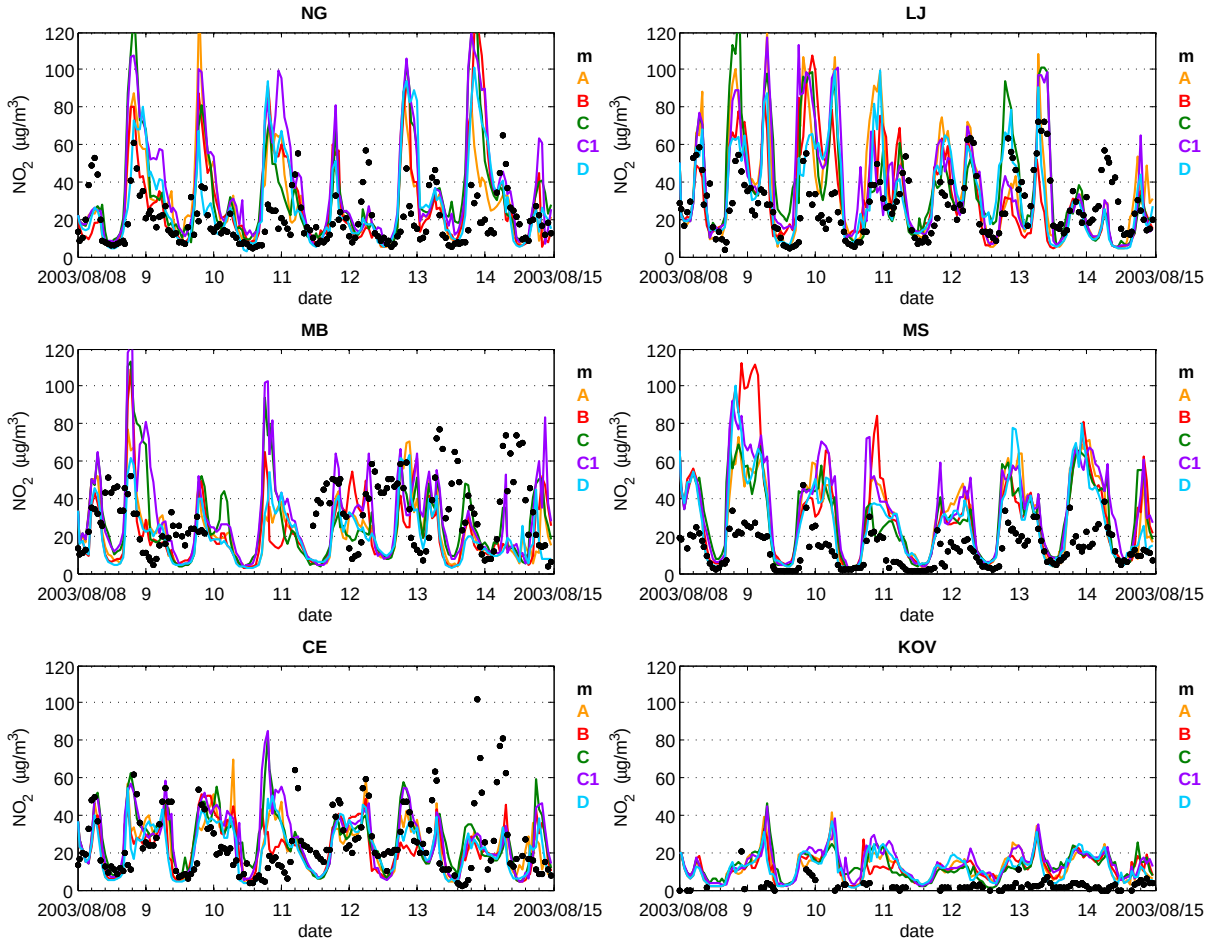

Figure F.9: The same as Fig. F.6, but for NO_2 hourly values.

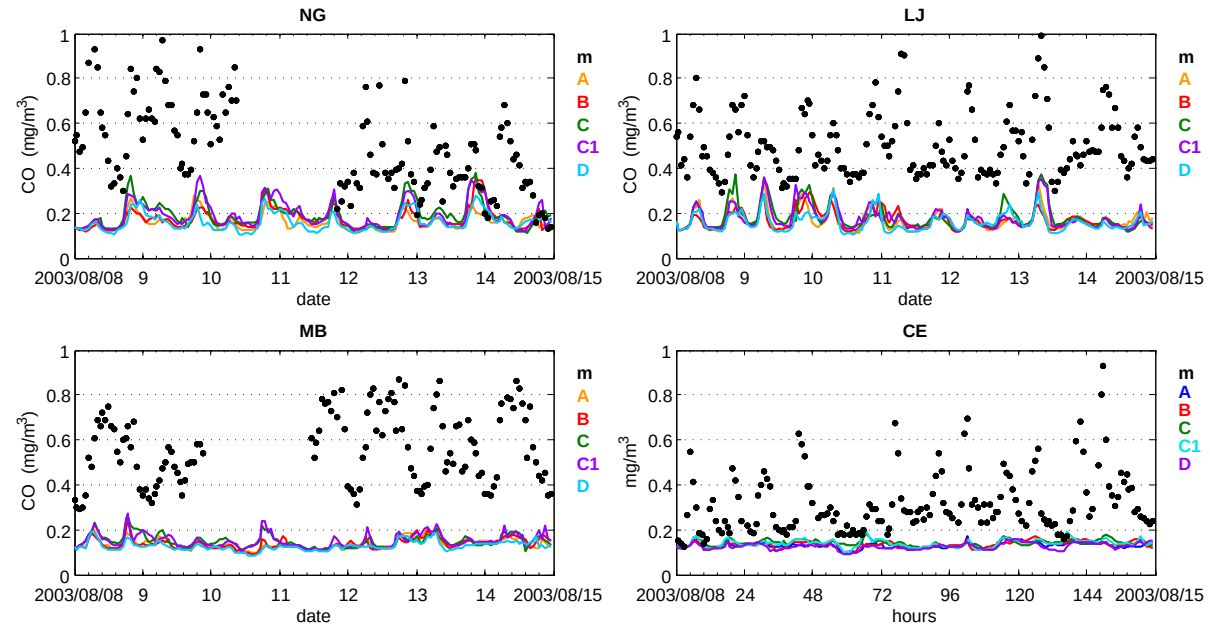

Figure F.10: The same as Fig. F.6, but for CO hourly values.

Appendix G

Results of sensitivity tests for Episode II

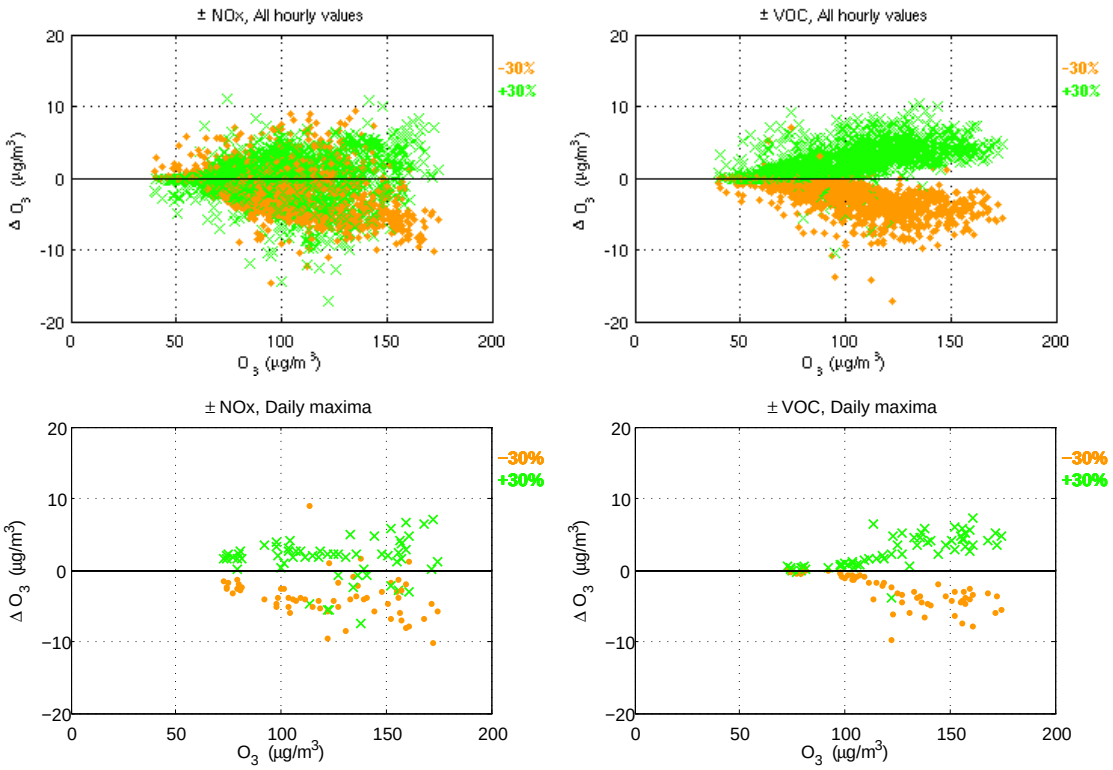

Figure G.1: Influence of ±30% NO_x or VOC bulk emission changes on simulated ozone. Shown are differences in ozone according to reference run for model points representing measuring sites over Slovenia for episode in June 2004. Left: run with ±30% NO_x emissions, Right: ±30% VOC. Upper and middle panels: all hourly ozone values during the 6-day simulation, Lower panels: daily maxima only. Ozone values on x axis correspond to the reference simulation.

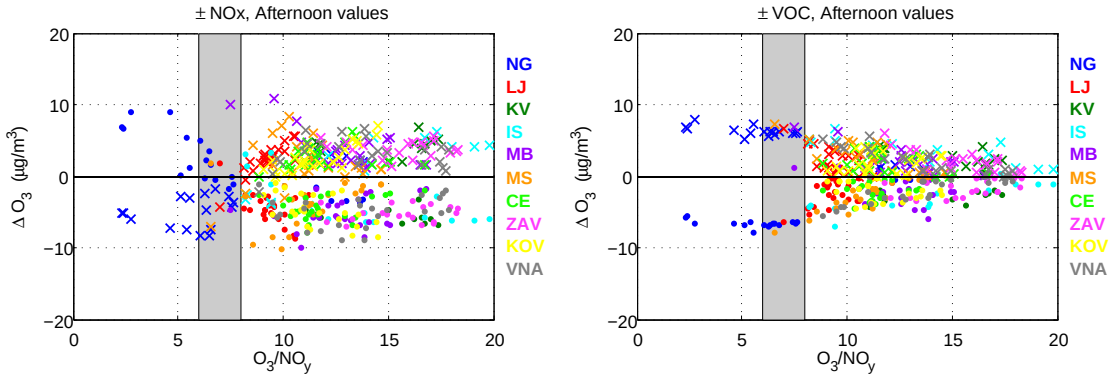

Figure G.2: Afternoon ozone changes (for hours 12 - 16 UTC during the 6-day simulation) for four emission scenarios (+30%:crosses, −30%: dots) as function of O_3/NO_y ratio. Left: ±30% NO_x, Right: ±30% VOC. Grey patch denotes the transition area between VOC and NO_x sensitive conditions, according to Sillman (1995).

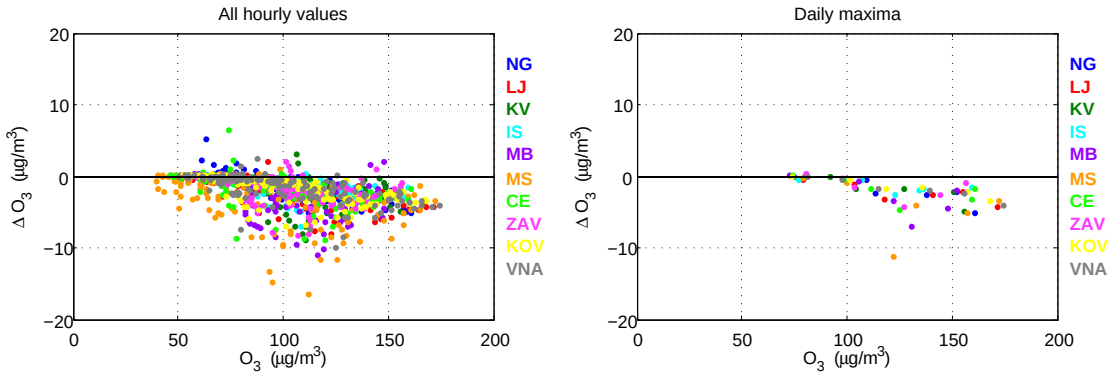

Figure G.3: Deviations in ozone values, simulated with two different VOC speciations for episode in June 2004. Left: all hourly ozone values, the points correspond to Slovenian ozone measuring sites, Right: daily maxima only. VOC1: VOC speciated as explained in Section 4.3, VOC2: VOC speciated according to Passant (2002). Differences are calculated as VOC2 minus VOC1 simulation. Ozone values on x axis are from VOC1 simulation.

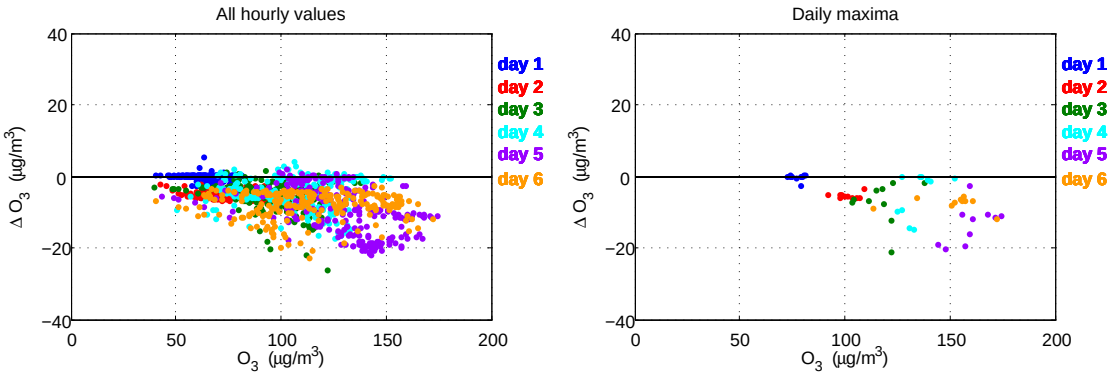

Figure G.4: Deviations in near ground ozone values as consequence of different chemical boundary conditions at domain D2 for episode in June 2004. The reference run is compared to the run with emissions outside domain D2 set to zero. Left: all hourly ozone values for model points that represent Slovenian measuring sites, Right: daily maxima only. Differences are calculated as modified run (no emissions outside) minus reference simulation. Ozone values on x axis are from the reference simulation.

Daljši slovenski povzetek

Troposferski ozon je sekundarni polutant. Tvori se v kompleksnih (foto)kemijskih reakcij iz primarnih polutantov, predvsem dušikovih oksidov, NO_x, ter hlapnih organskih spojin, VOC (volatile organic compounds), ob prisotnosti sončne svetlobe.

V disertaciji raziskujem značilnosti prostorske in časovne dinamike epizod z visokimi izmerjenimi prizemnimi koncentracijami ozona v Sloveniji. Čeprav se poslužujem tudi statističnih pristopov, pa je kot glavno orodje uporabljen sklopljen meteorološko-fotokemijskim model WRF-Chem, s katerim v visoki prostorski ločljivosti za izbrane epizode simuliram hkrati meteorološko dogajanje in širjenje polutantov ter (foto)kemijske reakcije med njimi.

Žal se pri modeliranju troposferskega ozona ne moremo izogniti napakam v rezultatih simulacij, ki izvirajo iz različnih virov negotovosti. Med najbolj prepoznavne vire negotovosti spadajo emisije različnih biogenih in antropogenih primarnih polutantov, začetna kemijska sestava atmosfere, koncentracije polutantov na robovih računskih domen ter meteorološki opis planetarne mejne plasti zraka tekom simulacije. V okviru svojega dela tako precej prostora namenim verifikaciji modelskih izračunov, pri kateri uporabljam meritve prizemnih spremenljivk (tako meteoroloških kot ekoloških), od vertikalnim meritev pa meteorološke sondaže.

Verifikacijo modelskih rezultatov nadgradim z analizo vplivov, ki jih imajo variacije v različnih virih negotovosti na simulairane vrednosti ozona. Na ta način skušam razumeti zakaj prihaja do odstopanj med meritvami in simularini vrednostmi ozona ter kolikšna je v resnici napovedna moč modela. S primerjavo učinka, ki ga imajo spremembe v antropogenih emisijah, začetnih in stranskih robnih kemijskih pogojih, opisu nekaterih fizikalnih procesov v planetarni mejni plasti zraka itd. na simulirane vrednosti ozona, skušam oceniti stopnjo problematičnosti različnih virov negotovosti.

V okviru tega poglavja se najprej podobno kot v sami disertaciji dotaknem rezultatov analize trajektorij (Žabkar et al., 2008), s katerimi študiram povezavo med izmerjenimi prizemnimi koncentracijami ozona ter izvorom zračnih mas. Nadaljujem z zgoščenim povzetkom konfiguracije modela WRF-Chem ter zelo kratko predstavitvijo antropogenih emisij, ki sem jih pripravila za potrebe simuliracij. Sledi predstavitev najpomembnejših rezultatov ter nekaj sklepnih misli za zaključek.

Analiza trajektorij: Povezava med koncentracijami prizemnega ozona v Sloveniji in izvorom zračnih mas

Do visokih koncentracij ozona v zraku prihaja, kadar je v zračnih masah akumuliranega dovolj skupnega onesnaženja (v ugodnem razmerju NO_x in VOC) ter so obenem vremenski pogoji ugodni za potek fotokemijskih reakcij. Poleg tega je za tvorbo ozona iz "svežih" emisij vedno potreben čas; tako se najvišje koncentracije ozona tipično pojavljajo v smeri vetra nekoliko stran od mestnih središč (oziroma večjih emisijskih virov).

Za akumulacijo zadostnih količin polutantov v zraku je običajno potrebnih vsaj nekaj dni ugodnih vremenskih razmer. Slovenija je majhna država, zaradi česar se pojavlja vprašanje, v kolikšni meri so visoke koncentracije ozona pri nas posledica lastnih emisij, oziroma kakšno vlogo pri visoki stopnji onesnaženosti igra prekomejni transport polutantov. Samo analiza trajektorij sicer za odgovor na to vprašanje ni dovolj, saj poleg transporta ne omogoča obravnave vpliva drugih procesov (kemijskih pretvorb, suhe depozicije, spiranja s padavinami, turbulentne difuzije). Nam pa trajektorije lahko pokažejo morebitno povezavo med visokimi koncentracijami ozona v Sloveniji in območji izven Slovenije, preko katerih potujejo zračne mase predno dosežejo naše kraje. To je bil tudi glavni namen te analize.

V okviru nekaterih prejšnjih raziskav je bila kot pomemben izvor predhodnikov ozona za območje Alp prepoznana Padska nižina (Seibert et al., 1997; Wotawa et al., 2000; Kaiser et al., 2007). Ker se najvišje koncentracije ozona na območju Slovenije običajno pojavljajo na Primorskem, in to ponavadi ob zahodnih smereh vetra, je bila postavljena hipoteza, da imajo onesnažene zračne mase iz Padske nižine pomemben vpliv tudi na kvaliteto zraka v Sloveniji. V okviru analize trajektorij je bil naš cilj preveriti to hipotezo, oziroma poiskati morebitna druga emisijska območja, ki pomembno vplivajo na koncentracije ozona v Sloveniji.

Metodologija

Vpliv regionalnega transporta polutantov na koncentracije ozona smo študirali za 4 merilna mesta: Ljubljano, Novo Gorico, Krvavec in Iskrbo. V letih 2003 do 2005 je bilo največ urnih preseganj ozona izmerjenih v Novi Gorici (skupno 162 ur s povprečno koncentracijo ozona nad opozorilno vrednostjo 180 μg/m^3). Sledi ji Ljubljana (merilno mesto za Bežigradom) s 33 urami, Krvavec s 23 in Iskrba s 16 urami z izmerjeno koncentracijo nad 180 μg/m^3. Do neke mere so visoke koncentracije ozona na mediteranskem delu Slovenije gotovo povezane z ugodnejšimi vremenskimi razmerami (vroča poletja, malo padavin, veliko sončnega sevanja), na vprašanje o izvoru primarnih polutantov pa iščemo odgovor s pomočjo trajektorij.

Za izračun trodimenzionalnih (3D) trajektorij smo uporabili meteorološka polja, izračunana z modelom ALADIN (Team, 2003) s horizontalno ločljivostjo 9.5 km in 37 vertikalnimi nivoji na območju 2° do 28° zahodne geografske dolžine in 36° do 54° severne geografske širine. Trajektorije so bile izračunane z modelom FLEXTRA (Stohl et al., 1995; Stohl and Seibert, 1998) za toplo polovico let (April-September) 2003 in 2004. Končne točke trajektorij so bile postavljene 50 m nad modelsko topografijo, njihovi časi prihoda na merilno mesto pa so bili vsake 3 ure (00, 03, ..., 21 UTC). Dolžina trajektorij je bila 96 ur, oziroma v primerih, ko je trajektorija prej "pobegnila" iz domene, ustrezno krajša.

V prvem delu postopka analize smo z metodo voditeljev (k-means; Moody and Galloway, 1988) trajektorije ločeno po merilnih postajah razvrstili v skupine podobnih trajektorij. V tem postopku smo uporabili le zadnjih 24 ur trajektorij, saj smo s tem lahko obdržali celoten nabor trajektorij - daljše trajektorije so občasno že "pobegnile" iz računske domene, metoda pa zahteva trajektorije enake dolžine. Veliko truda smo namenili iskanju *naravnih skupin* trajektorij, torej skupin, za katere v največji možni meri veljata lastnosti *interne kohezivnosti* in *externe korelacije*. V naslednjem koraku smo za vsako od dobljenih skupin trajektorij (tipičnih poti zraka na merilno mesto), statistično analizirali ter primerjali med skupinami izmerjene koncentracije ozona, značilnosti njihovih dnevnih hodov ter povezavo z izmerjenimi osnovnimi meteorološkimi spremenljivkami. Tem rezultatom smo dodali še polja s koncentracijo utežene gostote trajektorij (concentration weighted trajectory, CWT; Seibert et al., 1994) ter polja običajne številske gostote onesnaženih trajektorij.

Rezultati analize trajektorij

Posledica lege Slovenije v zavetrju Alp sta med drugim dve glavni smeri trajektorij, ki kažejo, od kod zračne mase v nižjih plasteh ozračja (v PBL) pritekajo v Slovenijo: iz severovzhoda (SV) in jugozahoda (JZ) (Slika H.1). V postopku razvrščanja v več kot dve skupini se skupini trajektorij s težiščnico iz ene od teh dveh smeri razcepita na daljše in krajše trajektorije, ki spet v povprečju dosežejo merilna mesta iz SV ali JZ. V našem primeru, ko je bilo število skupin 6 ali 7, pa se skupine dolgih trajektorij dalje razdelijo na skupine s težiščnimi trajektorijami, ki na večji oddaljenosti od merilnih mest (24 ur pred prihodom) izvirajo iz v povprečju precej različnih smeri. Nekoliko dugačna slika težiščnih trajektorij za Krvavec je posledica višje nadmorske višine tega merilnega mesta in posledično zmanjšanega vpliva Alpske pregrade na potovanje zračnih mas (Slika H.1).

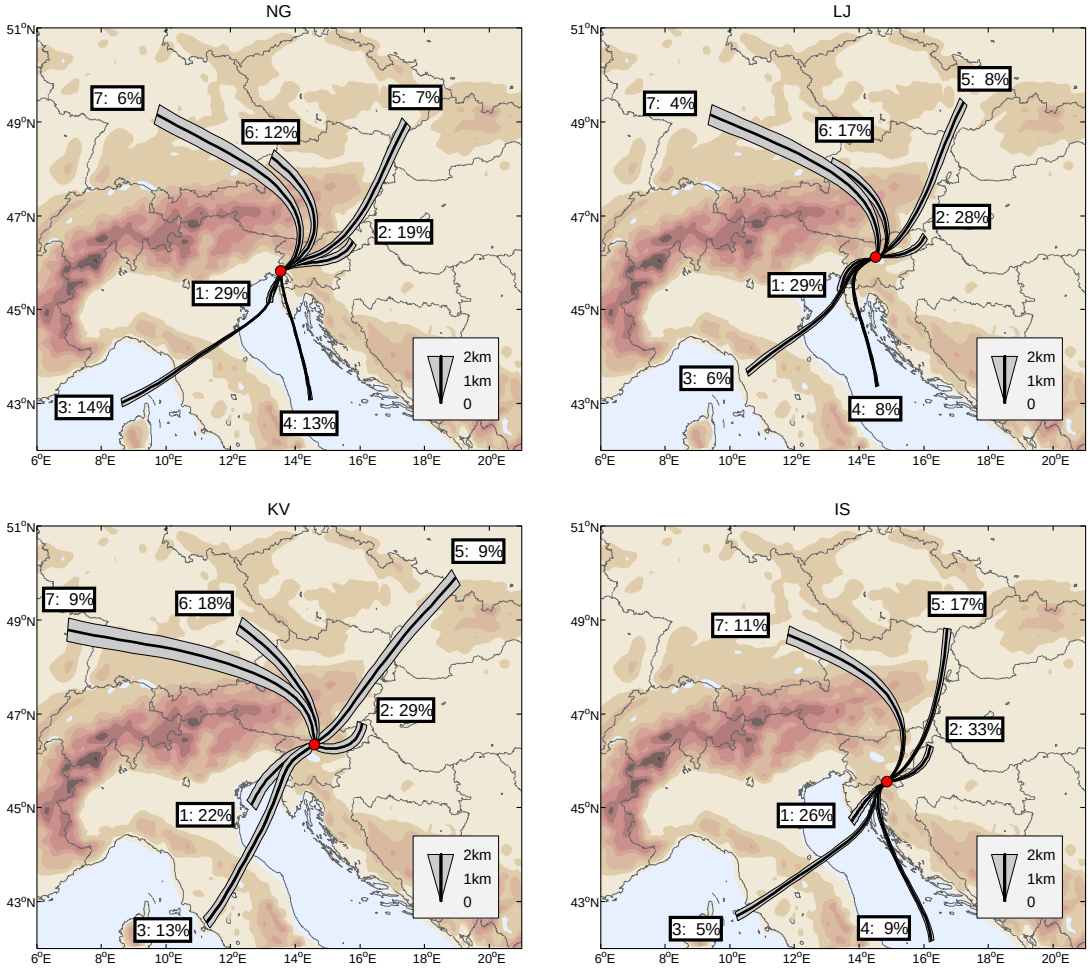

Slika H.1: Rezultati razvrščanja trajektorij v skupine. Prikazane so težiščne trajektorije skupin (tipične poti zraka) za Novo Gorico (NG), Ljubljano (LJ), Krvavec (KV) in Iskrbo (IS). Posamezne skupine so označene z zaporedno številko (izmerjene koncentracije ozona po skupinah padajo večinoma monotono od skupine 1 proti 7), na slikah pa je podan tudi delež trajektorij v vsaki od skupin. Širina težiščnih trajektorij je sorazmerna s povprečno višino težiščne trajektorije nad modelsko topografijo.

S statistično analizo izmerjenih prizemnih vrednosti meteoroloških parametrov in gostot ozona za posamezne skupine smo prišli do nekaterih zanimivih rezultatov. Za vsa 4 merilna mesta so dnevni maksimumi ozona statistično značilno najvišji v 1. skupini kratkih trajektorij, ki izvirajo v povprečju iz JZ smeri (t-test, stopnja tveganja manjša od 0.05). Po vrsti za merilna mesta NG, LJ, KV in IS, so povprečni enourni dnevni maksimumi ozona v 1. skupini 140, 127, 137 in 129 μg/m^3. Kratka dolžina trajektorij 1. skupine je posledica šibkega vetra. Zrak v teh skupinah torej v zadnjih 24-urah ni bil izpostavljen močni advekciji. Če temu dodamo še v povprečju visoke izmerjene temperature zraka v 1. skupini, lahko visoke koncentracije ozona v tej skupini razložimo z "ugodnimi" vremenskimi pogoji: visoke temperature omogočajo učinkovit potek fotokemijskih reakcij, šibki vetrovi pomenijo slabše mešanje zraka in neučinkovito redčenje koncentracij polutantov. Vsekakor pa vremenski pogoji ne razložijo povsem visokih koncentracij v tej skupini. Zelo podobni vremenski pogoji so namreč značilni tudi za 2. skupino kratkih trajektorij iz SV. Včasih, recimo za NG in KV, so temperature 2. skupine v povprečju še višje, padavinskih dni pa je na vseh merilnih mestih v tej skupini še manj. Kljub temu tako rezultati t-testa za dnevne maksimume ozona, kot rezultati Kruskall-Wallis testa za pripadajoče 3-urne maksimume ozona, potrjujejo, da so koncentracije ozona v 1. skupini trajektorij statistično značilno višje kot v 2. skupini. Očitno torej pretežno JZ izvor trajektorij 1. skupine igra pomembno vlogo na vseh merilnih mesti.

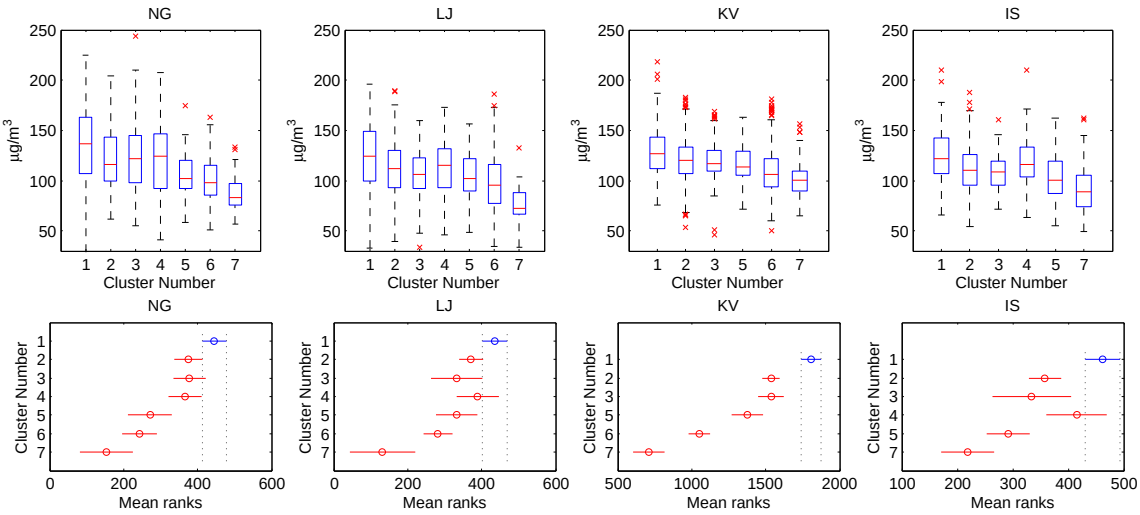

Slika H.2: Rezultati primerjave gostot ozona med skupinami trajektorij. Zaporedne številke skupin ustrezajo oznakam na Sliki H.1. Zgornja vrsta: okvirji z ročaji (box-and-whisker plots) za 3-urne maksimume ozona trajektorij (prikazan zgornji in spodnji kvartil, 1.5-kratnik kvartilov, mediana ter osamelci), ki dospejo na merilno mesto med 12 in 15 UTC (za NG, LJ, IS), torej v urah, ko so razmere običajno najbolj ugodne za tvorbo ozona. V primeru KV, ki se nahaja na večji nadmorski višini in ima povsem drugačeh dnevni hod ozona, pa so upoštevane vse trajektorije (00, 03, ..., 21 UTC). Spodnja vrsta: enako, le da so prikazani rezultati testa Kruskall-Wallis. Skupine, katerih območja (ranks) se ne prekrivajo, se statistično značilno v pripadajočih 3-urnih koncentracijah ozona razlikujejo med seboj.

Nadaljnje presenečenje predstavlja ugotovitev, da so gostote ozona v 2. skupini kratkih trajektorij pretežno iz SV smeri v povprečju nižje kot gostote ozona v skupini dolgih trajektorij 4. skupine iznad Jadrana (npr. LJ in IS, pa tudi NG, Slika H.2) ali skupini dolgih trajektorij 3.

skupine iz JZ. Zaradi močnih vetrov, pa tudi nekoliko nižjih temperatur, očitno v teh skupinah ne gre za ozon, ki bi se ob ugodnih vremenskih pogojih tvoril iz pretežno lokalnih emisij, pač pa so visoke izmerjene vrednosti posledica advekcije onesnaženih zračnih mas. Slednje potrjujejo tudi statistično značilno višje povprečne vrednosti ozona v 3. oziroma 4. skupini, izračunane za vse 3-urne vrednosti za merilna mesta NG, LJ in IS (t-test, p=0.05).

Dopolnitev do sedaj predstavljene clusterske analize, kjer smo analizirali prizemne vrednosti spremenljivk za vse trajektorije v skupini hkrati, je analiza posameznih trajektorij s pripadajočimi vrednosti ozona v končni točki (na merilnem mestu). Na Sliki H.3 desno so predstavljena polja številske gostote trajektorij z izmerjenimi maksimalnimi 3-urnimi koncentracijami v končni točki nad 165 μg/m^3. Zanimivo, praktično vse "onesnažene" trajektorije za Novo Gorico izvirajo iznad Tržaškega zaliva in dosežejo merilno mesto iz juga. Čeprav pričakujemo, da je ozon v Ljubljani primarno posledica tvorbe iz lokalnih emisij ob ugodnih vremenskih razmerah, pa tudi za to merilno mesto opazimo značilno pot onesnaženih trajektorij, ki izvirajo iz Severnega Jadrana, potujejo prek Tržaškega zaliva in dosežejo glavno mesto iz JZ. Pri Iskrbi je situacija podobna, le da tu za onesnažene trajektorije izstopa pot iznad Reškega zaliva preko Reke proti merilnem mestu. Za merilno mesto Krvavec, pa se poleg poti onesnaženih trajektorij iz JZ, kažejo tudi posamezni vplivi iz centralne Evrope; v polju številske gostote onesnaženih trajektorij se pojavijo namreč poti iz S ter SV.

Polja številske gostote onesnaženih trajektorij nam dajo informacijo o smereh potencialnih virov onesnaženja, ne pa nujno o njihovi lokaciji. Upoštevati je naprimer potrebno, da je lahko velika številska gostota onesnaženih trajektorij nad nekim območjem tudi posledica kanalizacije zraka (privetrna/zavetrna območja merilnega mesta). V ta namen so na Sliki H.3 desno prikazana tudi polja povprečnih 3-urnih maksimumov gostot ozona v končni točki trajektorij. Le ta kažejo, da so v povprečju opazno višje koncentracije ozona na vseh merilnih mestih povezane z zračnimi masami, ki izvirajo iznad severnega Jadrana in obalnih območij. Le pri Novi Gorici opazimo maksimum na območju izliva reke Pad v Jadransko območje, kar nakazuje na povečano verjetnost vpliva emisij Padske nižine na tem merilnem mestu. Na drugih merilnih mestih znakov morebitnega povečanega vpliva emisij Padske nižine ni opaziti. Ponovno pa se pri Krvavcu (rahlo tudi pri Ljubljani in Iskrbi) pojavijo poti višje gostote ozona v povezavi s potmi zraka, ki izvirajo iz centralne Evrope in v loku obidejo Alpe ter dosežejo Slovenijo iz SV.

Diskusija

Zanimivo, da se je kot najbolj verjeten izvor z ozonom onesnaženih zračnih mas za Slovenijo običajno pokazalo območje severnega Jadrana. Ker razen ladij tam ni prepoznavnih virov primarnih polutantov, se kot potencialni izvori onesnaženja ponujajo obalna območja - na obalah Tržaškega in Reškega zaliva se dejansko nahajajo pomembni industrijski viri (tovarne, pristanišči, termoelektrarne, rafinerija), podobno tudi ob italijanski obali. Direktnega vpliva emisij Padske nižine na ozon v Sloveniji z dosedanjimi rezultati ne moremo potrditi. Le analiza polj z ozonom uteženih trajektorij za Novo Gorico je pokazala povečano verjetnost vpliva Padske nižine. Zavedati pa se je potrebno, da ima Padska nižina kljub temu lahko pomemben vpliv na ozon v Sloveniji. Možno je recimo, da emisije Padske nižine prispevajo k širšemu jezeru onesnaženega zraka, ki se tvori nad mediteranskim območjem (tudi nad severnim Jadranskim morjem).

Vsekakor je pojav Jadranskega morja kot vira z ozonom onesnaženih zračnih mas za Slovenijo potrebno podrobneje raziskati. Možno je, da se onesnažene mase dejansko kopičijo nad morjem (če to drži, nas zanima zakaj je temu tako), ali pa Jadransko morje deluje le kot

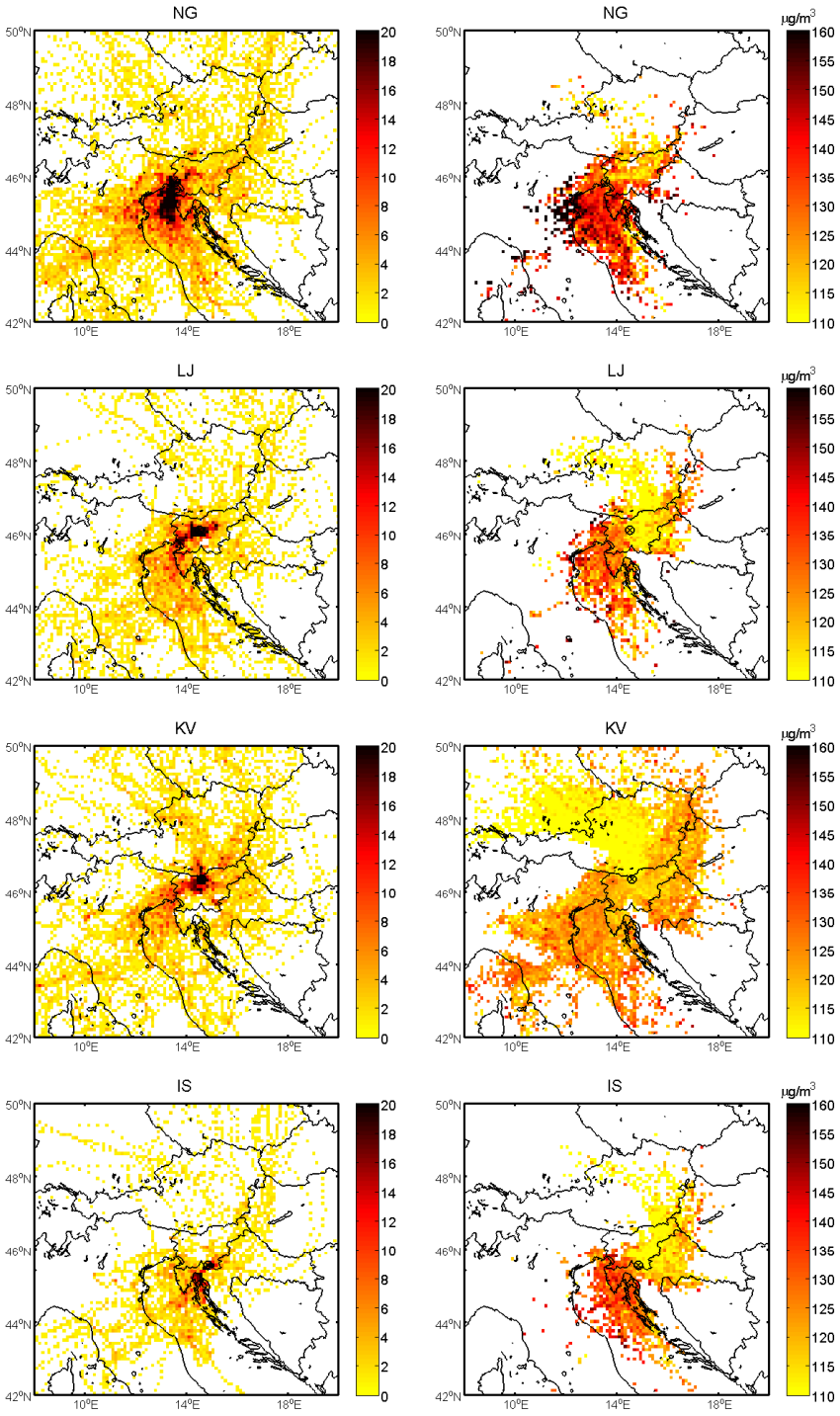

Slika H.3: Levo: številska gostota trajektorij z izmerjeno maksimalno 3-urno gostoto ozona nad 160 μg/m^3 na merilnem mestu. Desno: gostote ozona, izračunane kot povprečje 3-urnih maksimumov ozona, izmerjenih v končni točki trajektorij. Za LJ, NG in IS so povprečja računana le iz trajektorij, ki dospejo na merilno mesto ob 12:00 ali 15:00 UTC. Prikazane so vrednosti za kvadratke, ki jih prečka vsaj 10 trajektorij. Velikost mrežnih kvadratkov je 10×10 km^2.

navidezen vir onesnaženja (v tem primeru morda prihaja do pomembnega vnosa polutantov v zračne mase na njihovi poti iz obalnih emisij). Vsekakor je verjetno, da na nek način k Jadranskemu morju kot (navideznemu) viru z ozonom onesnaženih zračnih mas za Slovenijo pripomorejo procesi, povezani s spremembo lastnosti tal med kopnim in morjem. Iz tega razloga je bilo za razumevanje tega pojava nujno pomagati si s simulacijami, narejenimi z modelom, ki vključuje čimboljši opis vseh pomembnejših meteoroloških in kemijskih procesov. Izbrala sem model WRF-Chem, ki ga predstavljam v nadaljevanju.

Konfiguracija modela WRF-Chem

Model WRF-Chem (Skamarock et al., 2005, 2008; Peckham et al., 2008) je s kemijskim modulom sklopljena različica precej razširjenega mezo-meteorološkega modela WRF (Weather Research & Forecasting). Ker je dandanes sicer običajna praksa, da se za potrebe simuliranja onesnaženja uporablja dva ločena modela, meteorološkega in disperzijskega, je bistvena prednost modela WRF-Chem ravno sklopitev teh procesov v enem modelu. V primeru uporabe dveh ločenih modelov, se namreč za simuliranje disperzije in kemijskih pretvorb polutantov zaradi velike količine podatkov uporabljajo meteorološka polja, shranjena tipično v časovnem razmiku 1 ure. S tako grobo časovno sklopitvijo modelov se bistven del informacije meteoroloških polj izgublja. Poleg tega sklapljanje dveh modelov predstavlja vir napak v končnih izračunih tudi, ker parametrizacije nekaterih fizikalnih procesov v obeh modelih med seboj niso združljive. Napakam, ki izvirajo iz postopka sklapljanja dveh modelov, se tako v našem primeru zaradi uporabe meteorološko-fotokemijskega modela povsem izognemo.

V simulacijah sem s postopkom gnezdenja model poganjala na območjih računskih domen z ločljivostjo 27 km (D1), 9 km (D2) in 3 km (D3), prikazanih na Sliki H.4. V vertikali sem imela atmosfero opisano na 51 nivojih, pri čemer so bili nivoji bistveno gostejši v planetarni mejni plasti zraka (25 nivojev v spodnjih 2 km). Namen domene D1 je bil predvsem priprava čimbolj zanesljivih robnih pogojev za koncentracije polutantov na meji domene D2. S testiranjem vpliva kemijskih robov domene D2 na gostote ozona v Sloveniji sem namreč ugotovila, da je pomembno kakšne kemijske pogoje pripišem robovom domene D2. Obenem je domena D1 služila simuliranju sinoptičnega meteorološkega dogajanja nad Evropo. Cilj domene D2 je predvsem simulirati procese Padske nižine, Jadranskega morja, ter njihov vpliv na območje Slovenije v razmeroma grobi skali. Obenem je domena D2 služila kot vir robnih meteoroloških in kemijskih podatkov za domeno D3. Cilj domene D3 je v fini skali simulirati episode ozona na območju, ki nas najbolj zanima, torej nad Slovenijo in skrajnim SV delom Jadranskega morja. S

Robne meteorološke pogoje domene D1 ter začetne meteorološke pogoje v vseh domenah sem pripravila s pomočjo arhiviranih analiz modela ECMWF. Za opis koncentracij polutantov na robu domene D1 ter ob začetnem času pa sem uporabila v model vgrajene kemijske rutine, s katerimi dobimo sprejemljiv opis razporeditve polutantov v razmeroma čisti atmosferi. Da bi dobila smiselne koncentracije polutantov ob epizodah, ko je bila atmosfera onesnažena, sem tako poganjala model vsaj 3 ali 4 dni predno sem pričela z analizo rezultatov, običajno sem pričela z izračuni po izrazitem deževju (čiščenju atmosfere).

Poleg robnih meteoroloških in kemijskih pogojev model potrebuje še podatke o antropogenih emisijah (predstavljeno v naslednjem razdelku), biogenih emisijah (uporabim kar že vgrajene rutine za približen opis na osnovi temperature in vrste tal), ter podatke o lastnostih tal (uporabim USGS podatke).

Model ponuja vrsto možnosti za opis različnih fizikalnih (turbulenca, mikrofizikalnih pro-

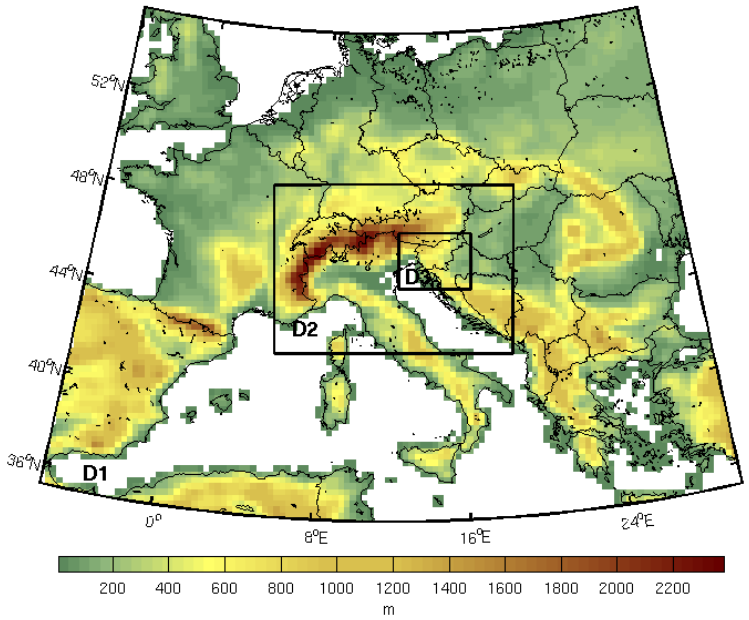

Slika H.4: Območja računskih domen D1, D2 in D3 s horizontalno ločljivostjo 27 km, 9 km and 3 km. Na območju vseh treh domen je narisana topografija z ločljivostjo zunanje D1 domene.

cesov, sevanja, procesov na površju tal, difuzija,...) in drugih procesov (fotoliza, biogene emisije,...). Primer tipične v disertaciji uporabljene nastavitve modela je prikazan v Prilogi D. Ker se je izkazalo, da ima modelski opis turbulence in procesov na površju tal pomemben vpliv na simulirane vrednosti ozona, v disertaciji prikažem rezutate, izračunane z različnimi parametrizacijami turbulence (PBL sheme) in tokov vlage in toplote na površju tal (LSM, land surface model).

Za verifikacijo modela sem uporabila prizemne meritve ozona na 11 postajah razporejenih po vsej Sloveniji, ter prizemne meritve meteoroloških parametrov na 15 postajah. Vertikalno strukturo atmosfere sem verificirala s pomočjo sondaž v Ljubljani, Udinah in Zagrebu.

Priprava antropogenih emisij za namen modeliranja ozona

Z izvedbenega vidika najbolj problematičen del moje raziskave je bila priprava baze podatkov o antropogenih emisijah. Za Slovenijo namreč do sedaj ni bilo na voljo emisijskih kart v obliki, kot jih potrebujemo za modeliranje ozona. Za omejena območja (za Ljubljano ali Zasavje) so v preteklosti že bile pripravljene emisijske karte s zelo dobro krajevno ločljivostjo (do 100 m), vendar ne za vse emisijske sektorje (brez kmetijstva, emisij iz industrijskih procesov, odlagališč itd.) in samo za skupne letne emisije ter brez specifikacije tipa hlapnih organskih spojin (razlaga v nadaljevanju). Za preostali del Slovenije, kot tudi za sosednje države (emisijske karte potrebujemo za celodno območje na Sliki H.4) so bile na voljo le emisijske karte EMEP (Vestreng et al., 2006). Slednje imajo zelo slabo krajevno (50×50 km^2) in časovno ločljivost (1 leto), ter so prav tako na voljo brez specifikacije po tipu hlapnih organskih spojin.

Troposferski ozon se tvori v zapletenih (foto)kemijskih procesih predvsem iz NO_x in VOC,

svojo vlogo pa imajo v teh procesih tudi drugi polutanti (CO, NH_3, SO_2, delci...). Posebej zahtevna je priprava hlapnih organskih spojin (VOC), saj ne le da obstaja nešteto različnih spojin, ampak se le te med seboj tudi močno razlikujejo v reaktivnosti oziroma vlogi, ki jo igrajo v kemijskih procesih, in s tem v učunku, ki ga imajo na koncentracije ozona. Pri modeliranju si v tej množici spojin in različnih pretvorb med njimi pomagamo s poenostavitvami. Sama sem v simulacijah uporabljala v model WRF-Chem vgrajen kemijski mehanizem RADM2 (Stockwell et al., 1990; Chang et al., 1989), ki ima opis kemijskih procesov osnovan na reakcijah med skupinami po reaktivnosti med seboj podobnih si organskih spojin (lumped species). V postopku priprave antropogenih emisij je bilo tako potrebno upoštevati razdelitev v skupine polutantov kot jih predvidi ta mehanizem.

Postopek priprave emisijskih je razmeroma podrobno je opisan v 4. poglavju disertacije. Na tem mestu na omenim le, da je bilo v okviru postopka priprave potrebno narediti naslednje: (i) pripraviti letne količine antropogenih emisij osnovnih polutantov (SO_x, NO_x, CO, NH_3, VOC) v dobri krajevni ločljivosti za celotno računsko območje na Sliki H.4, (ii) pripraviti letne, tedenske in dnevne hode polutantov po posameznih virih (ločeno za različne tipe industrije, prometa, mala kurišča, kmetijstvo itd.), ter (iii) določiti profile hlapnih organskih spojin za vsakega od virov ter zatem izvesti združevanje teh spojin v skupine, ki jih obravnavamo v modelu.

Rezultati numeričnih simulacij za izbrane epizode z visokimi izmerjenimi koncentracijami ozona

V disertaciji sem se odločila predstaviti rezultate simulacij za tri epizode tekom katerih so bile po Sloveniji izmerjene visoke gostote ozona. Epizode sem izbrala v letih 2003 do 2005. To je obenem tudi obdobje za katerega sem pripravila emisijske karte, za leti 2003 in 2004 pa je bila narejena tudi analiza trajektorij v povezavi s koncentracijami ozona v Sloveniji. V nadaljevanju izbrane epizode na kratko predstavim.

Celoten nabor dni za katere je bila vsaj enkrat v dnevu na vsaj enem od merilnih mest Nova Gorica, Ljubljana, Krvavec in Iskrba v letih 2003 - 2005 urna koncentracija ozona nad 165 $\mu g/m^3$ je prikazan v tabeli v Prilogi E. Za obravnavo v disertaciji sem se trudila izbrati med seboj različne epizode, tako po trajanju in krajevni razsežnosti, kot po pričakovanem izvoru (na osnovi 3D trajektorij) onesnaženih zračnih mas.

Kot so pokazali rezultati simulacij imajo obravnavane epizode podoben časovni razvoj, ki ga lahko razdelimo v značilne faze, s katerimi so povezane tudi nekatere značilnosti prostorske porazdelitve ozona po Sloveniji. V nadaljevanju tega poglavja bom razvoj epizod, omenjene faze ter njihove značilnosti tudi predstavila. Obenem, ker je model WRF-Chem nov in je hkrati prvič uporabljen za obravnavano geografsko območje, je pomemben del mojih rezultatov tudi verifikacija modela. Le ta pokaže v kolikšni meri se z modelom uspemo približati meritvam na območju razgibanega reliefa oziroma v čem je vrednost/pomanjkljivost modelskih simulacij. Verifikacijo v nadaljevanju nadgradim s testiranjem občutljivosti simuliranih vrednosti ozona na spremembe v emisijskih poljih, meteoroloških shemah modela, robnih in začetnih kemijskih pogojih, horizontalni ločljivosti modela. Na ta način skušam ugotoviti kolikšen oziroma kakšen vpliv imajo napake v različnih virih negotovosti (v emisijah, opisu nekaterih fizikalnih procesov, v robnih pogojih) na simulirane vrednosti ozona ter tako poskušati razložiti odstopanja med meritvami in modelom ter oceniti v kolikšni meri se pravzaprav lahko zanesemo na modelske rezultate.

Opis izbranih epizod ozona

I. Epizoda: 4 - 14 avgust 2003

Avgust 2003 je bil rekordno vroč, zabeležen je celo kot do sedaj najtoplejši mesec pri nas (MOP ARSO, 2003). Razlog za ekstremno visoke temperature, jasno nebo in sušo, zabeleženo po celotni Evropi, je bila blokada planetarnih zahodnih tokov (Slika H.5), ob kateri se je območje visokega zračnega pritiska raztezalo nad južno, zahodno ter centralno Evropo. Greben geopotenciala na 500 hPa se je nad Evropo formiral med 2. in 3. avgustom in vztrajal vse do 12. avgusta, ko je hladna fronta iz Atlantika pričela potiskati zračne mase proti vzhodu. Slovenijo je hladna fronta prešla v noči med 14. in 15. avgustom in s tem je bilo obenem prekinjeno tudi dolgotrajno obdobje visokih prizemnih koncentracij ozona.

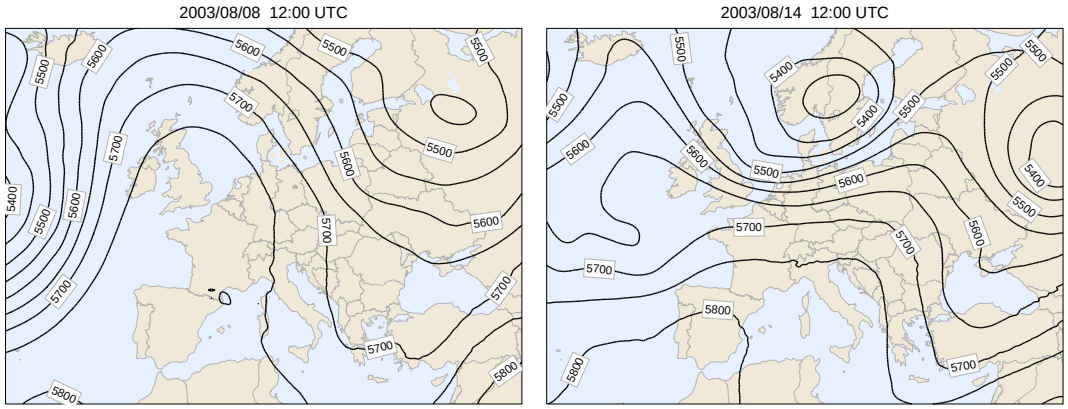

Slika H.5: Polje geopotenciala na 500 hPa ploskvi za 8. in 14. avgust 2003.

Prvič je bilo preseganje urne opozorilne vrednosti (180 μg/m^3) tekom te epizode izmerjeno 5. avgusta v Novi Gorici. Na ta dan so bile maksimalne dnevne gostote ozona blizu opozorilni vrednosti tudi na Krvavcu in Kovku. Z izjemo 7. avgusta, ko so bile tudi drugje po Sloveniji izmerjene nizke gostote ozona, so bili na Primorskem (v Novi Gorici) dnevni maksimumi ozona nad 180 μg/m^3 vse do vključno 14. avgusta. V preostalih delih Slovenije so bile do 11. avgusta urne gostote občasno blizu opozorilni vrednosti v Ljubljani, Iskrbi, Krvavcu in Kovku. Dne 11. avgusta so gostote ozona po Sloveniji nekoliko padle (razen na Primorskem), najvišje vrednosti ozona pa so bile sicer v kontinentalni Sloveniji izmerjene v zaključni fazi epizode, to je med 12. in 14. avgustom. V teh dneh so urne gostote ozona presegle opozorilno vrednost v Ljubljani, Iskrbi, Murski Soboti, Velenju in Kovku.

Iz 3D trajektorij za Novo Gorico za obdobje med 5. in 11. avgustom (Slika) je razvidno, da so zračne mase v tem obdobju izvirale iz centralne Evrope. Dan pred prihodom nad merilno mesto v Novi Gorici trajektorije običajno zaokrožijo nad severnim delom Jadranskega morja in nato iz južnih smeri (pogosto prek Tržaškega zaliva) dosežejo merilno mesto. V naslednjih treh dneh šibko obtekanje Alpske pregrade iz SV v nižjih plasteh troposfere postopno zamenja JZ veter. Zadnji dan epizode, torej 14. avgusta, pa že vse trajektorije v zadnjih 24 urah izvirajo iznad severnega Jadrana ter dosežejo merilna mesta z JZ vetrom. Trajektorije tekom te epizode ne kažejo povezave med zadrževanjem zračnih mas nad Padsko nižino in visokimi gostotami ozona v Sloveniji.

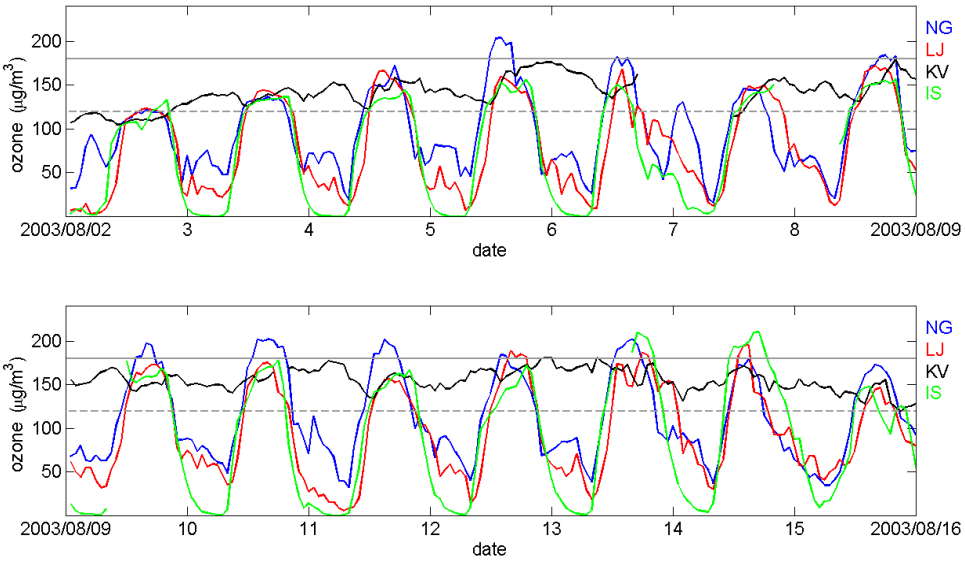

Slika H.6: Potek izmerjenih vrednosti ozona v μg/m^3 na štirih merilnih mestih v obdobju med 2. in 16. avgustom 2003. Rdeča črtkana črta označuje zakonsko določeno 1 urno opozorilno vrednost (180 μg/m^3), siva črtkana črta pa 8 urno ciljno vrednost za leto 2010 (120 μg/m^3).

II. Epizoda: 10 - 11 junij 2004

Gre za kratko, komaj dvodnevno epizodo z zelo visokimi izmerjenimi gostotami ozona na različnih merilnih mestih po Sloveniji. Kljub temu, da je bilo 10. junija v letu 2004 prvič, ko so urne gostote ozona presegle 165 μg/m^3 na vsaj eni od postaj v Tabeli E.1, je bil na ta dan denimo v Novi Gorici izmerjen maksimum ozona kar 210 μg/m^3.

V dneh pred epizodo se je nad zahodno, osrednjo ter južno Evropo formiralo območje visokega zračnega pritiska. Greben geopotenciala na 500 hPa, se je v teh dneh raztezal zahodno od Slovenije, nad Slovenijo so pihali SZ vetrovi. Vreme po Sloveniji je bilo večinoma jasno, dnevne temperature so iz dneva v dan naraščale, vendar so šele 10. in 11. junija presegle 30°C. V dneh epizode (10. - 11. junij) je anticiklon začel slabeti, v višjih plasteh pa so nad Slovenijo zahodni vetrovi prinašali topel in vlažen zrak. 3D trajektorije za 10. in 11. junij kažejo spremembo smeri vetra v nižjih plasteh. In sicer imamo v dneh 10. - 11. junij namesto šibkega obtekanja Alpske pregrade iz SV, značilnega za prejšnje dni, sedaj v nižjih plasteh izrazit JZ veter. Epizodo je prekinila hladna fronta, ki je 12. junija od zahoda dosegala Alpe in v noči med 12. in 13. junijem prešla Slovenijo.

Na osnovi 3D trajektorij bi lahko sklepali, da gre v primeru te epizode za izrazito advekcijo onesnaženih zračnih mas iznad Padske nižine z JZ vetrovi prek Slovenije proti SV. To je redek primer epizode v letih 2003 - 2005, za katero trajektorije v tako neposredni obliki nakazujejo vpliv Padskle nižine na visoke izmerjene koncentracije ozona v Sloveniji.

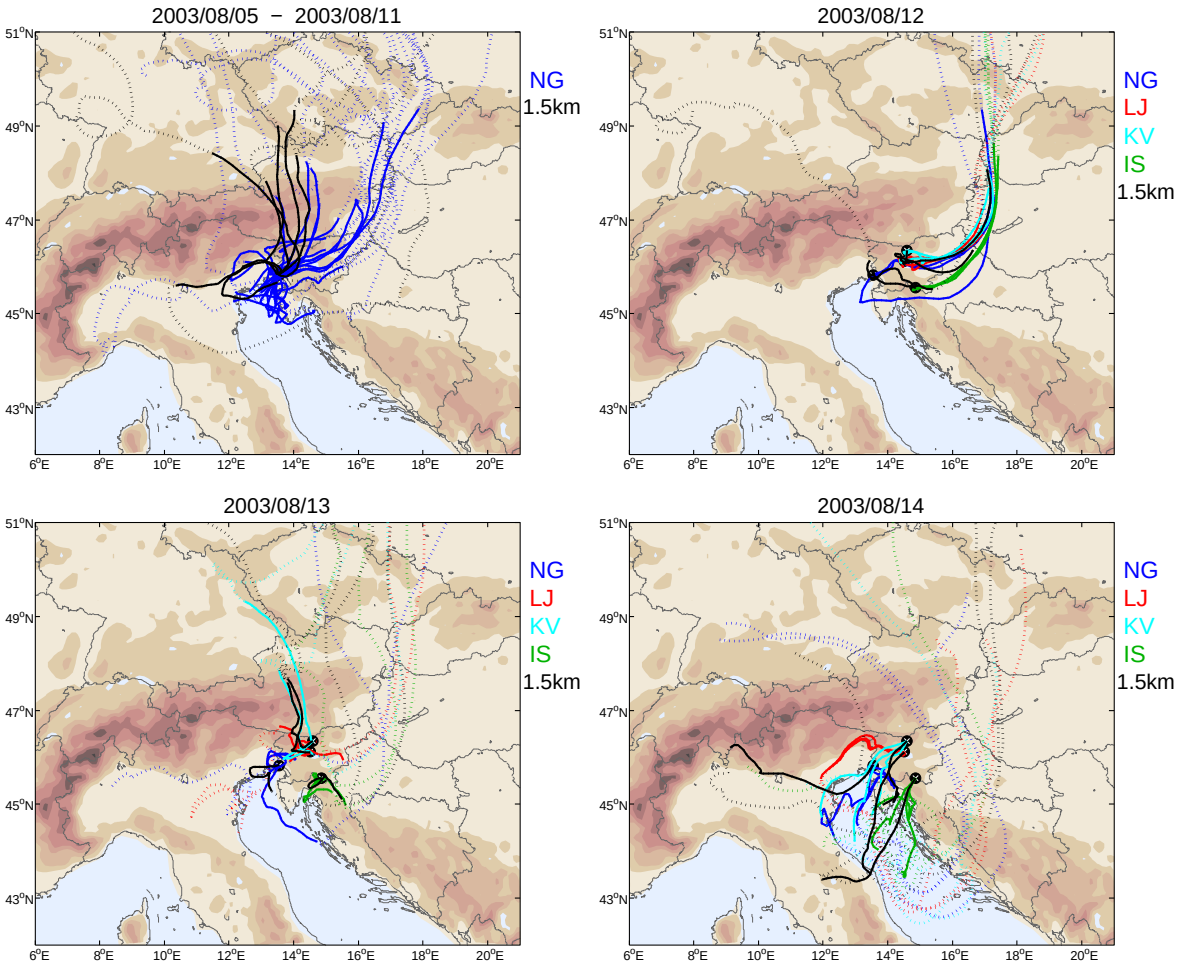

Slika H.7: 3D trajektorije s končnimi točkami na lokaciji merilnega mesta 50 m nad tlemi in 1500 m nad višino morja, izračunane tekom I. epizode. Čas prihoda nad merilno mesto je 9:00, 12:00 in 15:00 UTC za 50 m, ter 12:00 UTC za 1500 m trajektorije. Levo zgoraj: 5 - 11 avgust, trajektorije za Novo Gorico. Ostale slike: trajektorije za izbran dan za Novo Gorico, Ljubljano, Krvavec and Iskrbo. Podrobnosti glede izračuna trajektorij so opisane v poglavju o analizi trajektorij. Celotna dolžina trajektorij je 96 ur, zadnjih 24 ur pred prihodom nad merilno mesto so trajektorije risane s polno črto, preostanek vsake od 96 urnih trajektorij pa je narisan s črtkano črto.

III. Epizoda: 19 - 26 junij 2005

Tudi ta epizoda je povezana z nastankom območja visokega zračnega pritiska nad južno in zahodno Evropo v dneh med 17. in 23. junijem 2005, ozirom nad južno in vzhodno Evropo v naslednjih dveh dneh (med 24. in 25. junijem). V višjih zračnih plasteh so tudi tekom te epizode nad Slovenijo najprej prevladovali SZ vetrovi. S premikom grebena geopotenciala na 500 hPa ploskvi proti zahodu po 23. juniju pa se je veter v višjih plasteh nad Slovenijo počasi obrnil v zahodnik.

Temperature zraka na slovenski obali so že od 16. junija dalje dosegale ali presegale 30°C, medtem ko so bile v notranjosti nekoliko nižje, vendar še vedno visoke. Tekom epizode je prevladovalo pretežno jasno vreme. V dneh 22., 23. in 25. junija, so bile po Sloveniji lokalne plohe in nevihte. Od 26. junija dalje se pa so se krajevne plohe in nevihte pojavljale tekom celega dneva, spremljal jih je močan veter, nalivi in tudi toča.

Do vključno 24. junija so bile visoke gostote ozona izmerjene le na Primorskem, kjer so dnevni maksimumi dosegali tudi 200 $\mu g/m^3$. Le povprečne 8-urne vrednosti na Krvavcu so bile v teh dneh občasno nad 120 $\mu g/m^3$, medtem ko so bile sicer po Sloveniji vrednosti ozona nizke (v Ljubljani naprimer ves čas pod 150 $\mu g/m^3$). Dne 25. junija meritve pokažejo izrazito povišanje gostot ozona na različnih merilnih mestih po Sloveniji. Tako so na ta dan bile opozorilne urne vrednosti ozona presežene v Ljubljani, Krvavcu, Vnajnarjah in Zavodnjah. Po 25. juniju so izmerjene gostote ozona spet nizke, le v Novi Gorici dne 28. in 29. junija za kratek čas dosežejo opozorilno vrednost.

Poti 3D trajektorij s končnimi točkami 50 metrov nad merilnimi mesti so podobne kot v zadnjih dneh I. epizode. Izvirajo iz centralne Evrope, v loku iz SV obidejo Alpsko pregrado, večinoma potujejo nad Jadranskih morjem oziroma nad obalnim območjem in dosežejo merilna mesta z JZ. Pri trajektorijah s končno višino 1500 m je slika drugačna. Že v obdobju 22. - 24. junij ena od teh trajektorij zaokroži nad Padsko nižino, dne 25. junija pa je njihova pot povsem spremeni. Sedaj izvirajo iznad Ligurskega morja severno od Korzike, potujejo južno od Padske nižine in Severnih Apeninov, ter nato preko Severnega Jadranskega morja dosežejo Slovenijo iz jugozahoda.

Značilnosti referenčnih simulacij

Za vsako od epizod je bilo narejenih precej simulacij. Razlike med simulacijami so bile naprimer v pogostosti inicializacije meteoroloških polj, v izbiri shem za opis turbulence v planetarni mejni plasti (PBL shema), v izbiri modela za opis tokov toplote in vlage na površju tal (LSM, land surface model), ter nekaterih drugih kasneje opisanih robnih in začetnih pogojih.

Rezultati tako dobljenega ansambla rešitev so pokazali, da je težko izbrati konfiguracijo modela, ki bi bila v splošnem najboljša. Vsaka modelska rešitev je običajno imela nekatere prednosti in tudi kakšno slabost. Kljub temu sem se odločila definirati konfiguracijo modela, katere rezultate sem definirala kot referenčne. Z referenčno simulacijo vsake epizode sem nato lahko primerjala vplive, ki jih imajo različne spremembe v nastavitvah modela na simulirane vrednosti ozona.

V referenčnih simulacijah so bile vrednosti antropogenih emisij takšne, kot so opisane v poglavju o emisijah, konfiguracija domen je bila prav tako takšna kot je opisana v poglavju o konfiguraciji modela WRF-Chem, pri zagonu modela je bil uporabljen seznam možnosti, ki je prikazan v Prilogi D. Izpostavimo naj le, da sta bili v referenčnih simulacijah uporabljeni YSU PBL shema in Noah LSM.

Verifilkacija referenčnih simulacij je pokazala, da so dnevne temperature dobro sledile izmerjenim vrednostim, medtem ko so bile ponoči modelske temperetaure običajno previsoke. Pritisk je prav tako lepo sledil meritvam, sistematične napake so bile posledica odstopanj v dejanskem in modelskem reliefu. Simulirane vrednosti zralne vlage (razmerja mešanosti, v g/kg) so bile v modelu običajno sistematično prenizke, na nekaterih merilnih mestih po Sloveniji pa je bilo ujemanje razmeroma dobro. Vetrovno polje je v vseh simulacijah predstavljalo velik izziv. V glavnem je bilo v modelskih rezultatih moč razpoznati glavne značilnosti mezoskalnih cirkulacij zraka, predvsem to velja za Primorsko, kjer so bila dnevna nihanja vetrov zelo izrazita. Drugod po Sloveniji, kjer gibanja zraka niso bila tako izrazita, je imel model v

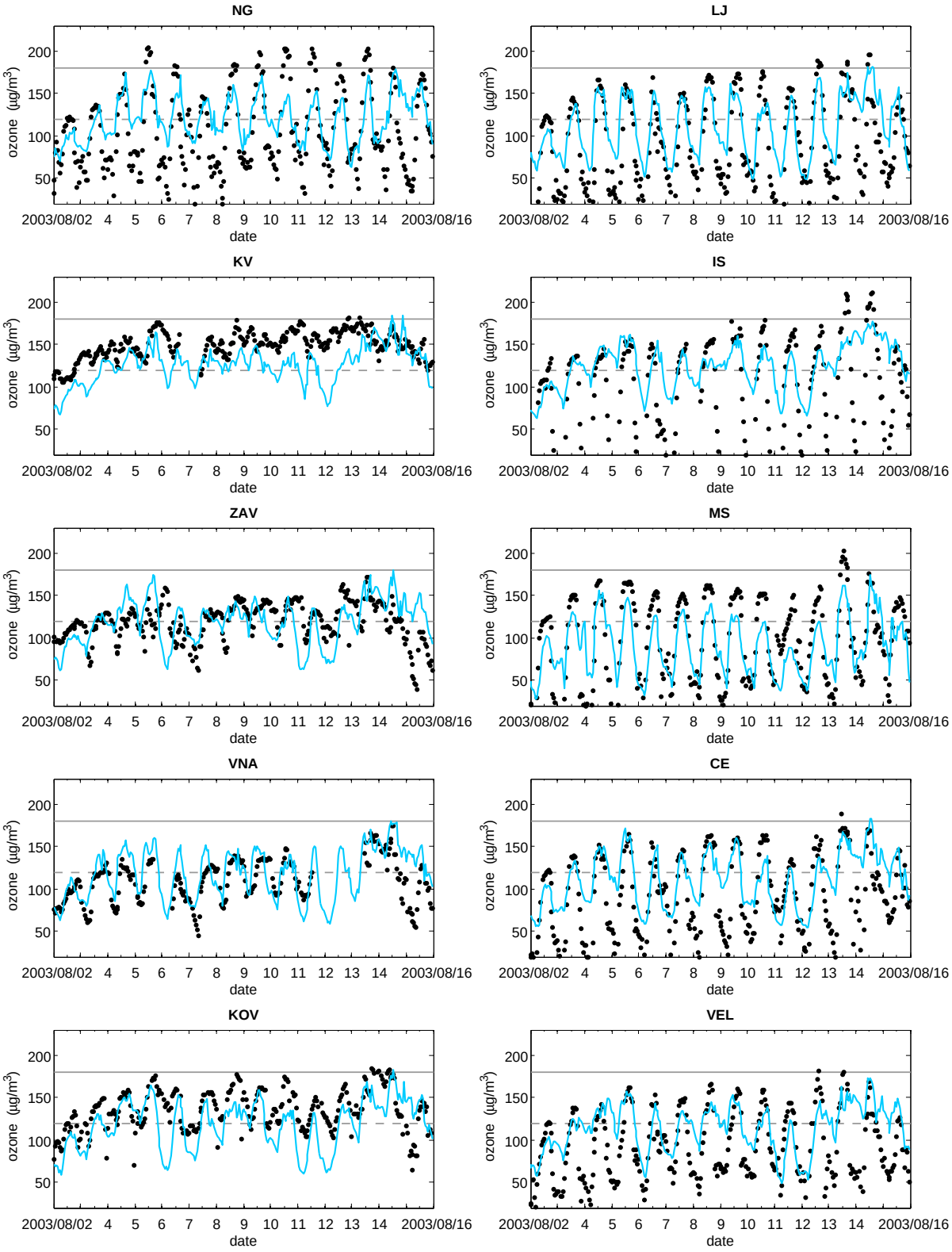

Slika H.8: Primerjava modelskih (modro) in izmerjenih (črno) urnih vrednosti ozona na postajah Nova Gorica, Ljubljana, Krvavec, Iskrba, Zavodnje, Murska Sobota, Vnajnarje, Celje, Kovk in Velenje. Siva črti: 1-urna opozorilna in 8-urna ciljna vrednost.

splošnem težave pri pravilnem opisu šibkih vetrov.

Primerjava simuliranih in izmerjenih vrednosti ozona je dala v nekaterih simulacijah boljše, v drugih pa slabše rezultate. Običajno je imel model največje težave približati se najvišjim koncentracijam na Primorskem (v Novi Gorici), čeprav je obenem dobro predvidel povišanje ozona na mediteranskem območju v primerjavi z ostalo Slovenijo. Poleg tega je model običajno precenil nočne vrednosti ozona, medtem ko je tudi sicer (ne le na Primorskem) običajno podcenil maksimume. Neujemanje ozona med modelom in meritvami je bilo tudi pogosto posledica težav pri pravilnem opisu šibkih gibanj zraka v planetarni mejni plasti, zaradi česar so v modelu nastopali maskimumi drugje kot v naravi. Primer primerjave simuliranih vrednosti ozona z meritvami za I. epizodo je prikazan na Sliki H.8.

Vpliv nekaterih modelskih parametrizacije na rezultate

Običajno se visoke koncentracije ozona pojavljajo v toplih mesecih ob dolgotrajnih anticiklonalnih situacijah, pri čemer je učinkovitost tvorbe ozona iz primarnih polutantov ob takšnem vremenu dalje odvisna predvsem od temperature ozračja, pa tudi od drugih meteoroloških parametrov, kot so vetrovnost, količina sončnega obsevanja, višina planetarne mejne plasti zraka, oblačnost in padavine.

Tabela H.1: Eksperimentalni zagoni modela.

Eksperiment	PBL shema	LSM shema	Sprememba razpoložljive vlage v tleh
A	MYJ	Noah	Ne
B	YSU	5-plastni model	Ne
C	MYJ	5-plastni model	Ne
C1	MYJ	5-plastni model	Da
D - referenčni	YSU	Noah	Ne

Z vidika modeliranja onesnaženosti ozračja predstavljajo te situacije s šibkim dinamičnim siljenjem v velikih skalah precejšen izziv. Problem predstavlja predvsem vetrovno polje, ki ga v planetarni mejni plasti določajo termično pogojeni lokalni vetrovi. Gre torej za šibke vetrove, pri katerih je velikostni red turbulentnih gibanj v opisanem tipu vremenskih situacij pogosto enak velikostnemu redu jakosti vetra. Opis turbulence prizemne plasti zraka v modelu tako lahko pomembno vpliva na modelske rezultate.

Tabela H.1: Vrednosti osnovnih statističnih parametrov za temperaturo, jakost vetra in zračno vlago, izračunane za 15 meteoroloških postaj. Izračuni so narejeni za urne vrednosti spremenljivk. ME - povprečna napaka, MAE - povprečna absolutna napaka, RMSE - koren povprečnega kvadrata napake.

	$T_{max}(^{\circ}C)$			v (m/s)			Q (g/kg)		
Exp	ME	MAE	RMSE	ME	MAE	RMSE	ME	MAE	RMSE
A	0.4	1.6	2.0	1.6	1.9	2.4	-1.6	2.3	2.9
B	-1.9	2.6	2.7	0.8	1.3	1.7	2.6	2.9	3.3
C	-5.1	5.3	5.6	0.9	1.4	1.8	3.6	3.7	4.3
C1	-2.7	3.2	3.3	1.1	1.5	2.0	2.8	3.0	3.5
D	-0.5	1.6	2.0	0.9	1.4	1.9	-1.9	2.5	3.1

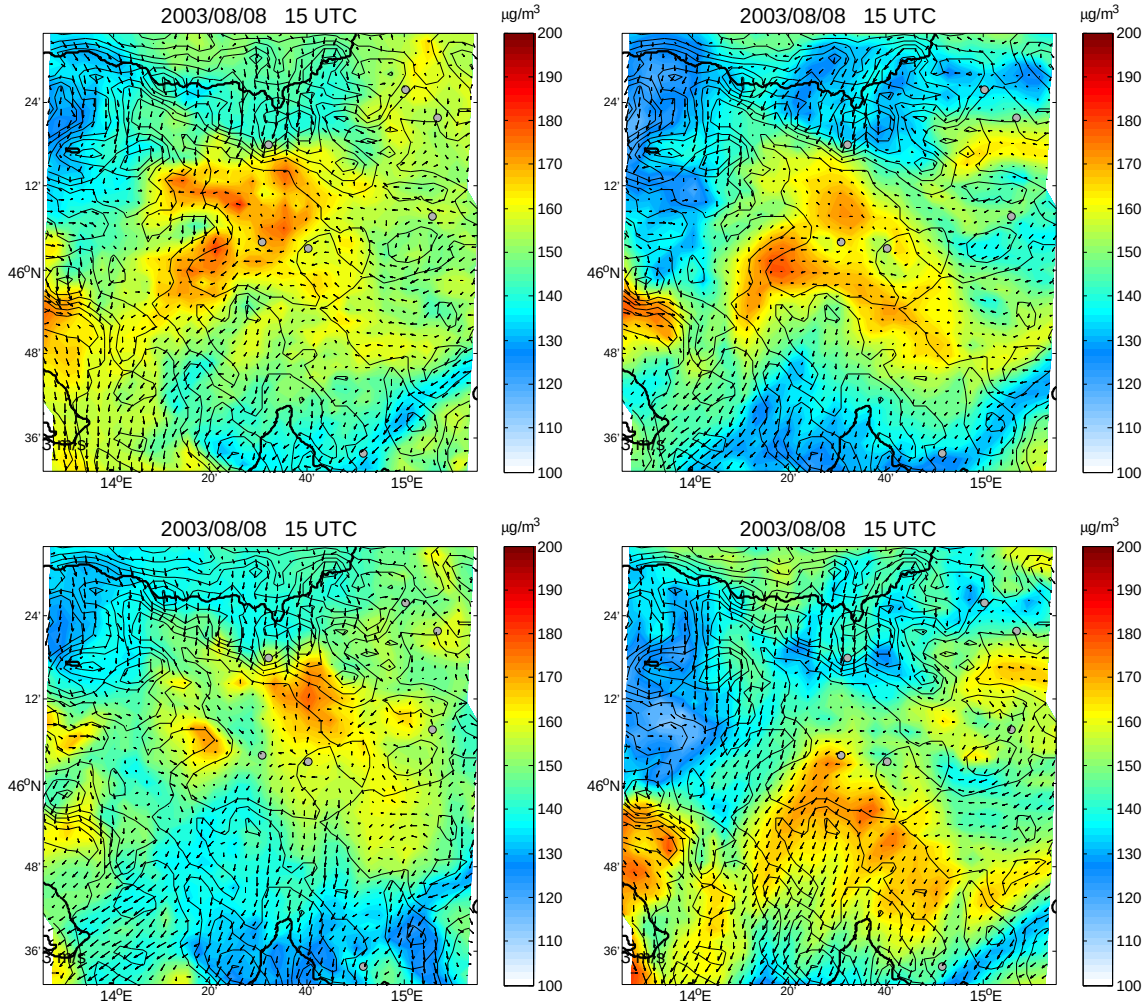

Slika H.9: Primerjava prizemnega polja ozona ter vetra na 10 m nad tlemi za dne 9. avgusta 2003 ob 15:00 UTC, po vrsti za eksperiment A, B, C1 in D. Prikazani so rezultati simulacij na območju znotraj notranje domene z ločljivost 3 km, velikem 36×36 modelskih točk. Tanke črne črte prikazujejo topografijo, močnejše pa obalo in državne meje.

Z namenom študirati vpliv opisa turbulence in ter opisa tokov toplote in vlage med tlemi in ozračjem, sem tako naredila dodatne eksperimentalne zagone modela za del I. epizode (od 8. avgusta dalje). Izbira shem v posameznem eksperimentu za parametrizacijo turbulence (PBL shema) ter shem za opis tokov na površju tal (LSM shema), je prikazana v Tabeli H.1. Model nudi dve možnosti za izbiro PBL sheme (MYJ and YSU) ter dve možnosti za LSM shemo (Noah in 5-plastni model), torej imamo skupno 4 konfiguracije modela. Izkazalo se je, da so z eno od teh konfiguracij (C) povezane velike sistematične napake nekaterih prizemnih meteoroloških spremenljivk, ki jih je bilo mogoče v precejšnji meri odpraviti z zmanjšanjem razpoložljive vlage v tleh. Tako je bila naboru 4 simulacij dodana še peta, C1, v kateri je bil parameter razloložljive vlage tal na večini območja (za 2 prevladujoči kategoriji rabe tal) spremenjen - popravljen na vrednost urbanih središč.

Tabela H.2 prikazuje primerjavo statistik, izračunanih za tri osnovne prizemne meteorološke spremenljivke, iz 15 meteoroloških postaj, vključenih v obravnavo v disertaciji. Kot posledica razlik v podrobnostih opisa planetarne plasti zraka, prihaja med eksperimenti tudi do

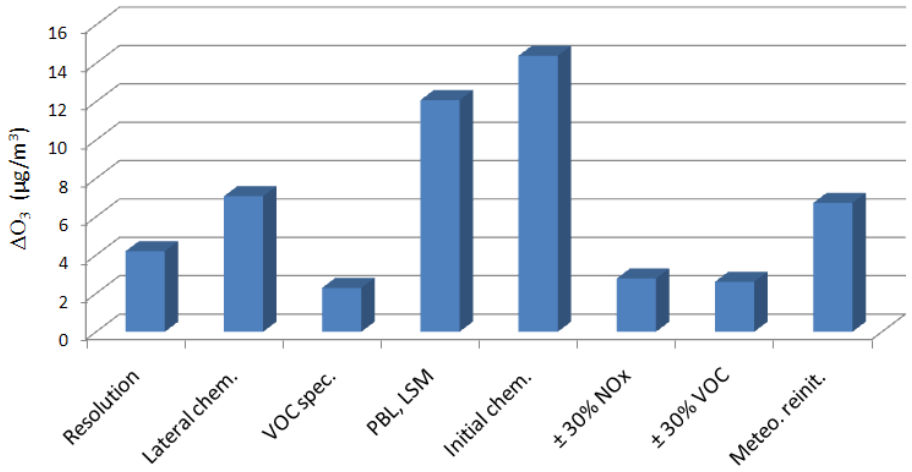

Slika H.10: Občutljivost simuliranih dnevnih maskimumov ozona na različne vire negotovosti. Prikazana je primerjava povprečnih absolutnih odstopanj (povprečeno po ekoloških postajah tekom epizode) od referenčne simulacije za drugi del I. epizode (8. do 14. avgust). Resolution: primerjava referenčne simulacije v 3 km horizontalni ločljivosti z rezultatom v 9 km ločljivosti; Lateral chem.: spremenjeni kemijski pogoji na robu srednje D2 domene; VOC spec.: drugačna razdelitev VOC po reaktivnosti v skupine; PBL, LSM: različne parametrizacije v modelu; Initial chem.: vpliv začetnih kemijskih pogojev; ±30% VOC and NO_x: povečanje ali zmanjšanje emisij za faktor 30%, Meteo. reinit.: večja pogostost re-inicializacije meteoroloških polj.

razlik v simuliranih poljih ozona. Slika H.9 tako primerja lego ljubljanskega ozona med štirimi eksperimenti. Očitno razlike v obravnavanih parametrizacijah povzročijo zadostne spremembe vetrovnega polja, da oblak onesnaženega zraka iz mesta Ljubljane zanese v različne smeri že po nekaj urah simulacije. Z daljšanjem časa simulacije pa se razlike stopnjujejo. Na žalost na osnovi meritev, ki jih imamo na razpolago, običajno ne moremo ugotoviti do katerega od predlaganih razvojev je v resnici prišlo, oziroma katera od simulacij je najboljša. Razlike med temi modelskimi simulacijami nam tako predstavljajo oceno negotovosti modelskih rezultatov zaradi napak pri meteorološkem opisu planetarne mejne plasti zraka.

Primerjava občutljivosti simuliranih vrednosti ozona na vire negotovosti

Opis planetarne plasti zraka pa ni edini vir napak v modelskih izračunih. Nasprotno, pri modeliranju ozona se srečujemo z mnogimi viri negotovosti, ki potencialno predstavljajo pomemben vir napak v rezultatih simulacij. Z namenom testirati in primerjani občutljivost modelskih izračuniv na različne vire negotovosti, sem za enako obdobje kot v prejšnjem odseku naredila dodatne ekperimente. V teh ekperimentih sem testirala vpliv negotovosti antropogenih emisij, robnih in začetnih kemijskih pogojev, horizontalne ločljivosti v modelu, pogostosti re-inicializacije meteoroloških polj in razdelitve antropogenih hlapnih organskih spojin v skupine po reaktivnosti.

Primerjava odstopanj v dnevnih maksimumi ozona (ne glede na čas nastopa maksimuma) med temi eksperimenti in referenčno simulacijo nam da oceno vpliva, ki ga imajo testirane

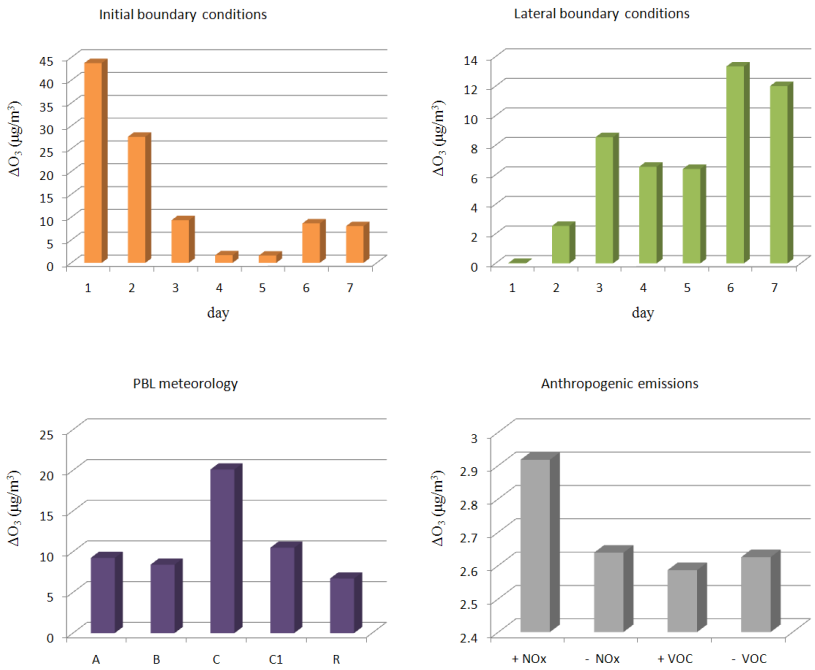

Slika H.11: Kot na prejšnji sliki, le da so rezultati podrobneje razdelani. Vpliv začetnih in robnih kemijskih pogojev je prikazan ločeno po posameznih dneh simulacije, vpliv meteorološkega opisa planetarne mejne plasti po posameznih eksperimentih (A - D, medtem ko R predstavlja veljo pogosto re-inicializacije meteoroloških polj), ter vpliv spremembe antropogenih emisij prav tako..

spremembe v konfiguraciji modela na najvišje vrednosti ozona (torej na tiste, ki nas najbolj zanimajo). Kot je razvidno iz Slike H.10, je višina dnevnih maksimumov najbolj odvisna od začetnih kemijski pogojev, sledi jim meteorološki opis planetarne plasti zraka, ter nato robni kemijski pogoji. Podrobneje so ti rezultati razdelani na Sliki H.11, kjer je vpliv začetnih in robnih kemijskih pogojev prikazan ločeno po vseh 7 dneh simulacije, vpliv meteorološkega opisa pa ločeno za vsakega od eksperimentov A - D ter za eksperiment s pogostejšo reinicializacijo meteoroloških polj (R). Vpliv 30% spremembe emisij NO_x oziroma VOC je prav tako prikazan ločeno po 4 eksperimentih.

Značilne faze epizod

Kljub temu, da so bile simulacije narejene za različne epizode (kriteriji podobnosti/različnosti so bili trajanje, razsežnost, poti 3D trajektorij), se je na koncu izkazalo, da imajo vse obravnavane epizode nekatere skupne značilnosti. Namreč, njihov časovni razvoj sestavljajo tri značilne faze, tesno povezane s sinoptično situacijo.

V prvi delu epizod sinoptično situacijo definira greben geopotenciala na 500 hPa ploskvi, ki se nahaja zahodno od Slovenije (kot npr. na Sliki H.5, levo). Slovenija se v tem času nahaja v območju visokega zračnega pritiska pri tleh, medtem ko v višjih zračnih plasteh pihajo SZ vetrovi, ki jih v spodnjih plasteh ozračja blokira Alpska pregrada. Deloma je, predvsem nad

SV Slovenijo, v nižjih plasteh prisotno obtekanje zraka iz SV, večinoma pa v nižjih plasteh ozračja nad Slovenijo ni prevladujočih splošnih tokov. Glavna gonilo gibanja zraka torej v tem obdobju predstavljajo pojavi v mezo skali (lokalni pobočni, dolinski, obalni vetrovi, toplotni otok nad mestom itd.).

Na obalnem območju se v tem obdobju razvijejo tipični termično pogojeni obalni vetrovi, ki se v primeru severnega Jadrana sklopijo oziroma nadaljujejo v pobočne vetrove v predgorju Alp in SZ ostankov Dinarskega gorstva. Podnevi tako prevladuje smer gibanja zraka z morja preko Furlanije in naprej proti vrhovom hribov, ponoči pa v obratni smeri, s hribov navzdol proti morju. Ob tako ustvarjenih cirkulacije ali celo re-cirkulacije zrakčne mase nad obravnavnavanim območjem lahko vztrajajo precej časa, kar omogoča, da se v njih iz emisijskih virov tega območja akumulirajo velike količine onesnaženja. Ker so obenem tekom te faze epizod vremenske razmere na mediteranskem območju običajno zelo ugodne za tvorbo ozona, končne koncentracije ozona lahko dosegajo zelo visoke vrednosti. Slovenija vzhodno od Alpsko-Dinarske pregrade v tem delu epizod bolj ali manj ločena od mediteranskih zračnih mas. V preostalih predelih Slovenije so v prvem delu epizod najvišje gostote ozona nekoliko nižje, pogostejša so preseganja 8-urnih vrednosti ozona, predvsem na območjih izven mestnih središč.

V drugem delu epizod, povezanem s premikom grebena geopotenciala na 500 hPa ploskvi proti vzhodu, nad Slovenijo zapihajo jugozahodni vetrovi, s katerimi so onesnažene zračne mase iznad Jadrana advektirane proti in čez Slovenijo. Ker je količina onesnaženja nad Jadranskim morjem lahko velika (onesnaženje akumulirano nad Jadranom s podobnimi mehanizmi tudi z obalnih območij Italije, Hrvaške, tudi Padske nižine), so v teh dneh ponekod v osrednji Sloveniji lahko izmerjene ekstremno visoke vrednosti ozona. To je torej razlog, zakaj je analiza trajektorij pokazala najvišjo pogostost visokih koncentracij ozona za trajektorije iz JZ smeri tudi za merilna mesta v osrednji Sloveniji.

Epizode prekine tretja faza, običajno je to prehod fronte, v kateri vrednosti ozona močno padejo. Poleg čiščenja atmosfere v primeru intenzivnih frontalnih padavin (rahle padavine ali razpršene plohe in nevihte ne počistijo atmosfere povsem) so faktorji, ki prispevajo k padcu gostot ozona tudi ohladitev spodnje troposfere ter sprememba jakosti in smeri zračnega toka nad Slovenijo.

Na Slikah H.12 in H.13 je prikazan prikazan primer časovnega razvoja za epizodo v Juniju 2005. Dne 21. junija je atmosfera še razmeroma čista, čeprav se že kažejo znaki akumulacije. V naslednjih dneh so na širšem obalnem območju gostote ozona zaradi akumuliranega onesnaženja in ugodnih vremenskih razmer zelo visoke, medtem ko se v preostali Sloveniji kažejo posamezni “oblaki” ozona. Dne 25. junija jugozahodni vetrovi ponesejo zračne mase iznad Jadrana skupaj z akumuliranim onesnaženjem čez Slovenijo.

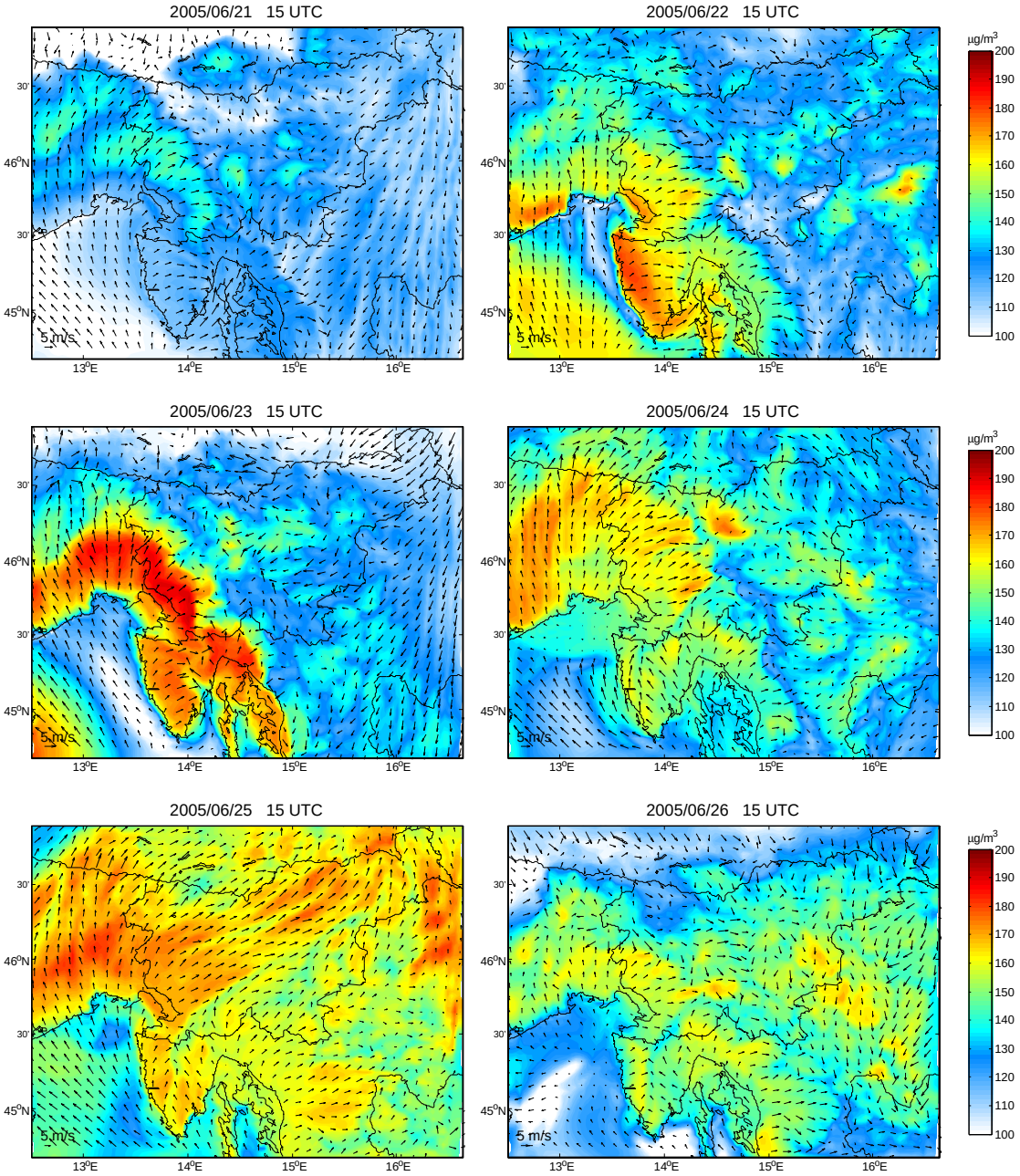

Slika H.12: Simulirane prizemne vrednosti ozona in veter 10 m nad tlemi tekom III. epizode (Junij 2005) na območju notranje domene z ločljivostjo 3 km. Prikazani so rezultati referenčne simulacije.

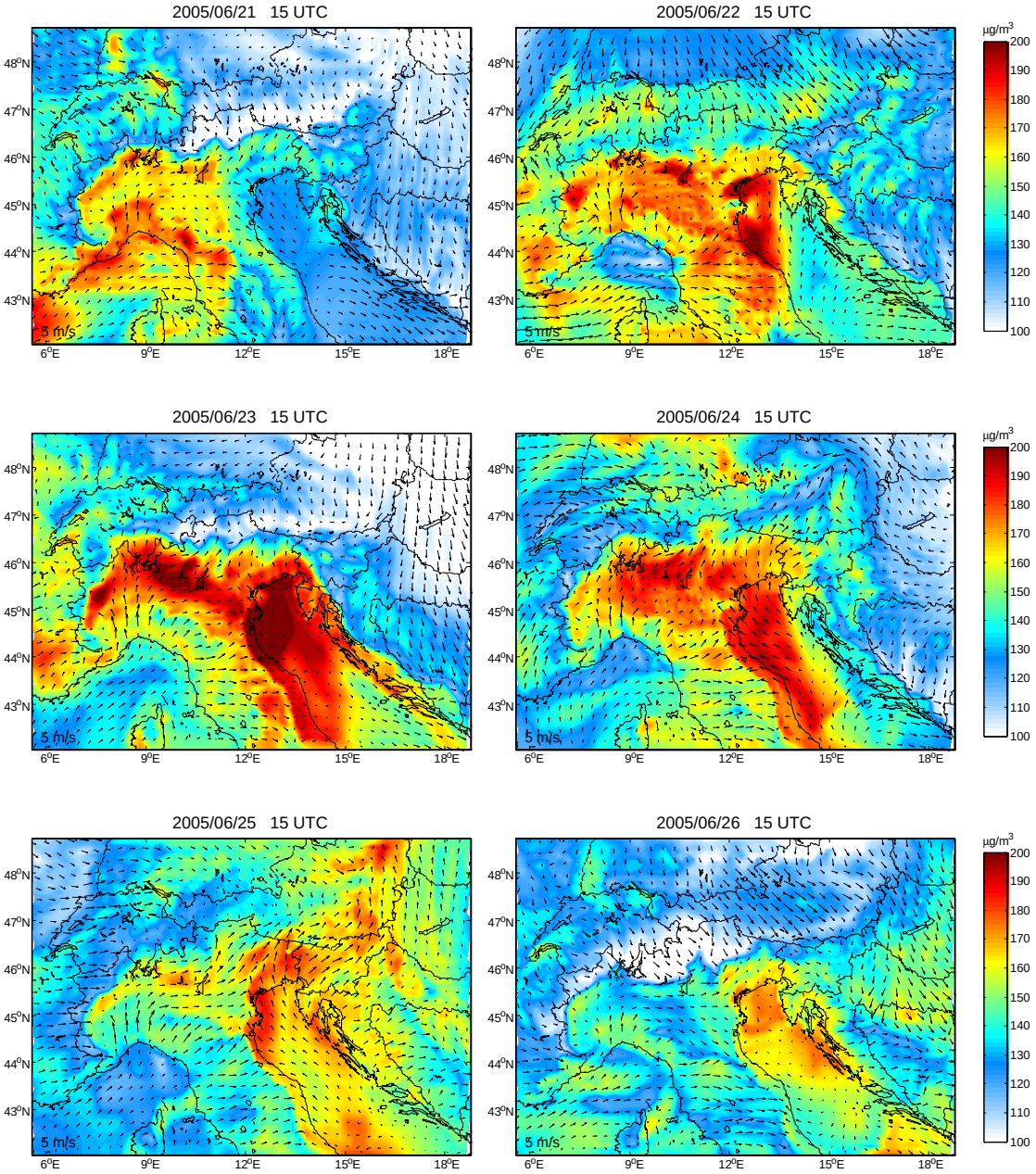

Slika H.13: Simulirane vrednosti ozona in veter na 8. modelskem nivoju (približno 270 m nad tlemi) tekom III. epizode (junij 2005). Prikazani so rezultati referenčne simulacije.

Zaključki

Rezultati analize trajektorij so pokazali, da so bile za obravnani topli polovici let 2003 in 2004 koncentracije ozona statistično značilno višje v skupinah kratkih (počasnih) trajektorij iz jugozahodne smeri. Kot skupno izvorno območje onesnaženih trajektorij se je izkazalo, da je področje severnega Jadrana, česar samo z analizo trajektorij ni bilo mogoče razložiti.

Modelske simulacije narejene za izbrane epizode so potrdile, da se tekom prve faze epizod

nad severnim Jadrana, obalnimi območji in Alpskimi pobočji, razvije tipična cirkulacija zraka, ki pripomore k akumulaciji velikih količin polutantov v zračnih masah nad tem območjem. Velika količina akumuliranega onesnaženja in hkrati ugodni meteorološki pogoji (visoke temperature, jasno nebo, brez padavin) pa omogočajo učinkovito tvorbo ozona, s čimer lahko razložimo večjo pogostost pojavljanja najvišjih gostot ozona na Primorskem tekom prve faze epizod. Gostote ozona v teh fazi na območju preostale Slovenije ne dosegajo tako visokih vrednosti, čeprav so izjemoma predvsem kot posledica tvorbe iz lokalnih emisij dnevni maksimumi lahko visoki tudi drugod.

V drugi fazi se z jugozahodnimi vetrovi onesnažene zračne mase premaknejo iznad severnega Jadrana proti osrednji Sloveniji, kar je v primeru obravnavanih epizod imelo za posledico ekstremno visoke izmerjene prizemne vrednosti ozona na nekaterih postajah v osrednji Sloveniji. To nam razloži vpliv onesnaženih zračnih mas z izvorom iznad severnega Jadrana na postaje v ne-mediteranski Sloveniji, ki ga je pokazala analiza trajektorij.

Čeprav so občasno visoke prizemne gostote ozona v osrednji in SV Sloveniji tekom prve faze epizod predvsem posledica tvorbe v PBL iz lokalnih emisij ob ugodnih vremenskih pogojih, pa ima določen vpliv tudi regionalni transport. Poskus s spremenjenimi kemijskimi pogoji na robu domene srednje domene (D2) je namreč pokazal, da se simulirane vrednosti dnevnih maksimumov ozona na postajah po Sloveniji znižajo za do 10 μg/m^3.

Onesnaženje se nad severnim Jadranom in obalnimi območji tekom prve faze epizod akumulira predvidoma prevsem iz obalnih virov ter emisij z območja Furlanske nižine, verjetno pa k temu bazenu onesnaženega zraka svoj delež prispevajo tudi emisije iz Padske nižine. Kvantitativno prispevek emisij Padske nižine tekom te faze zaenkrat ni bil ocenjen. V preteklosti se je občasno dogodilo (Epozoda 2) tudi, da je bilo onesnaženje iznad Padske nižine advektirano neposredno proti Sloveniji. Vsekakor pa se je v analiziranem obdobju treh let (2003 do 2005) to dogodilo zelo izjemoma.

Tabela H.3: Rezultati verifikacije simuliranih prizemnih vrednosti ozona. Prikazani so rezultati izračunov, narejenih za tri referenčne simulacije (tri epizode), za 11 merilnih mest ozona obravnavanih v dizertaciji. Pomen posameznih statistik je opisan v Prilogi A. Z izjemo UPA, MNBE in MNGE, ki so brezdimenzijske, so vrednosti izražene v enotah μg/m^3. Vrednosti ME, MAE in RMSE so izračunane ločeno za dnevne maksimume (ne glede na čas nastopa maksimuma) in za urne izmerjene vrednosti nad 100 μg/m^3.

ME_{max}	MAE_{max}	$RMSE_{max}$	ME_{100}	MAE_{100}	$RMSE_{100}$	UPA	MNBE	MNGE
-1.5	20.6	25.8	-2.1	20.5	26.2	0.06	1.2	15.6

Dnevni in letni hod ozona na višje ležečih območjih (merilna postaja Krvavec) ima svoje posebnosti. V poletnem času je v najtoplejših urah dneva običajno pod vplivom premešane plasti zraka, formirane nad Ljubljansko kotlino. Rahel minimum ozona v povprečnem dnevnem hodu za Krvavec ob 10:00 UTC ustreza času, ko premešana plast zraka doseže merilno mesto. Preostali del dneva, vključno z nočnimi urami, pa so relativno visoke vrednosti ozona posledica onesnaženih plasti, ki so bile vnešene v spodnjo prosto troposfero iz planetarne mejne plasti zraka tekom dneva in so nato dalje podvržene regionalnemu transportu. Občasno bi bile visoke vrednosti ozona na višje ležečih območjih lahko tudi posledica vdorov iz stratosfere, vendar bi bilo za potrditev vpliva stratosferskega ozona potrebno opraviti dodatne analize (študirati morebiten vpliv od primera do primera posebej).

Primerjava občutljivosti simuliranih vrednosti ozona na različne vire negotovosti je pokazala,

da so vrednosti ozona najbolj občutljive na začetne kemijske pogoje. Ta ugotovitev kaže na pomembnost akumulacije polutantov v zračnih masah pri tvorbi ozona. Dejstvo, da je po treh dneh simulacije vpliv začetnih kemijskih pogojev postal zanemarljiv, kaže da je v tolikšnem času onesnaženje nad opazovanim območjem doseglo nekakšno nasičenje. Vendar pa so na koncu obravnavane epizode, po 6 do 7 sneh simulacije, začetni kemijski pogoji postali spet bolj pomembni. Ker je v teh dneh prihajalo do advekcije onesnaženih zračnih mas iznad severnega Jadrana z jugozahodnimi vetrovi, je torej očitno, da je za dosego dokončne meje nasičenja onesnaženja nad širšim Mediteranom potreben daljši čas, oziroma da je bila v teh dneh Slovenija pod vplivom onesnaženja, ki se je v zračnih masah akumuliralo mnogo preteklih dni.

Naslednji najpomembnejši vpliv na simulirane vrednosti ozona nad razgibanim območjem Slovenije, pa se je izkazalo da ima meteorološki opis planetarne mejne plasti (PBL) zraka. Če se zdi, da je problem z opisom začetne kemijske sestave atmosfere nekako obvladljiv (simulacije začnemo mnogo dni pred pričetkom epizode, da omogočimo akumulacijo polutantov), pa so težave pri meteorološkem opisu PBL večje. Potrebne bi bile namreč dodatne, po možnosti celo trodimenzionalne meritve atmosfere, da bi lahko ugotovili katera od simulacij se bolj približa dejanskemu dogajanju. V kolikor bi nas zanimalo dogajanje nad omejenim območjem (naprimer nad Ljubljansko kotlino), bi potem z metodami siljenja lahko modelske rešitve bolj približali meritvam.

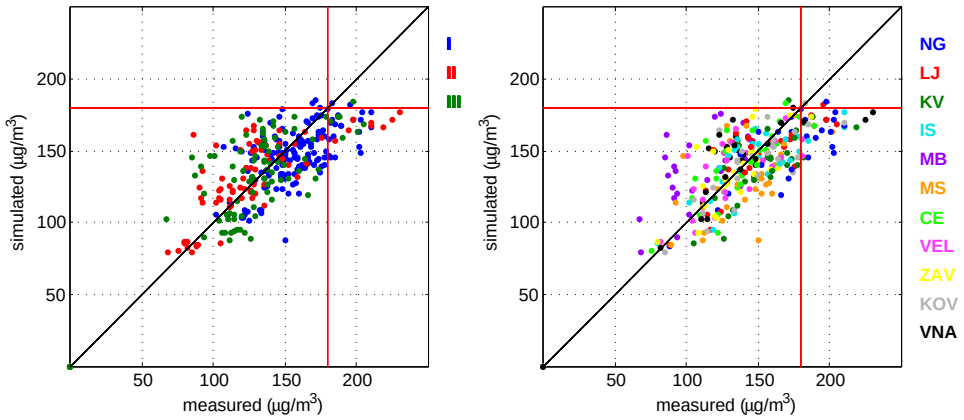

Slika H.14: Razsevni grafikon, primerjava simuliranih in izmerjenih dnevnih maksimumov ozona za referenčne simulacije epizod. Levo: točke obarvane glede na to za katero od treh epizod gre, Desno: glede na merilno mesto.

Robni kemijski pogoji so naslednji vir negotovosti, za katerega se je izkazalo, da ima lahko velik vpliv na simulirane vrednosti ozona, odvisno seveda od tega, kako daleč od območja zanimanja so postavljeni robovi domene, in kje se nahajajo najpomembnejši vplivni viri emisij. V našem primeru so bili robni kemijski pogoji testirani za srednjo D2 domeno, ki vključuje vse najpomebnejše potencialne vire emisij, tudi celotno Padsko nižino. Relativno velik vpliv teh robov kaže na pomembnost regionalnega transporta tudi v dneh, ko sicer prevladuje tvorba ozona iz lokalnih virov emisij.

Testiranje vpliva spremenjene količine antropogenih emisij NO_x in VOC za $\pm 30\%$ je pokazalo razmeroma majhen vpliv teh negotovosti na simulirane vrednosti ozona. Posledično torej ni za pričakovati, da bi napake v antropogenih emisijah bistveno vplivale na rezultate

simulacij. Edino območje, kjer ta trditev po vsej verjetnosti ne velja, oziroma kjer je možno, da je neujemanje med meritvami in modelom v precejšnji meri posledica napak v emisijah, je Primorska (oziroma Nova Gorica v disertaciji). Na tem območju imajo namreč na kvaliteto zraka pomemben vpliv emisije iz virov v sosednji Italiji, ki pa so bile zaradi nepoznavanja dejanskih lokacij velikih točkovnih in ostalih virov, ocenjene le s prostorsko prerazporeditvijo EMEP emisij ločljivosti 50×50 km glede na gostoto prebivalstva in rabo tal. Čeprav je iz modelskih rezultatov jasno sklepati na pospešeno tvorbo ozona nad tem območjem, pa so še posebej na posameznih lokacijah odstopanja v ozonu zaradi napak v prostorski razporeditvi emisij lahko precejšnja.

Zaradi različnih virov negotovosti z modelom ni bilo mogoče zelo natančno simulirati značilnosti prostorske in časovne dinamike ozona. Naprimer, z modelom običajno ni bilo možno natančno predvideti dejansko lokacijo in obseg najvišjih vrednosti ozona. V modelskih rezultatih so bili praviloma maksimumi ozona podcenjeni, enako preseganja mejnih vrednosti ozona, medtem ko so bili nočni minimumi ozona pogosto previsoki. Velikost sistematične napake je bila odvisna tudi od epizode in od merilne postaje. S Slike H.14 je denimo razvidno, da so najvišje precenitve izmerjenih vrednosti povezane s postajo v Mariboru, kar je bilo zaradi lokacije postaje blizu ceste pričakovano. Po drugi strani pa med najbolj opaznimi modelskimi podcenitvami dnevnih maksimumov ozona morda izstopa Nova Gorica. Kljub različnim negotovostim so nam rezultati simulacij omogočali prepoznati in razložiti nekatere pomembne značilnosti časovne in prostorske dinamike epizod z visokimi izmerjenimi vrednostmi ozona pri nas.

Izjava

Podpisana Rahela Žabkar izjavljam, da predložena disertacija predstavlja rezultate lastnega znanstveno-raziskovalnega dela.

Ljubljana, 5. marec 2009

Rahela Žabkar